

**EFFECTS OF INHALED NANOPARTICLES ON PLACENTAL NUTRIENT  
TRANSFER AND ENERGY METABOLISM**

By

JEANINE NICOLE D'ERRICO

A dissertation submitted to

The School of Graduate Studies

Rutgers, The State University of New Jersey

In partial fulfillment of the requirements

For the degree of

Doctor of Philosophy

Graduate Program in Toxicology

Written under the direction of

Dr. Phoebe Stapleton

And approved by

---

---

---

---

---

New Brunswick, New Jersey

October 2022

## ABSTRACT OF THE DISSERTATION

Effects of Inhaled Nanoparticles on Placental Nutrient Transfer and Energy Metabolism

By: JEANINE NICOLE D'ERRICO

Dissertation Director: Dr. Phoebe Stapleton, PhD

Inhalation of ultrafine particulate matter (PM<sub>0.1</sub>), otherwise known as nanoparticles (NPs), during pregnancy is of emerging concern due to known distribution throughout the body and impact on the developing offspring (i.e. fetal growth restriction). During pregnancy, the placenta serves as a protective barrier and conduit of glucose for the fetus. As a highly metabolically active tissue, the placenta needs a significant amount of glucose-derived energy to function. Together, this raises concern for NP-mediated placental toxicity with consequences for placental function and fetal development. Further, developmental growth patterns differ depending on the sex of the fetus, therefore there may be sex-dependent risk after gestational NP exposure. The hypothesis of this dissertation was that inhaled NP translocate to the placenta and impact placental glucose transfer and metabolism in a sex-dependent manner. Three specific aims were put forth; 1) characterize the distribution of NP aerosols in a pregnancy model, 2) evaluate maternal and fetal blood glucose concentrations and placental glucose transfer, and 3) assess placental energetic status and glucose metabolism. To recapitulate maternal NP exposure, pregnant Sprague-Dawley rats were administered whole-body exposure to titanium dioxide nanoparticle (nano-TiO<sub>2</sub>) aerosols. TiO<sub>2</sub> is a naturally occurring ore manufactured at the nanoscale for application in personal care products, pharmaceuticals, food and drink, and an array of other consumer products. Additionally, due to low reactivity profile, nano-TiO<sub>2</sub> is used to model toxicity for PM air pollution exposure. The findings of this dissertation demonstrate the systemic distribution of Ti in maternal, placental, and fetal tissues after gestational inhalation exposure to nano-TiO<sub>2</sub> aerosols. NPs were visualized intracellularly at the syncytiotrophoblast barrier inside nuclei, lysosomes, and embedded among

rough endoplasmic reticulum organelles. A significant reduction in glucose was identified in fetal blood. When stratifying the data by fetal sex, male fetuses had a significant lowering of blood glucose where females did not. Using ex-vivo placental perfusion a significant reduction in fluid flow through the uterine vasculature, but no change in placental glucose transfer to the umbilical vein, was identified. It was also determined that exposure does not reduce placental glucose transporter protein (GLUT1, GLUT3, GLUT4) expression or membrane localization. However, GLUT4 mRNA expression and fetal blood vessel area in the labyrinth zone were significantly reduced. Upon further investigation, changes in glucose metabolizing enzyme activity and energetic status in response to gestational nano-TiO<sub>2</sub> exposure were found; females significantly reduced glycolytic enzyme activity, whereas in male placentas enzyme activity was unchanged and energy status was compromised. Presented are the first evidence of sex-dependent reductions in glycolytic metabolism and energy in the placenta after maternal nano-TiO<sub>2</sub> inhalation. Altogether, the dissertation data support that inhaled NPs translocate to the placenta and lead to uterine vascular dysfunction. These may contribute to poor placental delivery of glucose, reduced placental glucose metabolism, and lowered fetal blood glucose transfer. Inadequate intrauterine conditions could lead to impaired fetal growth and predispose to life-long health consequences, particularly for males. The next research questions surround the sex-dependent changes to placental mitochondrial function and alternate nutrient metabolic pathways in response to gestational NP exposure. Offspring metabolic reprogramming and glucose tolerance from the intrauterine experience should also be explored. Overall, the information presented here is critical for educating the public and policy makers on the hazards of repeated NP inhalation exposure for pregnant women and their developing offspring.

## **DEDICATION**

This dissertation is dedicated to my parents Sonia and Ron D'Errico.

## ACKNOWLEDGMENTS

There are several people that I must thank for helping me get here. First and foremost, I must thank my advisor, Dr. Phoebe Stapleton. Thank you for allowing me to join your laboratory 5 years ago, and for the enormous amount of time and patience you dedicated to me while I've been learning since then. From you I learned how to be a stronger scientist, communicator, thinker, and writer. You are one of the smartest, most determined people I have ever met, and I know you will have a long successful career. To my committee, Drs. Lauren Aleksunes, Andrew Gow, Keith Cooper, and Nick Illsley, I am so grateful that you were always there for guidance. Thank you for all your time and intellectual contribution to the dissertation project. I must also mention Dr. Gary Grover who introduced me to Dr. Aleksunes as an undergraduate student in Rutgers Animal Sciences and has followed me closely ever since, I would not have found this program if it were not for you. I want to also thank Drs. Kenneth Reuhl and Ray Rancourt for all the conversations, science or personal-related, that I left feeling better from. Thank you for caring about me as a student as well as a person.

To my laboratory members: Sara Fournier, Chelsea Cary, Talia Seymore, and Jarett Reyes George. This work could not have been completed without you. Thank you for giving your time and energy to help with the necropsies, tissue collection, and tissue processing. More than that, thank you for all the laughs and support when things got tough. I enjoyed coming into the laboratory to work with each of you every day. To Chelsea in particular, I cannot express how grateful I am that you joined the lab. You were there to support me every step of the way during the last two years and for that I am so thankful. To the other wonderful friends who I happened to meet in graduate school: Sandra Minchala, Daniel Szatkowski, Talia Planas, Rulaiha Taylor, Danielle Kozlosky, and Zakiyah Henry, thank you so much for the fun and laughter in and outside of school because it truly helped

me get through. I have no doubt that our friendships will extend beyond graduate school and that all your futures are so bright.

To all my incredible friends outside of the graduate program, thank you for keeping me sane throughout this entire process. Thank you for your understanding when I was reclusive with my studies and for never making me feel badly when I had to focus and miss out. Thank you for always cheering me on, and most importantly thank you for not letting me forget to have fun.

To the JGPT moms: Eva Link, Liz Rossi, and Linda Everett. Thank you so much for always being available and more than willing to help with any administrative matter, but also for being so warm, kind, and willing to talk about anything. Your efforts make the program run smoothly.

I owe the biggest thank you's to my family. To my future in-laws: Lisa, Jim, Kyle, and Eric King. I have had some of the most fun times and belly-aching laughs with all of you. Thank you so much for welcoming me into your family 6 years ago and for all your love and support ever since. I am so excited to officially join your family. To my brother, Anthony, thank you for being you. You are my calm, cool, collected, polar-opposite sibling that I look to when I'm frantic and I thank you for always being a source of love and support. To my fur-baby, Jackson. Thank you for making me smile and laugh constantly, I think you are the best dog in the entire world.

Finally, to the people closest to me, who know me to the bone, and have seen me at my highest highs and lowest lows: my mom, dad, and fiancé. I could not have asked for a better support system to help get me through this program. I know I could probably never repay you for all the love and support you have given to help get me here. Mom and Dad, thank you for being the best pair of parents imaginable. Thank you for working so hard to give every opportunity you could to Anthony

and I as we were growing up. Mom, thank you for always being a listening ear, for reminding me to “get myself right”, and to just take deep breaths and do my best. Dad, thank you for giving me the realism and tough-love, and for helping me to find the strength in myself to push forward and finish strong when it felt like I had none. To Jameson King, my best friend and love of my life. You’ve loved and supported me through it all. I can honestly say this moment is as much yours as it is mine because I would not have gotten through if it were not for you. Thank you from the bottom of my heart.

## ACKNOWLEDGMENT OF PUBLICATIONS

### CHAPTER 2

**D'Errico J.N.**, Doherty C., Reyes George J.J., Buckley B., Stapleton P.A. Maternal, placental, and fetal distribution of titanium after repeated titanium dioxide nanoparticle inhalation through pregnancy. *Placenta*. 2022 Apr;121:99-108. doi: 10.1016/j.placenta.2022.03.008. Epub 2022 Mar 12. PMID: 35305398; PMCID: PMC9010360.

### APPENDIX 1

**D'Errico J.N.**, Stapleton P.A. Developmental onset of cardiovascular disease- could the proof be in the placenta? *Microcirculation*. Nov;26(8), (2018)

### APPENDIX 2

**D'Errico J.N.**, Fournier S.B., Stapleton P.A. Ex vivo perfusion of the rodent placenta. *Journal of Visualized Experiments*. May;(147), (2019)

### APPENDIX 3

**D'Errico J.N.**, Doherty C., Fournier S.B., Renkel N., Kallontzi S., Goedken M., Fabris L., Buckley B., Stapleton P.A. Identification and quantification of gold engineered nanomaterials and impaired fluid transfer across the rat placenta via ex vivo perfusion. *Biomedicine & Pharmacotherapy*. Sep;(117), (2019)

### APPENDIX 4

**D'Errico J.N.**, Fournier S.B., Stapleton P.A. Considering intrauterine location in a model of fetal growth restriction after maternal titanium dioxide nanoparticle inhalation. *Frontiers in Toxicology – Developmental and Reproductive Toxicology*. Mar;3:643804, (2021)

## TABLE OF CONTENTS

ABSTRACT OF THE DISSERTATION.....	ii
DEDICATION.....	iv
ACKNOWLEDGEMENTS.....	v
ACKNOWLEDGEMENT OF PUBLICATIONS.....	viii
TABLE OF CONTENTS.....	ix
LIST OF FIGURES.....	xiii
LIST OF TABLES.....	xvi
LIST OF ABBREVIATIONS.....	xvii
CHAPTER 1: GENERAL INTRODUCTION.....	1
1.1 Nanoparticle Inhalation and Fetal Growth Restriction.....	1
1.2 Titanium Dioxide Nanoparticles.....	2
1.2.1 Physiochemical Properties.....	4
1.2.2 Sources and Routes of Exposure.....	7
1.2.3 Inhalation and Distribution.....	8
1.2.3.1 Lung Exposure and Toxicity.....	9
1.2.3.2 Particle Translocation from the Lung.....	10
1.2.3.3 Target Organs and Toxicities of Inhaled Nanoparticles.....	12
1.2.3.4 Non-Pregnant Model Target Organs and Toxicities of Inhaled Nanoparticles.....	12
1.2.3.5 Target Organs and Toxicities During Pregnancy.....	19
1.3 Placental Anatomy and Physiological Functions.....	20
1.3.1 Uteroplacental Vasculature and Blood Flow.....	20
1.3.2 Hemochorial Placental Anatomy and the Human-Rat Comparison.....	23
1.3.3 Placental Physiological Functions.....	26
1.4 Placental Glucose Transport.....	27

1.4.1	Placental Glucose Transporter Proteins.....	28
1.4.2	Glucose Homeostasis During Pregnancy.....	29
1.4.3	Regulation of Placental Glucose Transport.....	30
1.4.4	Placental Glycogen Storage.....	31
1.5	Placental Energetics and Metabolism.....	32
1.5.1	Fetal Sex and Intrauterine Position-Dependent Differences in Placental Metabolism....	34
1.6	Research Hypothesis and Objectives.....	36
CHAPTER 2: MATERNAL, PLACENTAL, AND FETAL DISTRIBUTION OF TITANIUM AFTER REPEATED TITANIUM DIOXIDE NANOPARTICLE INHALATION THROUGH PREGNANCY.....		
		41
2.1	Abstract.....	42
2.2	Introduction.....	42
2.3	Materials and Methods.....	46
2.4	Results.....	50
2.5	Discussion.....	53
CHAPTER 3: REPEATED TITANIUM DIOXIDE NANOPARTICLE AEROSOL EXPOSURE REDUCES UTERINE ARTERY FLUID FLOW, PLACENTAL CAPILARY SIZE, AND FETAL GLUCOSE .....		
		70
3.1	Abstract.....	71
3.2	Introduction.....	71
3.3	Materials and Methods.....	76
3.4	Results.....	82
3.5	Discussion.....	84

CHAPTER 4: SEX-DEPENDENT PLACENTAL CHANGES IN GLUCOSE METABOLISM AND ENERGY STATUS IN RESPONSE TO MATERNAL TITANIUM DIOXIDE AEROSOL EXPOSURE.....	101
4.1 Abstract.....	102
4.2 Introduction.....	103
4.3 Materials and Methods.....	106
4.4 Results.....	114
4.5 Discussion.....	117
CHAPTER 5: OVERALL DISCUSSION.....	133
APPENDIX 1: DEVELOPMENTAL ONSET OF CARDIOVASCULAR DISEASE- COULD THE PROOF BE IN THE PLACENTA?.....	147
A-1.1 Abstract.....	148
A-1.2 Introduction.....	148
A-1.3 Review.....	149
A-1.4 Conclusion.....	164
APPENDIX 2: EX VIVO PERFUSION OF THE RODENT PLACENTA.....	172
A-2.1 Abstract.....	173
A-2.2 Introduction.....	173
A-2.3 Protocol.....	174
A-2.4 Representative Results.....	181
A-2.5 Discussion.....	182
APPENDIX 3: IDENTIFICATION AND QUANTIFICATION OF GOLD ENGINEERED NANOMATERIALS AND IMPAIRED FLUID TRANSFER ACROSS THE RAT PLACENTA VIA EX VIVO PERFUSION.....	191
A-3.1 Abstract.....	192

A-3.2 Introduction.....	192
A-3.3 Materials and Methods.....	196
A-3.4 Results.....	200
A-3.5 Discussion.....	201
APPENDIX 4: CONSIDERING INTRAUTERINE POSITION IN A MODEL OF FETAL	
GROWTH RESTRICTION.....	
A-4.1 Abstract.....	212
A-4.2 Introduction.....	213
A-4.3 Materials and Methods.....	216
A-4.4 Results.....	220
A-4.5 Discussion.....	222
References.....	243

## LIST OF FIGURES

Figure 1.1. Placental transfer of glucose from the maternal to the fetal circulation.

Figure 1.2. Cellular metabolism.

Figure 1.3. Schematic of normal and activated placental glycolytic activity in response to NP exposure theory.

Figure 2.1. Representations of nanoparticle aerosol characteristics during whole-body animal exposure taken on a single exposure day (4.20.21).

Figure 2.2. Ti concentrations in ppb measured in (A) maternal, (B) uteroplacental, and (C) fetal tissues on GD 20 using ICP-MS analysis.

Figure 2.3. Comparison between right and left sides of the reproductive tract.

Figure 2.4. Differential Ti tissue distribution outside of the lung in control and nano-TiO<sub>2</sub> exposed groups.

Figure 2.5. Placental accumulation of Ti (ppb) measured by ICP-MS analysis from nano-TiO<sub>2</sub> and filtered air exposed dams.

Figure 2.6. Transmission Electron Microscopy (TEM) image of particle distribution in the trophoblasts in the labyrinth zone of the placenta.

Figure 3.1. Maternal and fetal blood glucose concentrations.

Figure 3.2. Maternal and fetal gestational growth parameters after maternal nano-TiO<sub>2</sub> aerosol exposure.

Figure 3.3. Placental glucose transfer rate to the umbilical vein. Ex vivo placental perfusions from dams that were exposed to filtered air or nano-TiO<sub>2</sub> or that were naïve.

Figure 3.4. Fluid flow across the maternal uterine artery and through fetal umbilical vein.

Figure 3.5. Placental weight and morphometrics.

Figure 3.6. Expression of placental glucose transporter isoforms.

Figure 3.7. Placenta labyrinth zone syncytiotrophoblast immunolocalization of GLUT1 protein.

Figure 3.8. Placenta labyrinth zone syncytiotrophoblast immunolocalization of GLUT3.

Figure 3.9. Placenta labyrinth zone syncytiotrophoblast immunolocalization of GLUT4.

Figure 4.1. 10kDa spin column hemoglobin removal.

Figure 4.10 kDa spin column protein removal.

Figure 4.3. Hemoglobind<sup>TM</sup> optimization for hemoglobin removal.

Figure 4.4. Quantification of glucose and lactate from blood harvested from the fetal side of the labyrinth zone.

Figure 4.5. Hexokinase (HK) activity in placental labyrinth zone trophoblast tissue.

Figure 4.6. Phosphofructokinase (PFK) activity in placental labyrinth zone trophoblast tissue.

Figure 4.7. Lactate dehydrogenase activity (LDH) activity in placental labyrinth zone trophoblast tissue.

Figure 4.8. Measurement of cellular AMP from placental labyrinth zone trophoblast homogenates.

Figure 4.9. Measurement of cytosolic NAD and NAD<sup>+</sup>/NADH ratio from placental labyrinth zone trophoblast homogenates.

Figure 4.10. Placental junctional zone glycogen cell glycogen storage.

Figure A-1.1: Schematic of utero-placental vasculature.

Figure A-2.1: This figure represents the modified single vessel chamber.

Figure A-2.2: A closer view of the placental perfusion chamber.

Figure A-2.3: A view of the placental perfusion system.

Figure A-2.5: Schematic of placental perfusion system.

Figure A-2.5: Representative images of proof-of-principle experiments using Evan's blue dye.

Figure A-2.6: Data derived from the mock experiment.

Figure A-3.1: Schematic of placental perfusion methodology.

Figure A-3.2: Representative images of placental morphology after *ex vivo* perfusion.

Figure A-3.3: Quantification of Au-ENM concentration within the (A) uterine artery effluents and (B) fetal umbilical vein effluents over a 180-minute time course via ICP-MS analyses.

Figure A-3.4: Measurement of (A) maternal fluid flow across the uterine artery or (B) fluid flow across the placenta to the fetal compartment after Au-ENM infusion.

Figure A-3.5: Total Au-ENM transfer after the perfusion experiment was complete via ICP-MS analyses.

Figure A-4.1. Schematic of rodent uterine horn anatomy from the ventral aspect and acronym key.

Figure A-4.2. Fetal weight normalized by maternal weight on GD 20 and number of feti per uterine horn.

Figure A-4.3. Fetal weight normalized by maternal weight on GD 20 and number of feti per horn.

Figure A-4.4. Fetal weight normalized by maternal weight on GD 20 and number of feti per horn.

Figure A-4.5. Raw placental weights (g).

Figure A-4.6. Raw placental weight (g) at each intrauterine position for control and exposure groups.

Figure A-4.7. Placental efficiency calculated by fetal weight/placental weight.

Figure A-4.8. Placental efficiency, calculated by fetal weight/placental weight, for control and exposure groups.

## LIST OF TABLES

Table 2.1. Calculated NP lung burden with the following equation:  $D = F * V * C * T$ , where F is the deposition fraction (10%), V is the minute ventilation based on dam body weight (g), C equals the steady state mass concentration ( $\text{mg}/\text{m}^3$ ), and T equals the exposure duration (minutes).

Table 2.2. Ti in ppb measured in maternal, uteroplacental, and fetal tissues on GD 20 using ICP-MS analysis.

Table 3.3. Rank order of organs with expected highest to lowest relative Ti concentrations and actual relative concentrations (excluding lung).

Supplemental Table A-4.1: Table of effect sizes for traditional analysis approach (T-Test) and for our developed method (2-Way ANOVA).

## LIST OF ABBREVIATIONS

DLS, dynamic light scattering  
DOHaD, developmental origins of health and disease  
F-6-P, fructose-6-phosphate  
FGR, fetal growth restriction  
G-6-P, glucose-6-phosphate  
GD, gestational day  
HK, hexokinase  
ICP-AES, inductively coupled plasma atomic emission spectroscopy  
ICP-MS, inductively coupled plasma mass spectrometry  
IGF-1, insulin-like growth factor 1  
IGF-2, insulin-like growth factor 2  
LDH, lactate dehydrogenase  
NAD, nicotinamide adenine dinucleotide  
NADH, nicotinamide adenine dinucleotide (NAD) + hydrogen (H)  
Nano-TiO<sub>2</sub>, titanium dioxide nanoparticles  
NIOSH, National Institute for Occupational Safety and Health  
NPs, nanoparticles  
PAS, periodic acid-schiff  
PFK, phosphofructokinase  
PM<sub>0.1</sub>, ultrafine particulate matter  
PM<sub>2.5</sub>, fine particulate matter  
PSS, physiological saline solution  
RUPP, reduced uterine perfusion pressure  
SEM-EDX, scanning electron microscopy with electron dispersive X-ray analysis  
TEM, transmission electron microscopy  
TiO<sub>2</sub>, titanium dioxide  
UV, ultraviolet

## CHAPTER 1: INTRODUCTION

### 1.1 Nanoparticle Inhalation and Fetal Growth Restriction

Exposure to ultrafine particles (PM<sub>0.1</sub>) and engineered nanoparticles (NPs) have been linked with fetal growth restriction (FGR) and other pregnancy complications. Human studies have shown that pregnant women who are exposed to high levels of ambient air pollution (Nobles et al. 2019) or NPs in the work place (Manangama et al. 2019) have an increased likelihood for preterm delivery or FGR. Rodent studies that have recapitulated NP inhalation using nose-only cadmium oxide (Blum et al. 2012a) and whole-body titanium dioxide (TiO<sub>2</sub>) (Stapleton et al. 2013b) exposure schemes have also identified FGR outcomes. However, the mechanisms connecting gestational inhalation of NPs and reduced fetal growth remain obscure.

FGR is diagnosed as birth weight less than the 10<sup>th</sup> centile for gestational age-matched infants. Affecting up to 10% of human pregnancies worldwide, this condition constitutes a failure to meet the genetically pre-determined growth potential *in utero* (Colella et al. 2018). Currently, there are no interventions to improve an FGR diagnosis; the only available therapeutic approach is early delivery of the fetus (Alberry and Soothill 2007). FGR neonates are prone to a series of complications including asphyxia, hypoglycemia, hypocalcemia, jaundice, feeding difficulties, and neuro-behavioral abnormalities (Sharma et al. 2016). FGR diagnoses have also been linked with later childhood neurodevelopmental delays and adult cardiovascular disease, metabolic disease, obesity, and cancer (Velten et al. 2012). Thus, an FGR diagnosis has significant short and long-term health consequences.

A common cause of FGR is a maternal factor (e.g., malnutrition, preeclampsia, xenobiotic exposure) leading to placental dysfunction. For example, food deprivation and maternal malnutrition in developing countries is the most significant determinant of uteroplacental

insufficiency and FGR (Bergmann et al. 2008). Additionally, preeclampsia coincides with FGR in 22% of cases, where narrowing of uterine blood vessels may create nutrient restriction for the placenta (Zhu et al. 2020). Finally, maternal xenobiotics may also contribute to the development of FGR (Pintican et al. 2019; Zhu et al. 2021). There is strong evidence to suggest that cigarette smoke and air pollution contribute to the development of FGR through impairments to placental blood flow and nutrient transfer (Kawashima et al. 2014; Sastry 1991; van den Hooven et al. 2012). A great number of toxic heavy metals, pesticides, and solvents have shown similar outcomes (Kamai et al. 2019). Therefore, the evidence suggests that exposure to polluted air is an emerging maternal factor that can lead to reduced uteroplacental nutrient transfer to the fetus, thereby restricting fetal growth.

## **1.2 Titanium Dioxide Nanoparticles**

Titanium dioxide ( $\text{TiO}_2$ ) has been used as the pure white of the 20<sup>th</sup> century. Pure titanium was first discovered as a naturally-occurring mineral in the 1700's and extracted in small quantities to be used as a bright white pigment (Jorge et al. 2013). It was not until the early 1900's that mass production was made possible by two companies, the Titanium Pigment Corporation of Niagara Falls and the Titan Company (Habishi 2016). For the past century,  $\text{TiO}_2$  has been increasingly valued for its unmatched hue compared to other white pigments like lead or zinc. Today,  $\text{TiO}_2$  is the most coveted white pigment annually produced at 5 million tons (Skocaj et al. 2011).

Titanium dioxide can be intentionally engineered to fall in the nano-size range for unique and beneficial properties (Musial et al. 2020). Such properties include ultraviolet (UV) light absorption which has been applied in sunscreens and optimized over the years to be most efficient by decreasing  $\text{TiO}_2$  particle size from the micron to the nanoscale to achieve maximal absorptive cross section. At the nanoscale, the large band gap and band gap absorbance edge (413 nm for rutile, 388 nm for anatase) allows for stronger light (i.e., light falling in the UV range with wavelengths

between 100 and 400 nm) to be absorbed by electrons and excite them to cross the large band gap (Yang et al. 2004). This results in the excited electrons and electron holes to unite and rearrange, thus yielding the UV protective ability (Yang et al. 2004). Additionally, this property confers antimicrobial activity to nano-TiO<sub>2</sub> that is used in surface coatings and food, as UV light-excited electrons can also catalyze surrounding absorbents (i.e., water molecules) into strong oxidative species that can then damage the cell membranes and DNA of surrounding microbes (Desai and Kowshik 2009). Titanium dioxide nanoparticle (nano-TiO<sub>2</sub>) powders can be produced from bulk TiO<sub>2</sub> ore by the sulfate, chloride or sol-gel processes (Ramos-Delgado et al. 2016). Nano-TiO<sub>2</sub> is now one of the most manufactured NPs world-wide (Piccinno et al. 2012). Due to the sheer production and usage, it is important to characterize the properties and potential human health implications of this material.

An added advantage to understanding the health implications of nano-TiO<sub>2</sub> is extrapolation to health effects of PM air pollution. PM is categorized as fine (PM<sub>2.5</sub>) and ultrafine (PM<sub>0.1</sub>), which are particles less than 2.5 microns and 100 nanometers, respectively. Types of PM<sub>2.5</sub> and PM<sub>0.1</sub> include combustion particles, organic compounds, and metals (Kwon et al. 2020). Nano-TiO<sub>2</sub> represents a metal, the PM<sub>0.1</sub> particle in size, and it has a near neutral zeta potential in biological environments such as blood meaning it has a lower reactivity profile (Shi et al. 2013). Thus, it is a useful model to study toxicological outcomes after exposure to the PM component of air pollution. Additionally, it is not vulnerable to enzymatic degradation compared to the carbon-based NPs of carbon black, fullerenes, graphite, and multi- or single- walled carbon nanotubes (Vlasova et al. 2016), allowing for study of a persistent particle in the body. Modeling exposure with nano-TiO<sub>2</sub> can help follow up studies use NPs layered with additional and more complex physiochemical properties. Additionally, studies can include nano-TiO<sub>2</sub> as a reference material to ascertain which effects are due to or worsened by the added properties. For example, nano-TiO<sub>2</sub> can be used to compare the effects of more reactive or complex NPs (i.e. zinc, copper) that might not be related

to physical particle presence (Lanone et al. 2009). Overall, inhaled nano-TiO<sub>2</sub> can help inform the health effects that would occur after inhalation of PM component of air pollution.

### 1.2.1 Physiochemical Properties

The role of physiochemical properties in NP toxicological outcomes is enormous. A variety of properties such as chemical composition, size, shape, surface charge, zeta potential, light absorption and scattering, and photocatalytic activity can significantly influence the interactions between NPs and biological environments (Gatoo et al. 2014). In turn, the biological environment can also influence NP physiochemical properties (Jurašin et al. 2016). Nano-sized particles have consistently demonstrated to be more toxic than larger-scale counterparts, likely due to increased surface area and ability to breach biological barriers (Barua and Mitragotri 2014; Nurkiewicz et al. 2008). Therefore, it is vital to appropriately characterize and understand the physiochemical properties of TiO<sub>2</sub>, particularly at the nanoscale.

#### *Chemical composition*

TiO<sub>2</sub> is a naturally occurring oxide of the metal titanium that can be found in the earth's crust with a molecular weight of 79.9 g/mol. Its chemical composition is comprised of a single titanium atom configured with two oxygen atoms; several join to form crystal structures in the form of brookite, anatase, or rutile. On gross observation TiO<sub>2</sub> is a wispy, white, odorless powder.

#### *Shape*

Due to its small size, nano-TiO<sub>2</sub> has very different physiochemical properties compared to TiO<sub>2</sub> at larger sizes. As size decreases, the surface area, photocatalytic, and hydrophilic activity of the material increases. These properties that are unique at the nano size have toxicological implications including deeper lung access (Kwon et al. 2020) and distribution through biological barriers (Geiser et al. 2005). Nano-TiO<sub>2</sub> has shown cellular internalization (Lammel et al. 2019) that could lead to

disturbances of cell surface proteins (Soto et al. 2017), mitosis (Huang et al. 2009), survival (Biola-Clier et al. 2020), and metabolism (Tucci et al. 2013).

#### *Crystal form (shape)*

Individual nano-TiO<sub>2</sub> particles exist in either rutile, anatase, or brookite crystal forms. Each crystal shape confers a slightly different cellular interaction. Of the three polymorphs, rutile has the smallest band gap and is therefore the most chemically stable and commonly produced (Cui et al. 2016). One study using a mouse macrophage cell line demonstrated the important role crystal structure plays in the biological effects of NPs (Yu et al. 2017). Rutile and anatase nano-TiO<sub>2</sub> produced at similar size, surface area, and zeta potential showed that the rutile NPs have a stronger adsorption to phospholipids which are the main component of cell plasma and lysosomal membranes, and the anatase NPs have a greater affinity for proteins and can disturb mitochondrial function (Yu et al. 2017). Therefore, different crystal structures of the same type of NP can create preferential surface affinity for proteins or phospholipids and lead to damaging effects on different organelles. Additionally, the results from this study suggest that other nanotoxic outcomes may be distinctly due to the surface affinity or shape differences between rutile and anatase NPs. With respect to reactivity between anatase and rutile structures, anatase has demonstrated a higher ability to generate ROS due to larger band gap and energetic potential (Xue et al. 2010). Brookite is the least chemically stable phase as it has the largest band gap of the three polymorphs (Luo et al. 2016).

#### *Surface charge and zeta potential*

Surface charge plays a critical role in how NPs interact with their environment. Pure nano-TiO<sub>2</sub> has a negative charge that is inherent to its chemical and crystal construct. In a biological environment such as blood (range of 7.35 to 7.45 (Kellum 2000)), the zeta potential (i.e., charge that develops at the interface of a particle with a surrounding liquid) of nano-TiO<sub>2</sub> is approximately neutral to -

40 mV depending on the crystal form (Skocaj et al. 2011). An inverse relationship exists between pH and zeta potential of nano-TiO<sub>2</sub> which greatly influences particle reactivity (i.e., ability to produce ROS) (Delgado Alvarado et al. 2019).

Surface charge also has an influence on the adsorption of molecules in biological environments. The surface coating of biomolecules is called the “corona”. Depending on the charge of the NP, lipids or proteins may be attracted and adhere to the surface (Kopac 2021). The composition of the corona then largely determines cellular interactions and uptake, and therefore potential toxicity. Regarding nano-TiO<sub>2</sub>, Khan et al. recently characterized the surface-chemistry dependent behavior of the corona after uptake and sub-cellular localization using adenocarcinoma human alveolar basal epithelial cells (A549) (Khan et al. 2020). Their findings revealed that pure nano-TiO<sub>2</sub> rapidly exchanged corona molecules compared to modified nano-TiO<sub>2</sub>. This could indicate that pure nano-TiO<sub>2</sub> has complicated interactions with varying biological environments, which is an area that is not yet studied or completely understood.

#### *Light absorption and scattering*

Nano-TiO<sub>2</sub> is most often exploited for its light absorption and light scattering. Owing to chemical composition and nano-size, UVB (290-320 nm) and UVA (320-400 nm) are efficiently absorbed by the particle valance bands (Cole et al. 2016). Along with zinc oxide, nano-TiO<sub>2</sub> are applied to sunscreens to protect against the adverse effects of ultraviolet radiation (Smijns and Pavel 2011). Light in the visible range however is effectively scattered. Color cosmetics such as eye shadows, blush, highlighters, and foundations in loose or pressed powder forms utilize nano-TiO<sub>2</sub> to for a luminescent appearance when applied to the skin (Dréno et al. 2019). Both the light absorption and scattering effects are functions of the ~3.1 eV band gap width of nano-TiO<sub>2</sub> particles (Smijns and Pavel 2011).

### *Photocatalytic activity*

Photocatalytic activity of nano-TiO<sub>2</sub>, also attributed to energy band gap width, is exploited to be antimicrobial. Upon photoactivation by UVA, B, and C, visible and fluorescent light, and X-ray radiation, nano-TiO<sub>2</sub> donates electrons to surrounding oxygen molecules to generate strong oxidizing species (Molina-Reyes et al. 2020). Hydroxyl radical ( $\bullet$ OH) and other reactive oxygen species then oxidize surrounding organic material. It has been shown that these radicals can damage cell membranes and DNA of bacteria such as *Escherichia coli* (*E. Coli*) (Sunada et al. 2003). To take advantage of this property nano-TiO<sub>2</sub> is used in water treatments, self-cleaning surfaces such as windows and windshields, and smartphones where UV activation from the sun stimulates the photocatalytic activity of the particles.

### 1.2.2 Sources and Routes of Exposure

#### *Sources*

TiO<sub>2</sub> is commonly used in a wide range of commercial products including personal care, pharmaceutical, technological, food and drink. It is estimated that 36% of the TiO<sub>2</sub> in production exists at the nano scale (Wu and Hicks 2020). Currently, the National Institute for Occupational Health and Safety (NIOSH) recommends that workplace exposures for nano-TiO<sub>2</sub> do not exceed air concentrations of 0.3 mg/m<sup>3</sup> as a time-weighted average for up to 10 hours per day during a 40-hour work week (Skocaj et al. 2011). The prevalence of nano-TiO<sub>2</sub> is owed to the applicability of traits that physiochemical properties confer (i.e., UV absorption, visible light scattering photocatalytic activity, and white pearlescent coloring). Since the early 1900's, the primary use was for its bright white appearance and resistance to discoloration from UV exposure for products available to the general population (e.g., paints, paper, pharmaceutical tablets, and personal care, food, and drink). Up until 2015, Dunkin Donuts included nano-TiO<sub>2</sub> in their donut powdered sugar to achieve an appetizing white appearance (Blaznik et al. 2021). Until January 2022, the ingredient was allowed in candy, coffee creamer, baked goods and white sauces in the European Union under

the food additive alias of E171, but is now being phased out due to carcinogenicity concerns (Weir et al. 2012). The amount of material required to achieve the desired white opaque appearance is relatively low for nano-TiO<sub>2</sub>, meaning low costs and widespread use of the pigment for these product classes. The applicability of nano-TiO<sub>2</sub> has led to the mass production and integration of this material into products that are used daily by the general population. Consequently, there are commonplace opportunities for human exposure in the occupational, environmental, and domestic settings.

#### *Routes of exposure and systemic uptake*

Human exposure to nano-TiO<sub>2</sub> occurs through the dermal, gastric, and pulmonary routes during manufacturing or product use. There is minimal dermal nano-TiO<sub>2</sub> absorption according to *in vitro* studies using HaCaT keratinocyte cell line and *in vivo* studies on hairless rat skin (Adachi et al. 2010; Adachi et al. 2013; Crosera et al. 2015). Pulmonary and gastric routes are of further toxicological concern through subsequent absorption and distribution. Arguably, the most vulnerable route of entry into the body is through the lung due to the absence of first pass through the liver. Inhaled nano-TiO<sub>2</sub> may have a more direct path to systemic circulation over oral or dermal routes of exposure. Thus, pulmonary exposure is the focus of this dissertation.

#### 1.2.3 Inhalation and Distribution

Inhalation is a predominant human exposure route for nano-TiO<sub>2</sub> and an important means of systemic NP distribution. The respiratory tract is comprised of the upper airways (i.e., nasopharyngeal passage and larynx) and lower airways (i.e., trachea, bronchi, and alveoli). According to *in silico* models of healthy basal human respiration, the deposition fraction of NPs is not uniform throughout the respiratory tract (Löndahl et al. 2014). The tracheobronchial and alveolar segments were found to be the highest sites of deposition. The distribution pattern can be influenced by age (Keshavarzian et al. 2012), and pulmonary disease (Brown et al. 2002; Löndahl et al. 2012).

NPs can travel deeper into the human lungs compared to larger scale counterparts that are caught in upper airways and cleared via the mucociliary escalator (Möller et al. 2006; Wang et al. 2020). Braakhuis and colleagues compared the rat alveolar mass dose between inhaled 15 nm and 410 nm silver particles for 6 hours/day for 4 consecutive days and measured a 3.5 times higher concentration of 15 nm particles at that pulmonary location (Braakhuis et al. 2014). They further visualized the 15 nm silver particles within alveolar macrophages and lung epithelial cells. The extremely thin lung air-blood barrier (approximately 2  $\mu\text{m}$  in humans) may allow for the diffusion of NPs to the blood, interstitial space, or lymphatic fluid (Knudsen and Ochs 2018). Therefore, the potential for inhaled nano-TiO<sub>2</sub> to reach systemic circulation and cause disturbance in secondary tissues is of high concern.

#### 1.2.3.1 Lung Exposure and Toxicity

Laboratory animal studies can model pulmonary exposures to NPs via intratracheal instillation, nose-only, or whole-body inhalation. Intratracheal instillation is useful for examining the distribution and dose-dependent effects of nanomaterials at a relatively low cost and with simpler equipment. However, inflammation due to bolus dose effects have been reported, which do not occur in nose-only or whole-body inhalation studies (Morimoto et al. 2016). Additionally, installation requires animal anesthesia which may not be ideal for longer term repeated dose studies. Nose-only and whole-body inhalation exposures avoid bolus-dose inflammation and animal anesthesia; however, they also have their advantages and disadvantages. Nose-only exposures limit the amount of material waste as the exposure is directed to the animal due to the much smaller chamber volume. Additionally, this mode of exposure eliminates contamination from other routes of exposure. However, animal restraint is required to conduct nose-only exposures may cause undue stress to the animal. In comparison to nose-only exposure, whole-body does not require animal restraint and best recapitulates real-world exposures. However, this method involves some

material waste along the chamber walls, and the equipment and maintenance of whole-body inhalation facilities are expensive and require more advanced training and expertise (Oyabu et al. 2016). While each of the three methods have their advantages and limitations, all three are useful in modeling pulmonary exposure for toxicological profiling.

Real world pulmonary exposure to nano-TiO<sub>2</sub> aerosols can occur in occupational or domestic settings which may lead to adverse effects in the lung (Kwon et al. 2012). Animal models show whole-body aerosol exposures increase the number of immune cell populations in bronchoalveolar lavage (Baisch et al. 2014; Grassian et al. 2007), particle-laden alveolar macrophages (Geiser et al. 2008a), and fibrinolytic and proliferative histopathological lesions (Ma-Hock et al. 2009). Blackford et al. found that 24 hours after a single intratracheal instillation of TiO<sub>2</sub> particles that averaged less than 5 microns in diameter there were increases in pulmonary alveolar macrophages, neutrophils, inducible nitric oxide synthase gene expression and nitric oxide production (Blackford et al. 1997). Grassian et al. found that mice exposed via whole-body inhalation (4 hrs/day for 10 days) to 2 and 5 nm nano-TiO<sub>2</sub> had a moderate increase in alveolar macrophages 1- and 2-weeks post exposure cessation, which was ameliorated at 3 weeks post-exposure (Grassian et al. 2007). Together, the evidence shows a local inflammatory response and inability to clear particles after pulmonary deposition. Smaller particles may cause greater toxicity due to access to the deep lung, larger surface area, and uptake into alveolar epithelium (Thorley et al. 2014). Further, uptake of nano-TiO<sub>2</sub> has been shown to cause morphological damage to human alveolar epithelial cells *in vitro* (Park et al. 2007). These studies demonstrate the potential for inhaled nano-TiO<sub>2</sub> to promote inflammatory and structural damage to the lung and alveolar epithelial cells. In addition to being a target of NP-mediated toxicity, the alveolar epithelium may also serve as a gateway for systemic distribution.

#### 1.2.3.2 Particle Translocation from the Lung

The way(s) in which inhaled NPs, including nano-TiO<sub>2</sub>, access systemic circulation is still a topic of debate. The possible routes that have been put forth include 1) interstitial/lymphatic passage (Semmler-Behnke et al. 2007), 2) phagocytosis by alveolar macrophages and migration into systemic circulation (Geiser et al. 2008a), and 3) alveolar epithelial uptake and efflux into pulmonary microcirculation (Geiser et al. 2005). As it currently stands, there is stronger evidence for the majority of pulmonary nano-TiO<sub>2</sub> being cleared by migration into the alveolar microvasculature (Mühlfeld et al. 2007; Pujalté et al. 2017), compared to macrophage phagocytosis (Geiser et al. 2008b).

There is evidence from rodent studies demonstrating that inhaled nano-TiO<sub>2</sub> particles move into systemic circulation. Toxicokinetic distribution studies by nose-only or whole-body inhalation exposures have identified particles in extrapulmonary sites. Pujalté et al. administered adult male Sprague Dawley rats a single nose-only exposure to anatase nano-TiO<sub>2</sub> at a dose of 15.57 mg/m<sup>3</sup> over 6 hours and were sacrificed at varying time points over a 14-day period (0, 3, 6, 12, 24, 48 (2 days), 72 (3 days), 168 (7 days) and 336 (14 days) hours) to evaluate lung deposition, retention, and distribution (Pujalté et al. 2017). Using inductively coupled plasma mass spectrometry (ICP-MS), peak levels of titanium within the lungs were measured at 48 hours, which had a slight decline over the successive time points but remained at relatively high concentrations at day 14 (Pujalté et al. 2017). Although an order of magnitude lower than the lungs, this study found that the extrapulmonary tissues (blood, liver, kidneys, spleen) had detectable titanium levels. Blood levels of titanium rose during the 6-hour inhalation exposure with peak levels at 12 hours and return to baseline at day 7. In a study conducted by Yin et al., mice were put in whole-body inhalation chambers and administered  $6.34 \pm 0.22$  mg/m<sup>3</sup> of nano-TiO<sub>2</sub> aerosols for 8 hrs/day for 3 weeks (Yin et al. 2014). The toxicokinetic results also revealed the highest levels of titanium in the lungs and extrapulmonary tissues of blood, liver, kidney, and urine excrement having detectable amounts after the 3 week exposure (Yin et al. 2014). These studies not only provide evidence of nano-TiO<sub>2</sub>

translocation from the lung to secondary tissues, but also beg the question of potential toxic effects from direct NP interactions at these extrapulmonary sites.

#### 1.2.3.3 Target Organs and Toxicities of Inhaled Nanoparticles

The weight of evidence for the absorption and distribution of nano-TiO<sub>2</sub> after pulmonary exposure raises concern for toxicity to various organ systems. Inhaled nano-TiO<sub>2</sub> has been detected in the brain (Wang et al. 2007b), liver (Pujalté et al. 2017), kidneys (Pujalté et al. 2017), and spleen (Pujalté et al. 2017). Additionally, from investigations using alternate routes of exposure or PM inhalation, NPs have been found to distribute to and affect barrier (e.g., brain, testes), filter (e.g., liver, kidney, spleen, lymph node), reproductive and endocrine (e.g. ovary, thyroid, adrenal), and circulatory (e.g. heart, blood vessels) systems. These studies have been referenced where gaps in the literature on cell toxicity and organ function after nano-TiO<sub>2</sub> inhalation occur. While all these studies are critical, the model predominantly used is healthy male or non-pregnant female. Here summarized first is the literature on target organs and toxicities in the non-pregnant system. Then, the smaller collection of work that has begun to assess exposures using a pregnancy model is reviewed.

#### 1.2.3.4 Non-pregnant Model Target Organs and Toxicities

##### *Barrier system: brain and testes*

There are several blood barriers of the body that are meant to protect from harmful substances. Some examples include the blood-brain, blood-testes, blood-placenta, and blood-thymus barriers (Fröhlich 2002). Here is discussed the available literature on the possible NP breach of the blood-brain and blood-teste barriers and effects on the brain and teste tissues.

The blood-brain barrier is a tightly-sealed and highly selective barrier formed by specialized microvasculature along with astrocytes that together protect the brain from toxins, pathogens, and inflammation (Daneman and Prat 2015). In the rat, inhaled NPs may reach the brain by breaching the blood-brain barrier or by olfactory nerve pathway where central nervous system toxicity may occur (Elder et al. 2006). Using ICP-MS analysis, Wang et al. confirmed that single (Wang et al. 2008b) and subacute (Wang et al. 2008a) intranasally administered nano-TiO<sub>2</sub> aerosols to adult mice significantly increased the brain Ti concentrations compared with control. In addition to Ti measurement, particle accumulation was visualized in the hippocampus (Wang et al. 2008a). Lesions and oxidative stress to the brain were also found, suggesting that particle presence within neural tissue is the cause of the morphological and biochemical damage (Wang et al. 2008a). However, the mechanism of travel to the brain remains unclear.

*In vitro* and *in vivo* studies have helped to identify the molecular mechanisms of nano-TiO<sub>2</sub>-induced neurotoxicity. Oxidative stress, apoptosis, reduced mitochondrial membrane potential, inflammation, and disturbance of ATPases or neurotransmission have been identified in neurons *in vitro* (Liu et al. 2010; Wu et al. 2010; Xue et al. 2012). From *in vivo* mouse studies, oxidative stress, inflammation activation of apoptotic pathways has consistently been found after nano-TiO<sub>2</sub> respiration (Wang et al. 2008c; Ze et al. 2013). The functional consequences on recognition ability, spatial memory, and learning ability of nano-TiO<sub>2</sub> treated rodents indicates that particle deposition in the brain could lead to neurodegeneration (Song et al. 2015). The overall evidence shows that inhaled nano-TiO<sub>2</sub> can accumulate in neural tissue and cause local toxicity and lead to functional neurological impairments.

The blood-testes barrier is another physical barrier between the systemic blood circulation and the seminiferous tubules of the testes. Miura et al. reported that sperm motility and number were significantly reduced in mice after single intravenous injection of titanium NPs (Miura et al. 2019).

This study did not measure titanium content or visualize NP in the testes. However, by isolating mature spermatozoa and directly exposing to the NPs, they recapitulated the significant reduction in sperm motility, suggesting this effect may be due to direct particle exposure *in vivo*. Further, significant reductions in spermatozoa ATP content were identified, suggesting that the NPs may have a mitochondria functional effect. It is well understood that spermatozoa mitochondrial function is essential for sperm motility to reach and fertilize the oocyte (Boguenet et al. 2021), therefore these findings suggest that exposure may contribute to male infertility. Additionally, Abu Zeid et al. found juvenile rats given chronic oral nano-TiO<sub>2</sub> exposure had abnormal development and necrosis of the seminal vesicles (Abu Zeid et al. 2017). The seminal vesicles are a pair of small glands that secrete fluid important for sperm vitality and immunosuppression in the female reproductive tract. This finding further supports nano-TiO<sub>2</sub> exposure affects the teste that may have functional consequences on male fertility. Overall future work is needed to confirm NP breach of the blood-testes barrier.

*Filter system: liver, kidney, spleen, and lymph node*

The purpose of filter tissues in the body, such as the liver, kidney, spleen, and lymph node, is to detoxify and remove harmful substances from the systemic blood circulation. Therefore, after inhalation exposure NPs may be absorbed into systemic circulation and encounter these tissues where harmful effects on organ function may ensue.

The liver is a major blood-filtering organ that may accumulate NPs in systemic circulation. There is one study by Pujalté et al. that has measured Ti with ICP-MS in the liver after single nose-only nano-TiO<sub>2</sub> inhalation exposure (15 mg/m<sup>3</sup>) thus far (Pujalté et al. 2017). After oral nano-TiO<sub>2</sub> exposure (1, 4, and 16 g/kg body weight) in rats, Ti was also detected in the liver in all exposure groups measured by inductively coupled plasma atomic emission spectroscopy (ICP-AES) (Valentini et al. 2019). In addition, transmission electron microscopy (TEM) visualized hepatocyte

intracellular particle accumulation in lysosomes and free in cytoplasm. Together, these infer after multiple routes of exposure, nano-TiO<sub>2</sub> enters systemic circulation and directly interfaces with the liver. Visual identification of nano-TiO<sub>2</sub> within hepatocytes coincided with elevated oxidative stress markers, indicating direct particle interactions in the liver may lead to oxidative stress and cellular damage (Valentini et al. 2019). Wang et al. detected elevations in systemic alanine transaminase (ALT), aspartate aminotransferase (AST), and lactate dehydrogenase (LHD) in mice, suggesting nano-TiO<sub>2</sub> may lead to liver damage (Wang et al. 2007a). Although no study to date has focused on hepatotoxicity after nano-TiO<sub>2</sub> inhalation, current evidence supports that circulating nano-TiO<sub>2</sub> can accumulate in the liver and cause hepatocellular oxidative stress and liver damage (Ma et al. 2009).

In addition to the liver, the kidneys are a major blood filtration organ. There is evidence from rat models that inhaled nano-TiO<sub>2</sub> moderately accumulates within the kidneys (Pujalté et al. 2017), and leads to increased renal oxidative stress but without impact on kidney function (Liang et al. 2009). Aztatzi-Aguilar et al. found increased levels of kidney damage biomarkers ( $\beta$ -2-microglobulin and cystatin-C) and histological lesions of the kidney using PM<sub>2.5</sub> inhalation exposure in rats (Aztatzi-Aguilar et al. 2016). Wardoyo et al. exposed mice via whole-body inhalation to PM<sub>0.1</sub> and showed a dose-dependent increase in kidney particle accumulation along with kidney cell deformation (Wardoyo et al. 2018). The available studies using alternate routes of exposure to nano-TiO<sub>2</sub> (e.g. intraperitoneal injection) in rats found oxidative stress within the kidney and swelling of the glomeruli (Valentini et al. 2019). This together evidence suggests nano-TiO<sub>2</sub> can collect in renal tissue and cause oxidative stress.

Further assessments were conducted on the urine after nano-TiO<sub>2</sub> intraperitoneal injection, which can lead to systemic exposure via peritoneal drainage into the portal vein and inferior vena cava (Al Shoyaib et al. 2019). In a rat study, enzymatic markers of kidney function detected in the urine

indicated damage at the high dose (16g/kg body weight) (Valentini et al. 2019). From this study urine samples also quantified concentrations of metabolic byproducts, meaning cellular metabolism of the kidney is reduced with exposure. In contrast, the low-dose nano-TiO<sub>2</sub> (0.5g/kg body weight) increased metabolic byproducts (e.g.,  $\alpha$ -ketoglutarate, citrate, succinate, transaconinate, and acetate) in urine without apparent impact on renal function. The dose-dependent changes found in this study indicate possible cellular response by increased metabolism at a low dose but decreased metabolism at the high dose potentially due to cellular toxicity. Overall, the literature supports particle accumulation within renal tissue and dose-dependent oxidative stress, perturbed metabolism, histological damage, and functional perturbations to renal tissue.

The spleen is responsible for filtering the blood of foreign material, mounting immune responses to blood-borne pathogens, and clearing old or damaged red blood cells (Cesta 2006). In rats, the spleen has been shown to be susceptible to inhaled nano-TiO<sub>2</sub> accumulation (Pujalté et al. 2017). However, there are no studies that evaluate toxicity after pulmonary exposure. From toxicological assessments using oral exposure, it was found that chronic low-dose nano-TiO<sub>2</sub> led to significant reductions in immune cell populations and increases in apoptotic cytokine expression (Sang et al. 2012). Sheng et al demonstrated that oral nano-TiO<sub>2</sub> led to reduced immune capacity, oxidative stress, and apoptosis at multiple doses (Sheng et al. 2014). Due to the major splenic function of blood filtration, more work is required to fully understand the impact of inhaled nano-TiO<sub>2</sub> on this tissue.

The lymphatic system aids in the drainage of the blood circulation and immune surveillance (Cueni and Detmar 2008). Lymph nodes are a component of the lymphatic system that filter substances through the lymphatic fluid that drains from blood plasma (Cueni and Detmar 2008). One study in rats has detected Ti in lymph nodes after nano-TiO<sub>2</sub> inhalation (Pujalté et al. 2017), but there are no studies available that evaluate lymphatic effects after this route of exposure. Within 24 hours of

intradermal injection of nano-TiO<sub>2</sub>, significant changes in protein expression involved in the inflammatory response, lipid and fatty acid metabolism, mRNA processing, and nucleosome assembly were found in the lymph nodes of mice, providing some initial inferences on the potential effects of nano-TiO<sub>2</sub> in the lymph node (Gao et al. 2011). Given that circulating NPs may be drained by the lymphatic system and reach lymph nodes (Kourtis et al. 2013), further investigations on the lymph node immune function and health are required.

*Circulatory system: heart and blood vessels*

The circulatory system is comprised of the heart and a closed system of blood vessels including arteries, veins, and capillaries. The macrocirculation refers to the largest blood vessels including arteries and veins, and the microcirculation refers to the smallest blood vessels, including arterioles, capillaries, and venules (Rizzoni et al. 2009). The endothelium is the inner lining of blood vessels and is directly exposed to substances circulating in the blood. Inhaled NPs may translocate from the lung to the systemic circulation and directly affect the heart and blood vessels.

The heart has been shown to be vulnerable to accumulation and adverse effect from nano-TiO<sub>2</sub> particles. Transmission electron microscopy (TEM) analysis of rat cardiomyocytes after 2 mg/kg body weight nano-TiO<sub>2</sub> intratracheal instillation once per week for 6 weeks showed NP aggregates in the cytoplasm, along with obliterated myofibrils and swollen mitochondria (Rossi et al. 2019). Concomitantly, inflammatory and collagen deposition markers were elevated in heart tissue (Rossi et al. 2019). Functional impacts measured include increased cardiac excitability, arrhythmias, and blood pressure suggesting that inhaled nano-TiO<sub>2</sub> is internalized by cardiomyocytes and causes functional consequences to the tissue (Kan et al. 2014; Rossi et al. 2019). The evidence together shows direct particle effects on heart tissue function.

Vascular perturbations have been reported after nano-TiO<sub>2</sub> inhalation. While there are no available *in vivo* studies visualizing NP-endothelium interactions after nano-TiO<sub>2</sub> inhalation, an *in vitro* study using a human endothelial cell line shows phagocytosis and perinuclear deposition of the particles (Strobel et al. 2013). Considering an *in vivo* exposure model, endothelial exposure to circulating NPs would be at a lower concentration, but cellular internalization is still possible. *In vivo* inhalation has shown impact on function at the microvascular level, specifically by endothelium dependent and independent mechanisms that could be due to generation of ROS (Abukabda et al. 2017; LeBlanc et al. 2010). Further research on whether the effect on vascular function is due to direct particle interactions or indirect mechanisms of ROS generation are required. Taking this information together, pulmonary exposure to nano-TiO<sub>2</sub> results in impairments to heart and blood vessel function. This could have severe effects for proper blood pressure and tissue perfusion regulation.

*Reproductive and endocrine: ovary, thyroid, and adrenal*

Very little attention has been given to the effects of nano-TiO<sub>2</sub> inhalation on female reproductive organs. Most of the research conducted in this area pertains to the uterine vascular tree. Sprague Dawley rat nano-TiO<sub>2</sub> inhalation led to blunted uterine vasculature reactivity, increased vascular inflammatory markers, and increased leukocyte rolling through the estrous cycle (Stapleton et al. 2017; Stapleton et al. 2015c). In the non-pregnant female, these findings would mean poor uterine blood flow and increased inflammation that could hinder successful implantation and establishment of a pregnancy. More research on female reproductive health is urgently needed to fill the gaps in this area.

To date, there are no available human or animal studies that evaluate inhaled nano-TiO<sub>2</sub> accumulation and effects at endocrine tissues. However, Tassinari et al. focused on short-term (5 consecutive day) oral nano-TiO<sub>2</sub> exposure (0, 1, and 2 mg/kg body weight) in Sprague Dawley rats

and found sex-specific toxicity in response to exposure; females had histological changes of the adrenal and ovary and decreased testosterone levels at both doses, and males had reduced thyroid function and increased testosterone levels at the high dose (Tassinari et al. 2014). Conversely, there is evidence from aquatic models that indicates nano-TiO<sub>2</sub> does not disrupt the production of thyroid hormones or thyroid hormone receptors (Hammond et al. 2013; Miao et al. 2015). The conflicting evidence may be due to species specificities, *in vivo* vs *in vitro* experimental models, and oral vs whole body suspension in water or DMSO exposure routes. Thus, further research on endocrine tissue accumulation and function after nano-TiO<sub>2</sub> inhalation are urgently needed, as endocrine disruption can impact reproductive, metabolic, immune, and central nervous systems.

#### 1.2.3.5 Target Organs and Toxicities During Pregnancy

Pregnancy is a time of rapid, enormous cardiovascular expansion and adaptation to support the development of placental and fetal tissues. Provided the weight of evidence of inhaled nano-TiO<sub>2</sub> distribution and toxicity to secondary tissues, it is reasonable to have similar expectations during pregnancy. In fact, inhaled particle uptake and distribution may be enhanced by pregnancy-induced 50% increase in respiratory tidal volume and 40% increase in cardiac output (Soma-Pillay et al. 2016). To date, only a few studies have examined the toxicokinetics of nano-TiO<sub>2</sub> and detected amounts within the placental barrier and fetal tissues.

After a single intravenous injection of nano-TiO<sub>2</sub> on GD 16 in BALB/c mice, particles could be visualized in the placenta, fetal heart, and fetal brain by TEM analysis (Yamashita et al. 2011). Alternatively, chronic oral administration to pregnant Sprague Dawley rats between GD 6 and GD 19 at 0, 100, 300, and 1000 mg/kg body weight revealed nano-TiO<sub>2</sub> accumulation in the maternal liver and brain and the placenta, but only at the highest dose, found by ICP-MS (Lee et al. 2019). In contrast, female CD-1 mice orally dosed from GD 0 to GD 17 at 0, 25, 50, and 100 mg/kg body weight showed significant increases in maternal serum, placenta, and fetal titanium across all doses,

also detected by ICP-MS (Hong et al. 2017b). Evidently, particle deposition in the placenta and fetus is possible in a pregnancy model. Little to no work has been done to evaluate cellular placental effects after gestational nano-TiO<sub>2</sub> inhalation.

This section provides a summary of the physiochemical properties of nano-TiO<sub>2</sub> and current knowledge of their impact within cells, tissues, and organ systems. Notably, there is a paucity of information regarding the distribution of nano-TiO<sub>2</sub> after inhalation during pregnancy, as well as on the potential effects on the fetoplacental unit. What is consistent however is particle deposition leading to impaired health and function of cells and tissues. Given the placental role of regulating fetal growth and development, impaired function after nano-TiO<sub>2</sub> exposure may be deleterious for the fetus.

### **1.3 Placental Anatomy and Physiological Function**

The placenta is a fetal-derived tissue that invades into the arterioles of the uterine decidua. As a result, maternal blood can enter the placenta from the uterine vasculature. The placenta exchanges nutrient and waste substances, hormones, and cytokines and acts as a physical and biochemical protective barrier between maternal and fetal blood (Burton and Fowden 2015). Therefore, the normal growth and development of a fetus hinges on healthy vascular blood delivery and functioning of the placenta. Additionally, the placenta is the most species-specific tissue (Chavatte-Palmer and Tarrade 2016). Humans and rats have a similar hemochorial placentation type where maternal and fetal blood come in close contact separated by a two or three-layer epithelium, respectively (Furukawa et al. 2011). The following provides an overview of the similarities and differences between human and rat hemochorial placental anatomy and function.

#### **1.3.1 Uteroplacental Vasculature and Blood Flow**

In humans and rodents, a pair of uterine arteries are the main vessels that deliver blood to either side of uterus. Proximally, each uterine artery is an extension of the aorta and distally a branch of the internal iliac artery (Osol and Mandala 2009). Blood flow from the proximal and distal ends converge in the middle of length of the vessel; the bidirectional perfusion redundancy is important to maintain blood flow to the reproductive tissues in the case of uterine artery occlusion (Osol and Moore 2014). The uterine artery branches to form arcuate and then radial vessel networks that span the uterus (**Figure A-1.1**). The smaller radial arteries penetrate the myometrium and divide into straight (basal) arterioles that feed into the uterine endometrial spiral arterioles. Capillaries meet close to the luminal lining of the uterus to then drain and merge back through the uterine layers to eventually return to the heart through the inferior vena cava. The spiral arterioles are invaded by extravillous trophoblasts of the placenta during implantation, which is critical for establishing blood supply to the developing fetus later in pregnancy.

Specific to the rodent is a duplex or dual horn (**FigureA-4.1**). This anatomical shape of the uterus is meant to maximize surface area for the litter-baring species. The uterine artery runs widely spaced along either side of each horn. Where human arcuate arteries lead into the uterus, the rat has arcuate loop networks that bring blood back to the uterine artery to support the length of the horns supporting multiple fetuses, and tertiary radial arteries extend the arcuate loops down into the uterine muscle (Osol and Mandala 2009).

There are multiple factors that orchestrate enhanced uterine blood flow during pregnancy. A coordinated increase in maternal systemic cardiovascular and humoral modifications, increased vascular sensitivity to vasodilation and blunted vasoconstriction, uterine vascular remodeling, and invasion by the placenta occur. In the maternal compartment, the production of estrogen and progesterone by the placenta stimulates water reabsorption to increase blood and erythrocyte volume by the kidneys, and the presence of the placenta adds a low-resistance circuit that stimulates

an increase maternal cardiac output (Longo 1983). Meanwhile, the uterine vasculature undergoes remodeling and changes to reactivity. The uterine artery doubles in circumferential diameter to accommodate for a significant increase in blood volume, from  $\frac{1}{2}$  mL/min to 10 to 30 mL/min (Bullelli et al. 1986). Additionally, it is critical that uterine artery and branching arterioles (i.e., basal, radial, spiral) maintain compliance to meet placental and fetal demand for oxygen and nutrients through vasodilation. Local mediators released from the surrounding tissue or vessel itself also help balance vasodilation and vasoconstriction to meet the local metabolic demand. To enhance dilation, the endothelial cells of the uterine vasculature contribute to regulation of blood pressure and blood flow through the production and release of vasodilators nitric oxide and prostacyclin that then act on the smooth muscle (Sandoo et al. 2010). To achieve vessel dilation and optimal uterine blood flow, there is an increased production in vasodilator signals by the endothelium stimulated by systemic hormones, growth factors, and sheer stress, and in addition there is attenuated responsiveness to vasoconstrictive mediators such as thromboxane, norepinephrine, epinephrine, phenylephrine, and endothelin-1 (Weiner et al. 1989). A proper balance between relaxing and constricting factors during pregnancy is crucial to support blood flow to downstream developing tissues.

The invasion of the spiral arterioles by placental extravillous trophoblasts during implantation establishes uteroplacental blood flow. During the first trimester extravillous trophoblasts rupture and invade retrograde through these arterioles and form an intraluminal plug to permit slow permeation of plasma, but no true blood flow. Towards the second trimester the luminal plugs are converted into circumferential arteriolar stents. These stents hold the vessels open into the intervillous space and establish placental blood flow at low pressure (Browne et al. 2015). It is these cardiovascular adaptations at the systemic and uterine levels that are paramount for establishing normal pregnancy. Thus, any abnormalities could lead to severe downstream consequences to the placenta and developing fetus.

The placenta has a dual vascular circuit and counter-current pressure gradient coming from the maternal and fetal compartments (**Figure A-1.1**). Maternal blood flows through the uterine arteries to fill blood sinusoids of the placenta (labyrinth zone in rodents, intervillous space in humans). Pressure in the uterine arteries is maintained at 80-100 mm Hg, in the spiral arterioles 70 mm Hg, and 10 mm Hg in the blood sinusoids of the placenta (Wang Y and S. 2010). On the fetal side of the placenta, the umbilical artery perfuses the placenta at approximately 50 mm Hg (Damsky and Fisher 1998). Umbilical artery branches into stem arteries and then further into fetal blood capillaries that are near maternal blood bathing the sinusoids. Oxygen and nutrients are transferred to fetal blood in the fetal blood capillaries by diffusion or active transport. These capillaries then converge into the umbilical vein to return the oxygen and nutrient rich blood to the fetus. Because the umbilical vessels are of fetal origin, the terminology of vascular anatomy is like that of the pulmonary system, where the umbilical vein carries nutrient rich blood from the placenta and the umbilical artery returns blood that is nutrient depleted to the placenta. The pressure gradient across utero-placental-fetal blood circulation, along with proper vascular delivery of nutrient rich blood to the placenta, are critical to drive the exchange of nutrients and waste between mother and fetus.

### 1.3.2 Hemochorial Placental Anatomy: a Human-Rat Comparison

The placenta brings blood circulations between mother and developing fetus close together to allow for nutrient-waste exchange while maintaining a certain extent of physical separation. Across mammalian species, distinct anatomical nuances have evolved to determine the extent of the separation between circulatory systems. These differences have been classified into epitheliochorial, endotheliochorial and hemochorial placental types (Furukawa et al. 2014). The hemochorial placental type, possessed by humans, rats, mice, and other non-human primates, has the least separation with only a few cellular layers between maternal and fetal blood. The rodent placenta has five layers that separate maternal and fetal blood; cytotrophoblast, syncytiotrophoblast

I, syncytiotrophoblast II, basal lamina, and fetal endothelium. The human placenta has four layers; syncytiotrophoblast, cytotrophoblast, villous stroma and fetal endothelium. Gases, nutrients, and wastes are exchanged between these layers by passive diffusion, facilitative and active transport, and between cellular fenestrations (Gaccioli and Lager 2016). Compared to the other types of placentation, the hemochorial type has the smallest distance for substances to cross between blood circulations.

The hemochorial placenta can be grossly divided into the maternal (i.e., decidua, metrial gland) and fetal (i.e., trophoblast layer, fetal endothelium) zones (Furukawa et al. 2011). The maturity and thickness of each zone either increases or regresses as pregnancy continues (Furukawa et al. 2019). These zones are functionally similar between the human and rat, however different terminology is used to describe them.

#### *The maternal zone of the placenta*

The maternal zone of the hemochorial placenta includes the metrial glands, decidua basalis, and junctional zone. Metrial glands are present within the pregnant uterus and are comprised of comprised of a dynamic mixture of cell types including uterine natural killer (uNK) cells, decidualized endometrial stromal cells, fibroblasts, invasive trophoblasts, and the spiral arterioles (Picut et al. 2009). The decidua is located a layer beneath and are comprised of decidualized endometrial cells. These form during the reproductive cycle in response to estrogen and progesterone to provide a receptive uterus for blastocyst implantation (Ng et al. 2020). Ultimately these form a thin layer of cells at the surface of the placenta called the decidua basalis. The decidua basalis and metrial gland possess newly formed maternal blood vessels which serve as the anchorage point for placental invasion and the maternal-placental interface (Brosens et al. 1967). The decidua basalis also secretes immune factors, hormones, and molecules which recruit specific

immune cell populations required for placental tolerance, growth, and development (Mori et al. 2016a).

In the rodent placenta, there are three cell types that make up the junctional zone: 1) the spongiotrophoblast cells, which are the major cellular component of the junctional zone serving as a precursor lineage and structural support (Simmons and Cross 2005), 2) trophoblastic giant cells that demarcate the maternal-fetal separation and are the major endocrine contributors to the placenta, secreting prolactin as a systemic hormone/local cytokine to stimulate pregnancy expansion (Soares 2004), and 3) glycogen cells that are specialized trophoblasts that store glycogen and interface with the maternal decidua and spiral arterioles (Tunster et al. 2020). These three cell types make up the rodent junctional zone, wherein structural channels are formed to drain maternal blood into the labyrinth of the placenta.

#### *The fetal zone of the placenta*

The fetal zone of the hemochorial placenta is comprised of the labyrinth zone in the rodent and the functionally similar intervillous space in the human (Furukawa et al. 2011). The fetal zone contains spaces for maternal blood to seep in and contact a syncytium which is a triple layer (rodent) or double layer (human) of trophoblastic epithelium. Trophoblasts are a cell type that form the outer layer of the blastocyst and then a large component of the placenta. The invasive trophoblast lineage invades uterine spiral arterioles to anchor the placenta and access maternal blood circulation. The syncytiotrophoblast lineage forms a continuous layer of specialized cells that encapsulate fetal capillaries and is in direct contact with maternal blood (Soares et al. 2012). A fully mature syncytium is the functional unit of nutrient/waste exchange between mother and fetus (Ji et al. 2013). Additionally, it forms a physical and biochemical barrier that is selective in the transport of biomolecules to the fetal circulation, and it secretes numerous growth factors and hormones to

regulate fetal growth and development (Ji et al. 2013). Under the layers of syncytium lies a basal lamina that separates from the fetal capillary endothelium lining fetal blood capillaries.

### 1.3.3 Placental Physiological Functions

The placenta has three main physiological functions; 1) to provide a physical and biochemical barrier, 2) to produce and secrete hormones, and 3) mediate nutrient/waste exchange between maternal and fetal blood circulations (Griffiths and Campbell 2015). Together, these determine the health of a pregnancy and quality of the intrauterine environment for the developing fetus. This section briefly introduces each of these critical functions.

#### *Physical and biochemical barrier*

The placenta provides protection for the fetus by creating a selective barrier to substances that may be circulating in maternal blood. Physically, several epithelial layers (depending on species) collectively referred to as the syncytium create separation between maternal and fetal blood flowing through the placenta. This barrier is semi-permeable to maternal xenobiotics (Rudge et al. 2009), proteins (Lambot et al. 2006), hormones (Dahlerup et al. 2018), cytokines (Zaretsky et al. 2004), and blood cells (Hunziker et al. 1984). The syncytium is also equipped with enzymes and transporters to permit the metabolism and efflux of xenobiotics back into maternal circulation, performing functions analogous to the liver and limiting fetal exposure (Hemauer et al. 2010). These are the ways by which the placenta forms a physical and chemical barrier of protection to limit harm to the developing fetus.

#### *Endocrine*

A major function of the placenta is to produce and secrete hormones that act as autocrine, paracrine, and endocrine signaling factors to promote the expansion of pregnancy. A major source of hormone production is the syncytiotrophoblast layer, which possesses the enzymes necessary to produce

several hormones including human chorionic gonadotropin (hCG), human placental lactogen (HPL), placental growth hormone, progesterone, estrogens, leptin and resistin (Costa 2016). In rodents, another major source of hormones are the trophoblastic giant cells produce which produce placental lactogen I and II and proliferin (Nadra et al. 2006). The hormonal profile of the placenta changes from early placentation up to labor and delivery.

#### *Nutrient/waste exchange*

The most important function of the placenta is to promote the delivery of nutrients to and remove waste from the fetal blood circulation. Glucose travels from maternal to fetal blood by concentration-dependent kinetics (Hay 1994). Glucose is taken up from maternal blood by apical syncytial membrane GLUT1 and GLUT3 and diffuses to the fetal circulation through basolateral syncytial membrane GLUT1 and, upon insulin stimulation, GLUT4 (Hay 1994). Amino acids and fatty acids are taken up and transferred by specific active transporters (Hay 1994). Oxygen and carbon dioxide translocate by diffusion (Carter 1989). Waste products and carbon dioxide from the fetus are sent back through the umbilical cord and placenta to maternal blood for elimination.

#### **1.4 Placental Glucose Transport**

Glucose is the primary fuel used in cellular respiration under normal conditions (Hay 1991b). Depending on the conditions of the cell it is possible for carbohydrates, fatty acids, and proteins to be fed into the Krebs cycle. Most carbohydrates, including glucose, can enter the Krebs cycle as pyruvate generated from the glycolysis pathway which yields a net of 2 ATP. Fatty acids can be oxidized through beta oxidation in the matrix of the mitochondria and enter the glycolysis as glycerol, or the Krebs cycle as acetyl CoA. The metabolism of fatty acids produces more ATP than glucose, however it is slower and requires a higher rate of oxygen consumption per mole of ATP generated compared to glucose metabolism (Leverve et al. 2007). Amino acids derived from proteins can also enter the Krebs cycle after deamination to generate energy. However, unless the

cell is in a state of starvation or excess protein, it is more energetically favorable to recycle amino acids to build other proteins than to break amino acids down for energy production (Martínez-Reyes and Chandel 2020). Therefore, of the energy substrates, glucose is most rapidly and efficiently metabolized to produce ATP, and is the only nutrient that can produce energy in the form of net 2 ATP in the absence of oxygen (Brosnan 1999).

The syncytium of the placenta is an active cellular layer that requires a large amount of glucose to generate ATP. In the placenta, glucose is acquired from maternal blood as it bathes the apical membrane of the syncytium (**Figure 1.1**). The syncytiotrophoblast utilizes up to 80% of glucose that enters the cell for its own metabolic need with the remainder to be transferred to the fetus (Hay 1991b). Fetal glucose provision is indispensable for fetal growth and development and is therefore important to understand the processes that regulate placental glucose transfer.

#### 1.4.1 Placental Glucose Transport Proteins

Glucose transport proteins are crucial for cell uptake of glucose to sustain aerobic metabolism. Isoforms germane to the human and rodent placenta are GLUT1, GLUT3, and GLUT4 (Furukawa et al. 2019). D-glucose is the primary substrate for these three isoforms. The GLUT family of glucose transporter proteins contain 13 isoforms and are encoded by the SLC2 genes (Holman 2020). The general structure includes 12 transmembrane  $\alpha$  helical domains with the C-terminal and N-Terminal facing intercellularly (Cheeseman and Long 2015). A glutamine residue facing extracellularly has been suggested to be important for glucose substrate selectivity (Mueckler et al. 1994).

GLUT1 and GLUT3 in the placenta are asymmetrically distributed between the microvillous and basal membranes of the syncytium (**Figure 1.1**). GLUT1 is expressed on both microvillous and basal membranes, with relatively higher expression in the microvillous aspect (Furukawa et al.

2019). GLUT3 expression is restricted to the microvillous membrane. GLUT3 has a higher affinity for glucose relative to GLUT1, and it has been shown in human placentas that GLUT3 is upregulated by the syncytiotrophoblast in response to increased glucose requirements (Chang et al. 2021). In human cases of restricted fetal growth, up-regulation of GLUT3 has been documented (Janzen et al. 2013). Studies on the human placenta showed transporters GLUT1 and GLUT3 were upregulated with maternal pulmonary exposures (e.g., cigarette smoking) (Walker et al. 2019). GLUT4 is an insulin-sensitive isoform and can be recruited from the cytoplasm to the basal membrane (James-Allan et al. 2019a).

#### 1.4.2 Glucose Homeostasis During Pregnancy

Pregnancy presents a unique challenge where glucose from the maternal diet must be allocated for maternal and fetal tissues. To achieve this, maternal blood glucose concentrations are maintained at higher levels compared to non-pregnant state by a period of insulin insensitivity (Sonagra et al. 2014). During the first few weeks of pregnancy, placental-derived factors (e.g., human placental lactogen, placental growth factor, placental derived human growth hormone, progesterone, cortisol, and prolactin) interfere with insulin receptor activation in peripheral tissues such as adipose and skeletal muscle (Newbern and Freemark 2011). As a result of insulin insensitivity, post-prandial glucose levels are higher relative to the non-pregnant state to ensure availability for the fetoplacental unit (Butte 2000). This adaptation occurs to accommodate fetoplacental glucose uptake and prevent maternal hypoglycemia (Di Cianni et al. 2003).

To maintain glucose homeostasis, a concentration gradient from higher (i.e., maternal) to low (i.e., fetal) circulations and proper expression and function of placental glucose transport proteins (GLUTs) are required (Illsley and Baumann 2020). Glucose moves across the placental barrier by facilitated diffusion down a concentration gradient from maternal blood, to syncytiotrophoblast cytoplasm, to fetal blood. The transport is facilitated by GLUT isoforms on the microvillous (i.e.,

GLUT1, GLUT3) and basal (i.e., GLUT1, GLUT4) membranes (Illsley and Baumann 2020). Previously, it was thought that the placental syncytium was an indolent barrier without the capacity to sense and respond to the maternal environment. However, there is now evidence that nutritional signals from both sides of the barrier, including maternal nutrient bioavailability and fetal demand, are interpreted by the placenta (Díaz et al. 2014). The placenta is able to respond by adjusting nutrient transport protein expression to maintain appropriate levels of glucose transfer to the fetus (Bell and Ehrhardt 2002). Failure to adjust according to maternal glucose concentrations can result in FGR or fetal macrosomia. Thus, glucose homeostasis during pregnancy largely determines fetal growth outcomes.

#### 1.4.3 Regulation of Placental Glucose Transport

Maternal, fetal, and placental factors regulate the transport of glucose across the placenta. This can be achieved by the up- or down-regulation of GLUT isoforms, predominantly GLUT1 and GLUT3, and in some cases the up-regulation of the insulin sensitive GLUT4. The expression of GLUT isoforms is dependent on the stage of pregnancy, where more placental glucose uptake is required as pregnancy progresses. Maternal endocrine factors such as insulin-like growth factor 1 (Baumann et al. 2002), corticotropin releasing hormone (Gao et al. 2012), glucocorticoids (Hahn et al. 1999), and insulin (James-Allan et al. 2019a) have been shown to activate cognate receptors on the microvillous membrane of the placenta. Additionally, placental oxidative stress (Lappas et al. 2012) and hypoxia (Zamudio et al. 2006) both reduce the expression of GLUT1 in human placentas.

Maternal nutrition greatly influences placental and fetal growth and has been shown to regulate the expression of placental nutrient transporters. There are currently two proposed models to describe fetoplacental response to reduced maternal nutrition: 1) the *placental response model* where the placenta downregulates nutrient transporter expression to match nutrient availability and thus FGR would ensue, and 2) the *fetal demand model* where the fetus sends signals to the placenta to

upregulate nutrient transporters to maintain growth despite limited maternal supply, which is a fetal compensatory response. There is evidence to support both models exist independently and together, although these are dependent on species, and the window and type of nutrient restriction, and sex of the fetus. Maternal nutritional changes may affect placental nutrient and oxygen levels and metabolism, which can be sensed by intracellular regulators such as glycogen synthase, AMK-activated kinase, and mTOR (Jansson et al. 2012).

#### 1.4.4 Placental glycogen storage

Glucose is stored in the form of glycogen, which is a multistranded polysaccharide of glucose. Glycogen is made and stored in cells of the liver, skeletal muscle, and placenta (Adeva-Andany et al. 2016). When energy is needed, glycogen can be rapidly cleaved to liberate individual glucose molecules. Both the human and rodent placentas possess glycogen stores. In the rodent, specialized trophoblasts called glycogen cells are present in the junctional zone where there are histologically apparent as cell masses (Woods et al. 2018). In humans, glycogen is stored in the syncytiotrophoblasts. The function of glycogen storage in the placenta is still up for debate; however, it is theorized that the carbohydrate is stored for the placenta or fetus in case of reduced maternal glucose availability or increased placental need (Hay 2006). The importance of placental glycogen balance is underscored by excessive and depleted amounts correlating with restricted fetal nutrition and growth (Akison et al. 2017).

According to the metabolic demands of the feto-placental unit, glycogen synthase and glycogen phosphorylase coordinate the glycogen synthesis and breakdown, respectively. In times of high fetal glucose demand, such as late pregnancy, glycogen stores are relatively depleted and activity of synthase decreases and phosphorylase increases (Gabbe et al. 1972). This a placental mechanism of ensuring optimal fetal growth just before term and delivery. These enzymes have been shown to respond to the metabolic demands and glycemic state. Gewolb et al. induced gestational diabetes

in a Sprague Dawley rat model and observed the activity of placental synthase to be significantly higher, and phosphorylase significantly lower than controls, on the latter 4 days of gestation (Gewolb et al. 1983). In times of placental stress and dysfunction, induced by cholera toxin, the ratio of enzymatic activity reverses causing a liberation of glucose and depletion of glycogen reserve (Barash and Shafrir 1990). The literature in this area has been primarily devoted to gestational diabetic model, leaving a large knowledge gap around placental glycogen metabolism with xenobiotic exposure.

### **1.5 Placental Energetics and Metabolism**

The placenta is a highly metabolically active tissue performing constant hormone production, absorption of nutrients and expulsion of waste. Of the most energetically demanding functions are the large production of protein hormones (Napso et al. 2018), ATPase-driven transport of substances across the syncytium (Johansson et al. 2003), and continual growth and development (Murray 2012). It has been estimated that 40% of oxygen and as much as 80% of glucose taken up is consumed by the placenta (Carter 2000; Hay 1991b). While free fatty acids and amino acids are important for cellular metabolism, the preferred method of ATP production is by glucose metabolism and oxidative phosphorylation.

In all mammals, placental energy requirements are met predominantly by glucose metabolism and oxidative phosphorylation (Carter 2000) (**Figure 1.2**). Glucose metabolism, or glycolysis, is a series of enzymatic steps that transform a glucose molecule into pyruvate while creating energy in the form of 2 molecules of ATP. This process is regulated in all cells by specific regulatory enzymes in the pathway that are irreversible and rate-limiting. These include Hexokinase (HK) and Phosphofructokinase (PFK) (Zuo et al. 2021). HK is a major rate-limiting enzyme that phosphorylates glucose to glucose-6-phosphate (G-6-P) using ATP as a phosphoryl donor. This is the first reaction of glucose metabolism and effectively traps the glucose molecule in the cell. HK

expression is regulated by the Akt/mTOR nutrient sensing pathway (Roberts and Miyamoto 2015). The activity of HK is negatively regulated by its product, G-6-P (Roberts and Miyamoto 2015). The product of HK, G-6-P can then enter the pentose phosphate, glycogenesis, hexosamine biosynthetic, or glycolysis pathways. The second rate limiting irreversible reaction that commits glucose to glycolysis pathway is carried out by PFK. PFK converts fructose-6-phosphate (F-6-P) to fructose- 1,6-bisphosphate using ATP as a phosphoryl donor. The activity of PFK is regulated according to the cell's energy status; negatively regulated by ATP and citrate, and positively regulated by ADP (Nakajima 1995). Once F-6P is committed to glycolysis by PFK, a cascade of enzymatic reactions uses ATP and nicotinamide adenine dinucleotide (NAD)<sup>+</sup> to yield four ATP (net 2 ATP), two NADH, and two pyruvate molecules.

The product of glycolysis, pyruvate, is the critical output that is then used to provide further energy for the cell. The oxygen availability provided from the bloodstream for the cell determines whether this will occur through aerobic or anaerobic metabolism. Under normal oxygen conditions, pyruvate will enter the Krebs cycle to drive production of 32 to 34 ATP molecules in the mitochondria (Gray et al. 2014). Conditions of low oxygen, such as during hypoxia or ischemia, will stimulate the enzyme LDH to use nicotinamide adenine dinucleotide + H (NADH) as a cofactor to convert pyruvate to lactate and NAD<sup>+</sup> (Gray et al. 2014). As a result of the NADH turnover, NAD<sup>+</sup> can be used as a cofactor again for earlier glycolysis enzymes to support a net of 2 ATP generation through the glycolysis pathway. Therefore, pyruvate and LDH play an important role in cellular energy generation by linking glycolysis with oxidative phosphorylation during varying oxygenation conditions. During early embryo implantation, the initial placental development occurs under low oxygen conditions driven by anaerobic metabolism. Following this, endovascular invasion into the uterine spiral arterioles establishes blood flow and thus oxygenation of the placenta (Thompson et al. 2016). From this point on the placenta extracts oxygen and glucose from maternal blood for oxidative phosphorylation or transfer to the feto-placental unit.

The placenta can shift its metabolic profile in response to challenges presented by the mother or fetus (Vaughan and Fowden 2016). Maternal conditions such as low nutrient availability, extreme temperature or altitude, physical activity and xenobiotic exposure can all affect placental physiology and may necessitate adaptation to sustain pregnancy. The fetus can also signal mismatches between nutrient provision and fetal growth rate and stimulate the placenta to deliver more nutrients to the fetus (Angiolini et al. 2011). Glucose-6-phosphatase, an enzyme responsible for hydrolyzing G-6-P to yield a free glucose molecule, can reverse the HK reaction that keeps glucose molecules trapped within a cell. This enzyme is critical in regulating blood glucose levels, and is expressed predominantly in the liver, kidney cortex, small intestine (van Schaftingen and Gerin 2002). Glucose-6-phosphatase activity has also been identified in the human placenta, fetal liver, and decidual tissue and is thought to be important in balancing consumption by placental glucose metabolizing pathways (Carter and Weber 1966). While it has yet to be studied in the syncytiotrophoblast of the placenta, the HK/glucose-6-phosphatase ratio is likely regulated to increase or decrease delivery of free glucose to the fetal compartment by adding or removing a phosphate group from glucose molecules that enter the syncytial cells. As it has been shown in a diabetic mouse model, this ratio is increased indicating increased glucose utilization in response to hyperglycemia (Belfiore et al. 1989). Additionally, the fetal expression of insulin-like growth factor-1 (IGF-1) and IGF-2 can regulate glucose transfer to the fetus by up-regulating glucose transporter protein (GLUT) expression (Baumann et al. 2014; Fowden 2003). Interestingly, it has been shown that male fetuses undergo an elevated response to the effects of IGF-2 in late pregnancy compared to females (White et al. 2018). This suggests placental cues to contour metabolism and nutrient utilization are dependent on the sex of the fetus.

### 1.5.1 Fetal Sex and Intrauterine Position-Dependent Differences in Placental Metabolism

Fetal sex has been shown to play a role in fetal growth potential. Males are biologically programmed for maximal growth compared with female counterparts, and evidence from human pregnancies shows that this programming starts in utero (Broere-Brown et al. 2016b). In a prospective study in pregnant women, males had significantly larger crown-rump length in the first trimester and head and abdominal circumferences at birth (Broere-Brown et al. 2016a). Further, it has been shown that male fetuses are more likely to have poor outcomes under conditions of growth restriction (Di Renzo et al. 2007; Ingemarsson 2003). Given that the placenta is responsible for nutrient provision, it is possible that sex-dependent differences in growth is a result of differences in placental nutrient transfer.

Intrauterine position has been described as a factor in fetal growth in both human (Gonser et al. 1996; Kalanithi et al. 2007) and animal (McLaurin and Mactutus 2015) studies. In a rat model, it has been shown with radioactive tracer that blood flow between the right and left uterine horns is not equal and favors the right uterine horn (Even et al. 1994). Additionally, this model showed that blood flow is highest at the ovarian and cervical ends and lowest towards the middle (Even et al. 1994). This effect may reasonably lead to position-specific effects on the placenta and its functioning. A position-dependent expression of glucose transport proteins and coenzyme transport and metabolism has been shown in a gilt model, suggesting that implantation position in the uterus influences placental transfer of nutrients to the fetus (Che et al. 2016). However, there has been little attention given to the impact of environmental exposures affecting the fetoplacental unit by intrauterine position. Our laboratory was the first to conduct a study assessing fetal growth by position in response to inhaled nano-TiO<sub>2</sub> in 3 gestational windows (appendix 4), where the findings identify the middle position of the right horn having the most severe reduction after exposure on gestational day (GD) 4 and GD 17 (D'Errico et al. 2021). This finding is in line with the work by Even et al., where they identified that uterine blood flow is lowest in the middle of the horn, and that blood flow to the right horn should be greater than the left under normal conditions (Even et

al. 1994). In our study, placental weight and efficiency in the middle position of the right uterine horn were impacted after GD 17 exposure in this study. To understand the underpinnings of these outcomes, further placental vascular and metabolic assessments as well as NP deposition throughout the reproductive tract are required to explain positional effects on fetal weight given the evidence that intrauterine position may influence fetoplacental growth outcomes.

A placental shift in metabolism, such as an increase in glucose metabolism and oxygen consumption, to support a compensatory response to NP exposure may explain reduced fetal nutrition and growth. In an FGR model put forth by Illsley et al., maternal hypoxia leads to placental metabolic reprogramming, wherein syncytial ATP/protein synthesis is maintained and glucose transfer to the fetus reduces (Illsley et al. 2010a). In this model, cellular metabolism shifts to an increased placental glucose consumption to maintain ATP-driven processes, thereby limiting glucose availability for the fetus (**Figure 1.3**). This placental outcome may also apply to gestational nano-TiO<sub>2</sub> exposure and contribute to reduced placental glucose transfer and fetal growth.

## 1.6 Research Hypothesis and Objectives

Taking all the information presented into consideration, a central hypothesis has been put forth: NP aerosols during pregnancy can travel to the placenta and increase placental metabolism of glucose, thereby decreasing the rate of glucose transfer to the fetus. Sex-dependent and intrauterine position-dependent effects will also be explored. Three specific aims were employed to test the central hypothesis:

Aim 1. Characterize the distribution of nano-TiO<sub>2</sub> in a pregnancy model.

Aim 2. Evaluate maternal and fetal blood glucose concentrations and placental glucose transfer.

Aim 3. Assess placental glucose metabolism and energetic status.

This research ventures into the effects of NPs inhalation on placental metabolism and effects on fetal nutrient provision and growth. These studies are the first to show reduced blood glucose concentrations in the fetus where males are more severely impacted compared to female. Placental glucose transfer to the fetal compartment was significantly reduced after gestational exposure, particularly in males. Sex-dependent changes in placental glucose metabolism were identified in response to exposure. Overall, this work aims to increase our understanding of placental and developmental toxicology, and the occupational, domestic, and environmental hazard of inhaled NPs for pregnancy.

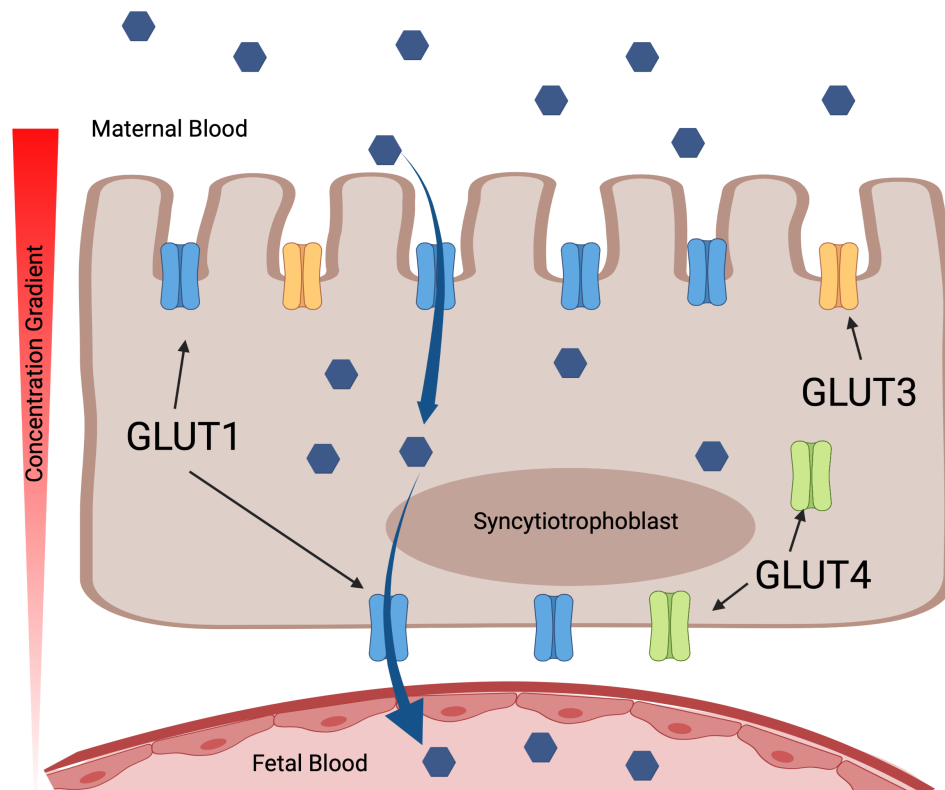


**Figure 1.1. Placental transfer of glucose from the maternal to the fetal circulation.** The syncytiotrophoblast cell type (continuous layer referred to as the syncytium) separates maternal and fetal blood circulations and establishes a high-to-low concentration gradient. Glucose diffuses down its concentration gradient through apical and basolateral glucose transporter protein isoforms. Isoforms GLUT1 and GLUT3 are localized to the apical (maternal-facing) membrane, and GLUT1 and GLUT4 are localized to the basolateral (fetal-facing) membrane.

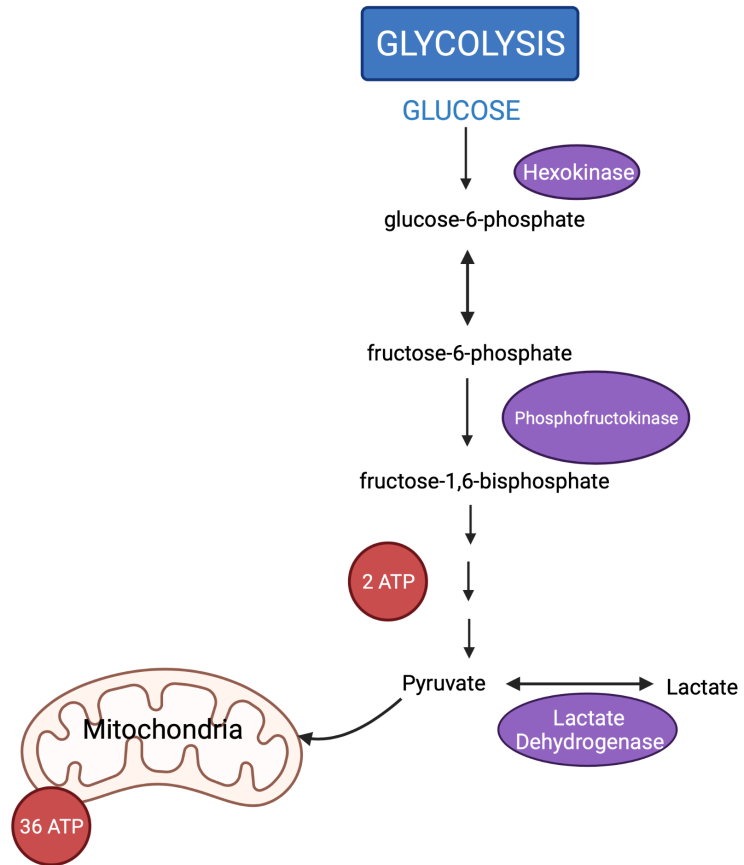


**Figure 1.2. Cellular metabolism.** Cellular energy in the form of ATP is generated by glycolysis (net 2 ATP) conversion of glucose to pyruvate which then enters the mitochondria for oxidative phosphorylation (36 ATP). Image created with BioRender.com.

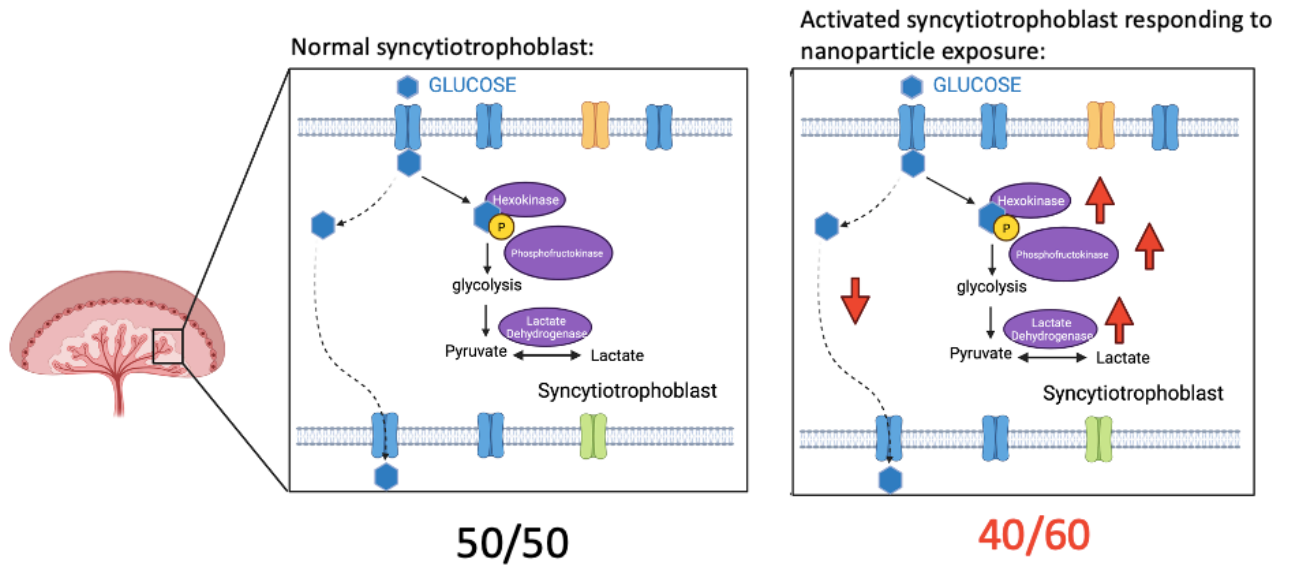


**Figure 1.3. Schematic of normal and activated placental glycolytic activity in response to NP exposure theory.** NP stress response increases the activity of placental glycolytic enzymes and glucose metabolism thereby reducing the concentration of glucose free to diffuse to the fetal circulation.

**CHAPTER 2: Maternal, Placental, and Fetal Distribution of Titanium After Repeated  
Titanium Dioxide Nanoparticle Aerosol Inhalation Through**

Jeanine N D'Errico<sup>a</sup>, Cathleen Doherty<sup>b</sup>, Jarett J Reyes George<sup>a</sup>, Brian Buckley<sup>a,b</sup>, Phoebe A  
Stapleton<sup>a,b</sup>

**Affiliations:**

a. Department of Pharmacology and Toxicology, Ernest Mario School of Pharmacy, Rutgers University, 160 Frelinghuysen Rd., Piscataway, NJ 08854, USA; b. Environmental and Occupational Health Sciences Institute, 170 Frelinghuysen Rd., Piscataway, NJ 08854, USA

## 2.1 Abstract

Epidemiological studies have associated ambient engineered nanomaterials or PM<sub>0.1</sub>, collectively referred to as NPs, with adverse pregnancy outcomes including miscarriage, preterm labor, and FGR. Evidence from non-pregnant models demonstrate that NPs can cross the lung air-blood barrier and circulate systemically. Therefore, inhalation of NPs during pregnancy leading to fetoplacental exposure has garnered attention. The purpose of this study was to evaluate the distribution of inhaled nano-TiO<sub>2</sub> from the maternal lung to maternal, placental, and fetal systemic tissues. Pregnant Sprague Dawley rats were administered whole-body exposure to filtered air or of nano-TiO<sub>2</sub> aerosols ( $9.96 \pm 0.06 \text{ mg/m}^3$ ) between GD 4 and 19. On GD 20 maternal, placental, and fetal tissues were harvested then digested for ICP-MS analysis to measure concentrations of titanium (Ti). TEM was used to visualize particle internalization by the placental syncytium. The results demonstrate the extrapulmonary distribution of Ti to various maternal organs during pregnancy. Our study found Ti accumulation in the decidua/junctional and labyrinth zones of placentas obtained throughout all sections of the uterine horns regardless of fetal sex. Furthermore, NPs deposited in the placenta, identified by TEM, localized intracellularly within nuclear, endoplasmic reticulum, and vesicle organelles. This study characterized the systemic distribution and placental accumulation of Ti after nano-TiO<sub>2</sub> aerosol inhalation in a pregnancy model. These findings raise concerns for poor air quality for pregnant women and potential contributions to adverse pregnancy outcomes.

## 2.2 Introduction

Ambient PM<sub>0.1</sub> are aerosols with diameters of 0.1  $\mu\text{m}$  (100 nm) or less. Due to their small size, PM<sub>0.1</sub>, otherwise recognized as NPs, can cross biological barriers with considerable ease (Bachler et al. 2015; Elder et al. 2006; Fazlollahi et al. 2013). Over recent years, the global increases in aerosolized particulate matter (Cohen et al. 2017), as well as the rapid development of engineered NPs, raises the potential for inhalation and systemic distribution of NPs across the pulmonary air-

blood barrier. Particle translocation from the lungs has been demonstrated in normal healthy humans (Miller et al. 2017; Nemmar et al. 2002) and controlled animal studies (Pujalté et al. 2017; Schleh et al. 2013); therefore, consideration is growing for underrepresented individuals, such as pregnant women and their children, who may be more vulnerable to these exposures. Recent work gives cause for concern over maternal inhalation of ambient NPs during pregnancy and their distribution (Liu et al. 2021). Analysis of human placentas collected at birth suggested that inhaled NPs by the mother can travel through the placenta. Using electron microscopy and energy dispersive X-ray spectroscopy, one study found PM consistent with the morphology, clustering, and chemical construct of  $PM_{0.1}$  from combustion-associated processes on the fetal side of 5 out of 5 placentas after real-world exposure throughout pregnancy (Liu et al. 2021). Additional evidence from pregnant animal studies reveal that lung exposures to nano-polystyrene (Fournier et al. 2020) and engineered nano-silver (Campagnolo et al. 2017b) led to their distribution to the placenta and fetus. Furthermore, pregnancy complications (e.g., miscarriage, FGR) are observed in both human and animal studies which suggests a link between pulmonary NP exposure, systemic distribution, and adverse pregnancy outcomes (Campagnolo et al. 2017b; D'Errico et al. 2021; Fournier et al. 2020). Altogether, the evidence supports that NPs inhaled during pregnancy can disseminate through the body, reach the placenta and fetus, and evoke pregnancy complications.

Characterizing absorption and distribution are critical components to understanding the toxicokinetics of NPs that enters the body. Previous work using a healthy male Sprague Dawley rat model has identified that after nose-only exposure, the highest concentrations NPs accumulate in the lung and a certain fraction are absorbed and distributed to secondary tissues, namely the liver and kidneys (Pujalté et al. 2017). During pregnancy, the drastic physiological changes that occur may alter the absorption and distribution to secondary tissues. For instance, a 30-40% increase in tidal volume, 45% elevation in blood volume, and augmented uterine artery dilation and blood flow occur to shunt more oxygen and nutrition to the uterus and placenta (Soma-Pillay et al. 2016).

However, these physiological changes may also amplify the inhalation fraction of ambient particles and delivery of absorbed particles towards the reproductive tissues. Additionally, blood perfusion through the liver (Nakai et al. 2002) and kidneys (Dunlop 1981) is augmented during pregnancy. Together, these suggest that the maternal liver, kidneys, and reproductive tissues may be key sites of NP distribution and accumulation in a pregnancy model. These are important knowledge gaps on the distribution of inhaled NPs during pregnancy.

The placenta, a transient but critical tissue that embeds into the maternal uterus, may be damaged after NP inhalation exposure during pregnancy. Copious amounts of maternal blood circulate through the placenta and bathe a syncytium that is 2 or 3 layers thick in a human or rodent, respectively. The syncytiotrophoblast is the most important cell type of the placenta forming a syncytium and performing the critical functions of 1) fetal barrier protection, 2) expression of plasma membrane receptors that regulate protein synthesis, 3) production and secretion of peptide hormones (e.g., human chorionic gonadotropin), and 4) transport of substances across to the fetal blood circulation. Chemicals or pollutants such as NPs within maternal blood can directly encounter the syncytium. *In vitro* experiments have shown primary human syncytial cells to internalize and accumulate metallic NPs (Aengenheister et al. 2019). Once internalized, NPs mainly distribute to lysosomal vesicles while some remain freely suspended in cytoplasm (Zhang et al. 2018b). Other intracellular consequences include NP-protein aggregation, increased endoplasmic reticulum stress, mitophagy and increased intracellular ROS (Zhang et al. 2018b). Cellular damage to the placenta may cause serious organ dysfunction. NP-mediated decreases in uterine invasion (Zhong et al. 2020) and increases in uterine vascular resistance (Abukabda et al. 2019) have been empirically shown to lead to poor placental perfusion. Additional studies have shown decreased placental growth after NP inhalation in rats (Bowdrige et al. 2019), barrier integrity after NP ingestion in mice (Teng et al. 2020), and hormone secretion after NP incubation with primary human placental trophoblast cells (Nedder et al. 2020). Increased inflammatory cytokine secretion

(Campagnolo et al. 2017b) and trophoblast shedding (Teng et al. 2020) from NP exposure have also been found, all of which can result in attenuated barrier and nutrient provision for the fetus. While these findings are critical to the field, there are inherent limitations. Studies utilize *in vitro* or *ex vivo* models may apply NP doses significantly higher than physiological transport would permit of NP to elicit effects. Those employing short and direct lung instillation exposure schemes (e.g., single or acute exposure timelines and direct intratracheal instillation) often make for difficult extrapolation to the human population who often experience chronic and repeated exposure to ambient NPs. Therefore, it is critical to utilize a recurring whole-body exposure scheme throughout pregnancy to evaluate whether inhaled ambient NP aerosols translocate from the lung to the placenta and are internalized within the syncytium.

Fetal sex plays a major role in the outcomes of placental mediation of maternal stress (Wainstock et al. 2015), uptake of xenobiotics (D'Errico et al. 2021), and likelihood of developing gestational disorders such as preterm birth (Challis et al. 2013). A sex-dependent placental accumulation of various metals has been found in humans, where placentas from male fetuses accumulated higher concentrations of soluble silver (Ag) and titanium (Ti) compared to those from females (Li et al. 2019). The sexual dimorphisms in responses to maternal stress are likely due to sex-specific regulatory pathways of the placenta contributed from X- and Y- linked genes and sex-dependent epigenetic machinery. For example, it has been shown that maternal high fat diet during pregnancy can lead to sex-dependent changes the methylation on 9 out of 20 imprinted genes in mouse placenta (Gabory et al. 2012). Another emerging and potentially significant contributor to pregnancy outcomes includes intrauterine positioning of the placenta and fetus (D'Errico et al. 2021; Zia 2013). Differences were identified in fetal weight between uterine horns and specific horn locations after maternal nano-TiO<sub>2</sub> inhalation in a Sprague Dawley rat model (D'Errico et al. 2021). Therefore, these factors likely play a role in placental uptake of NPs.

Here a whole-body inhalation exposure to NP aerosols throughout gestation is employed to simulate environmental or occupational workplace exposures as previously identified (Stapleton et al. 2013b). To achieve this, titanium dioxide NPs (nano-TiO<sub>2</sub>), a widely used engineered nanomaterial and common surrogate for PM<sub>0.1</sub> exposures, was leveraged. The hypothesis of this study is that Ti will be quantified in all secondary maternal, utero-placental, and fetal tissues and NPs will be visualized in the syncytium after gestational nano-TiO<sub>2</sub> aerosol inhalation. Furthermore, fetal sex- or intrauterine position- specific Ti accumulation was expected. Our aims were to 1) describe the Ti distribution from the pulmonary space to maternal, placental, and fetal tissues, 2) measure Ti accumulation on the maternal and fetal sides of the placenta by sex and intrauterine position, and 3) visualize intracellular localization of NP within placental syncytium.

## **2.3 Materials and Methods**

### *Nanoparticle characterization*

Nano-TiO<sub>2</sub> powder was purchased from Evonik (Aeroxide TiO<sub>2</sub>, Parsippany, NJ). Using dynamic light scattering (DLS) techniques with a Zetasizer Nano ZS by Malvern, the crystalline composition of the powder was previously determined to be composed of 80% anatase and 20% rutile, primary particle size  $21 \pm 6.1$  nm and surface area 48.08 mg<sup>2</sup>/g (Fournier et al. 2019a).

### *Animal model*

Time pregnant Sprague Dawley rats were purchased from Charles River Laboratories (Kingston, NY) on GD 1 or 2 and housed in the Rutgers School of Public Health vivarium on GD 2 or GD 3. Animals were single housed and had *ad libitum* access to food (Purina 508 Rodent Chow) and water and were given a 24–48-hour acclimation period prior to first handling. All procedures were approved by the Institutional Animal Care and Use Committee of Rutgers University.

### *Whole-body nanoparticle exposure*

Between GD 4 and GD 19 animals were administered whole-body exposure to HEPA filtered air or nano-TiO<sub>2</sub> aerosols in our custom rodent inhalation facility (IESt techno, Morgantown, WV) (Fournier et al. 2019b). Both the HEPA filtered air control group and nano-TiO<sub>2</sub> group had a sample size of 6 dams. Animal exposures occurred for 4 hours/day 5 days/week with a total of 12 exposure days during gestation. The size distribution and concentration of the particles were monitored in real-time by a scanning mobility particle sizer (SMPS, TSI, Shoreview, MN) and a particle counter (General Purpose Water-based Condensation Particle Counter, TSI, Shoreview, MN), respectively. Animals were exposed to an ambient particle concentration of  $9.96 \pm 0.06 \text{ mg/m}^3$  within the chamber (**Figure 1**). The average aerosolized NP agglomerate size was determined to be  $175.91 \pm 3.35 \text{ nm}$ . The concentration of the particle aerosols was confirmed via gravimetric sample collection on a 47-nm PTFE membrane filter and an XP2U microbalance (Mettler Toledo, Switzerland) (Yi et al. 2013). For each individual animal the total lung deposition was calculated using a method previously described (Stapleton et al. 2015c) with the following equation:  $D = F * V * C * T$ , where F is the deposition fraction (10%), V is the minute ventilation based on dam body weight (g), C equals the steady state mass concentration ( $\text{mg/m}^3$ ), and T equals the exposure duration (minutes). The average sum of lung burdens for each exposure day considering clearance equated to  $194.81 \pm 1.89$  (**Table 1**).

#### *Tissue collection*

At approximately 9:45 AM on GD 20 animals were placed under anesthesia with 5% induction and 3% maintenance doses of isoflurane gas. The uterine horns were removed, and animals were humanely euthanized according to IACUC approved protocols. During this step maternal whole blood was collected from the thoracic cavity after heart removal. The right and left uterine horns were further dissected to harvest right and left ovarian and uterine samples. Placentas at the ovary, middle, and cervical sections of the right and left uterine horns were quartered. One quarter of each placenta was further dissected to separate the maternal (decidua/junctional zone) and fetal

(labyrinth) zones. Umbilical cord, liver, heart, and whole blood were collected from fetuses in the middle position of each uterine horn. Fetal sex was recorded by testes or uterine horn visualization. Maternal tissues that were sampled for collection were the lungs (caudal lobe), thoracic aorta, apex of the heart, liver, kidney cortex, spleen, and pancreas. Tissue samples were subsectioned to <0.2 g and were snap frozen in liquid nitrogen and stored at -80 °C until further processing.

#### *Inductively Coupled Plasma Mass Spectrometry (ICP-MS)*

Ti concentrations in tissue and blood samples were quantified using ICP-MS analysis. Tissue and blood samples were snap frozen in liquid nitrogen and later transferred to Teflon vials (Savillex). To each sample weighing over 0.15 g, 1 mL of concentrated HNO<sub>3</sub> was added. Samples weighing below 0.15 g received 0.5 mL of concentrated HNO<sub>3</sub>. Samples were then sonicated for 1 hour and subsequently set on a hot plate (110-130 °C) for at least 6 hours. Once tissues were visibly dissolved, samples were cooled completely and vented by loosening the Teflon vial cap. Uncapped samples were placed on a hotplate encased in polypropylene drying box to prevent contamination, to evaporate until about 95% of the acid had vaporized. Samples were then further digested with 1 mL of 8 N HNO<sub>3</sub> and 20 µL of HF and heated (120 °C) on the hotplate for 3 hours, to ensure TiO<sub>2</sub> was dissolved. For dilution and transfer, condensate was collected with the rest of the sample by rolling the liquid along Teflon vial walls and pouring the total sample into metal-free polypropylene centrifuge tubes. Samples were diluted with MilliQ water to produce an acid concentration of 5% HNO<sub>3</sub> and 0.1% HF ready for ICP-MS analysis.

Ti concentrations in digested samples were quantified using a Nu AttoM high resolution ICP-MS, at medium resolution (3000) to remove interferences. The operating conditions were as follows: RF power of 1524 W, carrier gas flow of 1.00 L/min Ar, and nebulizer gas flow of ~36 psi Ar. Three replicates of masses <sup>47</sup>Ti and <sup>49</sup>Ti were measured in deflector scan mode with 100 ms peak

dwell time, 100 sweeps/cycle, and averaged (RSD <5%). Calibration standards were prepared daily with Ti concentrations ranging from 0.01 – 10 ppb, in 5% HNO<sub>3</sub>, with an instrument detection limit <0.10 ppb Ti, and a method detection limit of 10 ppb. Sample concentrations were extrapolated using a linear regression through at least five standards, with a correlation coefficient > 0.999 for all runs. Procedural blanks were prepared with each batch of samples following the same protocol, with average blank contribution of 0.29 ppb. Final concentrations were blank corrected by subtracting the average blank concentration, corrected for dilution volume of the sample. Quality control standard (PAS-28) were repeatedly measured after every sixth sample to account for instrument drift and monitor reproducibility and reproduced with RSD <5% (n=24).

#### *Transmission Electron Microscopy (TEM) Imaging*

Placental units (uterine artery segment, entire arcuate and radial network connecting to the uterine myometrium and placenta, and umbilical cord) were harvested at necropsy from the middle section of the right uterine horn. The placentas were rinsed and then submerged in cold (4 °C) phosphate buffered saline and cannulated by the uterine and umbilical artery with steel blunt tip needles. A physiological saline solution (130 mM NaCl, 4.7 mM KCl, 1.18 mM KH<sub>2</sub>PO<sub>4</sub>, 1.17 mM MgSO<sub>4</sub> 7H<sub>2</sub>O, 1.6 mM CaCl<sub>2</sub>, 14.9 mM NaHCO<sub>3</sub>, 0.026 mM EDTA, and 5.5 mM glucose) was used to flush tissue of blood for 20 minutes or until tissue appeared devoid of blood at 80 µL/min using 50 mL syringe perfusion pump. The tissue was then perfused with a 2.5% glutaraldehyde, 4% paraformaldehyde fixative solution at 80 µL/min for 20 minutes. After fixation the uterine muscle was peeled away, and a 1 mm punch biopsy tool was used to sample from the center of the placenta. The biopsy samples spanned from the decidua, through the junctional and labyrinth zones and ended at the chorionic plate. The biopsied tissue was immediately drop fixed into a glass vial containing 4 mL of 2.5% glutaraldehyde and 4% paraformaldehyde fixative solution and stored at 20°C until further processing. Samples were subsequently dehydrated in a graded series of acetone

and embedded in Embed812 resin. Sections 90 nm thin were cut on a Leica UC6 ultramicrotome and stained with saturated solution of uranyl acetate and lead citrate. Images were captured with an AMT (Advanced Microscopy Techniques) XR111 digital camera at 80Kv on a Philips CM12 transmission electron microscope.

#### *Data presentation and statistics*

All organ data except for placenta are presented as one tissue per dam. For placenta, data are presented as a per dam average of 3 placentas from the right uterine horn and 3 placentas from the left uterine horn. Because not all ICP-MS data were normally distributed, a rule was set forth where values that were one or more order of magnitude above the mean for that tissue group were considered technical outliers and removed. To determine the appropriate statistical test for comparison between exposure groups for each tissue type a Shapiro-Wilk normality test was performed. This test assesses whether a data set is well-represented by a normal Gaussian distribution, and that there is an equal probability of each value to fall above or below the mean value of the data set. Data where both groups passed the normality test ( $p > 0.05$ ) were assessed by Student's t-test. Data where at least one group did not pass the normality test ( $p < 0.5$ ) were assessed by Mann-Whitney U test. Alpha was set to 0.05 for both tests. Right and left sides of the reproductive tract are presented and analyzed by Two-way ANOVA with Sidak's multiple comparisons test. Data are displayed as mean  $\pm$  standard error of the mean (SEM). Samples that were below detectable limits were replaced by numerical values of the instrument's limit of detection. Statistics were conducted and graphs created using GraphPad Prism 8 (Version 8.4.3).

## **2.4 Results**

### *Maternal lung deposition of NPs*

The total, daily, and additive lung deposition of NPs were calculated for each experimental group (**Table 2.1**). After considering daily deposition and clearance from repeated exposures, the total lung deposition for the nano-TiO<sub>2</sub> group was calculated to be  $194.81 \pm 1.89$  ug.

*Distribution of Ti to maternal, placental, and fetal tissues*

The distribution of Ti was quantified in both exposed and control tissues (**Table 2.2 and Figure 2.2**). The Ti quantified in maternal lung tissue was  $232404.8 \pm 18223.3$  ppb indicating successful pulmonary exposure utilizing the whole-body aerosol chamber (**Figure 2.2a**). The right and left uterine horns from nano-TiO<sub>2</sub> exposed dams had significantly more Ti detected compared to the filtered air control dams (**Figure 2.2b**). The right ovary also accumulated significantly more Ti after nano-TiO<sub>2</sub> inhalation exposure (**Figure 2.2b**). Regarding fetal tissues, the right umbilical cord and left fetal heart had significant Ti accumulation in the nano-TiO<sub>2</sub> exposed group (**Figure 2.2c**).

Comparisons were made between ovaries, uterine tissue, placenta decidua and placenta labyrinth of the right and left reproductive tract for the filtered air group and nano-TiO<sub>2</sub> exposed group (**Figure 2.3**). No significant differences were found between the right or left side for any tissue in either exposure group.

Background Ti concentrations in the control group are consistent with previous literature evaluating nano-TiO<sub>2</sub> biodistribution (Lee et al. 2019; Pujalté et al. 2017). Upon further investigation, it was found the maternal rodent diet was likely to be a source of Ti. A set of 3 Purina chow pellets were subjected to the same sample digestion protocol and using ICP-MS an average of  $12,606.0 \pm 6,359.5$  ppb of Ti was measured. Therefore, all animals were also exposed to Ti through ingestion.

Maternal, uteroplacental, and fetal organs were ranked by expected relative distribution in a pregnancy model based on previous work in a non-pregnant model (Pujalté et al. 2017) and

considering the physiological changes during pregnancy (Soma-Pillay et al. 2016). The relative quantification of Ti between exposure groups is presented in **Table 2.3**. These values are presented as a percent of total ppb. Furthermore, the distribution percentage to tissues outside of the lung in rank order (highest to lowest) after inhalation exposure are presented (**Figure 2.4**). Maternal and fetal hearts accounted for over 30% of Ti translocation in controls, whereas most of the Ti (i.e., 19.24%) was identified in the maternal liver after gestational inhalation of nano-TiO<sub>2</sub> aerosols.

#### *Distribution of Ti by placental zone, uterine position, and fetal sex*

Ti concentrations were analyzed by uterine and placental anatomical position as well as by fetal sex (**Figure 2.5**). In exposed animals there was on average  $40.6 \pm 7.2$  ppb measured on the maternal side (decidua/junctional zone) of the placenta and  $36.3 \pm 11.1$  ppb quantified on the fetal side (labyrinth) indicating no preferential zone for Ti accumulation (**Figure 2.4A**). Similarly, there was no difference in the Ti amount detected in the either maternal or fetal placental zone for the filtered air group with an average of  $37.4 \pm 8.1$  ppb and  $29.7 \pm 7.0$  ppb, respectively. There was also no overall difference in the amount of Ti detected on the right vs. left uterine horn, however the highest location of accumulation for the left horn was the cervical position and for the right horn was the ovary position (**Figure 2.4B**). In contrast, the filtered air group showed more Ti detection on the left uterine horn compared to the right. Regarding fetal sex in both the filtered air and nano-TiO<sub>2</sub> exposed group, more Ti was measured in the maternal zone for the males and in the fetal zone for the females (**Figure 2.4C**).

#### *Intracellular localization of nanoparticles*

NP agglomerates were visualized in 0 out of 4 filtered air placentas and 4 out of 4 nano-TiO<sub>2</sub> exposed placentas (**Figure 2.6**). 3,000x magnification demonstrates NP agglomerates within the syncytium inside of the nucleus, rough endoplasmic reticulum, and intracellular vesicles (**Figure 2.6A, 2.6B**). 3,800x shows microvilli extending into maternal sinus and presence of NP

agglomerates within the cell in nano-TiO<sub>2</sub> exposed dams. Agglomerates are embedded in rough endoplasmic reticulum and vesicles near the plasma membrane surface (**Figure 2.6C, 2.6D**). 10,000x magnification shows high magnification of space between cells and that NP agglomerates are present within confines of cell membrane from exposed placentas and are near rough endoplasmic reticulum and plasma membrane vesicles (**Figure 2.6E, 2.6F**).

## 2.5 Discussion

This study aimed to examine the systemic distribution of inhaled NP aerosols during pregnancy utilizing nano-TiO<sub>2</sub> as a model particle. There was a particular emphasis on the placenta, as this is the protective barrier for the fetus and previous work in mice and rats has found links between inhalation exposure and perturbations to pregnancy health (e.g., miscarriage, FGR) (Campagnolo et al. 2017b; Fournier et al. 2020). Evidence in support of inhaled Ti translocation to secondary maternal organs, the placenta, and fetal tissues was identified. Further, there was accumulation in both the decidua/junctional zone and labyrinth zone of the placenta and at each intrauterine position. Accumulation did not differ based on fetal sex.

This study verified the translocation of nano-TiO<sub>2</sub> from the lungs to extrapulmonary maternal tissues. These results support previous findings that inhaled NP using nano-TiO<sub>2</sub> as a model particle translocate and deposit in tissues secondary from the lung. Pujalté et al. found detectable Ti in the blood, lymph nodes, liver, kidneys, and spleen in male Sprague Dawley rats within 3 hours after a single inhalation exposure of 20 nm nano-TiO<sub>2</sub> (Pujalté et al. 2017). In another study using a male rat model, Ti persisted in the liver and spleen up to 180 days after exposure cessation (Gaté et al. 2017). While our study did not include a time course or recovery period component, it contributes to the body of evidence that inhaled NP aerosols exit the lung and embed in other organs. Tuswbbhis study provided a more traditional toxicological evaluation by identifying organs of distribution in a pregnancy model after inhalation exposure. Using this data, the percent deposition of Ti within

the maternal lung and extrapulmonary tissues was calculated (**Table 2.3**). This information may inform future study determination of the appropriate *in vitro* dosing based on percent of material translocated after pulmonary inhalation exposure.

Our samples derived from control filtered air exposures had detectable Ti. This allows for the differential analysis of Ti deposition after oral or pulmonary exposure (**Figure 2.4**). In the control (ingestion only) group, higher accumulation of Ti was identified in the maternal and fetal heart tissue, followed by the fetal whole blood, umbilical cord, placenta decidua, and placenta labyrinth. For the nano-TiO<sub>2</sub> exposed group the secondary sites of highest accumulated Ti were the maternal liver, fetal whole blood, and fetal heart (**Figure 2.4**). These outcomes indicate important sites of Ti distribution and accumulation with different exposure routes. Importantly, fetal whole blood and fetal hearts accumulate relatively high concentrations of Ti in both scenarios, implying the fetal circulation filters out maternal xenobiotics. Future investigations should further examine inhalation and ingestion NP administration and compare the distribution profiles. Alternatively, future studies may obtain Ti-free animal feed to remove any background contribution of elemental Ti for analysis.

During pregnancy the placenta typically acts to function as a protective barrier to prevent harmful substance(s) transfer to the fetus. Previous rodent studies have also detected nano-TiO<sub>2</sub> within placental and fetal tissue (Hong et al. 2017a; Lee et al. 2019; Yamashita et al. 2011); however, these were identified after oral or intravenous exposure only. In a mouse model, silver NPs (e.g., 18-20 nm) have been identified within dam organs, placentas, and fetuses via TEM imaging coupled with single particle ICP-MS after repeated nose-only exposure to nano-silver aerosols (Campagnolo et al. 2017a). Fetal loss, reduced blood estrogen levels, and placental inflammation were also detected in these dams after exposure (Campagnolo et al. 2017a). Using optical imaging and dark-field microscopy, our laboratory recently identified the deposition and transfer of nanosized polystyrene particles within maternal, placental, and fetal tissues after maternal

pulmonary exposure in late pregnancy using a Sprague Dawley rat model (Fournier et al. 2020). Previous studies in rats have also utilized fluorescently-labeled NP deposition by placental zone and found partial deposition in the chorionic plate, but not with consideration for other variables such as implantation in different uterine locations or fetal sex (Ho et al. 2017).

In this study, we found evidence of Ti deposition (ICP-MS) and particulate deposition (TEM) in the placenta. However, when considering these results together there is discord due to the Ti contamination in the ICP-MS results. More specifically, Ti measurements from labyrinth zone tissue obtained from all placentas (**Table 2.2**), placentas from the right uterine horn (**Figure 2.2B**), and placentas from the middle of the right uterine horn (**Figure 2.5B**) had similar concentrations of Ti (ppb) in both exposure groups. Whereas the TEM analysis, which was conducted on labyrinth from placentas harvested from the middle of the right uterine horn, identified particulate in nano-TiO<sub>2</sub> exposed placentas only. It is difficult to reconcile this information together, as if both groups were exposed to Ti through the diet, but the nano-TiO<sub>2</sub> exposed group had the additional Ti exposure through inhalation, it would be expected that the ICP-MS data would measure Ti in both groups but with higher concentrations in the nano-TiO<sub>2</sub> exposed group. However, this is not what we observed. There are a few possible explanations for the inconsistencies between the ICP-MS and TEM results. First, all animals had the same ad libitum access to the rodent chow, however it is possible that the chow did not have consistent pellet-to-pellet or batch-to-batch levels of Ti resulting in each animal consuming variable amounts. Additionally, food consumption for individual animals was not recorded in this study, but it is possible that decreased food consumption occurred for animals in the nano-TiO<sub>2</sub> exposure group. This would bring control Ti values closer to exposed values in the ICP-MS data, but the Ti would not be visualized with TEM in control placentas if present as a soluble element. Second, there could have been events during sample collection or processing that led to inadvertent additional contamination of control samples from dissection tools, laboratory equipment and surfaces, or laboratory air. Third, the discrepancy

between ICP-MS and TEM data could be due to the section of the placenta that the tissue sample originated from. From the same placenta, ICP-MS tissue was dissected from an outer quarter of the which was then further dissected to separate decidua from labyrinth zone, and TEM samples were taken as punch biopsies from the center. It is possible that Ti deposition is more variable around the outer edges of the placental disc, and that ICP-MS sampling would have been better performed from the center of the placenta consistent with the TEM sampling. To help resolve these disparities, further studies can use a chow diet that is confirmed to be free of Ti to help minimize the oral source of Ti. Separate dissection tools and surgical areas for control and exposed tissues can be maintained to help minimize any lab contamination. The region of placental sampling should be consistent as possible for quantitative (ICP-MS) and qualitative (TEM) analyses. Additionally, applying Scanning electron microscopy with energy dispersive X-ray spectroscopy (SEM-EDX) on Raman spectroscopy placentas of both exposure groups can help identify the elemental composition of the particles *in situ*, and if there is Ti present in filtered air placentas that are not visualized with microscopy. Despite the incongruity in the data, there is support that the placenta is an imperfect barrier and may be permeated by elemental Ti and nanosized xenobiotic particles.

There is strong evidence to suggest that adverse placental outcomes affecting pregnancy can be influenced by intrauterine positioning (Zia 2013) and fetal sex (Rosenfeld 2015). Our previous work in a Sprague Dawley rat model investigated maternal nano-TiO<sub>2</sub> inhalation and FGR and found differences in fetal weight reduction on GD 20 depending on uterine horn (i.e. right vs. left), position within that horn (i.e. ovary end, middle, or cervical end), and timing of maternal exposure (D'Errico et al. 2021). In this study, there were no significant differences in amount of Ti deposition per intrauterine position after a repeat exposure duration during pregnancy. Further work may investigate NP deposition after the varying exposure timepoints of early, mid-, and late gestation. Fetal sex was assessed in this study due to the role it plays in nutrient uptake by the placenta. It has been theorized in humans that male fetuses exert higher demand for nutrient uptake from the mother

for maximal growth and thus receive more blood flow (Alur 2019a). Increased perfusion to male fetuses may result in larger particle deposition. Our findings revealed no significant difference in decidua/junctional zone Ti accumulation. Together, these results show accumulation of Ti regardless of intrauterine location, placental zone, or fetal sex after maternal repeated inhalation exposure.

Placental NP uptake can lead to transport to the fetus. Evidence from rat *in vivo* (Fournier et al. 2020), *in vitro* (Aengenheister et al. 2018a), and *ex vivo* (D'Errico et al. 2019; D'Errico et al. 2019a; Fournier et al. 2020) studies conclude that NPs can access the fetal compartment (Bongaerts et al. 2020). Our laboratory confirmed that nanopolystyrene beads instilled in the rat lung translocate to the placenta and fetus 24 hours after maternal exposure (Fournier et al. 2020). Furthermore, we demonstrated that this was due to placental transfer by monitoring NP transfer from maternal uterine artery injection to the fetal effluent in *ex vivo* placental perfusion (Fournier et al. 2020). Another used an *in vitro* co-culture model of the placental barrier and *ex vivo* placental perfusion to measure gold nanoparticle uptake and transfer to the fetal compartment (Aengenheister et al. 2018a). After placental translocation of NPs, TEM revealed that fetal hepatocytes and neurons can endocytose silica and TiO<sub>2</sub> NPs, which can then localize to nuclei and rough endoplasmic reticulum (Yamashita et al. 2011). In addition, numerous ramifications for progeny neurodevelopment (Engler-Chiurazzi et al. 2016; Umezawa et al. 2012), cardiovascular (Fournier et al. 2021; Hathaway et al. 2017; Stapleton et al. 2015e), immune (El-Sayed et al. 2015), and reproductive (Yoshida et al. 2010) functions, and overall genetic profiles (Stapleton et al. 2018b) have been documented after *in utero* NP exposures in rodent models (Hougaard et al. 2015a). Our study supports that inhaled Ti can access the fetal compartment. Furthermore, this study offers a unique perspective in specific locations of accumulation that highlight areas of potential fetal toxicity and vulnerability. The umbilical cord, the conduit carrying fetal blood to and from the placenta, had detectable Ti suggesting it may be transported to fetal blood by the placenta. In addition, the current

study demonstrated fetal liver and heart accumulation after maternal pulmonary exposure. Interestingly, the fetal tissue with highest accumulation of Ti was whole blood, further demonstrating transplacental transfer to the fetal circulation. This result suggests that Ti circulates around the developing fetal tissues, but it is not known whether these particles are free or protein-bound before eventually depositing within tissue. Overall, fetotoxicity and long-term progeny health outcomes may be due to *in utero* exposure, direct NP translocation to the fetal compartment, local inflammation, and reactive stressors (e.g., oxygen, nitrogen), and possible cellular internalization by the feto-placental tissues.

There are some limitations to our experimental design for this study. First, the exposure period spanned from pre-implantation (GD 4) up to 24-48 hours prior to delivery (GD 19) and did not include sub-groups of animals to gather time course data of NP distribution and accumulation. Future studies may include this analysis to provide snapshots at each trimester. While this was not within the scope of the current study, it may provide useful for understanding changes in NP distribution during gestation. Additionally, the ingestion exposure to Ti is an unintended confounding factor for the Ti measurements in the nano-TiO<sub>2</sub> exposed group. ICP-MS is unable to differentiate between elemental Ti and Ti NPs after the digestion protocol. Therefore, it is unknown whether the Ti measured from the tissues and rodent diet were in NP or metal element contaminant form (Kim et al. 2018).

Overall, this study evaluated the systemic distribution of Ti after NP aerosol inhalation in a pregnancy model. The results from this study infer that secondary tissues, including the placenta and fetus, are vulnerable to these types of exposures that may occur from environmental particulate matter air pollution, or occupational and domestic exposure to engineered NPs. Given the many critical roles the placenta plays during pregnancy to guard fetal development, further research to

investigate how placental NP aerosol exposure and deposition may impact placental function are warranted.

## FIGURES:

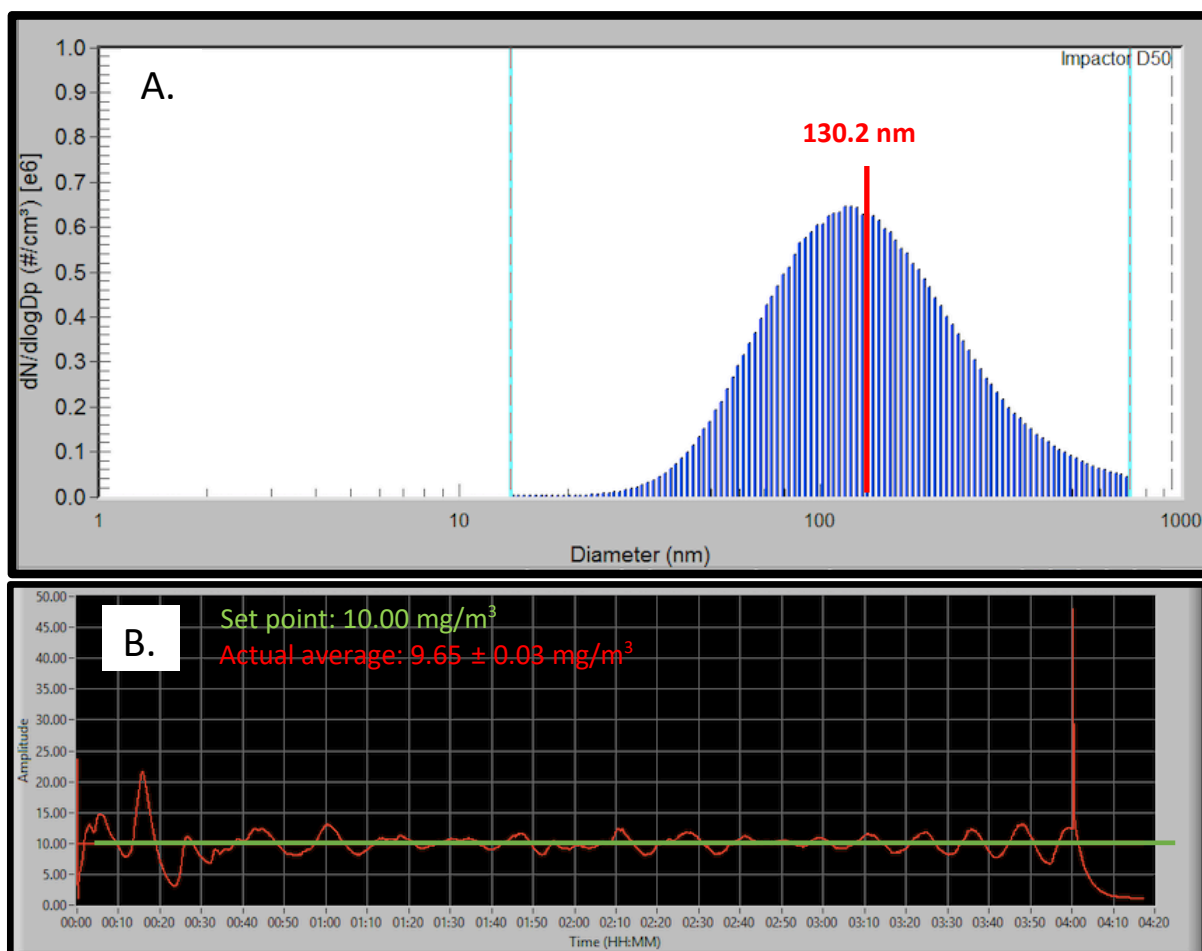


**Figure 2.1. Representations of nanoparticle aerosol characteristics during whole-body animal exposure taken on a single exposure day (4.20.21).** A. A representative histogram of the particle size distribution measured within the chamber in real-time by a Scanning Mobility Particle Sizer (SMPS). The SMPS determined the median aerosolized particle diameter to be 130.2 nm for this sample of chamber air. B. Real-time nanoparticle concentration monitoring within the exposure chamber over the span of a 4-hour nano-TiO<sub>2</sub> exposure. The overall average chamber particle concentration for this exposure was 9.65  $\pm$  0.03  $mg/m^3$  and the peak amplitude was 48.01  $mg/m^3$ .

Treatment Group	n	Total Deposition (μg)	Daily Deposition Considering Clearance (μg)	Additive Daily Deposition Considering Clearance (μg)
Filtered Air Control	6	0	0	0
Nano-TiO <sub>2</sub> Exposed	6	608.79 ± 5.90	16.23 ± 0.16	194.81 ± 1.89

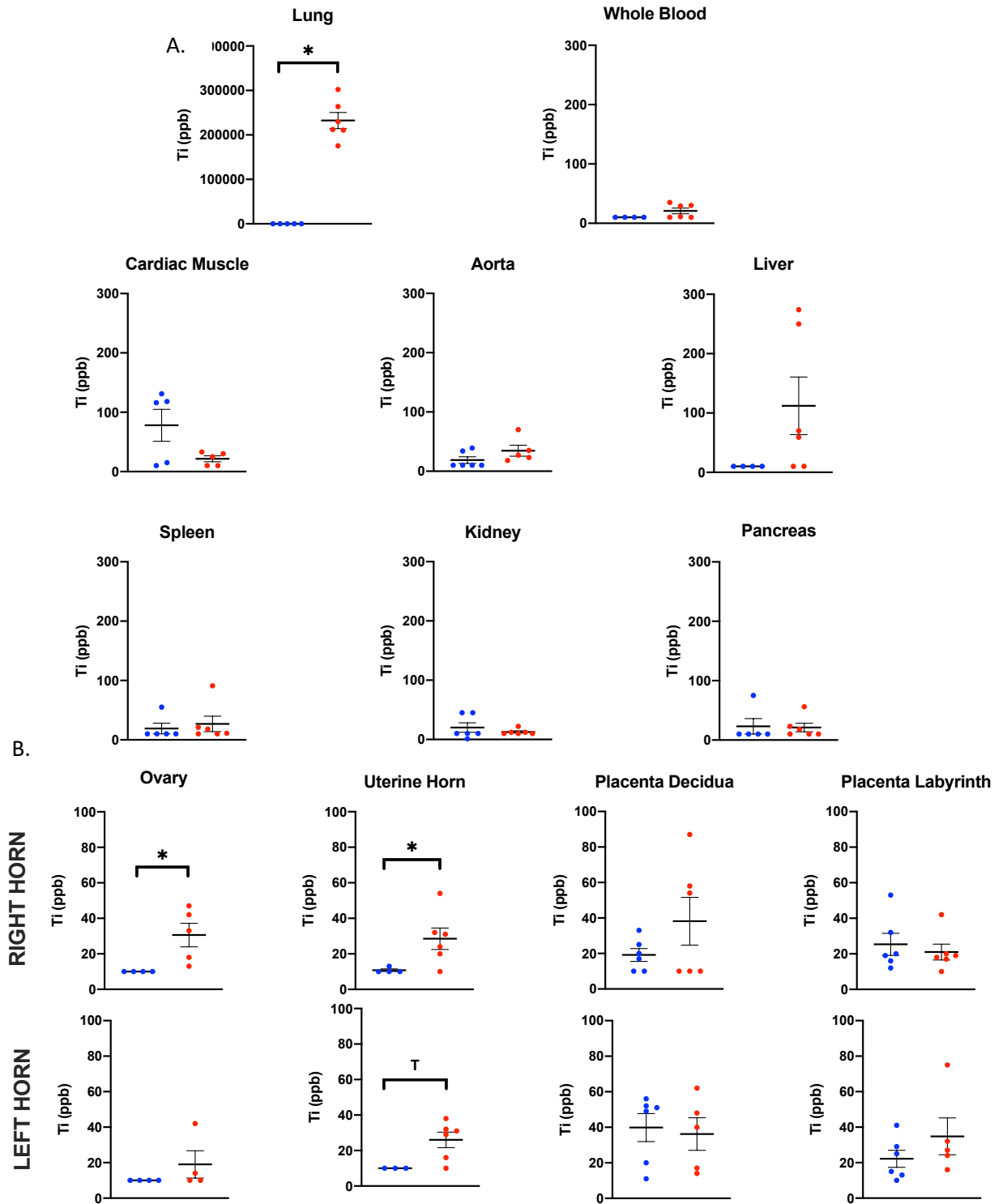
**Table 2.1. Calculated NP lung burden with the following equation:  $D = F * V * C * T$ , where F is the deposition fraction (10%), V is the minute ventilation based on dam body weight (g), C equals the steady state mass concentration (mg/m<sup>3</sup>), and T equals the exposure duration (minutes). Mean ± SEM reported. The average additive sum of lung burdens for each exposure day considering clearance equated to 194.81 ± 1.89 μg.**

Tissue	Filtered Air (ppb)	Nano-TiO <sub>2</sub> (ppb)	Student's t-test p-value	Mann-Whitney U test p-value
Maternal whole blood	10.0 ± 0.0	20.8 ± 4.8		0.10
Aorta	18.9 ± 5.7	34.7 ± 9.3		0.14
Heart	105.1 ± 37.7	31.8 ± 10.0		0.30
Lung	45.6 ± 17.6	232404.8 ± 18223.3	* < 0.01	
Liver	10.0 ± 0.0	104.4 ± 50.5		0.10
Kidney	21.7 ± 7.4	12.7 ± 1.9		0.80
Pancreas	23.2 ± 13.2	21.1 ± 7.4		0.62
Spleen	19.0 ± 9.0	26.8 ± 13.0		0.27

Right ovary	10.0 ± 0.0	33.7 ± 7.4		*0.02
Right uterus	10.8 ± 0.8	30.2 ± 7.1		*0.04
Right placenta decidua/junctional	19.2 ± 3.6	35.0 ± 16.0	0.20	
Right placenta labyrinth	25.3 ± 6.2	16.8 ± 1.8		0.68
Left ovary	10.0 ± 0.0	22.0 ± 10.1		0.43
Left uterus	10.0 ± 0.0	28.0 ± 4.7		<sup>T</sup> 0.07
Left placenta decidua/junctional	39.8 ± 7.8	29.8 ± 8.4		0.66
Left placenta labyrinth	22.2 ± 4.8	24.8 ± 3.4	0.27	

Right umbilical cord	13.0 ± 3.0	35.0 ± 12.5		*0.04
Right fetal liver	20.0 ± 10.0	23.0 ± 12.3		0.42
Right fetal heart	61.3 ± 24.3	53.7 ± 14.9	0.80	
Right fetal whole blood	46.2 ± 11.6	83.3 ± 33.5	0.25	
Left umbilical cord	21.8 ± 11.8	37.5 ± 7.8		0.20
Left fetal liver	13.8 ± 3.8	10.8 ± 2.4		0.60
Left fetal heart	21.0 ± 11.0	48.4 ± 6.0		<sup>T</sup> 0.07
Left fetal whole blood	27.5 ± 10.4	60.3 ± 17.4	0.16	

**Table 2.2. Ti in ppb measured in maternal, uteroplacental, and fetal tissues on GD 20 using ICP-MS analysis.** Limit of Detection = 10 ppb. N=6 dams per group. Data analyzed only by Student's t-test or Mann-Whitney U test according to the results from a distribution test, the section under the appropriate statistical test for each tissue present p-value and the section under the inappropriate test are grayed out, mean ± SEM reported. \* =  $p \leq 0.05$ , T =  $\leq 0.07$



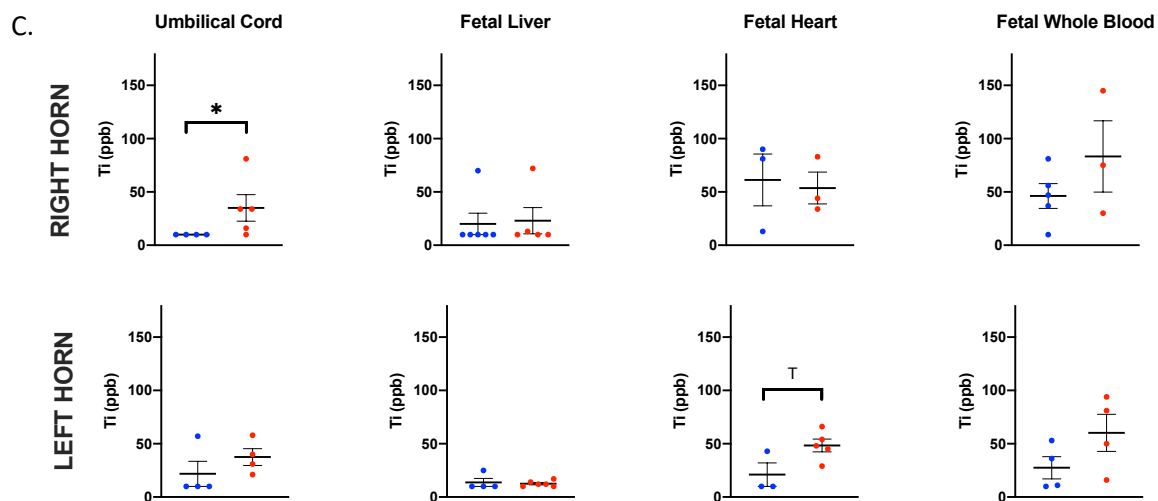


**Figure 2.2. Ti concentrations in ppb measured in (A) maternal, (B) uteroplacental, and (C) fetal tissues on GD 20 using ICP-MS analysis.** Limit of Detection = 10 ppb. N= 6 dams per group. Analysis by Student's t-test or Mann-Whitney U test depending on distribution, mean  $\pm$  SEM reported. \* =  $p \leq 0.05$ , T =  $\leq 0.07$

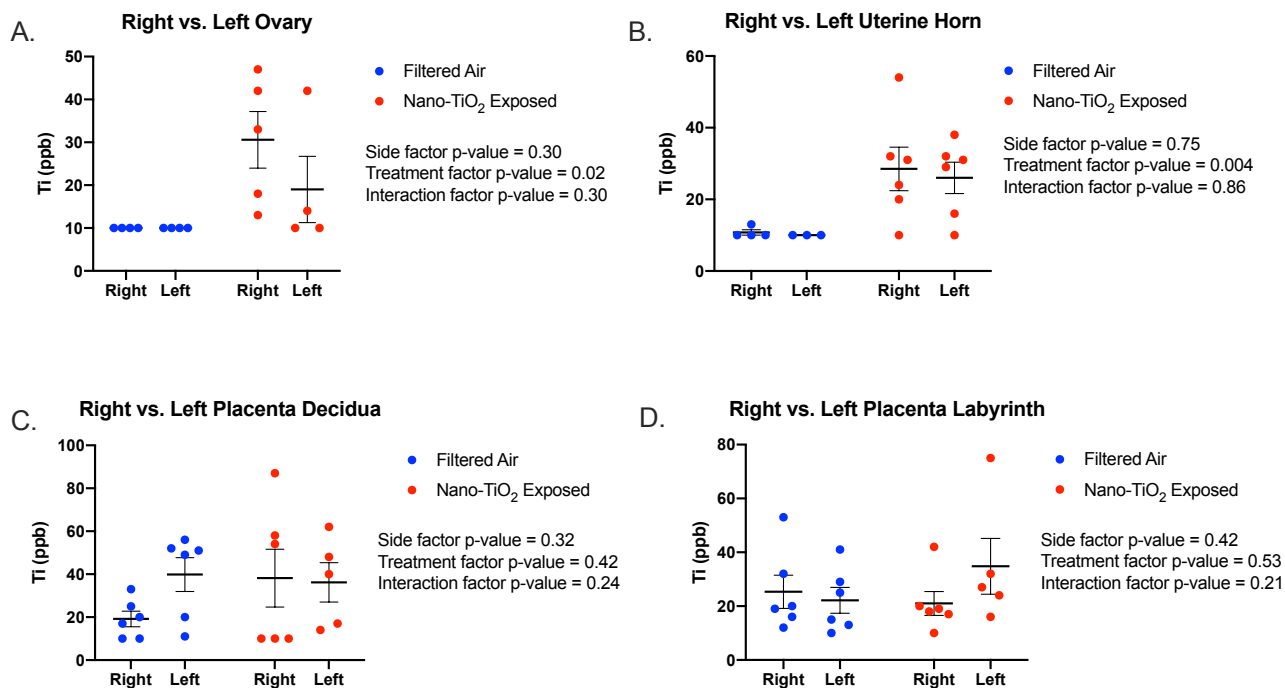


**Figure 2.3. Comparison between right and left sides of the reproductive tract. A.** Ovary from right and left uterine horn for each exposure group. **B.** Uterine horn tissue from right and left uterine horns for each exposure group. **C.** Placental decidua tissue from right and left uterine horns for each exposure group. **D.** Placental labyrinth tissue from right and left uterine horns for each exposure group. Analysis by two-way ANOVA and Sivak's multiple comparison post hoc correction. Mean  $\pm$  SEM reported.

Organ	Expected exposure order (highest to lowest Ti concentration)	Actual exposure order (highest to lowest Ti concentration)	Actual % of Nano-TiO <sub>2</sub>
Maternal Liver	1	1	19.24
Maternal Kidney	2	15	2.33
Uterus	3	9	5.02
Placenta Decidua	4	4	6.87
Placenta Labyrinth	5	8	5.03
Maternal Spleen	6	10	4.95
Maternal Aorta	7	6	6.39
Maternal Whole Blood	8	13	3.84
Maternal Heart	9	7	5.87
Maternal Pancreas	10	12	3.90
Ovaries	11	11	4.69
Umbilical	12	5	6.65
Fetal Liver	13	14	3.02
Fetal Whole Blood	14	2	12.93
Fetal Heart	15	3	9.28
<b>Total Ti (ppb)</b>			<b>542.59</b>

**Table 3.3. Rank order of organs with expected highest to lowest relative Ti concentrations and actual relative concentrations (excluding lung).** Data presented as a percent of the total of average Ti measured in nano-TiO<sub>2</sub> exposed.

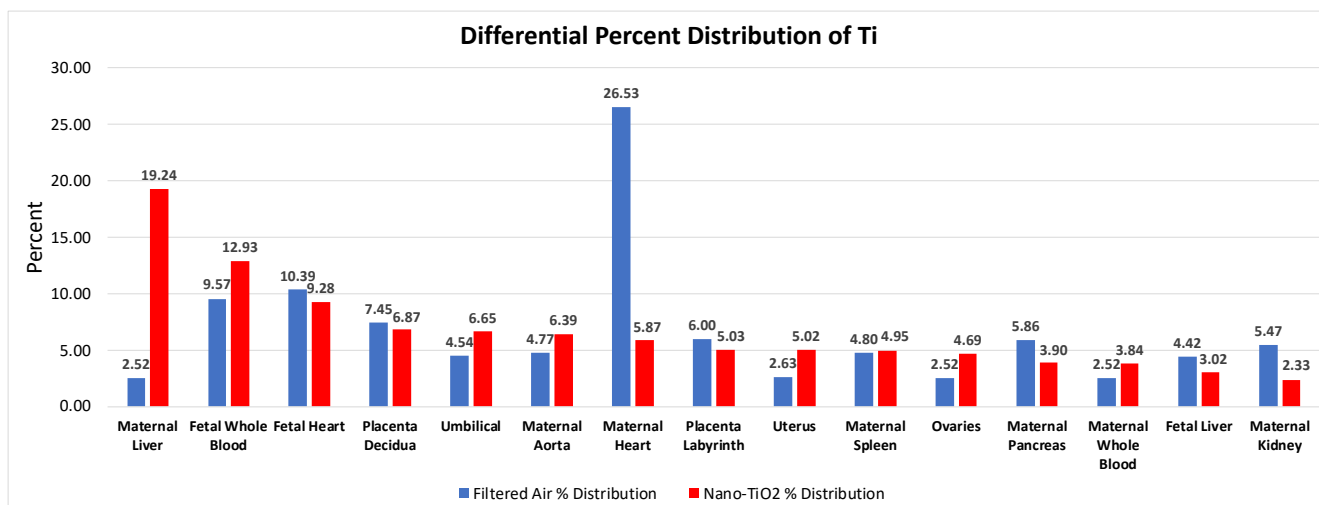


**Figure 2.4. Differential Ti tissue distribution outside of the lung in control and nano-TiO<sub>2</sub> exposed groups.** Data are displayed as percent of total Ti excluding the maternal lung in each group.

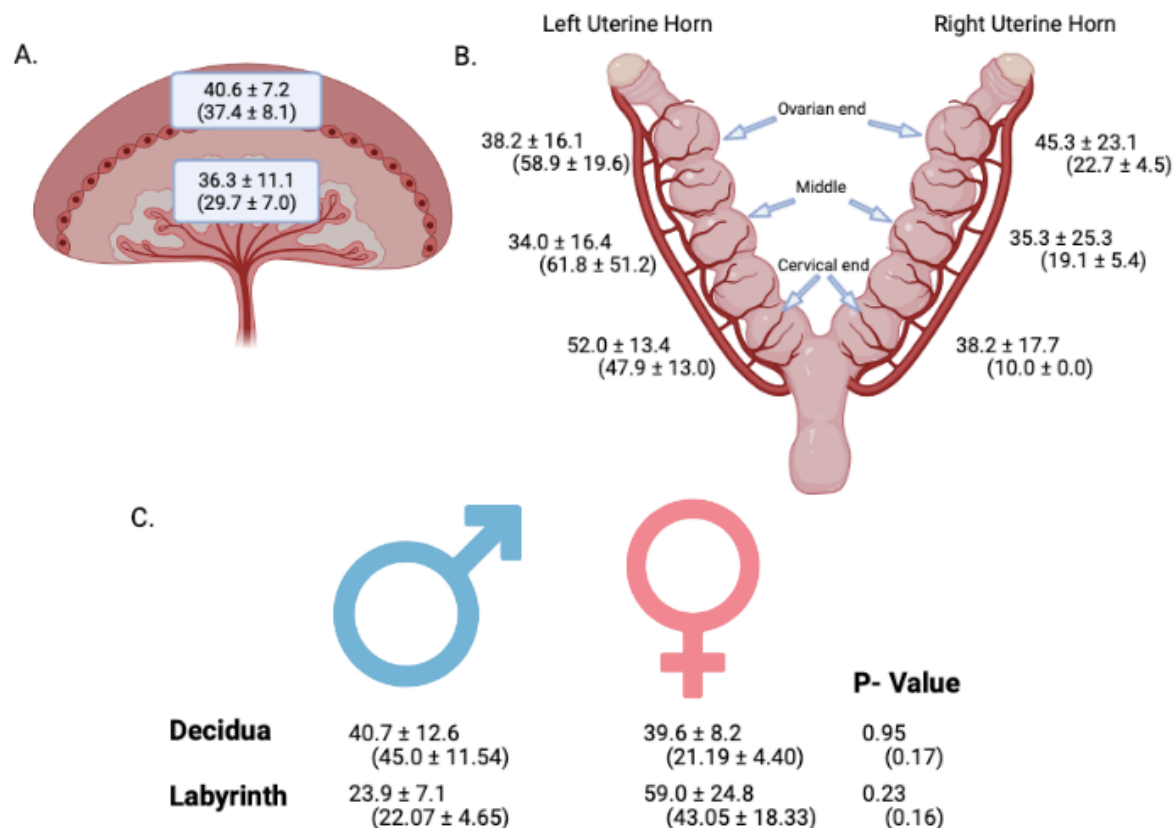


**Figure 2.5. Placental accumulation of Ti (ppb) measured by ICP-MS analysis from nano-TiO<sub>2</sub> and filtered air exposed dams.** **A.** Mean ± SEM values of Ti in ppb measured in the maternal zone (decidua/junctional zone) and fetal zone (labyrinth) of all exposed placentas. **B.** Mean ± SEM values of Ti in ppb measured in exposed placentas from left and right horns in ovarian end, middle, and cervical end locations. **C.** Mean ± SEM values of Ti in ppb measured in male and female placentas. Data are presented as exposed means ± SEM and (control means ± SEM). N=6 dams. Analysis by Student's t-test, mean ± SEM reported. Images created with BioRender.com.

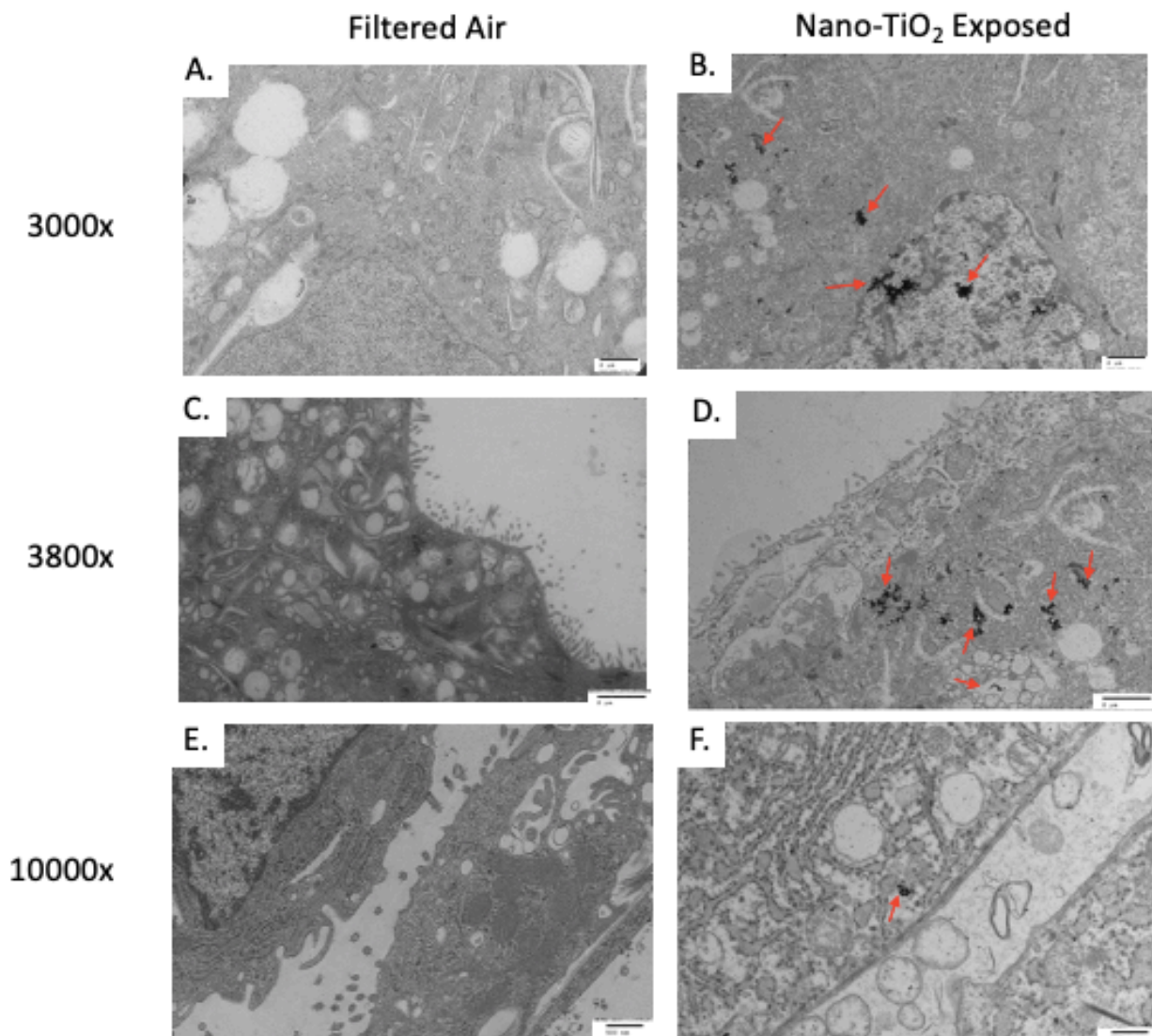


**Figure 2.6. Transmission Electron Microscopy (TEM) image of particle distribution in the trophoblasts in the labyrinth zone of the placenta.** Representative images (A-D scale bar 2 μm, E and F scale bar 500 nm). Particles were visualized in 0 of 4 filtered air placentas (2 males, 2 females) and 4 of 4 nano-TiO<sub>2</sub> exposed placentas (1 male, 3 females). All placentas were harvested from the middle section of the right uterine horn.

**CHAPTER 3: Repeated Titanium Dioxide Nanoparticle Aerosol Exposure Reduces Uterine Artery Fluid Flow, Placental Fetal Capillary Size, and Fetal Glucose**

Jeanine N D'Errico<sup>a</sup>, Pedro Lauro<sup>b</sup>, Chelsea M Carey<sup>a</sup>, Alex Lu<sup>a</sup>, Phoebe A Stapleton<sup>a,c</sup>

**Affiliations:**

4. Department of Pharmacology and Toxicology, Ernest Mario School of Pharmacy, Rutgers University, 160 Frelinghuysen Rd., Piscataway, NJ 08854, USA; b. Histopathology Core Facility, 41 Forgon Road, Piscataway, NJ 08854, USA, c. Environmental and Occupational Health Sciences Institute, 170 Frelinghuysen Rd., Piscataway, NJ 08854, USA

### 3.1 Abstract

Human and animal studies have linked FGR with maternal inhalation of ambient particulate matter (PM). FGR is a complex disorder often due to reduced placental nutrient transfer. Glucose is a critical nutrient for fetal growth. It unknown whether placental transfer of glucose is reduced after maternal PM inhalation. The objective of this study was to utilize nano-TiO<sub>2</sub>, a commonly used surrogate for PM, to test placental glucose transfer to the fetus. Further, placental morphometrics, fluid flow dynamics, and GLUT expression and membrane localization were assessed. Time-pregnant Sprague Dawley rats were administered whole-body inhalation exposure between GD 4 and 19 to HEPA filtered air or nano-TiO<sub>2</sub> ( $9.72 \pm 0.27 \text{ mg/m}^3$ ). On GD 20 blood glucose concentrations were measured, *ex vivo* placental perfusions were conducted, and placental tissues were harvested. Morphometrics analyzed the size of maternal blood sinus and fetal capillary. The placental mRNA and protein expression of GLUT1, GLUT3 and GLUT4 were evaluated with qPCR and Western blotting, respectively. Finally, immunohistochemistry evaluated the polarized membrane expression of glucose transporter protein isoforms. The results show that maternal weight gain and maternal glucose concentrations were unaffected with exposure. Fetal blood glucose concentrations were significantly reduced in a sex-dependent manner. Uterine artery fluid flow and fetal capillary size in the placenta were significantly reduced. There was no change to placental glucose transfer rate measured *ex vivo*. Additionally, there was no change in mRNA and protein expression for GLUT1 and GLUT3, and a reduction in GLUT4 mRNA. Immunolocalization of GLUT1 to the apical and basolateral membranes, GLUT 3 to the apical membrane, and GLUT4 to the perinuclear region of syncytiotrophoblasts did not change between exposure groups. Overall, it has been found that gestational nano-TiO<sub>2</sub> inhalation leads to reductions in uterine artery fluid flow, fetal blood vessel area of the placenta, and fetal blood glucose.

### 3.2 Introduction

FGR is a pregnancy disorder where optimal growth *in utero* is not achieved. The principal pathology of this condition often involves placental insufficiency, leading to reduced fetal nutrition and growth (Malhotra et al. 2019). This impact during fetal development can set the stage for immediate and long-term consequences for neurological (Miller et al. 2016), cardiovascular (Masoumy et al. 2018), and metabolic (Rueda-Clausen et al. 2010; Simmons et al. 2001) function, influencing life-long offspring health (Armengaud et al. 2021).

Epidemiological studies demonstrate FGR has been correlated with high ambient ultrafine particle ( $PM_{0.1}$ ), or nanoparticle (NP), environments including urban (Shao et al. 2020), domestic (Abusalah et al. 2012), and occupational settings (Manangama et al. 2019; Norlén et al. 2019). Animal studies that recapitulate these maternal exposures found reductions to placental weight and morphology in mice (Veras et al. 2008) and fetal weight in rats (Stapleton et al. 2013b). Further, repeated nano- $TiO_2$  aerosol exposure to simulate PM in rats has identified offspring reductions in short term memory and initial motivation (Engler-Chiurazzi et al. 2016), blunted coronary arteriole dilation tested through endothelium-dependent and -independent mechanisms (Fournier et al. 2021; Stapleton et al. 2015e), reduced cardiomyocyte mitochondrial oxidative phosphorylation and cardiac contractility (Hathaway et al. 2017; Stapleton et al. 2015e), and ablated uterine vascular mechanotransduction, endothelium-dependent dilation, and mitochondrial respiration capacity (State 3) (Stapleton et al. 2015a). While the mechanisms to explain how NP ambient inhalation exposure leads to these offspring outcomes remain unclear, initial evidence suggests that maternal exposure impacts the placenta. For example, one mouse study that administered  $PM_{0.1}$  by intratracheal instillation on 6 days during pregnancy found the exposure promoted placental inflammation and oxidative stress and reduced methylation of renin-angiotensin system related elements associated with an increase in adult offspring blood pressure (Morales-Rubio et al. 2019). Another study administering whole-body  $PM_{2.5}$  to pregnant Wistar rats for 15 days identified reduced placental invasion and angiogenesis and blunted placental mass, size, and surface area

(Soto et al. 2017). Finally, a pregnant C57BL/6 mouse study administering PM<sub>2.5</sub> by nasopharyngeal aspiration found placental proliferation was reduced, and placental nutrient transporter mRNA expression modified with increased amino acid transporters (Snat1, Snat4) and glucose uptake transporter (Glut3), and decreased long-chain polyunsaturated fatty acid transporters (Fatp1, Fatp4) measured on GD 18.5 (Zhu et al. 2021). Collectively, this information suggests that FGR and adult neurologic and cardiovascular health outcomes may be centered around gestational NP inhalation impact on placental morphology and function.

The placenta is a transient organ established during pregnancy for the purposes of fetal protection and nutritional transfer. Vacant spaces, referred to as intervillous space in humans and labyrinth sinusoids in rodents, serve as basins filled with maternal blood (Furukawa et al. 2019). Maternal blood bathes the placental syncytium, layers of epithelia separating maternal and fetal circulations where nutrient transport takes place. Although in different species and anatomical configurations, the morphology and thickness of the placenta and syncytium, respectively, have been shown to be critical for nutrient transfer to the fetus across mammalian species (Furukawa et al. 2014). In addition, the surface area of the syncytium can influence the capacity for nutrients to translocate across the membrane by passive diffusion (e.g. glucose, oxygen) (Griffiths and Campbell 2015; Van Gronigen Case et al. 2021). According to Fick's law of diffusion, a reduction in surface area would decrease the rate of diffusion per unit time (Griffiths and Campbell 2015). Therefore, placental weight, syncytial surface area and thickness are important indicators of maternal-fetal nutrient exchange (Roland et al. 2012). The current literature correlates ambient PM<sub>2.5</sub> exposures, which encompasses particles in the nano range, with changes in placental surface area shown in rats (Soto et al. 2017), and barrier structure and altered nutrient transporter expression in rats and mice (Soto et al. 2017; Zhu et al. 2021). Furthermore, reduction in maternal-fetal nutrient transfer and significant decreases in placental and fetal weight have been found after exposure to PM<sub>2.5</sub> (Liu et al. 2016). This evidence together supports gestational NP inhalation reduces syncytial surface

area, placental size, and nutrient transport capacity which may impede fetal growth and development.

As the principal energy substrate for protein synthesis and growth, glucose is a paramount nutrient for the developing fetus and has been shown to have a strong linear correlation with fetal weight in humans (Geurtsen et al. 2019). The robustness of this influence is exemplified in human maternal conditions such as malnourishment (e.g., maternal hypoglycemia) that results in growth-restriction (Lumey et al. 1993), and gestational diabetes (e.g., maternal hyperglycemia) that results in macrosomic newborns (Scholl et al. 2001). Therefore, deviations in fetal weight could be traced back to intrauterine glucose supply. During development, all glucose acquired by the fetus is sourced from maternal blood (Kalhan and Parimi 2000). Maternal blood glucose concentrations are tightly regulated during fasting and post-prandial states to accommodate for feto-placental glucose removal (Montaner et al. 2002). Glucose passively diffuses down a concentration gradient between maternal blood (highest), syncytial cytoplasm (lower), and fetal blood (lowest) (Cetin et al. 2011). Because glucose is a critical fuel for fetal growth and entirely acquired from maternal blood, reductions in fetal glucose due to maternal hypoglycemia may contribute to reduced fetal growth outcomes.

The critical process of glucose transfer to the fetus is enabled by glucose transport proteins (GLUTs) embedded along the placental syncytium (Illsley and Baumann 2020). The syncytiotrophoblast has a unique polarity of glucose transporter isoforms GLUT1, GLUT3, and GLUT4. GLUT1 is expressed and trafficked to both the apical (maternal-facing) and basolateral (fetal-facing) membranes with higher expression on the apical membrane (Smith et al. 1992). This asymmetry is critical to maintain the glucose concentration gradient and passive diffusion to the fetus. GLUT3 is primarily found in the apical membrane and thought to aid in glucose uptake for the syncytium itself. Kinetically, GLUT3 has a much higher affinity for glucose ( $K_m$  2 to 5 times

higher) which possibly aids to support very high syncytial cell glucose uptake and utilization (Hay 2006). GLUT4 is an insulin-regulated isoform that has cytosolic expression for the rapid recruitment to the basolateral membrane (Ericsson et al. 2005). There is much less dependency on GLUT4 near term compared to the first trimester, however the isoform has been detected near term in human (James-Allan et al. 2019b) and rodent (Xing et al. 1998) placentas. Inadequate expression and/or function of placental glucose transporter proteins can result from environmental exposures, as seen with cadmium (Xu et al. 2016) and triclosan (Cao et al. 2017) in mice, and human studies have shown that reduced expression of these transporters can result in reduced fetal glucose transfer and growth (Jansson et al. 1993). To our knowledge, the expression and polarized localization of glucose transporter isoforms has yet to be studied after ambient NP inhalation during pregnancy.

Accumulating evidence suggests that the sex of the fetus influences placental responses to external stimuli, such as changes in maternal nutrient availability (Mao et al. 2010) and environmental exposures (Rosenfeld 2012). Interestingly, male and female placentas from pregnant C57BL/6J mice have shown distinct differences in metabolism at baseline; female placentas had markedly higher concentrations in metabolites from fatty acid oxidation suggesting female placentas prefer lipids as energy substrate compared to male placentas (Saoi et al. 2020). Furthermore, when provided with a high fat or low fat diet, studies have found a divergent response based on fetal sex; female placentas change gene expression in response to changes in maternal diet more dramatically than male placentas (Mao et al. 2010). This interesting distinction may be due to male fetuses maintaining a high demand for nutrient provision in favor of maximal intrauterine growth, where females undergo relatively less growth to adapt to nutrient scarcity (Rosenfeld 2015). Few studies have considered placental response to maternal NP exposure based on fetal sex. One study conducted on 1,190 mother-newborn pairs (635 males, 555 females) in Changsha, China found maternal exposure to air pollution resulted in poor neonatal neurobehavioral scores in male subjects as compared to females (Chen et al. 2020b). However, this study did not evaluate placental nutrient

transfer or birth weight. Altogether, the placental response to maternal NP inhalation may vary by fetal sex.

Overall, reductions in maternal and fetal glycemia or alterations in placenta glucose transporter expression and function have yet to be studied in the context of maternal ambient NP inhalation during pregnancy. The purpose of this study was to investigate maternal and fetal blood glucose concentrations and sex-dependent differences after gestational exposure to nano-TiO<sub>2</sub> aerosols. To further study potential impacts on the placenta, glucose transfer to the umbilical vein and GLUT1, GLUT3, and GLUT4 expression and localization were assessed.

### **3.3 Materials and Methods**

#### *Nanoparticle characterization*

Nano-TiO<sub>2</sub> powder was acquired from Evonik (Aeroxide TiO<sub>2</sub>, Parsippany, NJ). Using DLS techniques with a Zetasizer Nano ZS by Malvern, the crystal structure composition was previously determined to be 80% anatase and 20% rutile, primary particle size  $21 \pm 6.1$  nm and surface area 48.08 mg<sup>2</sup>/g (Fournier et al. 2019b).

#### *Animal exposure*

Time pregnant Sprague Dawley rats were purchased from Charles River Laboratories (Kingston, NY) and housed in the Rutgers School of Public Health vivarium on GD 2 or GD 3. Animals were single housed and had *ad libitum* access to food (Purina 508 Rodent Chow) and water. A 24–48-hour acclimation period was given prior to first handling. All procedures were approved by the Institutional Animal Care and Use Committee of Rutgers University.

Between GD 4 and GD 19 animals were administered whole-body exposure to HEPA filtered air or nano-TiO<sub>2</sub> aerosols in our custom rodent inhalation facility (IEStechno, Morgantown, WV). The

HEPA filtered air control group had an n of 9 dams and nano-TiO<sub>2</sub> group had 15 dams. All dams were given 3 cheerios when being placed in the inhalation facility for enrichment purposes. Animal exposures occurred for 4 hours/day 5 days/week. The size distribution and concentration of the particles were monitored in real-time by a scanning mobility particle sizer (SMPS, TSI, Shoreview, MN) and a particle counter (General Purpose Water-based Condensation Particle Counter, TSI, Shoreview, MN), respectively. The concentration of the particle aerosols was confirmed via gravimetric sample collection on a 47-nm PTFE membrane filter and an XP2U microbalance (Mettler Toledo, Switzerland).

#### *Tissue collection*

Dams were fasted on the night of GD 19 and necropsied at approximately 9:45 AM on GD 20. Animals were placed under 5% induction and 3% maintenance isoflurane gas anesthesia. The right and left uterine horns were identified and excised from the abdomen. Six placentas from each dam were separated from respective fetus and sectioned along the sagittal plane into two halves; one half drop-fixed into 10% neutral buffered formalin and the other halved again and snap-frozen in liquid nitrogen. All tissues were stored at -80 °C until further molecular assessment. Fetal sexing was conducted at necropsy by visual identification of testes or uterine horns.

#### *Blood glucose quantification*

Blood glucose concentrations within maternal and fetal blood were measured at necropsy on GD 20 using a TRUTrack blood glucose meter (Trividia Health, Inc., Fort Lauderdale, FL). Maternal blood was sampled from the thoracic cavity after heart removal. Fetal blood was sampled from the trunk after decapitation.

#### *Ex vivo placental glucose perfusion*

Maternal and fetal physiological saline solutions (PSS) were prepared in advance with 180  $\mu\text{g}/\text{mL}$  and 40  $\mu\text{g}/\text{mL}$  glucose concentrations, respectively, and warmed to body temperature ( $37^\circ\text{C}$ ) to recapitulate in-life maternal blood circulation. Both PSS solutions also contained 130 mM NaCl, 4.7 mM KCl, 1.18 mM  $\text{KH}_2\text{PO}_4$ , 1.17 mM  $\text{MgSO}_4 \cdot 7\text{H}_2\text{O}$ , 1.6 mM  $\text{CaCl}_2$ , 14.9 mM  $\text{NaHCO}_3$ , and 0.026 mM EDTA. At necropsy the right uterine horn was removed from the body and placed in a warm bath of PSS. A uteroplacental unit that was central to the horn and had a segment of uterine artery that was connected to the length of an arcuate artery was selected to permit for successful cannulation and perfusion. From the selected utero-placental tissue, the uterine muscle was cut on either side and then moved aside to access the fetal pup. The amniotic membrane was separated from the fetal surface of the placenta. The umbilical cord was unraveled and ligated to separate the fetal pup. Using care, the umbilical artery and umbilical vein were separated for later cannulation with stainless steel needles. Finally, the entire placental unit (uterine vasculature, uterine muscle, placenta, umbilical cord) was cut away from the rest of the horn and moved to a modified single vessel chamber (D'Errico et al. 2019a; D'Errico et al. 2019c). The maternal uterine artery was cannulated at the proximal and distal ends and tied with sterile nylon sutures. The umbilical artery and umbilical vein were cannulated with 23 gauge and 25 gauge blunt stainless steel needles, respectively, and secured with braided silk sutures.

The maternal uterine artery was perfused with a PSS under conditions that aim to recapitulate maternal blood flow *in vivo*; glucose concentration 180  $\mu\text{g}/\text{mL}$ , gasses bubbled were 21%  $\text{O}_2$  and 5%  $\text{CO}_2$ , and flow adjusted using a pressure control system so that the pressure was maintained at 80 mm Hg. Similarly, the umbilical artery was perfused with PSS containing glucose concentration of 40  $\mu\text{g}/\text{mL}$  and pressure was maintained at 50 mm Hg gravimetrically. Perfusate was sampled from the distal end of the uterine artery and umbilical vein every 20 minutes for a duration of 60 to 80 minutes. A TRUTrack glucometer (Trividia Health, Inc., Fort Lauderdale, FL) was used to test transfer of glucose across the placenta over time course. In a subset of naïve animals, continuous

uterine artery infusion of a PSS solution containing 10  $\mu$ M Cytochalasin B (C2743, Sigma-Aldrich, St. Louis, MO), an inhibitor of GLUT1 and GLUT3 glucose uptake (Reckzeh and Waldmann 2020), was used as a positive control.

#### *Placental weight and morphometrics*

All placentas and fetuses from each litter were weighed. Placental efficiency ratios were calculated by dividing fetal weight by placental weight. Sagittally cut and drop-fixed placentas were subjected to hematoxylin and eosin staining. Using a JENOPTIK GRYPHAX camera microscope (Jenoptik AG, Jena, Germany), labyrinth zones were visualized on glass slides. Representative images were taken at 40X. Maternal blood spaces were identified as larger and irregularly shaped spaces with mature red blood cells, and fetal capillaries were identified by endothelial lining and single file nucleated immature red blood cells (Coan et al. 2004). Using ImageJ software, the perimeter of maternal blood space and fetal blood vessels were traced, and the area (pixels<sup>2</sup>) was calculated. For each H&E slide, 4 maternal and 4 fetal blood spaces were obtained and averaged for final analysis.

#### *Maternal and fetal weight*

Dam body weights were recorded on each exposure day (GD 4 to GD 19) and on day of necropsy (GD 20). To account for litter size influencing maternal gestational weight gain, to litter size was used to normalize maternal weight (maternal weight- maternal GD 4 weight) / litter size). On GD 20, body weight and crown-to-rump length were recorded for all fetuses in each litter.

#### *Quantitative RT-PCR*

One quarter of a whole placenta was homogenized in RNAzol using a TissueLyser adapter (Qiagen, Hilden, Germany) for 4 minutes at 50 Hz. RNase-free water was added to samples which were then kept on ice for 15 minutes and centrifuged at 12,000 g for 15 minutes at 4 °C. Isopropanol was used to precipitate RNA as a pellet which was then washed twice with 75% ethanol. Samples were

left uncapped to evaporate ethanol and RNA pellets were resuspended in RNase-free water. Integrity and concentration of RNA were evaluated with a Nanodrop 2000 spectrophotometer (ThermoFisher Scientific, Waltham, MA). RNA integrity was further confirmed by running an aliquot on an agarose gel stained with ethidium bromide and visualization of 28S rRNA and 18S rRNA bands. Complementary DNA was generated with a High Capacity cDNA Reverse Transcription kit (Applied Biosystems, Foster City, CA). SYBR Green Real-Time qPCR Master Mix (4368814, Applied Biosystems, Waltham, MA) was used for the detection of amplified product signals. Quantitative PCR was performed using ViiA7 RT-PCR system (Applied Biosystems, Waltham, MA). Primers were purchased from IDT Technologies (Coralville, IA). Target genes were normalized to  $\beta$ -Actin as a reference gene. Each sample was analyzed in duplicate.

**Table 1. Primer Sequences for qPCR.**

Gene	Forward	Reverse
GLUT1	ACGTCCATTCTCCGTTTCAC	TCCCACGGCCAACATAAG
GLUT3	GAC CAA GCG ACG GAG ATC	AGA GCT CCA GCA CAG TGA CC
GLUT4	AGG CAC CCT CAC TAC CCT TT	ATA GCC CTT TTC CTT CCC AA
$\beta$ -actin	AGCGTGGCTACAGCTTCACC	AAGTCTAGGGCAACATAGCACAGC

#### *Western blotting*

The placental protein expression of GLUT1, GLUT3, and GLUT4 were assessed by Western Blot. Primary antibodies were GLUT1 (1:1,000; 12939S, Cell Signaling, Danvers, MA), GLUT3 (1:1,000; MA5-32697 Invitrogen, Waltham, MA), GLUT4 (1:1,000; 2213S, Cell Signaling, Danvers, MA), and  $\beta$ -actin (1:1,000; 4970S, Cell Signaling, Danvers, MA). Secondary antibodies linked with HRP (anti-rabbit; 1:2,000; 7074S, Cell Signaling, Danvers, MA or anti-mouse; 1:2,000; 62-6520, ThermoFisher Scientific, Waltham, MA) were used to detect primary antibodies.

Chemiluminescent HRP-bound proteins were visualized using SuperSignal™ West Dura Extended Duration Substrate (34075, ThermoFisher Scientific, Waltham, MA). Target proteins were normalized to  $\beta$ -actin as the loading control. Semi-quantitative analysis of band intensities was conducted with AlphaView software (ProteinSimple, Biotech, Minneapolis, MN).

### *Immunohistochemistry*

Sagittally cut and drop-fixed placenta samples were sliced and embedded in paraffin wax. Sections were deparaffinized, dehydrated through a graded ethanol series, and subjected to heat-induced epitope retrieval with citrate buffer, pH 6.0 for 20 min at 98 ° C using a pressure cooker. Incubation of primary antibody Rabbit monoclonal anti-GLUT1 (Abcam ab15730, Cambridge, UK) was applied to sections at dilution of 1:750 for 1 hour followed by an incubation in the secondary antibody Horse anti-Rabbit IgG Polymer (Vector MP6401, Burlington, Ontario,) for 30 minutes. Incubation of primary antibody Rabbit monoclonal anti-GLUT3 (Invitrogen MA5-32697, Waltham, MA) was applied to sections at dilution of 1:250 for 1 hour followed by an incubation in the secondary antibody Horse anti-Rabbit IgG Polymer (Vector MP6401, Burlington, Ontario,) for 30 minutes. Incubation of primary antibody Rabbit polyclonal anti-GLUT4 (Invitrogen PA5-80022, Waltham, MA) was applied to sections at dilution of 1:750 for 1 hour followed by an incubation in the secondary antibody Horse anti-Rabbit IgG Polymer (Vector MP6401, Burlington, Ontario,) for 30 minutes. DAB chromogen substrate (Vector Labs SK-4105) was added for 5 minutes for development of brown color followed by 1 minute in Hematoxylin (Vector H-3404) for background blue color.

### *Statistics*

Unless otherwise stated, all fetal and placental data are presented as litter averages. Maternal and fetal blood glucose concentrations were analyzed by Student's t-test. Perfusate glucose and flow data were analyzed by Student's t-test for each time point and AUC. Maternal gestational weight

gain was assessed by Student's t-test for each exposure day. Data for fetal and placental weight, crown to rump length, and placental efficiency were analyzed by Student's t-test. All data sets stratified by fetal sex were analyzed by two-way ANOVA with Sivak's multiple comparison post hoc correction. Statistics were conducted and graphs created using GraphPad Prism 8 (Version 8.4.3)

### 3.4 Results

#### *Animal whole-body aerosol exposures*

Dams were subjected to nano-TiO<sub>2</sub> aerosols within a whole-body exposure chamber for 4 hours/day, 5 days/week. The overall average NP concentration and size were  $9.72 \pm 0.27$  mg/m<sup>3</sup> and  $193.09 \pm 11.46$  nm, respectively. A representative figure of the size distribution and concentration within the exposure chamber is presented in Chapter 2, Figure 1, where the median particle size was 130.2 nm (Chapter 2, Figure 1A) and average particle concentration was  $9.65 \pm 0.03$  mg/m<sup>3</sup> (Chapter 2, Figure 1B). The average lung deposition considering repeated exposure and clearance was  $158.38 \pm 1.36$  µg.

#### *Maternal and fetal blood glucose*

Overnight fasted maternal and fetal blood glucose concentrations were measured on GD 20 (**Figure 3.1**). Nano-TiO<sub>2</sub> exposure had no effect on maternal blood glucose concentration (**Figure 3.1a**). There was a statistically significant 21% reduction in fetal blood glucose after in utero exposure to nano-TiO<sub>2</sub> (**Figure 3.1b**). When stratified by fetal sex, males had a significant 25% reduction while females had a 17% reduction in blood glucose (**Figure 3.1c**).

#### *Maternal gestational weight gain, fetal length, and fetal weight*

Maternal gestational weight gain and fetal weight and length were measured (**Figure 3.2**). There was no significant difference in maternal gestational weight gain between exposure groups from

GD4 to GD 20 (**Figure 3.2a**). Fetal crown-to-rump length did not differ by exposure group or fetal sex (**Figure 3.2b, Figure 3.2c**). Fetal weight did not differ between exposure groups or by fetal sex (**Figure 3.2d, Figure 3.2e**).

#### *Placental transfer of glucose*

Glucose transfer to the fetal side of the placenta was measured over *ex vivo* time course placental perfusion (**Figure 3.3**). There was no reduction of glucose transfer to the umbilical vein at any time point after in-life exposure to nano-TiO<sub>2</sub> or CytoB infusion compared to filtered air (**Figure 3.3a**). Comparison of the estimated total glucose transferred over the 60-minute perfusion for each exposure group also revealed no differences (**Figure 3.3b**).

#### *Fluid flow across uterine artery and through umbilical artery*

The volume of fluid collected from the distal end of the uterine artery and umbilical vein was measured at each time point of placental perfusion (**Figure 3.4**). There was a significant reduction in volume crossing the uterine artery at the 40-, 60-, and 80-minute timepoints after in-life nano-TiO<sub>2</sub> exposure (**Figure 3.4a**). Area under the curve shows a 48% reduction in flow, although this did not reach statistical significance (**Figure 3.4b**). No change in fluid flow was found coming through the umbilical vein (**Figure 3.4c**). Area under the curve shows no difference in fluid flow (**Figure 3.4d**).

#### *Placental weight, efficiency, and morphometrics*

Placental weight, efficiency, and morphometrics were assessed on GD 20 placentas (**Figure 3.5**). No significant difference in placental weight (**Figure 3.5a**) or efficiency (placental to fetal weight ratio) (**Figure 3.5b**). There was no significant change in surface area of maternal blood space. Fetal blood vessel area was significantly reduced by 28% after nano-TiO<sub>2</sub> exposure (**Figure 3.5c**).

Representative hematoxylin and eosin stained labyrinth zone from male and female placentas per exposure group that were used for the morphometric analysis are presented (**Figure 3.5d**).

#### *Placental mRNA and protein expression of GLUT1, GLUT3, and GLUT4*

There was no difference in the placental mRNA expression of GLUT1 or GLUT3. There was a significant 34% reduction in the mRNA expression of GLUT4 (**Figure 3.6a**). There was no difference in the protein expression of GLUT1, GLUT3, or GLUT4 (**Figure 3.6b**).

#### *Syncytiotrophoblast membrane localization and expression of GLUT1, GLUT3, and GLUT4*

GLUT 1 protein had immunopositive staining in the labyrinth zone of male and female placentas from filtered air and nano-TiO<sub>2</sub> exposed groups (**Figure 3.7a-d**). Syncytiotrophoblasts positively stained on membranes facing maternal blood sinusoids and fetal blood spaces. There was no significant difference in GLUT1 staining by exposure (**Figure 3.7g**), or by fetal sex (**Figure 3.7h**). GLUT3 had immunopositive staining in the labyrinth zone of male and female placentas (**Figure 3.8a-d**). GLUT 3 is localized to syncytiotrophoblast facing maternal blood sinusoids. There was no difference in GLUT1 staining by exposure (**Figure 3.8g**) or by fetal sex (**Figure 3.8h**). This immunohistology for GLUT isoforms in the rat placenta is consistent with previous literature (Furukawa et al. 2019). GLUT4 had faint perinuclear staining (**Figure 3.9a-d**). There was no significant difference in GLUT4 intensity by exposure (**Figure 3.9g**), or by fetal sex (**Figure 3.9h**).

### **3.5 Discussion**

Human and animal studies have connected gestational NP inhalation with reduced fetal growth and long-term health consequences. In the clinic, neonates with growth restriction often present with hypoglycemia (Yamaguchi et al. 1997). The goal of the current study was to test the hypothesis that reduced placental transfer of glucose contributes to FGR after maternal inhalation of nano-TiO<sub>2</sub>, and to explore possible effects on maternal glycemia and placental glucose transporters.

A critical finding of this study is the significant 21% reduction in fetal blood glucose after maternal repeated nano-TiO<sub>2</sub> whole-body exposure. Further, this outcome had a greater impact on male fetuses compared to female. With the caveat that the studies were underpowered, a significant reduction in uterine artery fluid flow was identified along with a significant reduction in fetal capillary size, but no change to maternal blood space. Reduced placental glucose transfer to the fetal compartment during the perfusion time-course was not found. Additionally, the mRNA expression and perinuclear staining intensity of placental GLUT4 was significantly reduced. There were no changes found in the mRNA and protein expression or membrane staining intensity of placental GLUT1 or GLUT3. Interestingly, there were no changes found with placental or fetal weight. There were also no exposure-related impacts on maternal blood glucose concentration or gestational weight gain.

Significant reduction in fetal blood glucose after repeated maternal nano-TiO<sub>2</sub> inhalation was identified from this study. This result is consistent with other pathologies (e.g., preeclampsia, hypoxia) leading to FGR that have been strongly associated with neonatal hypoglycemia (Illsley et al. 2010b; Yamaguchi et al. 1997). To our knowledge, this is the first study to identify fetal hypoglycemia that could lead to FGR after gestational NP inhalation. This result may have severe consequences to fetal neurodevelopment, as low glucose availability impairs brain function and leads to seizure or long-lasting brain injury (Su and Wang 2012). Previous work has demonstrated that prenatal nano-TiO<sub>2</sub> exposure produces deficits in behavior and cognition detected in adult male rats (Engler-Chiurazzi et al. 2016). This study did not include females for comparison; therefore, it is not known if this effect is male-specific. However, the long-term effects on behavioral end points may be related to intrauterine fetal glucose concentrations. In addition, reduced glucose during the perinatal period can lead to metabolic reprogramming for a “famine” environment outside of the womb and alter postnatal glucose homeostatic regulation (Sadiq et al. 1998). This finding serves

as a major contribution to the field of Developmental Origins of Health and Disease (DOHaD). Unfortunately, the mechanisms are currently unclear.

The glycemic status of the mother during pregnancy dictates the placental and fetal supply of glucose. From blood samples obtained from dams at the same time as fetal collection, no difference in glucose concentrations was found. This indicates maternal glycemia is appropriately maintained, and the potential for fetoplacental acquisition should not be impaired. Interestingly, nano-TiO<sub>2</sub> has been previously found to alter maternal glucose concentrations during pregnancy in rats (Mao et al. 2019). However, this was after oral administration and found to be due to alterations of the gut microbiota. Our study agrees with another that assessed maternal inhalation of fine particulate matter (PM<sub>2.5</sub>) during gestation in mice and found maternal glucose concentrations were not changed with exposure (Soto et al. 2017). The results from our study highlight the influence of route of exposure and impact on maternal systemic glucose homeostasis, where oral exposure, but not inhalation, has an impact.

A surprising inconsistency with this study compared to historical work is that fetal weight was not significantly reduced. There are several possible explanations for this which were not evaluated in this study. First, a compensatory increase in an alternate nutrient, such as lipids or amino acids, may explain the similarly achieved fetal weight. Previous work in mice has demonstrated that the placenta may adapt and increase the transport of amino acids to the fetus in attempt to achieve appropriate fetal growth (McIntyre et al. 2019). Alternatively, the results of the current study may disagree with previous work due to the outsourcing of time-pregnant animals from Charles River Laboratories (Kingston, NY), whereas previous work mated in-house (Stapleton et al. 2013b). Regardless, fetal hypoglycemia may still have significant metabolic and developmental consequences for the offspring.

The placenta is responsible for the transfer of glucose from maternal to fetal blood. Studies in mice have suggested that placental nutrient transport is decreased in FGR (McIntyre et al. 2019) as well as after maternal NP exposures (Zhu et al. 2021). In this study an *ex vivo* placental perfusion methodology, previously utilized to follow maternal-to-fetal transfer of gold (D'Errico et al. 2019a) and plastic (Fournier et al. 2020) NPs in rats, was used to follow glucose transfer after in-life exposure for filtered air or nano-TiO<sub>2</sub>. In our results, the glucose concentration was not reduced in umbilical vein effluent from placentas that were exposed to nano-TiO<sub>2</sub> compared to those that were exposed to filtered air. This observation was consistent for the overall estimated total glucose transferred to the umbilical vein for the perfusion period. This result is in contrast with human FGR pregnancies that have shown reductions in umbilical vein uptake of glucose (Cetin et al. 2020). To date, this is the first study to test glucose transfer from the maternal uterine circulation to the fetal compartment after maternal NP inhalation. From these studies, a significant reduction in the volume of fluid perfused across the uterine artery was identified. This is in support of the outcome of uterine vascular dysfunction, consistent with our lab's previous findings (Stapleton et al. 2013b). Overall, these results suggest nano-TiO<sub>2</sub> contributes to uteroplacental vascular dysfunction, which may lead to poor placental blood flow and nutrient delivery.

Placental weight, efficiency, and surface area are important morphological markers of placental toxicity. Surprisingly, this study did not demonstrate significant reductions to placental weight and efficiency with maternal inhalation of nano-TiO<sub>2</sub>. This finding disagrees with another rat study that found increased placental weight and decreased placental efficiency; however, this was after a single maternal nano-TiO<sub>2</sub> inhalation exposure on GD 10 (Bowdridge et al. 2019). In other mouse studies, maternal lung exposure to PM<sub>0.1</sub> resulted in significantly reduced placental weights (Morales-Rubio et al. 2019), and PM<sub>2.5</sub> led to decreased placental mass, size, and surface area (Soto et al. 2017). Our conflicting findings could be explained by differences in the physiochemical properties of nano-TiO<sub>2</sub> compared to PM which is a more complex mixture of organic and inorganic

particles and liquid droplets, as well as timing and duration of NP inhalation exposure during pregnancy. Nevertheless, in this study a reduction of placental weight and efficiency (fetal to placental weight ratio) was not found. To further evaluate anatomical changes to the placenta, the surface area of maternal blood sinusoids and fetal blood capillaries were quantified. There was no change in maternal blood sinusoids in exposed placentas. However, a significant reduction in fetal blood capillary area was identified, which can be indicative of reduced surface area for nutrient uptake to the fetal circulation. Previous literature has also found reductions to placental surface area in mice, further supporting the hypothesis that changes to placental morphology contribute to insufficient nutritional support for the fetus (Soto et al. 2017). Placental morphometrics should therefore be further studied with maternal NP inhalation exposures.

To further explore the mechanisms behind reduced fetal glucose, the mRNA and protein expression and syncytiotrophoblast localization of placental glucose transporter isoforms GLUT1, GLUT3, and GLUT4 were evaluated. In human models of reduced birth weight, such as high altitude pregnancy (maternal hypoxia), a downregulation of GLUT1 expression in the basolateral syncytial membrane is observed (Zamudio et al. 2006). This finding would suggest glucose diffusion to the fetal compartment is restricted. Herein, no change in placental mRNA and protein expression of GLUT1 or GLUT3 or staining intensity and localization of GLUT1, GLUT3 or GLUT 4 by exposure group was found. However, a significant reduction in GLUT4 mRNA was identified. In literature using adipocytes to study diabetes mellitus, it has been shown that increased cAMP levels and cellular insulin resistance can decrease the expression of GLUT4 (Flores-Riveros et al. 1993). One *in vitro* study demonstrated cAMP repression of GLUT 4 mRNA transcription on 3T3-L1 adipocytes by treating with 8-Br-cAMP compared with a forskolin treatment, a well-known activator of adenylyl cyclase to increase intracellular cAMP, and measured a 70% decrease in GLUT4 mRNA in both treatment groups (Kaestner et al. 1991). Another *in vitro* study using 3T3-F442A adipocytes showed that cAMP blocks insulin receptor activation and up-regulation of

GLUT4 mRNA transcription and protein translation (Yu et al. 2001). Together, these studies demonstrate the influence of cAMP and insulin on the regulation of GLUT4 expression, and that they may be involved in the downregulation found in this study. It is also important to note that GLUT4 has low expression and involvement in placental glucose transport at term in human, mouse, and rat placentas (Xing et al. 1998), which agrees with our high qPCR Ct values (above 29) and faint immunohistochemistry staining. Additionally, the reduction in GLUT4 mRNA did not translate into significant reductions in protein or perinuclear protein intensity, although these studies would have benefited for a higher sample size to increase statistical power. Further, the GLUT4 immunohistochemistry stained for protein in the perinuclear region of the cell and not in the basolateral syncytiotrophoblast cell membrane where it would be participating in glucose transport to the fetus. Thus, it is difficult to contribute these findings to the fetal reduction in blood glucose. Overall, the GLUT isoform evaluation indicates that the presence of transporters in the appropriate membranes is not altered with exposure, and thus is not a contributor to the reduction in fetal blood glucose. A higher sample size would be necessary to corroborate the conclusion. Alternate mechanisms such as transporter activity or altered membrane insertion must also be explored. Increased placental glucose storage (e.g., glycogen stores), and/or placental hypermetabolism of glucose with maternal NP inhalation could explain reduced fetal hypoglycemia and remain as new research frontiers.

It is important to mention the few limitations to this study. First, the consumption and transfer of oxygen by the placenta was not measured in placental perfusion experiments. Oxygen is a critical determinant of cellular glycolysis and respiration, and previously has been shown to be tied to the ability of the placenta to transfer glucose to the fetal circulation (Zamudio et al. 2010). Where feasible, future experiments should measure placental oxygen consumption as a variable in glucose transport studies. Second, the dissection to perform the *ex vivo* uteroplacental perfusion from the rodent uterine horn results in vascular openings (i.e. arcuate arteries, radial arteries) from which

perfusion fluid can escape into the vessel chamber bath. This technical limitation makes it not possible to quantify fluid movement between the uterine and fetal circulations or calculate placental glucose consumption by subtracting umbilical vein from uterine artery concentrations. Third, the apical and basal syncytial membranes were not isolated and purified for mRNA and protein quantification of glucose transporter proteins, which are asymmetrically expressed on either side. Future work can utilize differential centrifugation and  $Mg^{2+}$  precipitation protocols previously established (Chassen et al. 2020). Additionally, it is important to consider that many nutrients, not just glucose, are critical to support fetal growth and development (e.g. amino acids, fatty acids, micronutrients). These other nutrients were not evaluated in this study and could have been increased in delivery as compensation to sustain fetal growth (Aiko et al. 2014; Chassen et al. 2020). Future work should assess the transport of other types of nutrition to the fetus in models of maternal NP inhalation. Finally, the analyses of placental glucose transport rate, fluid flow, fetal blood vessel area by treatment and by fetal sex, and membrane GLUT intensity by fetal sex are underpowered. Therefore, additional samples are required to corroborate the initial findings from this study.

Overall, this study utilized a model of repeated whole-body nano-TiO<sub>2</sub> inhalation exposure and found significant impacts in fetal blood glucose concentrations in a sex-specific manner. Using an *ex vivo* placental perfusion methodology, evidence of uterine vascular dysfunction after gestational exposure was identified. Additionally, a significant reduction in fetal blood capillary area suggesting exposure may reduce placental surface area for nutrient uptake was measured. Reductions in maternal blood glucose bioavailability and GLUT1, GLUT3, and GLUT4 expression and syncytial localization has been ruled out as contributors to the reduced glucose phenotype of the fetuses. Given the numerous studies that have found adult consequences to cardiovascular, metabolic, and neurological health after gestational exposure, these findings are extremely important for understanding the intrauterine environment that may set the stage for these outcomes.

Future work is required to clarify the mechanisms underlying fetal hypoglycemia after maternal NP inhalation exposures.

**Figures:**

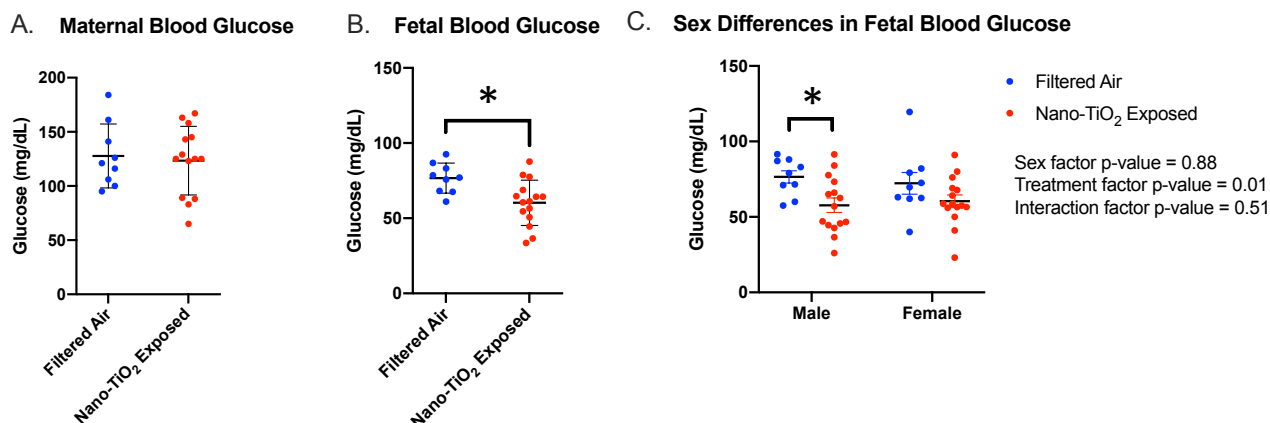


**Figure 3.1. Maternal and fetal blood glucose concentrations.** **A.** Maternal overnight fasted blood glucose concentrations between exposure groups on GD 20. N = 9-15 dams. Analysis by Student's t-test, mean and SEM reported. **B.** Fetal trunk blood glucose concentrations differ by 21% between exposure groups on GD 20. N = 9-15 dams per group. Analysis by Student's t-test, mean and SEM reported. **C.** Male and female fetal trunk blood glucose concentrations between exposure groups differ by 25% and 17%, respectively, on GD 20. N = 6 dams per group. Analysis by two-way ANOVA and Sivak's multiple comparison post hoc correction. Mean and SEM reported. \*= p < 0.05.

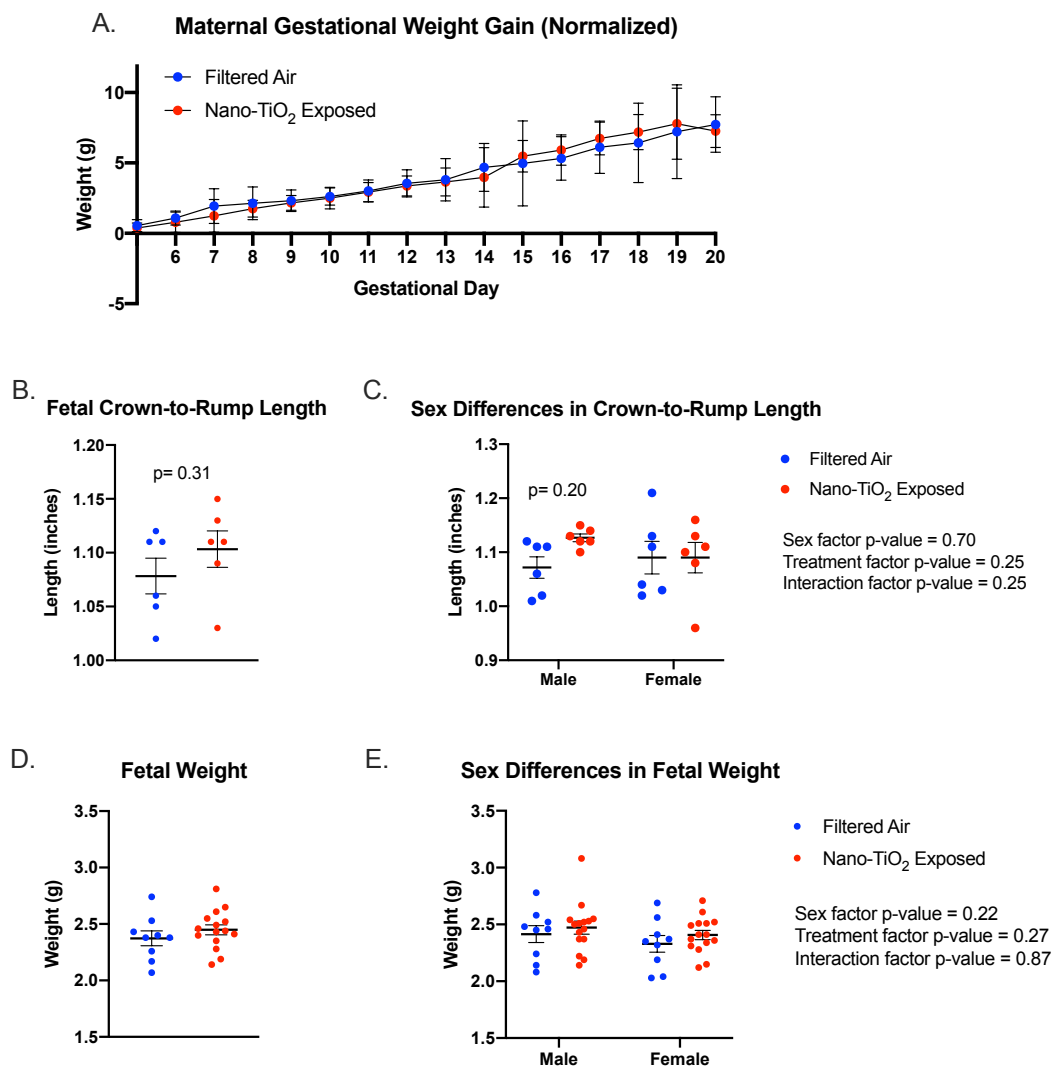


**Figure 3.2. Maternal and fetal gestational growth parameters after maternal nano-TiO<sub>2</sub> aerosol exposure.** **A.** Maternal weight gain over exposure period starting on GD 4 and ending at necropsy on GD 20. Maternal weight on GD 4 is subtracted from maternal weight on each subsequent day and then divided (normalized) by litter size. N = 9-15 dams per group. Analysis on each GD by Student's t-test, mean  $\pm$  SEM reported. **B.** Crown-to-rump length of a subset of fetuses between exposure groups on GD 20. N = 6 dams per group. Analysis by Student's t-test, mean  $\pm$  SEM reported. **C.** Male and female fetal crown-to-rump length of a subset of fetuses by exposure group on GD 20. N = 6 dams per group. Analysis by two-way ANOVA and Sivak's multiple comparison post hoc correction. Mean  $\pm$  SEM reported. **D.** Raw fetal weight between exposure groups on GD 20. N = 9-15 dams per group. Analysis by Student's t-test, mean  $\pm$  SEM reported. **E.** Male and female fetal weight by exposure group on GD 20. N = 9-15 dams per group. Analysis by two-way ANOVA and Sivak's multiple comparison post hoc correction. Mean  $\pm$  SEM reported.

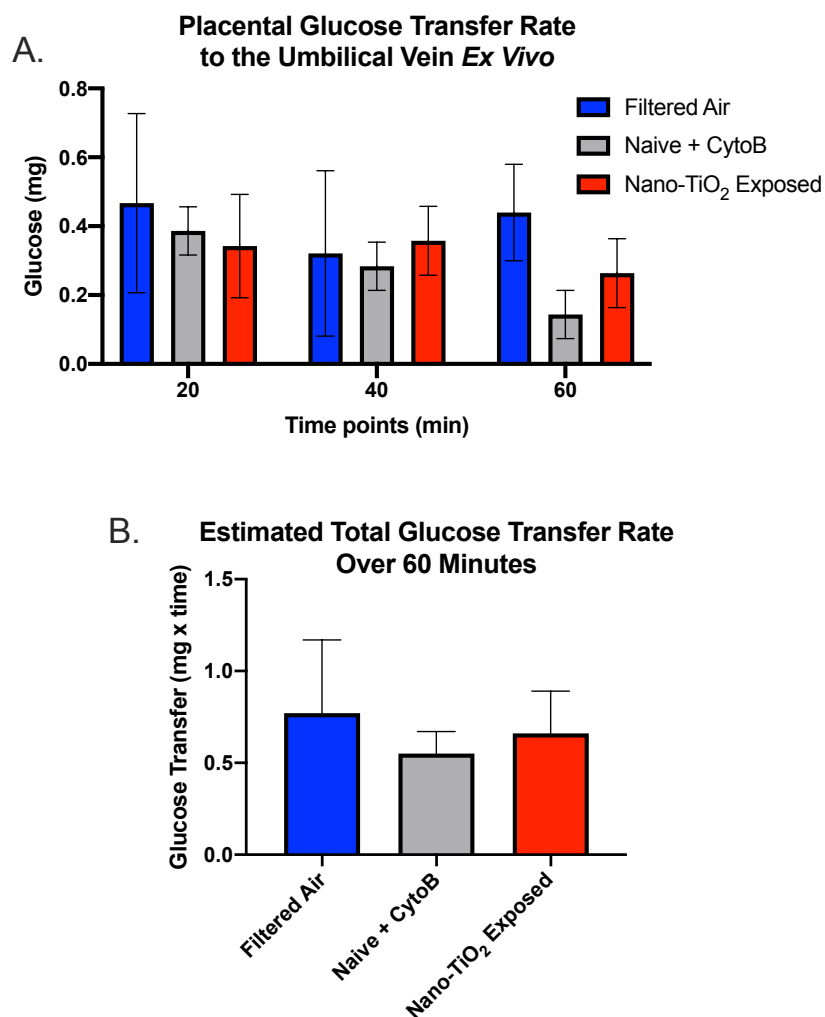


**Figure 3.3. Placental glucose transfer rate to the umbilical vein. *Ex vivo* placental perfusions from dams that were exposed to filtered air or nano-TiO<sub>2</sub> or that were naïve.** Values measured over time from umbilical vein effluent. **A.** Glucose concentration and effluent volume was measured from the umbilical vein at t = 20, 40, 60 minutes. n = 4 dams per group (4 placentas from male fetuses in filtered air group, 3 placentas from male fetuses and 1 placenta from a female fetus in nano-TiO<sub>2</sub> exposed group). As a positive control, 10  $\mu$ M of known glucose uptake inhibitor cytochalasin b (CytoB) was infused into naïve placentas through the uterine artery. Glucose concentration and effluent volume was measured from the umbilical vein at t = 20, 40, and 60 minutes. n = 3 dams. Analysis of glucose concentration at each time point by two-way ANOVA with Tukey's multiple comparisons test, mean  $\pm$  SEM reported. **B.** Estimated total glucose transfer to umbilical vein over perfusion time. Analysis by one-way ANOVA with Tukey's multiple comparisons test, mean  $\pm$  SEM reported.

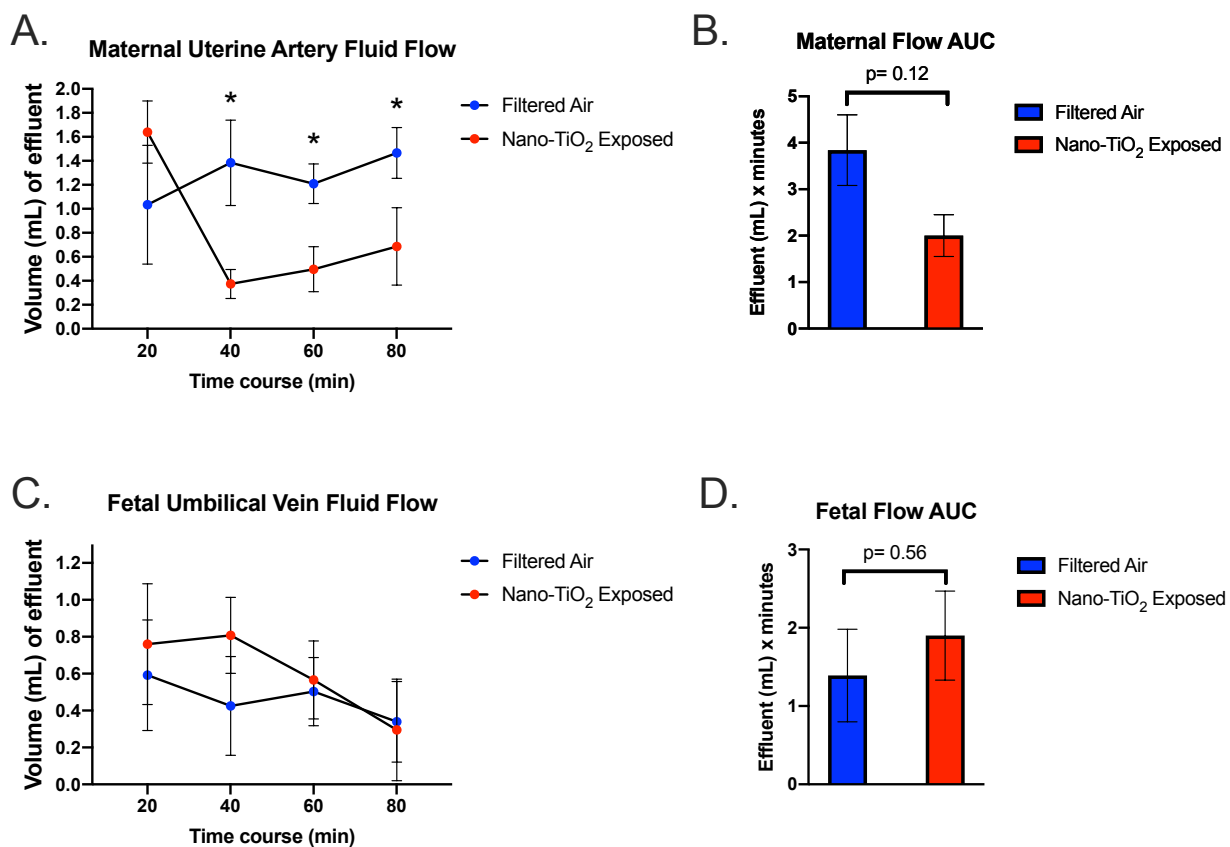


**Figure 3.4. Fluid flow across the maternal uterine artery and through fetal umbilical vein. A.** Fluid flow across the uterine artery pressured at 80 mmHg. Volume of effluent collected and measured from distal end of artery at 20, 40, 60, and 80 minutes.  $n = 4$  dams per group (4 placentas from male fetuses in filtered air group, 3 placentas from male fetuses and 1 placenta from a female fetus in nano-TiO<sub>2</sub> exposed group). Analysis of flow volume at each time point by Student's t-test, mean  $\pm$  SEM reported. \* =  $p < 0.5$ . **B.** Area under the curve analysis of fluid flow through uterine artery over time. Analysis by Student's t-test, mean  $\pm$  SEM reported. **C.** Fluid flow from umbilical vein pressurized at 50 mmHg at 20, 40, 60, and 80 minutes.  $n = 4$  dams per group (4 placentas from male fetuses in filtered air group, 3 placentas from male fetuses and 1 placenta from a female fetus in nano-TiO<sub>2</sub> exposed group). Analysis of flow volume at each time point by Student's t-test, mean  $\pm$  SEM reported. **D.** Area under the curve analysis of fluid flow from umbilical vein over time. Analysis by Student's t-test, mean  $\pm$  SEM reported.

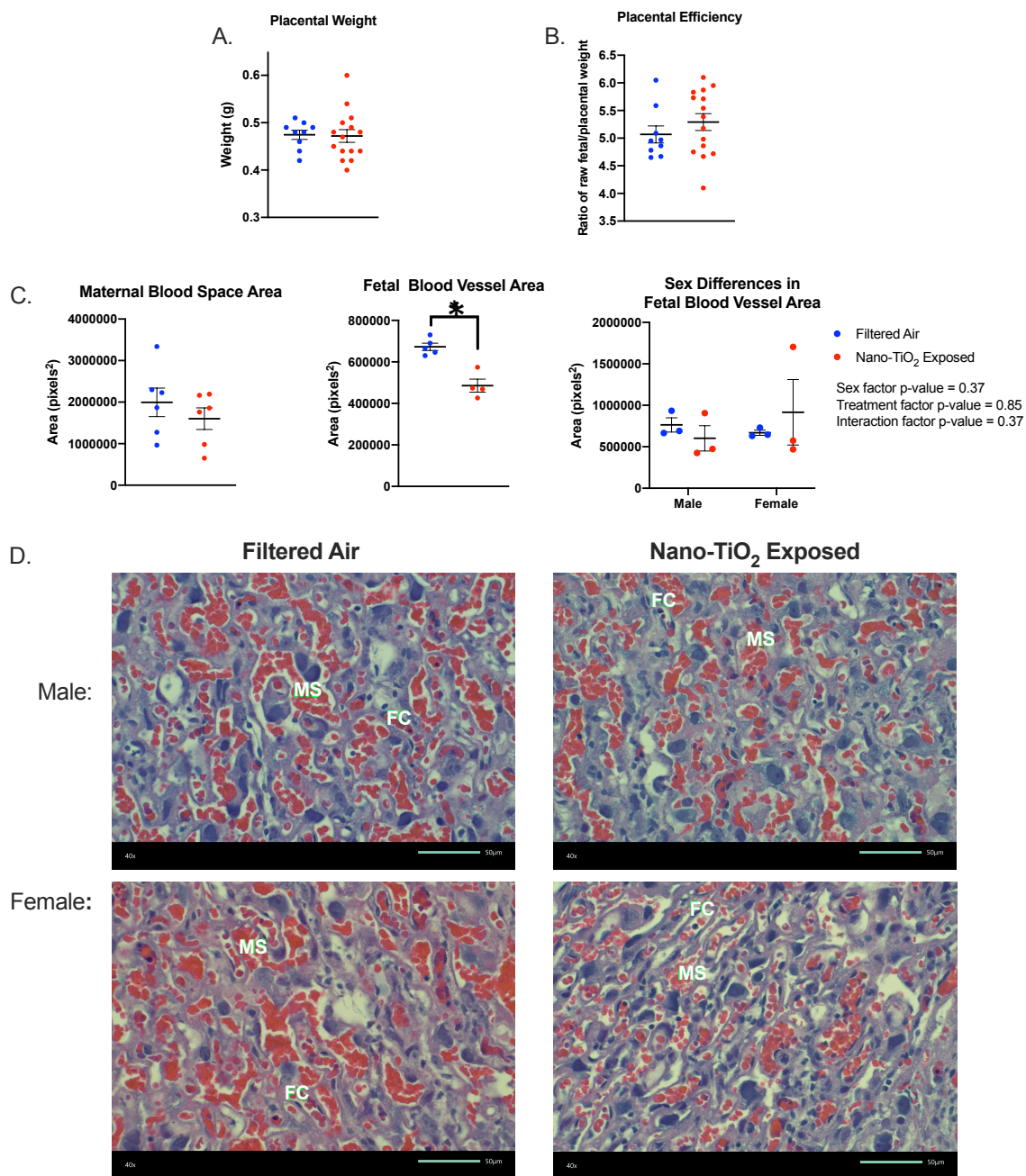


**Figure 3.5. Placental weight and morphometrics.** **A.** Raw placental weights between exposure groups on GD 20. N = 9-15 dams per group. Analysis by Student's t-test, mean  $\pm$  SEM reported. **B.** Placental efficiency (ratio of fetal weight to placental weight) between exposure groups on GD 20. N = 9-15 dams per group. Analysis by Student's t-test, mean  $\pm$  SEM reported. **C.** Area of maternal blood sinusoid and fetal blood capillary of placentas by treatment group and by fetal sex. n = 4-6 dams per exposure group, 3 male and 3 female in each group. Outliers removed by Grubbs' Test. Analysis by Student's t-test, mean  $\pm$  SEM reported. \* = p < 0.05. Analysis by fetal sex by two-way ANOVA and Sivak's multiple comparison post hoc correction. Mean  $\pm$  SEM reported. **D.** Representative H&E staining of the labyrinth zone from male and female placentas between exposure groups. MS= maternal sinusoid, FC= fetal capillary (40X magnification, scale bar = 50 $\mu$ M).

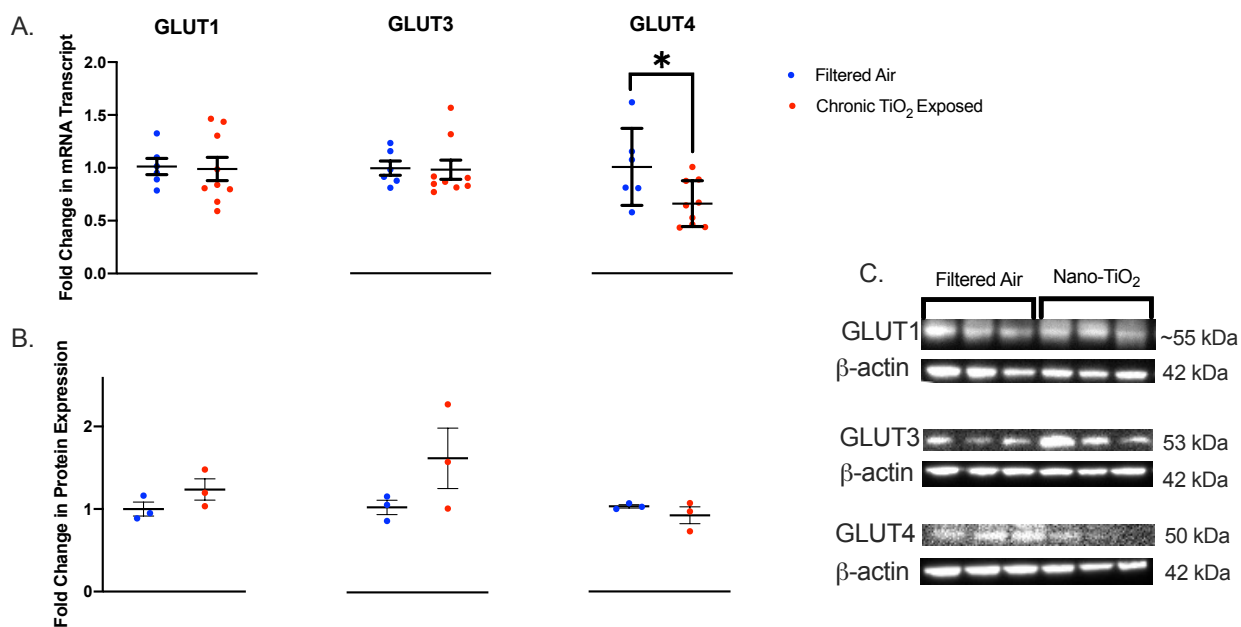


**Figure 3.6. Expression of placental glucose transporter isoforms.** **A.** Placental mRNA expression of GLUT1, GLUT3, and GLUT4 at GD 20 between exposure groups.  $n = 6-9$  dams per group. Analysis by Student's *t*-test, mean  $\pm$  SEM reported.  $* = p < 0.05$ . **B.** Placental protein expression of GLUT1, GLUT3, and GLUT4 on GD 20 between treatment groups.  $n = 3$  dams per group. Analysis by Student's *t*-test, mean  $\pm$  SEM reported. **C.** Immunoblots of individual samples for GLUT1, GLUT3, GLUT4. B-actin was used as the loading control.

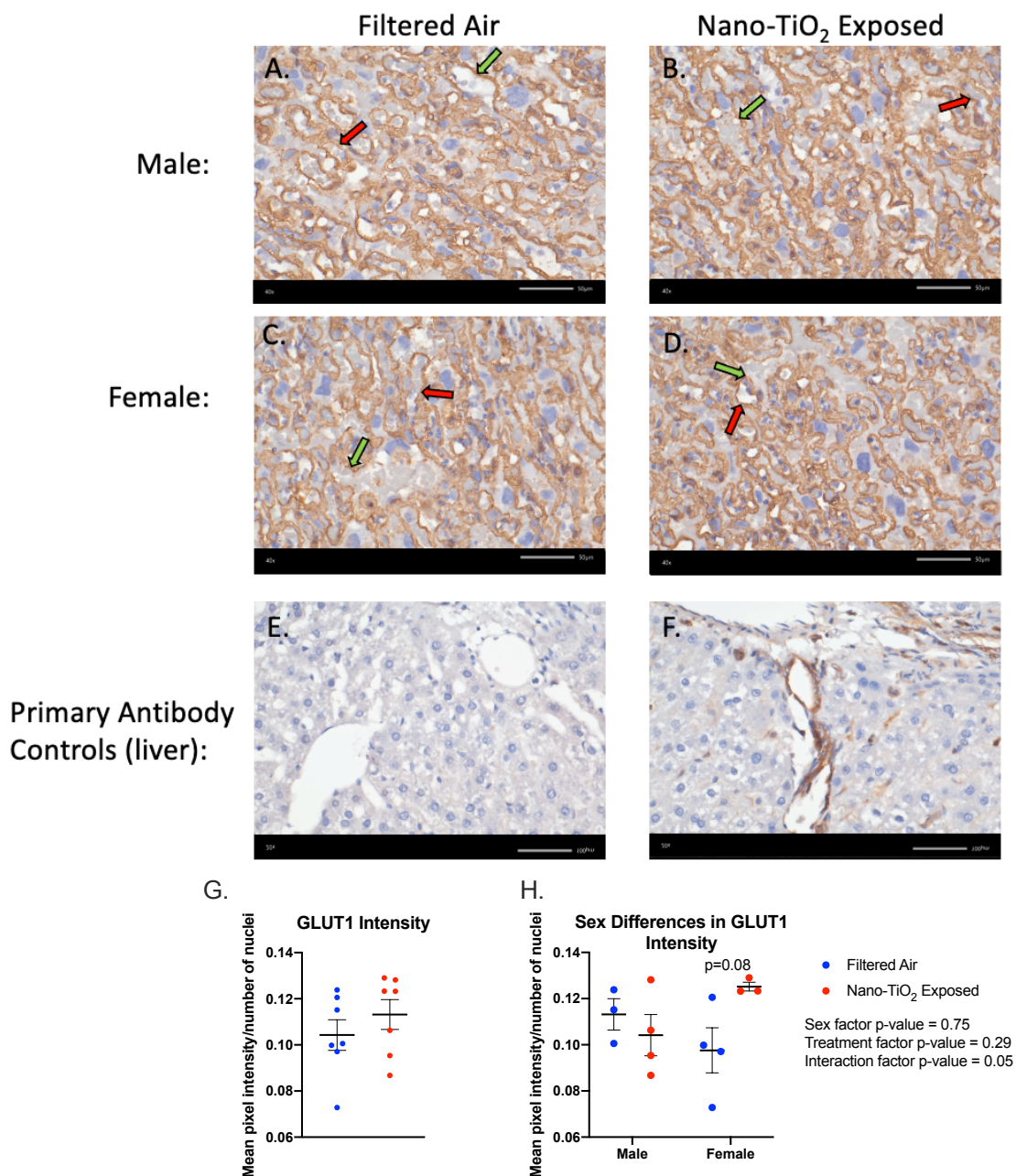


**Figure 3.7. Placenta labyrinth zone syncytiotrophoblast immunolocalization of GLUT1 protein.** GLUT1 protein is stained brown in color. Green arrow = immunolocalization on the maternal blood sinus facing membrane. Red arrow = immunolocalization on the fetal capillary facing membrane. (40X, scale bar 50  $\mu$ M) **A, C.** Representative filtered air exposed placentals, male and female. **B, D.** Representative nano-TiO<sub>2</sub> exposed placentals, male and female. **E.** Negative control liver (no primary antibody applied) (20 X, scale bar 100  $\mu$ M). **F.** Positive control liver (20x, scale bar 100  $\mu$ M). **G.** Intensity of GLUT1 staining normalized by number of nuclei by treatment group. n = 6 dams per group, 1-2 placentas per dam. Analysis by Student's t-test, mean  $\pm$  SEM reported. **H.** Intensity of GLUT1 staining normalized by number of nuclei by treatment group by fetal sex. Analysis by two-way ANOVA and Sivak's multiple comparison post hoc correction. Mean  $\pm$  SEM reported.

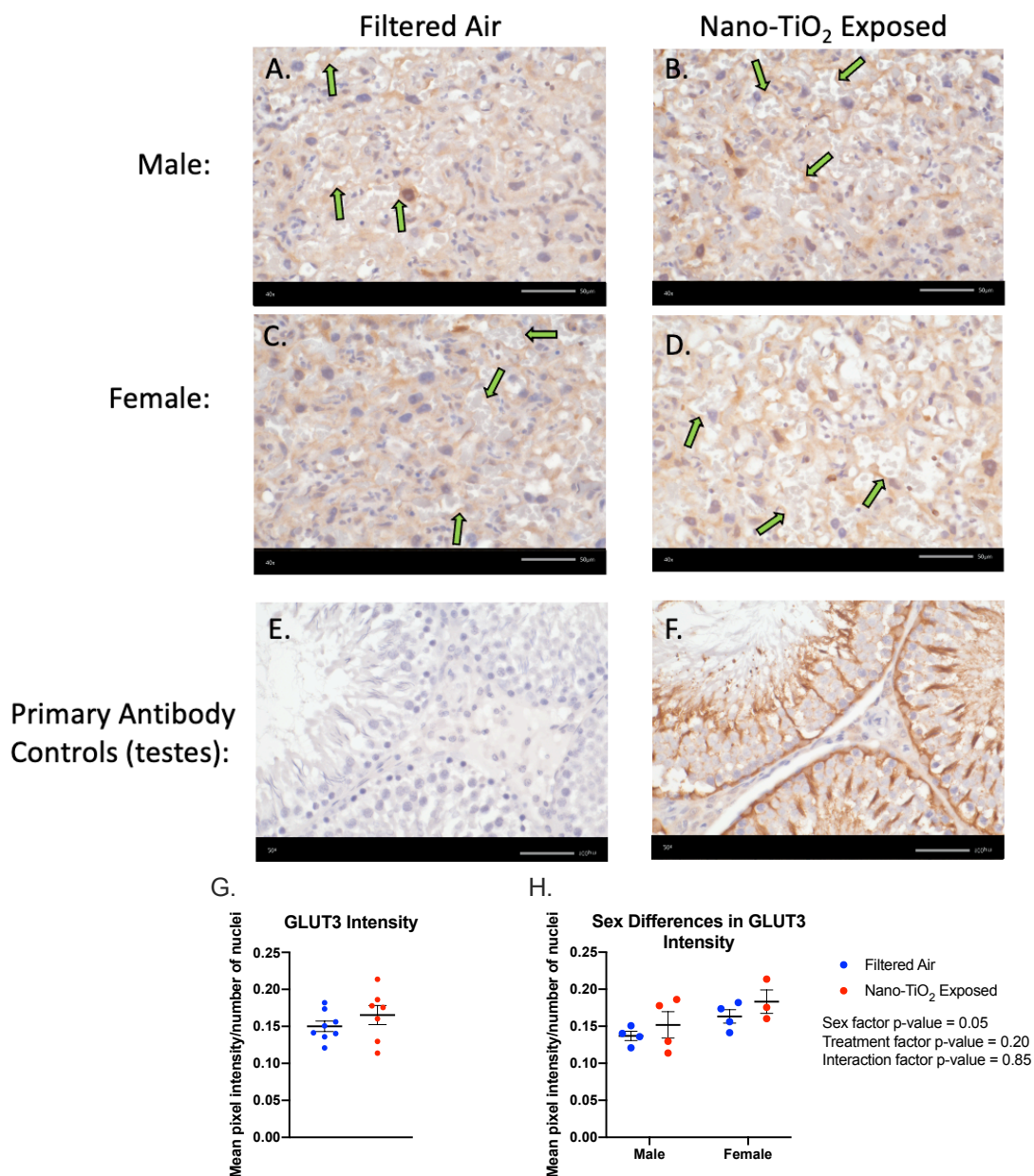


**Figure 3.8. Placenta labyrinth zone syncytiotrophoblast immunolocalization of GLUT3.** GLUT3 protein is stained brown in color. Green arrow = immunolocalization to the maternal blood sinus facing membrane. (40X, scale bar 50  $\mu$ M) **A, C.** Representative filtered air control placentas, male and female. **B, D.** Representative nano-TiO<sub>2</sub> exposed placentas, male and female. **E.** Negative control testes (no primary antibody applied) (20 X, scale bar 100  $\mu$ M). **F.** Positive control testes (20 X, scale bar 100  $\mu$ M). **G.** Intensity of GLUT3 staining normalized by number of nuclei by treatment group. n = 6 dams per group, 1-2 placentas per dam. Analysis by Student's t-test, mean  $\pm$  SEM reported. **H.** Intensity of GLUT3 staining normalized by number of nuclei by treatment group by fetal sex. Analysis by two-way ANOVA and Sivak's multiple comparison post hoc correction. Mean  $\pm$  SEM reported.

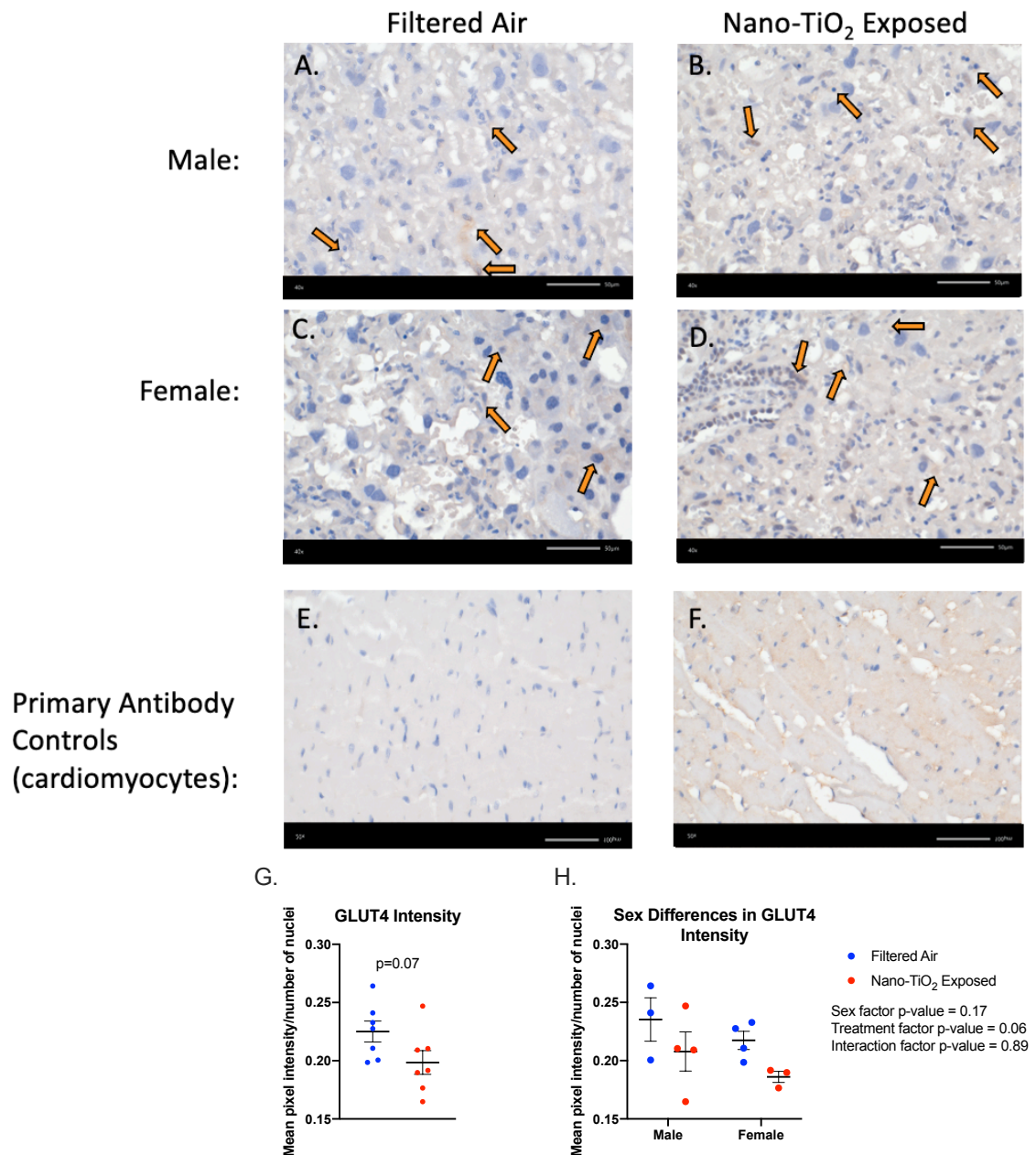


**Figure 3.9. Placenta labyrinth zone syncytiotrophoblast immunolocalization of GLUT4.** GLUT4 protein is stained brown in color. Orange arrow = perinuclear immunolocalization in the cytosol (40X, scale bar 50  $\mu$ M) **A, C.** Representative filtered air control placentas, male and female. **B, D.** Representative nano-TiO<sub>2</sub> exposed placentas, male and female. **E.** Negative control cardiomyocytes (no primary antibody applied) (20 X, scale bar 100  $\mu$ M). **F.** Positive control cardiomyocytes (20 X, scale bar 100  $\mu$ M). **G.** Intensity of GLUT4 staining normalized by number of nuclei by treatment group.  $n = 6$  dams per group, 1-2 placentas per dam. Analysis by Student's t-test, mean  $\pm$  SEM reported. **H.** Intensity of GLUT4 staining normalized by number of nuclei by treatment group by fetal sex. Analysis by two-way ANOVA and Sivak's multiple comparison post hoc correction. Mean  $\pm$  SEM reported.

**CHAPTER 4: SEX-DEPENDENT PLACENTAL CHANGES IN GLUCOSE  
METABOLISM AND ENERGY STATUS IN RESPONSE TO MATERNAL TITANIUM  
DIOXIDE NANOPARTICLE AEROSOL EXPOSURE**

Jeanine N D'Errico<sup>a</sup>, Pedro Lauro<sup>b</sup>, Chelsea M Cary<sup>a</sup>, Phoebe A Stapleton<sup>a,c</sup>

**Affiliations:**

- a. Department of Pharmacology and Toxicology, Ernest Mario School of Pharmacy, Rutgers University, 160 Frelinghuysen Rd., Piscataway, NJ 08854, USA; b. Histopathology Core Facility, 41 Gordon Road, Piscataway, NJ 08854, USA, c. Environmental and Occupational Health Sciences Institute, 170 Frelinghuysen Rd., Piscataway, NJ 08854, USA

#### 4.1 Abstract

Human and animal studies have correlated particulate matter (PM) inhalation with FGR. FGR is often due to reduced fetal nutrition. From the work in chapter 3, our laboratory has modeled maternal PM inhalation with nano-TiO<sub>2</sub> and identified a reduction in fetal blood glucose while maternal blood glucose was unchanged. Notably, this was more severe if the conceptus was male. The placenta is responsible for glucose transfer during pregnancy. It also has a high requirement for glucose to sustain high metabolic activity. It was hypothesized that gestational nano-TiO<sub>2</sub> exposure leads to increased placental glucose metabolism and decreased placental energy status, thereby reducing the amount of glucose available for fetal supply. Additionally, these changes were expected to occur to a greater extent in male placentas. To test this theory, time-pregnant Sprague-Dawley rats were exposed to HEPA filtered air or nano-TiO<sub>2</sub> aerosols ( $9.96 \pm 0.06 \text{ mg/m}^3$ ) between GD 4 and GD 19. Animals were necropsied on GD 20 where fetal sex was determined by testes or uterine horn visualization. Blood collected from the fetal circulation in the placenta was assayed for glucose and lactate. Labyrinth zone tissue was harvested for cellular HK, PFK, and LDH activity. Colorimetric assays were used to evaluate AMP and NAD<sup>+</sup>/NADH ratios. Junctional zone Periodic Acid Schiff (PAS) staining aided in visualization of placental glycogen reserves. Blood glucose from the fetal side of the placenta was significantly reduced, but lactate concentration was unchanged. Male placentas had 66% HK activity decrease, however PFK and LDH activity were increased by 57% and 46%, respectively. Additionally, a significant 35% increase in AMP and 41% increase of total NAD was measured. In contrast, in female placentas had HK and PFK activities decreased by 60% and 67%, respectively, and LDH activity was increased by 19%. Additionally, a 9% reduction in AMP and significant 41% increase in total NAD was identified. No difference in NAD<sup>+</sup>/NADH or glycogen reserves was found in placentas for either sex. The results from this study demonstrate a sex-dependent change in glucose metabolism and energetic status in response to gestational nano-TiO<sub>2</sub> exposure; female placentas reduced

glycolytic activity however were not energetically compromised, whereas male placentas did not exhibit significant change to glycolytic activity but remained at a compromised energetic state. The decrease or lack of change in glycolytic enzyme activity per sex and significant increase in LDH activity are not in line with a shift to anaerobic metabolism from placental ischemia or hypoxia. It can be concluded from these data that glycolysis is not increased with nano-TiO<sub>2</sub> exposure. Additionally, increased or decreased oxidative phosphorylation in females and males, respectively, cannot be ruled out. A switch to an alternate metabolic fuel, such as fatty acids in female placentas, is another theory that cannot yet be excluded. In conclusion, sex-dependent decreases in glucose metabolism and energy status were identified and may play a role in compromised placental nutrient transfer to the fetus.

#### **4.2 Introduction**

NP exposure, encompassing the fields of PM<sub>0.1</sub> and engineered nanomaterials, has been linked with negative effects during pregnancy (Zheng et al. 2016). Human and animal studies have identified fetal abnormalities (i.e., FGR (Blum et al. 2017), preterm birth (Zhang et al. 2020)) and increased risk for offspring disease (i.e., cardiovascular disease, Type 2 diabetes, cancers, and learning disorders (Simmons 2009)), making gestational exposure to NPs a public health issue concerning our future generations. Contributing to this body of research, our laboratory has identified a model of fetal hypoglycemia after gestational PM exposure. However, the link between maternal exposure and neonatal outcomes has yet to be identified.

Studies have consistently found that the placenta is impacted after maternal NP inhalation. Two mouse studies that have administered nose-only nano-silver or single-wall carbon nanotubes repeatedly through gestation incited release of inflammatory mediators from the placenta (Campagnolo et al. 2017a; Pietroiusti et al. 2011). A multi-walled carbon nanotube study in mice found a decrease in the number and size of blood vessels in the placenta (Qi et al. 2014). Other

studies have found that maternal exposure to PM<sub>10</sub> and PM<sub>2.5</sub> disrupted protein transport, ATP-dependent processes, and damaged mitochondrial function by decreasing DNA content of the placental syncytiotrophoblasts (Deysenroth et al. 2021; Janssen et al. 2012). Due to the positioning of the placenta between maternal and fetal blood circulations and responsibility for nutrient transfer, the placenta should be a key focus of toxicologic assessment after NP exposure.

The syncytiotrophoblasts of the placenta form a unique epithelium with regards to glycolysis and glucose transport to the fetus. The placenta is situated to absorb and transfer nutrients to the fetal blood in support of growth and development. However, the syncytiotrophoblasts are also evolving and highly metabolically active (Vaughan and Fowden 2016). Glucose is vital to maintain normal cellular energy and function, and aberrant glucose metabolism has been linked with a range of gestational pathologies (i.e. preeclampsia) (Wallis et al. 2008). Glucose is a paramount energy source largely metabolized by the syncytiotrophoblast cells. In sheep it has been shown that approximately 50% of total glucose supplied to the uterus near term is oxidized by the placenta, with another 20% being sent to the fetus and the remainder converted to lactate (Gu et al. 1987). ATP-driven processes such as protein production of hormones and nutrient transport consume as much as 50% of total ATP use in the ovine placenta (Hay 1991a). Therefore, the placenta requires a large amount of glucose-derived energy and must balance this against the evolving glucose demands of the fetus (Michelsen et al. 2018). If this biology is disturbed, it may be central to the pathogenesis of many gestational disorders.

There are several approaches that can be used to evaluate glycolytic activity of the placenta. A general approach to measure glycolytic flux in *ex vivo* tissue or *in vitro* cell culture is indirect quantification by measuring glucose uptake and lactate excretion (TeSlaa and Teitell 2014). Bringing this approach into *ex vivo* human and rodent placenta models, measurement of glucose and lactate on the fetal side of the syncytium can infer syncytial glucose consumption and lactate

production. Additionally, harvesting placental labyrinth tissue to measure the activity of the rate limiting enzymes of glycolysis, namely HK and PFK, can give an indication of the maximum possible flux through the glycolytic pathway (TeSlaa and Teitell 2014) (**Figure 1.2**). HK is the first enzyme of glycolysis that traps glucose within cells by using ATP to convert glucose to G-6-P (Roberts and Miyamoto 2015). G-6-P can then enter the pentose phosphate pathway or continue down the glycolytic pathway. PFK irreversibly commits G-6-P to the glycolytic pathway (Nakajima 1995). There are some studies that have used enzyme activity assays to understand this pathway in the placenta (Khoja and Salem 1991; Maria Edesina Aguiar 1980). Therefore, extracellular glucose and lactate in combination with glycolysis enzyme activity can provide information on the glycolytic activity.

Some *ex vivo* and *in vitro* evidence links alterations in placental glucose metabolism with reduced glucose transfer. Under anoxic conditions, *ex vivo* perfused human placentas uptake and consume more glucose from the maternal compartment and transport less to the fetal compartment (Illsley et al. 1984). At high altitude (>2700 m above sea level), the human placenta metabolizes more glucose and transports less as indicated by markedly reduced umbilical venous glucose measurements (Zamudio et al. 2010). When placental demand for glucose increases modeled as conditions such as glycolytic stimulation for anerobic metabolism in BeWo *in vitro* transwell studies, transepithelial transport to the fetus diminishes (Vardhana and Illsley 2002). Conversely, human placentas from preeclamptic pregnancies complicated by FGR had low levels of pyruvate and lactate indicative of impaired glycolysis (Bloxam et al. 1987). Unfortunately, this study did not assess offspring glucose concentrations at birth. Products of tobacco smoke have also been shown to cause hypoxia to the syncytiotrophoblast in humans, which results in cellular respiration enzyme activity changes (Kaiglová et al. 2001). For example, human exposure to environmental cigarette smoke throughout pregnancy increased placental LDH activity and is associated with hypoxia and a shift towards anerobic metabolism (Kaiglová et al. 2001). Altogether, the evidence suggests that

changes in placental glucose metabolism after various maternal stressors may explain reduced glucose availability to the fetus and elevate the risk for disorders (e.g., FGR, fetal hypoglycemia). Currently, there is a gap of knowledge about gestational exposure to environmental NPs that cause changes to enzymatic activities involved in glycolysis of the placenta.

Maternal exposures have been shown to affect offspring development in a sex-dependent manner in rodent models (Bara et al. 2018; Schneider et al. 2016). The placenta is one of the earliest organs developed after fertilization that carries the X- and Y- chromosome-linked genes, giving rise to some sex-specific processes. One such critical process that has been well-studied is growth trajectory, where it has been shown in mice models that sex hormones and growth factors play a role in nutrient sensing and transfer depending on fetal sex (Mao et al. 2010). Thus, sex-dependent differences in metabolism may be the molecular mechanisms connecting gestational exposure and sex-related outcomes for the offspring. To date, this has not been looked at within the context of NP exposure and placental metabolism.

The purpose of this study was to evaluate the sex-dependent changes in placental glycolysis and energy status in response to maternal nano-TiO<sub>2</sub> inhalation. To this end, nano-TiO<sub>2</sub> was utilized as a model to simulate gestational aerosol exposure.

### **4.3 Materials and Methods**

#### *Chemicals*

Protease inhibitor cocktail II was purchased from Calbiochem (539136, San Diego, CA). Hemoglobind<sup>TM</sup> was purchased from BioTech Support Group (H0145-05, Monmouth Junction, NJ). 10kDa Spin Columns were purchased from Abcam (ab93349, Cambridge, UK). Peirce BSA Assay kit was purchased from ThermoFisher (23225, Waltham, MA).

### *Whole-body nanoparticle exposure*

Time pregnant rats (Charles River Laboratories (Kingston, NY) (n=6 dams per group) were administered whole-body exposure to HEPA filtered air or nano-TiO<sub>2</sub> between GD 4 and GD 19 as described in previous chapters. Animals were exposed to aerosols at an average concentration of  $9.96 \pm 0.06$  mg/m<sup>3</sup> and particle size of  $175.91 \pm 3.35$  nm.

### *Perfusion of placental labyrinth blood*

Animals were placed under anesthesia with 5% induction and 3% maintenance of isoflurane gas. The right uterine horn was removed and further dissected to isolate placental units (i.e., uterine artery segment, entire arcuate and radial network connecting to the uterine myometrium and placenta, and umbilical cord) for transfer to a modified microvessel chamber as previously described for *ex vivo* placental perfusion (**Appendix 2**) (D'Errico et al. 2019). Blood present in the labyrinth zone on the fetal side of the placenta was perfused out with 100  $\mu$ L of PSS and collected from the umbilical vein for further processing.

### *Glucose and lactate quantification*

Blood glucose concentrations on the fetal side labyrinth tissue was measured using TRUTrack blood glucose meter (Trividia Health, Fort Lauderdale, FL). Blood lactate concentrations were measured using an L-Lactate Assay Kit (ab65331, Abcam, Cambridge, UK).

### *Tissue collection and processing*

From each dam, six placentas were collected (right and left horn ovary, middle, and cervical positions) to ensure enough tissue was collected for each subsequent analysis and to represent a mix of implantation sites. One quarter of each placenta was cut away and further dissected to separate decidua/junctional tissue from the labyrinth tissue. Labyrinth tissue was then further dissected into 3 aliquots. For each placenta the sex of the respective fetus was determined by

visualization of testes or uterine horns and recorded. Samples were snap frozen as quickly as possible in liquid nitrogen to reduce tissue degradation and stored at -80 °C for further processing.

*Sample hemoglobin removal by 10kDa spin column and Hemoglobind<sup>TM</sup>*

Hemoglobin is an effective light absorber at wavelengths below 600 nm (Uyuklu et al. 2011). The kits selected to assay our desired small molecule concentrations and enzyme activities require absorbance measurements at 450 nm and 570 nm. Therefore, the presence of hemoglobin from red blood cell rupture due to the freeze-thaw process of labyrinth tissue samples presented an optical density interference and required removal to proceed. To separate the desired analytes from the interfering hemoglobin, two approaches were developed depending on the molecular weight of the analyte. First, for measurement of small molecule concentrations (i.e., AMP, NAD<sup>+</sup>/NADH) a spin column with a 10 kDa (ab93349, Abcam, Cambridge, UK) pore size was used to trap larger molecules (i.e., hemoglobin in tetramer or monomer configuration) (**Figure 4.1**) and other proteins larger than 10 kDa (**Figure 4.2**) before the column. Samples were added to pre-column compartment and centrifuged at 12,000 (AMP) or 13,000 g (NAD<sup>+</sup>/NADH) for 30 minutes at 4 °C. This allowed for flow through and collection of smaller molecules for quantification without hemoglobin or protein interference. Second, for large enzyme activity assays (i.e., HK, PFK, and LDH that weigh approximately 100 kDa, 85 kDa, and 140 kDa, respectively), a 1:1 volume of the product Hemoglobind<sup>TM</sup> (H0145-05, Biotech Support Group, Monmouth Junction, NJ) was added to all samples. Samples were then mixed on a plate shaker for 10 minutes and centrifuged at 10,000 g for 2 minutes at 4 °C to pellet Hemoglobind<sup>TM</sup>:Hemoglobin complexes. The hemoglobin-free supernatant was then collected and transferred to new microtubes in preparation for enzymatic activity analyses.

To confirm hemoglobin removal by both 10 kDa spin column and Hemoglobind<sup>TM</sup> approaches, UV spectrum measurements were taken using a NanoDrop<sup>TM</sup> 2000/2000c spectrophotometer (ND-

2000, Thermo Fisher, Waltham, MA). For the first approach using 10 kDa spin columns, 2  $\mu$ L samples were taken from the crude sample homogenate before centrifugation, and after centrifugation from the pre-column and post-column compartments for UV spectrum analysis (**Figure 4.1A and 4.1B**). From this, optical densities at 540 nm were used to calculate molarity of oxyhemoglobin present in the sample using the Beer Lambert Law (**Figure 4.1C**). Similarly, for the Hemoglobind<sup>TM</sup> approach, UV spectrum measurements were taken from 2  $\mu$ L samples before and after addition to the samples to ensure the appropriate ratio (4:1, 3:1, 2:1, 1:1) of sample to Hemoglobind<sup>TM</sup> for optimal hemoglobin removal (**Figure 4.3**). The concentration of oxyhemoglobin in the samples were calculated using the Beer Lambert Law according to the following equation:  $A = \epsilon bc$ , where  $A$ = absorbance,  $\epsilon$ = molar extinction coefficient,  $b$ = length of path light, and  $c$ = concentration. The molar extinction coefficient used for oxyhemoglobin at 540 nm was 53,236  $\text{cm}^{-1}/\text{M}$  (Prahl 1998) and length of path light for the spectrophotometer was 0.1 cm.

#### *Hexokinase enzyme activity*

Hexokinase Activity Colorimetric Assay Kit was purchased from Abcam (ab136957, Cambridge, UK). In this assay, HK converts glucose to G-6-P, which is then oxidized by G-6-P dehydrogenase to form NADH. The NADH produced from this reaction then donates a proton to a dye (Formazan) to produce a blue colored product with a strong absorbance at 450 nm. The absorbance is proportional to the amount of NADH produced by HK enzyme activity. Labyrinth tissue aliquots were thawed (10 mg), washed thoroughly in ice-cold PBS, and homogenized in 200  $\mu$ L of ice cold Assay buffer with a 1:500 mixture of Calbiochem Protease Inhibitor Cocktail IV. Samples were centrifuged at 12,000 g for 5 minutes at 4°C. The supernatant was transferred to a new microfuge tube and a 1:1 volume of Hemoglobind<sup>TM</sup> (H0145-05, Biotech Support Group, Monmouth Junction, NJ) was added to the sample. Samples were left on a plate shaker at 90 rpm for 10 minutes at room temperature then centrifuged at 9,000 g for 10 minutes at 4 °C to pellet hemoglobin complexes.

The resulting clear supernatant was transferred to a new microfuge tube. A protein assay (Pierce BSA Protein Assay Kit 23225) was conducted on all samples. 0

A NADH standard curve was prepared for end concentrations of 0, 2.5, 5, 7.5, 10, and 12.5 nmol/well. From the protein assay, a calculated volume of each sample was added in duplicate so that 40  $\mu$ g of protein was added to the assay plate. A 5  $\mu$ L volume of a positive control provided by the manufacturer was added in duplicate. All samples and positive controls were brought up to 50  $\mu$ L with assay buffer. 50  $\mu$ L of a reaction mix were added to each sample and positive control. Optical densities were read at 450 nm at 30 and 40 minutes while incubating at room temperature. Enzyme activity for each sample was determined by NADH (nmol) produced per minute of reaction time per mg protein.

#### *Phosphofructokinase enzyme activity*

6-Phosphofructokinase Activity Colorimetric Assay Kit was purchased from Abcam (ab155898, Cambridge, UK). In this assay, PFK uses ATP to convert F-6-P to fructose-diphosphate and ADP. ADP is then converted to AMP and NADH in the presence of the assay kit substrate and enzyme mix. The NADH produced from this reaction then donates a proton to a colorless dye (Formazan) which then produces a blue colored product with a strong absorbance at 450 nm. The absorbance is proportional to the amount of NADH produced by PFK activity. Labyrinth tissue aliquots were thawed (20 mg), washed thoroughly in ice-cold PBS, and homogenized in 100  $\mu$ L of ice-cold assay buffer that contained a 1:500 mixture of Calbiochem Protease Inhibitor Cocktail IV. Samples were centrifuged at 12,000 g for 10 minutes at 4 °C. Supernatant was transferred to a new tube and a 1:1 volume of HemogloBind™ (H0145-05, Biotech Support Group, omouth Junction, NJ) was added to the sample to bind and remove hemoglobin. Samples were left on a plate shaker at 90 rpm for 10 minutes at room temperature then centrifuged at 9,000 g for 10 minutes at 4 °C to pellet

hemoglobin complexes. The resulting clear supernatant was transferred to a new microfuge tube. A protein assay (Pierce BSA Protein assay Kit 23225) was conducted on all samples.

A fresh NADH standard curve was prepared for end concentrations of 0, 2, 4, 6, 8, and 10 nmol/well. From the protein assay, volumes were calculated to add 100  $\mu\text{g}$  of protein to each well in two sets of duplicates (Sample and Sample Background Control). A positive control provided by manufacturer was added in triplicate of 10  $\mu\text{L}$ . All samples and positive control wells were brought up to 50  $\mu\text{L}$  with assay buffer. 50  $\mu\text{L}$  of a reaction mix was added to each standard, sample, and positive control. 50  $\mu\text{L}$  of a background reaction mix that did not contain the enzyme substrate was added to sample background control wells. Optical densities were read at 450 nm at 1 and 20 minutes while incubating at 37  $^{\circ}\text{C}$ . The average absorbance values for samples were corrected by the average absorbance values from background control samples. Enzyme activity for each sample was determined by NADH (nmol) produced per minute of reaction time per mg protein.

#### *Lactate dehydrogenase activity*

A Lactate Dehydrogenase Colorimetric Assay kit was purchased from BioVision (K726-500, San Francisco, CA). In this assay protocol LDH reduces  $\text{NAD}^+$  to NADH. The NADH produced from this reaction then reduces a probe that is colorless under basal conditions to produce a yellow-colored product with strong absorbance at 450 nm. The absorbance is proportional to the amount of NADH produced by LDH enzyme activity. Labyrinth tissue aliquots were thawed (75 mg), washed in ice-cold PBS, and homogenized in 500  $\mu\text{L}$  ice cold assay buffer with a 1:500 mixture of Calbiochem Protease Inhibitor Cocktail IV. Samples were centrifuged at 10,000 g for 15 minutes at 4  $^{\circ}\text{C}$ . The supernatant was collected and transferred to a new microfuge tube. A 1:1 volume of Hemoglobind<sup>TM</sup> (H0145-05, Biotech Support Group, omouth Junction, NJ) was added to the samples. Samples were left on a shaker at 90 rpm for 10 minutes at room temperature then centrifuged at 9,000 g for 10 minutes at 4  $^{\circ}\text{C}$  to pellet hemoglobin complexes. The resulting clear

supernatant was transferred to a new microfuge tube. A protein assay (Pierce BSA Protein Assay Kit 23225) was conducted on all samples.

A standard curve of 0, 2, 4, 6, 8, and 10 nmol NADH was prepared fresh. A volume of 5  $\mu$ L of each sample was added in duplicate, where the concentration of protein in the sample was later calculated from the protein assay. A 2  $\mu$ L volume of a positive control provided by the manufacturer was added in duplicate. All sample and positive control wells were brought up to 50  $\mu$ L with assay buffer. A volume of 50  $\mu$ L of assay buffer was added as background control. A reaction mix was prepared and 50  $\mu$ L added to all standard, sample, and positive control wells. Optical densities were measured at 450 nm at 0, 1, and 2 minutes while incubating at 37°C. The average absorbance values for samples were corrected by the average absorbance values from assay buffer background. Enzyme activity for each sample was calculated by NADH (nmol) per minute of reaction time per mg protein.

#### *Cellular AMP*

AMP Colorimetric Assay Kit was purchased from BioVision (K229-100, San Francisco, CA). In this assay protocol AMP is converted to pyruvate by pyruvate phosphate dikinase in the presence of pyrophosphate and phosphoenolpyruvate. Pyruvate is then enzymatically converted to an oxidizing agent that oxidizes a colorless probe to a yellow- colored product with strong absorbance at 570 nm. The absorbance is proportional to the concentration of AMP in the sample. Two aliquots of 10 mg labyrinth tissue were thawed, washed thoroughly in ice-cold phosphate buffered saline (PBS) and homogenized in ice-cold assay buffer with 50 passes of Dounce homogenizer. Samples were left on ice for 10 minutes then centrifuged for at 10,000 g for 10 minutes at 4 °C. Supernatants were collected and filtered through at 10kDa spin column at 12,000 g for 30 minutes at 4 °C. The flow through was collected for a protein assay (Pierce BSA Protein Assay Kit 23225) and for AMP analysis.

For AMP Colorimetric Assay 10  $\mu\text{L}$  of sample flow through were added to a 96 well plate. A subset of samples for each treatment group were used as AMP Spike and another subset for background control. A standard curve of 0, 2, 6, 8, and 10 nmol AMP was prepared. Optical densities for the standard curve and samples were read at 570 nm after 35 minutes of incubation at 37  $^{\circ}\text{C}$ . AMP was normalized to sample mg protein determined by protein assay.

#### *Cellular NAD<sup>+</sup>/NADH*

NAD<sup>+</sup>/NADH Colorimetric Assay Kit was purchased from Abcam (ab65348, Cambridge, UK). In this assay, a NAD cycling mix specifically acts on NADH and NAD<sup>+</sup> in an enzyme cycling reaction which turns a colorless probe a yellow-colored product that has a strong absorbance at 450 nm. Labyrinth tissue aliquots (20 mg) were thawed, washed thoroughly in ice-cold PBS, and added to a sterile microfuge tube in 400  $\mu\text{L}$  of ice-cold assay buffer. Tissues were rapidly homogenized with 50 passes of sterile hand Dounce homogenizer. Samples were centrifuged at top speed for 5 minutes at 4  $^{\circ}\text{C}$ , transferred to a 10kDa spin column, and centrifuged again at 13,000 g for 30 minutes at 4  $^{\circ}\text{C}$ . From the flow through, a protein assay (Pierce BSA Protein Assay Kit 23225) and NAD<sup>+</sup>/NADH Colorimetric Assay were conducted. For the samples designated as NADH, the sample NAD<sup>+</sup> was decomposed by placing on a heating block at 60  $^{\circ}\text{C}$  for 30 minutes.

For the NAD<sup>+</sup>/NADH assay a fresh NADH standard curve of 0, 20, 40, 60, 80, and 100 pmol/well was prepared. A volume of 25  $\mu\text{L}$  of each sample was added in duplicate. Sample volumes were brought up to 50  $\mu\text{L}$  with assay buffer. A NAD cycling reaction mix was prepared and 50  $\mu\text{L}$  added to each standard and sample well. The plate was left to incubate for 5 minutes at room temperature. A volume of 10  $\mu\text{L}$  of NADH Developer was then added to each well and assay plate was mixed on jitter bug. Optical densities were read at 450 nm after 60 minutes of incubation at room temperature. NAD<sup>+</sup> and NADH were normalized to sample mg protein determined by protein assay.

### *Glycogen storage*

Placentas were cut in half using a sterile razor blade and drop-fixed in 10% neutral buffered formalin. Tissues were sliced in paraffin sections, deparaffinized and hydrated with water. A 0.5% periodic acid solution was applied for 5 minutes then rinsed in distilled water. Slides were placed in Schiff reagent for 15 minutes to stain glycogen magenta, washed in water for 5 minutes, and counterstained hematoxylin for a background blue color for 1 minute. Slides were washed in water for 5 minutes, dehydrated and cover slipped.

### *Statistics*

A Shapiro-Wilk test was performed on data presented by treatment group to confirm normal distribution and then were analyzed by Student's t-test. Data presented by treatment group by fetal sex were analyzed with a two-way ANOVA with a Sidak's multiple comparisons test. Statistics were conducted and graphs created using GraphPad Prism 8 (Version 8.4.3)

## **4.4 Results**

### *Demonstration of hemoglobin and protein removal by 10 kDa spin column using naïve labyrinth tissue*

Microfuge columns with 10 kDa pore sizes were used to remove hemoglobin (**Figure 4.1A**) and protein (**Figure 4.2A**) from tissue homogenate supernatant samples that might interfere with AMP and NAD<sup>+</sup>/NADH assays. Hemoglobin was concentrated pre-spin column and removed from sample flow-through demonstrated at the 410 nm peak (**Figure 4.1B**). An average of 84.8% of protein was removed by centrifugation with a spin-column by comparing crude homogenate and post-centrifugation flow through (**Figure 4.2B**).

### *Hemoglobin removal by HemogloBind™*

Hemolysis presented an optical density interference issue when homogenizing placental labyrinth tissue to evaluate large enzyme activities by colorimetric analyses. The product HemogloBind™ is engineered to deplete hemoglobin from hemolyzed blood or tissue samples. Hemoglobin has a strong spectrum peak at 540 nm. Herein different ratios of sample to HemogloBind™ were tested and the UV spectrum of each sample was measured (**Figure 4.3A**). Optical density at 540 nm was used to compare and ascertain the best ratio for hemoglobin depletion (**Figure 4.3B, 4.3C**).

#### *Extracellular glucose and lactate*

Significantly lower blood glucose concentrations (22%) indicate less placental transfer and possibly increased glucose consumption by the placenta (**Figure 4.4A**). No change in lactate (5.8 nmol/μL vs 5.9 nmol/μL) suggests there is no change in the production of lactate by the labyrinth zone (**Figure 4.4B**).

#### *Hexokinase activity*

In placentas from nano-TiO<sub>2</sub> exposed dams, there was a 63% reduction in HK enzymatic activity (**Figure 4.5B**). Male placentas had a 66.1% reduction and female placentas had a 60% reduction in activity compared to filtered air control counterparts, suggesting a decreased HK potential for activity after nano-TiO<sub>2</sub> exposure (**Figure 4.5B**).

#### *Phosphofructokinase activity*

A 33% reduction in activity was found in nano-TiO<sub>2</sub> exposed placentas (**Figure 4.6B**). In male placentas, PFK activity was increased by 57%. In contrast, activity was significantly reduced by 67% in female placentas (**Figure 4.6B**). These results suggest PFK activity potential may be reduced specific to female placentas after nano-TiO<sub>2</sub> exposure.

#### *Lactate dehydrogenase activity*

A significant 49% increase in LDH activity was found in placentas from nano-TiO<sub>2</sub> exposed dams (**Figure 4.7B**). Male placentas exhibited a 46% increase and females exhibited a 19% increase in activity (**Figure 4.7B**). These results may suggest reduced oxygen tension of the placenta and/or reduced pyruvate availability as a substrate for the Krebs cycle after nano-TiO<sub>2</sub> exposure.

#### *Cellular AMP quantification*

There was no difference in cellular AMP between exposure groups (**Figure 4.8B**). When stratifying data by fetal sex, male placentas had a significant 35% increase in AMP, whereas females had a 9% decrease (**Figure 4.8B**). These data could indicate male placentas are energetically compromised after nano-TiO<sub>2</sub> exposure.

#### *Cellular NAD<sup>+</sup>/NADH quantification*

There was significantly more NAD available in tissue from nano-TiO<sub>2</sub> exposed placentas (**Figure 4.9B**). When stratified by fetal sex, this was also true for female exposed placentas compared to female filtered air control (**Figure 4.9B**). The ratio of NAD<sup>+</sup> to NADH was unchanged, indicating no impact on redox potential or generation of cellular energy due to nano-TiO<sub>2</sub> exposure (**Figure 4.9C**).

#### *Glycogen stores*

Placental glycogen storage deficit in male and female placentas was assessed histologically in the glycogen storage cells of the junctional zone by periodic acid-schiff (PAS) stain. Male and female placentas maintained glycogen stores after maternal nano-TiO<sub>2</sub> exposure, indicating no glycogen depletion and glucose mobilization occurred (**Figure 4.10**).

## **4.5 Discussion**

There is little known about the stress response of the placenta after maternal NP exposure. Glycolytic activity and energy status has not been investigated as a mechanism to connect placental metabolism with fetal adverse outcomes such as growth restriction or hypoglycemia. Thus, the purpose of this study was to assess placental glycolytic activity and energy status in response to maternal NP inhalation and stratify this response by fetal sex. Our findings indicate that glycolytic enzyme activity was reduced in female placentas, an indication of less reliance on glucose metabolism. Further, the energy status of male placentas was compromised with exposure, suggesting increased ATP consumption or decreased ATP production. Placental increase in ATP consumption and increased need for glucose may affect the glucose transferred to the fetal compartment measured by fetal blood glucose in the labyrinth zone of the placenta. Interestingly, male placentas were energetically compromised and did not significantly reduce glycolytic activity. Conversely, female placentas were not energetically compromised and reduced activity of glycolytic enzymes. Overall, we found evidence to support perturbed glycolysis and energy homeostasis after maternal NP inhalation throughout pregnancy that may contribute to placental glucose transfer to the fetus.

A critical and unexpected finding in this study was the attenuation of glycolytic enzyme activity and increase in LDH activity. Glycolysis is a tightly regulated metabolic pathway where the rate of enzymes such as HK or PFK are modified according to the energetic needs of the cell. In general, the rate of these enzymes are controlled by the concentration of glucose entering the cell, the relative concentration of critical enzymes, and competition of cofactors and intermediates (Lenzen 2014). One study showed HK activity was downregulated in human endometrial tissue and contributed to the development of preeclampsia (Lv et al. 2018), where another found that experimentally induced gestational diabetes in rats down regulated placental PFK activity (Khoja and Salem 1991). Together, this suggests that placental glycolytic activity is sensitive to the concentration of glucose delivered to uteroplacental tissue by maternal blood. Similarly, a down-

regulation in these enzyme activities in response to maternal NP inhalation was identified, although the mechanisms remain obscure. This could be due to nanoparticle induced ROS (Lee et al. 2016) and/or poor uteroplacental blood flow that has been found in rat models (Stapleton et al. 2013b). Albeit in a different tissue, our findings appear consistent with the effects of whole-body exposure to PM<sub>2.5</sub> on the reduction of glucose metabolism in the livers of mice (Reyes-Caballero et al. 2019). Interestingly, this study also found that exposure increased the oxidative branch of the pentose phosphate pathway, an alternate shunt for glucose to generate ATP, and increased de novo synthesis of fatty acids, another potential energy substrate, in the livers of mice. Therefore, next research should assess if the pentose phosphate pathway and fatty acid findings are consistent in the placenta after maternal NP exposure, which could be the alternate route of energy production and homeostasis in female placentas. Regarding LDH activity, an increase in activity is often associated with reduced oxygen tension as in tissue due to anoxia or hypoxia (Almeida-Val et al. 2011). However, this should also coincide with an increase in glycolytic activity to maintain cellular energy levels, which was not seen from these data. Together, this suggests that the placenta is not anoxic or hypoxic, and therefore is not shifting towards anerobic glucose metabolism. It is possible that the syncytiotrophoblast cells have uncoupled glycolysis with the Krebs cycle. This would allow pyruvate produced from the glycolysis pathway to be converted to lactate and serve as alternate energy fuel for the fetus, and for another substrate (i.e., fatty acids) to feed into the Krebs Cycle for oxidative phosphorylation. However, from the data collected it is difficult to pinpoint the metabolic shifts at play.

The discoveries from this study were in support of the theory that placental energy status may be reduced from NP inhalation exposure. The placenta is a highly metabolically active tissue requiring ATP to maintain homeostasis, protein production, and ATP-driven transporter processes (Hay 1991a). Janssen et al. have identified that PM<sub>10</sub> exposure during pregnancy reduced mitochondrial DNA content as a marker of mitochondrial damage in human placentas, suggesting reduced energy

may be due to impairments in mitochondrial ATP production (Janssen et al. 2012). Drawing upon experiments using other tissues may help further inform the impact on placental mitochondria after NP exposure (Ducray et al. 2017). Hathaway et al. found that gestational whole-body nano-TiO<sub>2</sub> exposure in rats decreased basal and maximal respiration, decreased complex I and complex IV activities, and increased proton leak in the mitochondria in the cardiomyocytes of progeny (Hathaway et al. 2017). Together, these studies provide information on the potential negative effects of NPs on mitochondrial ATP production and cellular energy homeostasis. While there were no assessments of the mitochondria included in this study, male placentas appeared unable to maintain energy levels indicated by the significant elevation in cellular AMP. The next research should include a comprehensive evaluation of mitochondrial respiration and membrane potential to determine if these are impaired in male placentas.

Another intriguing finding from this study was that cellular ratio of NAD<sup>+</sup> to NADH were unchanged but a significant increase in overall cellular NAD was identified. The placenta, in addition to the lung and small intestine, are especially equipped for *de novo* synthesis of NAD<sup>+</sup> from dietary L-tryptophan (Yamazaki et al. 1985). NAD<sup>+</sup> is generated via this pathway to maintain cellular redox homeostasis and promote oxidative metabolism (Xiao et al. 2018). Interestingly, recent literature using monocyte-derived endothelial-like cells *in vitro* has shown that the production of NAD via this pathway is up-regulated under conditions of low oxygen tension, possibly as a compensatory mechanism help maintain cellular energy metabolism (Herbert et al. 2011). Importantly, NAD can also be synthesized by the salvage pathway, where niacinamide (NAM) is metabolized by a group of ATP-dependent isozymes called nicotinate mononucleotide adenylyltransferases (NMATs) (Xiao et al. 2018). The current study limitations do not allow for illustration of the exact reasons that may be leading to the significant increase in total NAD, nor which pathway may be increasing NAD synthesis. Therefore, investigation of transcription and activities of key NAD synthetic enzymes of the *de novo* (tryptophan 2,3-dioxygenase (TDO),

idoleamine 2,3-dioxygenase (IDO), and salvage (NMAT, NAMPT, NAD<sup>+</sup> synthase) pathways could be conducted. The current data do suggest that the increase in NAD synthesis may have been triggered to aid in metabolic homeostasis and promote oxidative phosphorylation due to decreased placental energy status. This may be due to the impact of nano-TiO<sub>2</sub> exposure on uterine vascular compliance leading to reduced nutrient-rich blood perfusion to the placenta, as these pathways have been shown to be stimulated under conditions of nutrient restriction (Cantó et al. 2015).

Studies have begun to delve into the sex-dependent phenotypes in placental function and metabolism. Early studies have revealed distinct metabolic phenotypes associated with fatty acid oxidation, purine degradation, and metabolic function (Saoi et al. 2020). Additionally, placenta has been found to respond to changes detected in maternal blood stream based on the sex of the fetus as seen in the mouse (Gabory et al. 2012). Our study aligns with this body of literature, where the placental response to maternal NP inhalation was sex specific. Male placentas were found to utilize glycolysis by increasing PFK activity but were significantly energetically deficient, whereas female placentas did not utilize glycolysis and were not energetically deficient. The literature also states that males exhibit “risky” behavior *in utero* in terms of rapid growth and maxing out nutrient consumption compared to females (Eriksson et al. 2010). Our study is in line with this logic, where male placentas increase glycolysis and are energetically compromised. Female mitochondria are efficient at switching to fatty acid beta-oxidation under circumstances that demand an increase in ATP (Ventura-Clapier et al. 2019). Therefore, female placentas may be using fatty acids to generate acetyl Co-A for the Krebs Cycle to maintain ATP production by the mitochondria. Future research should identify the sex specific perturbations as well as adaptations by the placenta to NP exposure.

There are several important limitations to this study. Although the sample size for treatment and sex related differences is insufficiently powered, the data show promising indications of perturbations in energy metabolism based on the sex of the fetus. Furthermore, while the samples

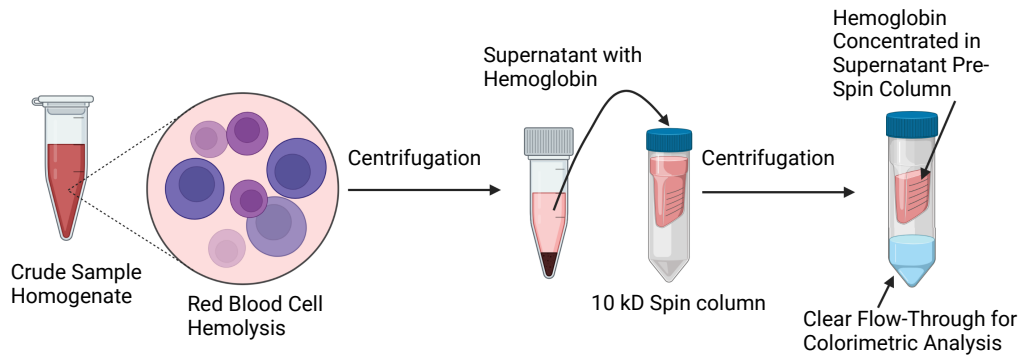
were specifically harvested from the labyrinth zone of the placenta, this tissue is a heterogenous mixture of maternal and fetal blood cells. Therefore, any lysed red blood or other hemopoietic cells may have contributed to the endpoints chosen. To verify these findings, future experiments could enrich placental labyrinth tissue for syncytiotrophoblasts before homogenization or conduct an *in vitro* study with primary rat syncytiotrophoblasts. The enzyme assays chosen to assess the potential for activity, not the actual flux of metabolic intermediates occurring within the cell. The next study can utilize the Seahorse XF Glycolysis Stress Test kit, as this analysis measures glucose flow through the glycolytic pathway within placental tissue. This information will shed light on if glycolysis rate is down after maternal nano-TiO<sub>2</sub> inhalation. In addition, the mRNA and protein expression of HK, PFK, and LDH can be evaluated for exposure impact on transcription or translation of these glycolytic enzymes that is impacting movement through the glycolysis pathway. Future work should also include analysis of glucose-6-phosphatase which is an enzyme responsible for balancing the activity of HK by hydrolyzing G-6-P to yield a free glucose molecule for transport across the syncytial basolateral epithelium. This enzyme is critical in regulating fetal blood glucose levels, and its activity after maternal NP exposure would aid in determining placental capacity to meet fetal nutrient demand.

In conclusion, this was the first study to evaluate the effect of inhaled NPs on placental glycolytic metabolism and energy status with an emphasis on fetal- sex differences. It has been identified that inhalation during pregnancy reduces placental glycolytic activity and energy state. While from this work it is difficult to identify the metabolic shifts at play, it was determined that NP inhalation likely does not lead to an increase in glycolysis or anaerobic metabolism, nor does oxidative respiration appear to be upregulated for male placentas or decreased for female placentas. It was also observed that redox potential is not reduced with exposure. It remains plausible that there may be a metabolic switch to an alternate substrate, such as fatty acids in female placentas, an upregulation in NAD synthesis to aid in energy metabolism, and that mitochondrial function may

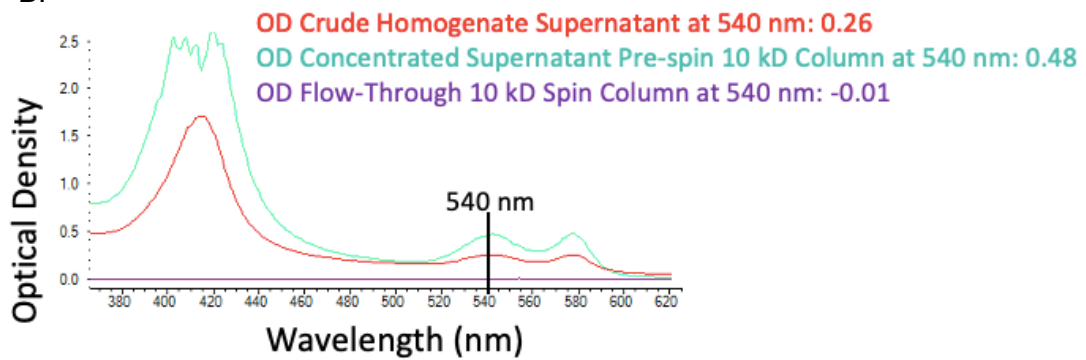
be maintained in females and impaired in males. The metabolic changes identified in the placenta may have downstream consequences for fetal nutrient delivery. Overall, these findings identify a developmental risk for exposure to air pollution and the potential for developmental origins of disease for the offspring. Further studies investigating glycolytic flux, mitochondrial respiration, and metabolic substrate switch from carbohydrates are urgently needed.

**Figures:**

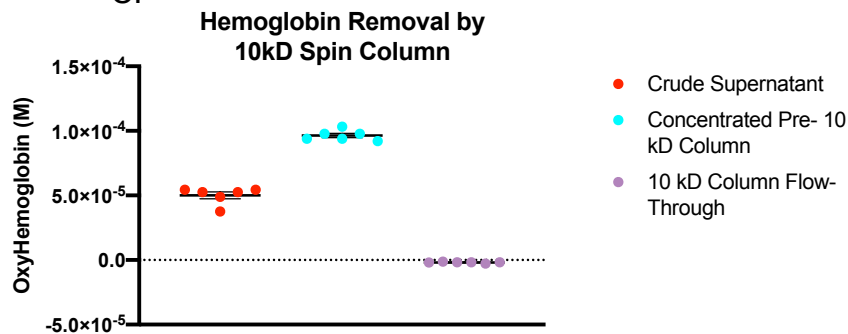
A.



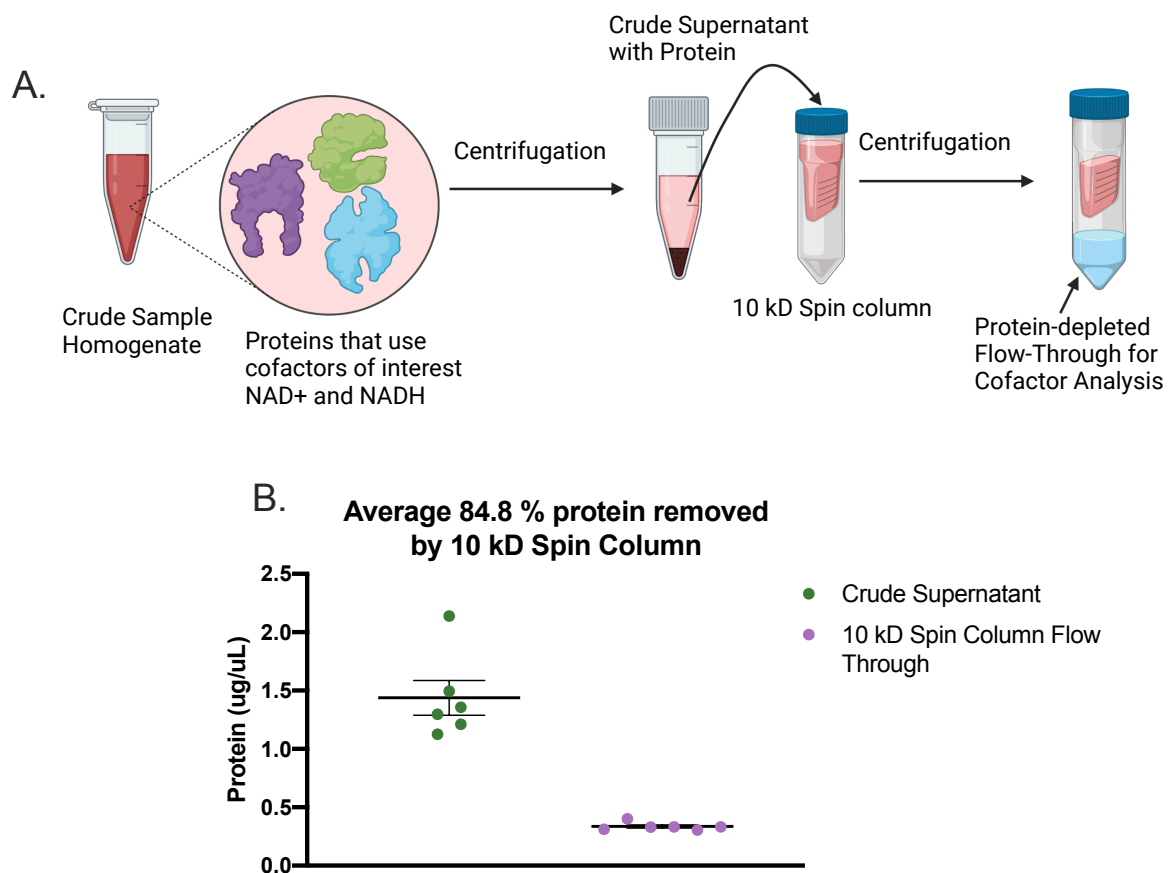
B.



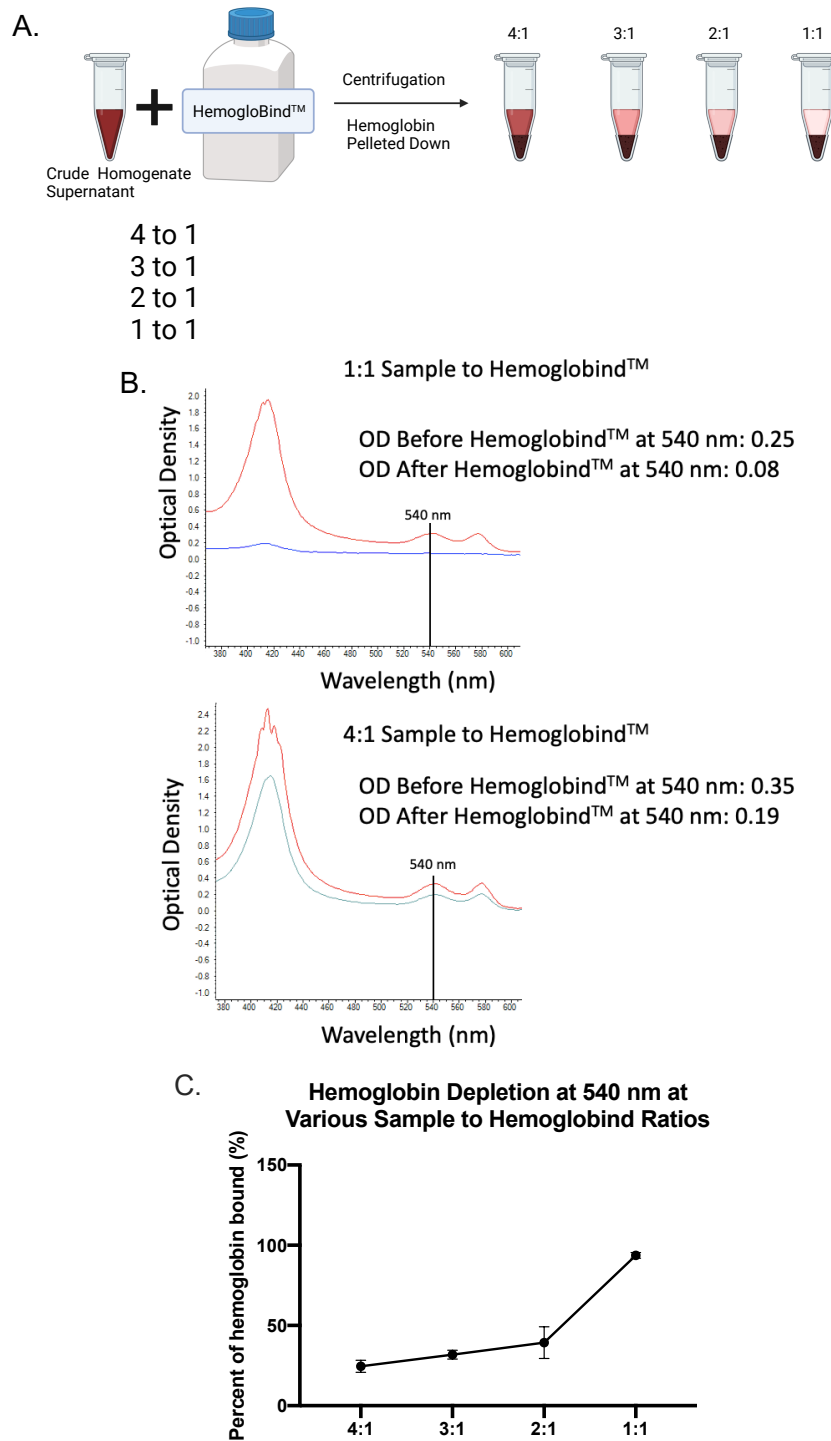
C.



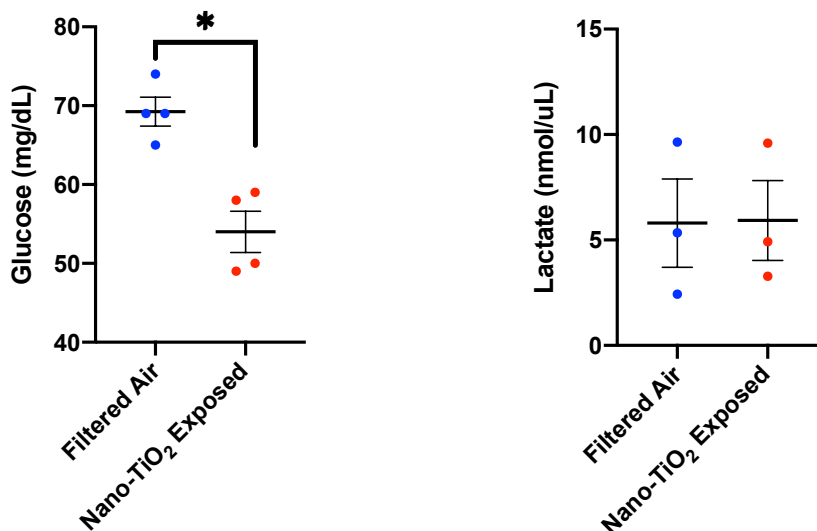
**Figure 4.1. 10kDa spin column hemoglobin removal.** A. Method development for sample hemoglobin removal using 10 kDa spin columns. B. Representative UV spectra of a crude sample homogenate (red), concentrated homogenate before spin column after centrifugation (green) and sample homogenate flow-through (purple). Hemoglobin presence in naïve placenta homogenates were measured by optical density at 540 nm. C. Concentration (M) of sample homogenate supernatant (crude, pre-column concentrated, and flow-through). N=6 labyrinth zone samples from naïve placentas. Mean  $\pm$  SEM reported.



**Figure 4.2 kDa spin column protein removal. 2.** **A.** Method development to remove protein from sample homogenates using 10 kDa spin columns. **B.** Average homogenate sample protein removed after centrifugation with a 10 kDa spin column. Protein was quantified by Pierce BCA Protein Assay.



**Figure 4.3. HemgloBind™ optimization for hemoglobin removal.** **A.** Method development of Hemoglobin removal from placental homogenate sample after addition of HemgloBind™. **B.** Representative UV spectra of samples before and after addition of HemgloBind™. Optical densities are reported at 540 nm. **C.** Average amount of hemoglobin removed from sample at various concentrations of HemgloBind™ to sample.

**A. Labyrinth Fetal Blood Glucose**    **B. Labyrinth Fetal Blood Lactate**

**Figure 4.4. Quantification of glucose and lactate from blood harvested from the fetal side of the labyrinth zone.** **A.** Glucose concentration within placental labyrinth zone blood between treatment groups on GD 20. N= 4 dams per group (all male placentas). Analysis by Student's t-test, mean  $\pm$  SEM reported. \* =  $p < 0.05$ . **B.** Lactate measured within placental labyrinth zone blood between treatment groups on GD 20. N=3 dams per group (all male placentas). Analysis by Student's t-test, mean  $\pm$  SEM reported.

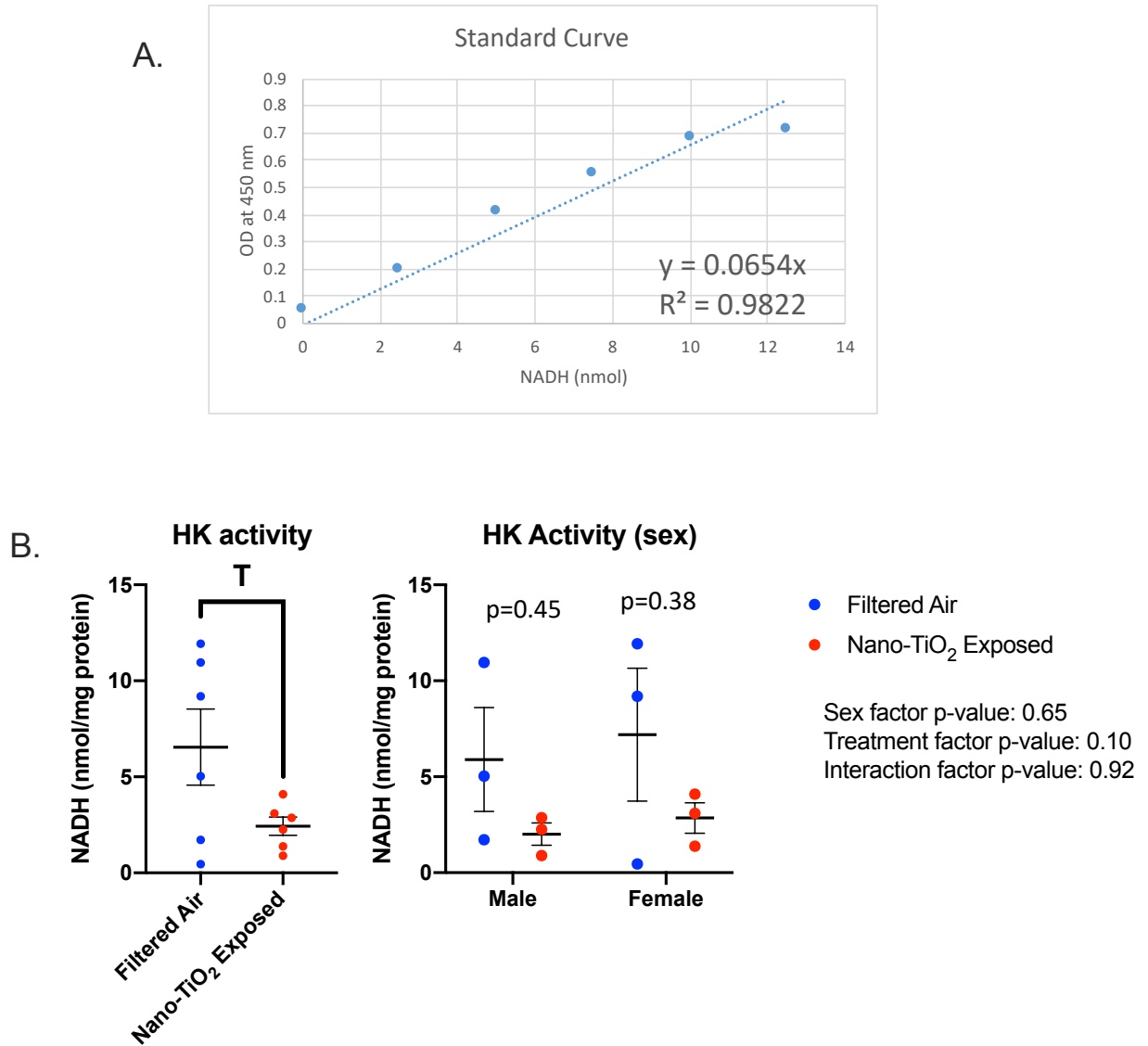


**Figure 4.5. Hexokinase (HK) activity in placental labyrinth zone trophoblast tissue. A.** Standard curve for NADH (nmol) generated by HK activity. **B.** HK activity (nmol NADH per minute per mg protein) measured from placental labyrinth zone trophoblast cell homogenates by treatment group and fetal sex. n= 6 dams per group. Analysis by Student's t-test, and fetal sex analysis by 2way ANOVA and Sivak's multiple comparison post hoc correction. Mean  $\pm$  SEM reported. T= p < 0.07.

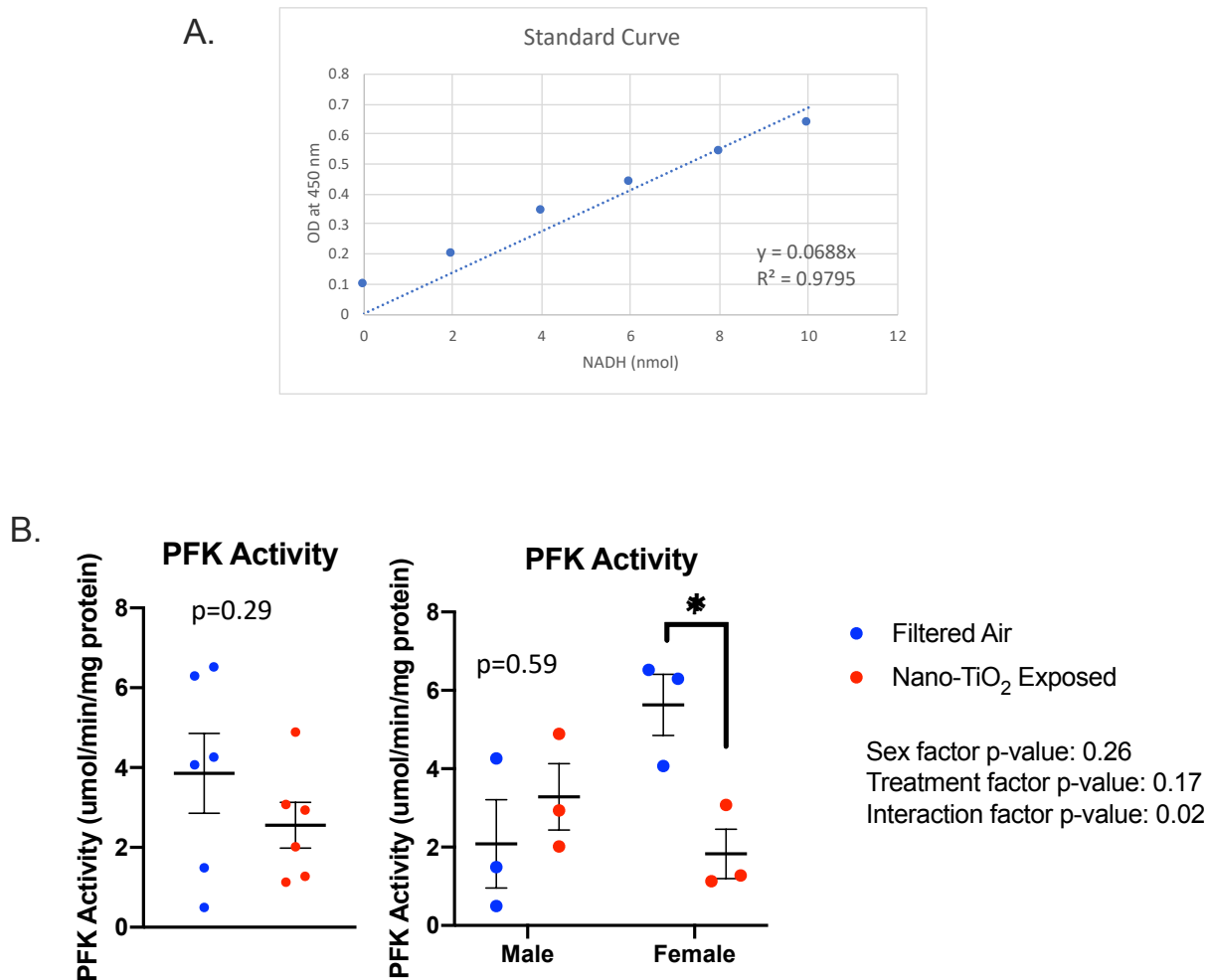


**Figure 4.6. Phosphofructokinase (PFK) activity in placental labyrinth zone trophoblast tissue.** **A.** Standard curve for NADH (nmol) generated by PFK activity. **B.** PFK activity (nmol NADH per minute per mg protein) measured from placental labyrinth zone trophoblast cell homogenates by treatment group and fetal sex.  $n=6$  dams per group. Analysis by Student's t-test, and fetal sex analysis by 2way ANOVA and Sivak's multiple comparison post hoc correction. Mean  $\pm$  SEM reported.  $*=p < 0.05$ .

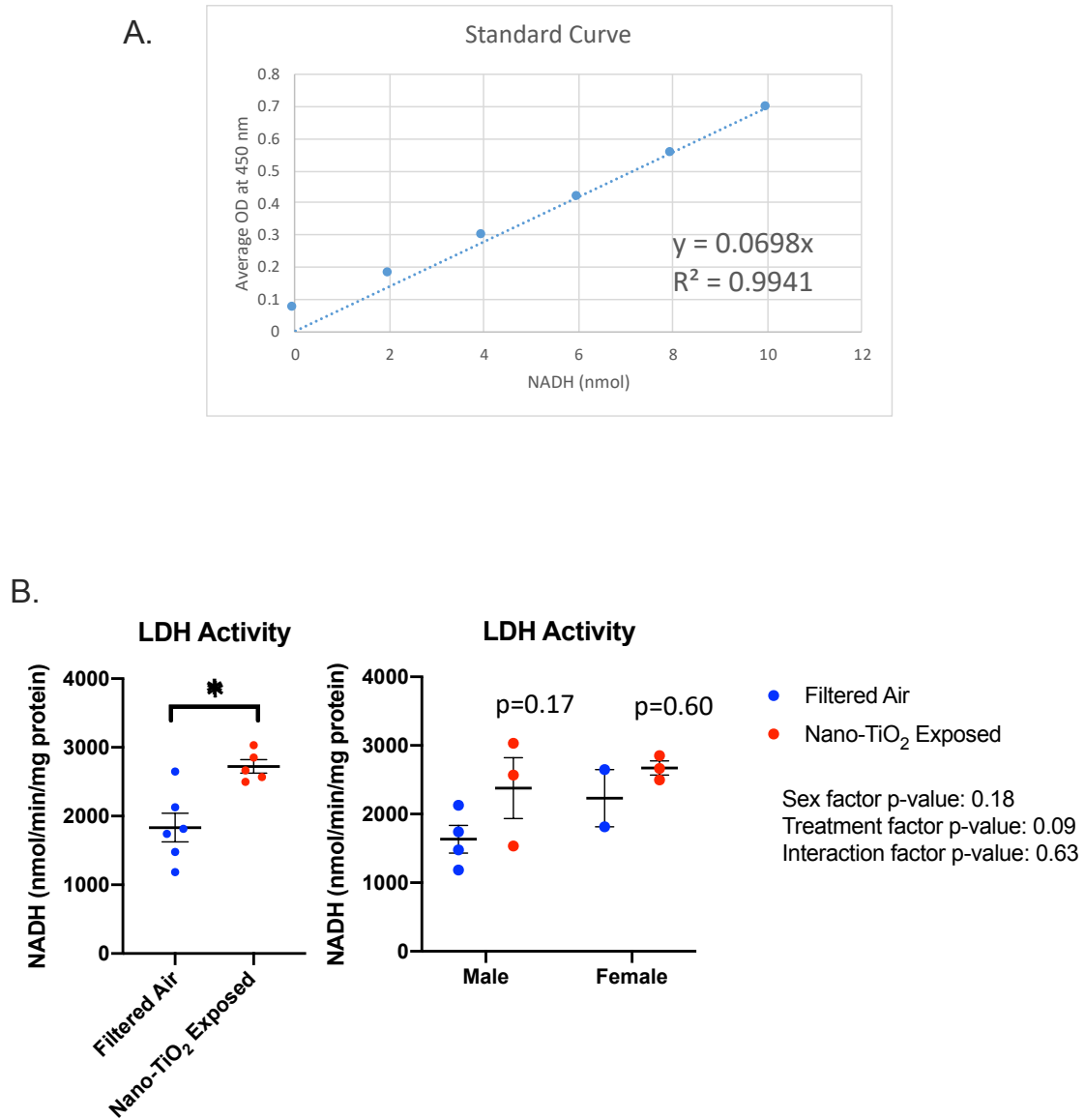


**Figure 4.7. Lactate dehydrogenase activity (LDH) activity in placental labyrinth zone trophoblast tissue.** A. Standard curve for NADH (nmol) generated by LDH activity. B. LDH activity (nmol NADH per minute per mg protein) measured from placental labyrinth zone trophoblast cell homogenates by treatment group and fetal sex. n= 6 dams per group. Analysis by Student's t-test, and fetal sex analysis by 2way ANOVA and Sivak's multiple comparison post hoc correction. Mean  $\pm$  SEM reported. \* =  $p < 0.05$ .

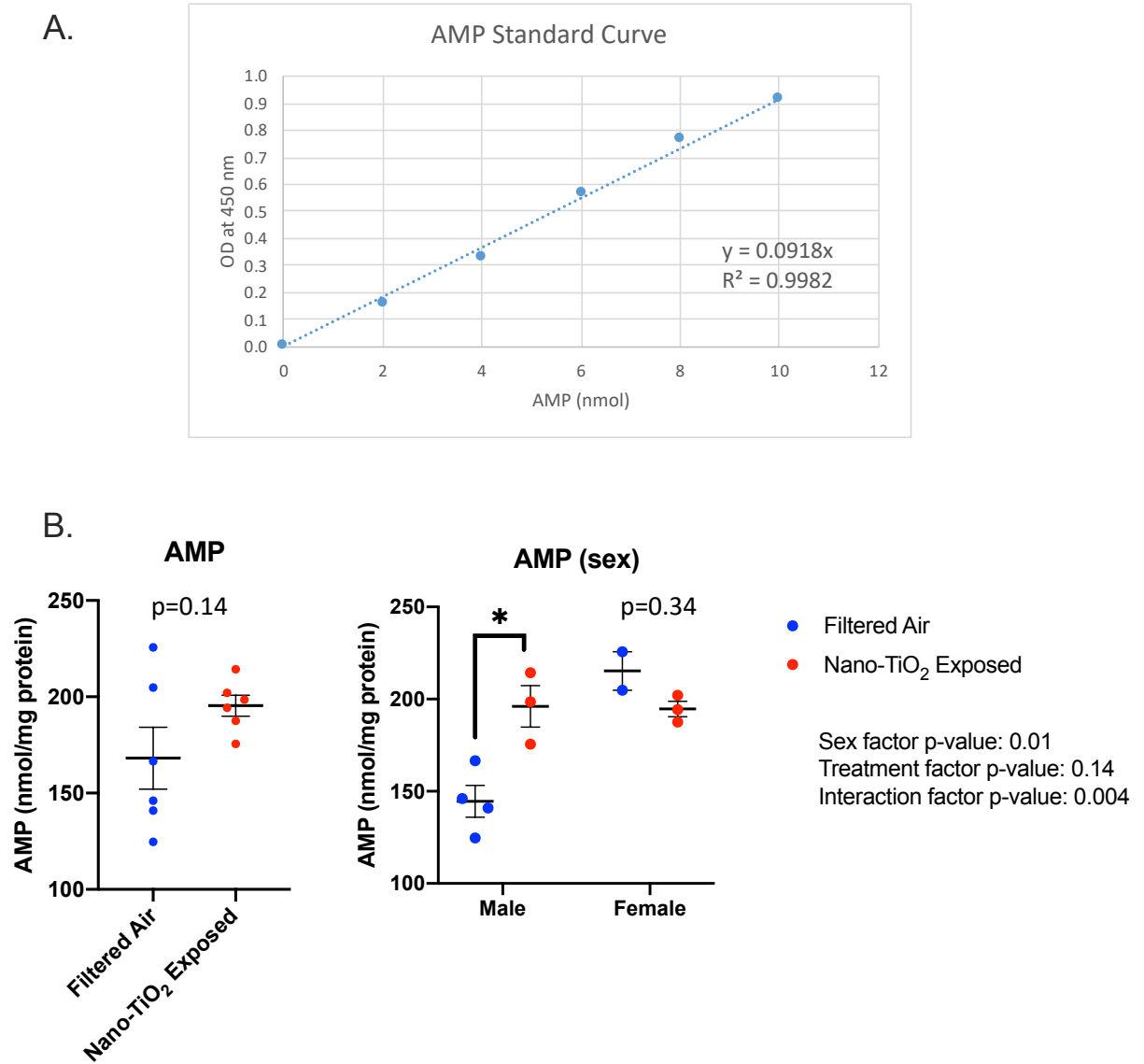


**Figure 4.8. Measurement of cellular AMP from placental labyrinth zone trophoblast homogenates.** **A.** Standard curve of AMP (nmol). **B.** Total AMP (nmol/mg protein) measured from placental labyrinth zone trophoblast cell homogenates by treatment group and fetal sex.  $n=6$  dams per group. Analysis by Student's  $t$ -test, and fetal sex analysis by 2way ANOVA and Sivak's multiple comparison post hoc correction. Mean  $\pm$  SEM reported.  $*$  =  $p < 0.05$ .

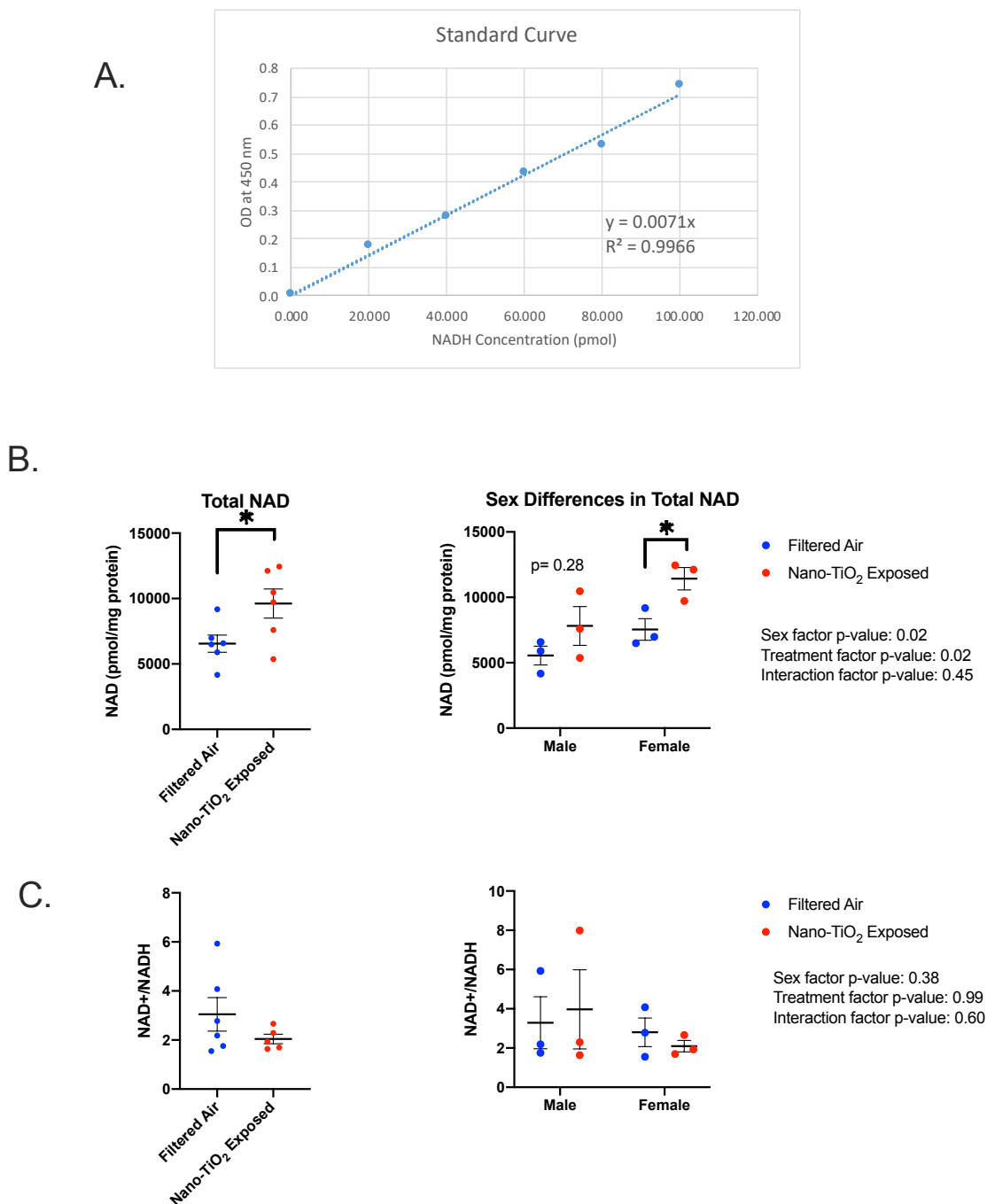


**Figure 4.9. Measurement of cytosolic NAD and NAD<sup>+</sup>/NADH ratio from placental labyrinth zone trophoblast homogenates. A.** Standard curve of NADH (pmol). **B.** Total NAD (pmol) by treatment group and fetal sex.  $n=6$  dams per group. Treatment group analysis by Student's t-test, and fetal sex analysis by 2way ANOVA and Sivak's multiple comparison post hoc correction. Mean  $\pm$  SEM reported.  $*$  =  $p < 0.05$ . **C.** NAD<sup>+</sup>/NADH ratios by treatment group and fetal sex.  $n=6$  dams per group. Outlier determined by Grubbs' test and removed. Analysis by Student's t-test, and fetal sex analysis by 2way ANOVA and Sivak's multiple comparison post hoc correction. Mean  $\pm$  SEM reported.

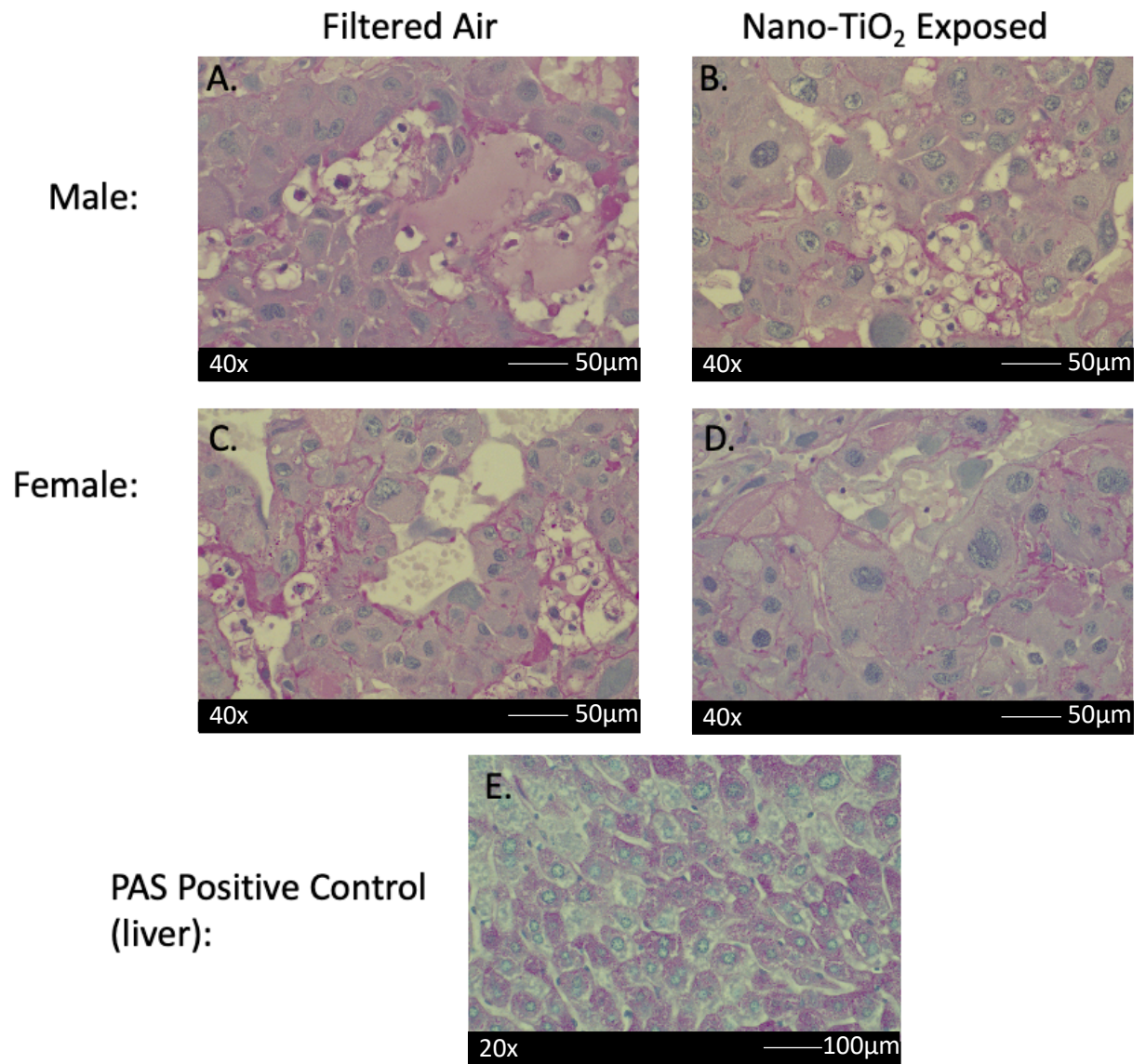


**Figure 4.10. Placental junctional zone glycogen cell glycogen storage.** PAS stains glycogen a magenta color. **A, C.** Representative filtered air control placentas, male and female. **B, D.** Representative nano-TiO<sub>2</sub> exposed placentas, male and female. **E.** PAS positive control liver. N= 6 dams per group.

## CHAPTER 5: OVERALL DISCUSSION

Exposure to particulate air pollution during pregnancy has been linked with fetal morbidity and mortalities including low birth weight (Tapia et al. 2020; Wojtyla et al. 2020). Birth weight outcomes are limited by the capacity of the placenta to transfer nutrition. However, the effects of particulate air pollution inhalation on placental transfer of nutrition, namely glucose, to the fetus are understudied. Thus, there is a need to understand how exposure may impact placental function and potentially contribute to reduced fetal growth and related pregnancy disorders.

The overall objective of this dissertation was to identify whether inhaled NPs translocate to the placenta and to evaluate the effects on placental glucose transfer to the fetus and glucose metabolism. I hypothesized that inhaled NP aerosols during pregnancy can travel to the placenta and increase placental metabolism of glucose, thereby decreasing the concentration of glucose transferred to the fetus. Three specific aims were developed to test the central hypothesis: 1) characterize the distribution of nano-TiO<sub>2</sub> in a pregnancy model, 2) evaluate maternal and fetal blood glucose concentrations and placental glucose transfer, and 3) assess placental glycolytic activity and energetic status. From this work, the evidence collected was in support of inhaled NP translocation to the placenta and decrease in fetal blood glucose, and against the theory that glucose metabolism is increased in the placenta.

The Chapter 2 evaluated the distribution of inhaled nano-TiO<sub>2</sub> to secondary maternal, placental, and fetal tissues. Previous studies observed that inhalation of various types of ambient NP, including exposure to homogenous engineered nanomaterials (Bowdridge et al. 2019; Campagnolo et al. 2017a) and heterogenous particulate matter (Blum et al. 2017), was associated with adverse pregnancy outcomes. Additionally evidence from non-pregnant human (Burch 2002) and rat models (Pujalté et al. 2017) demonstrated that inhaled NPs enter systemic circulation and are

detectable in secondary tissues after single exposures. Therefore, there was a need to identify and describe the distribution of chronically inhaled NPs in a pregnancy model. Elemental Ti was found in the maternal lung and secondary tissues (i.e., whole blood, heart, aorta, kidney, liver, spleen, and pancreas) after nano-TiO<sub>2</sub> inhalation. Ti was also found in both zones of the placenta (i.e., decidua/junctional zone, labyrinth zone), and NPs were visualized intracellularly in the syncytium of the labyrinth zone. Fetal tissues (i.e., umbilical cord, whole blood, liver, heart) also contained Ti. Together, these data support the translocation of inhaled NPs to secondary tissues during pregnancy including the placenta. Chapter 3 set out to evaluate placental morphometrics and glucose transfer capability. Previous studies have linked FGR to maternal NP exposure but have not tested reduced nutrient transport as a possible factor (Mozafari et al. 2020; Wojtyla et al. 2020). Gestational nano-TiO<sub>2</sub> inhalation significantly reduced fetal blood glucose concentrations measured on GD 20 with a greater reduction in males. With the caveat that the studies were underpowered, no change was found in the rate of glucose transfer *ex vivo*. However, fluid flow through the uterine artery and placental fetal capillary area were reduced. There were no significant changes found to maternal glucose, maternal, placental, or fetal weights, or placental GLUT expression or localization between exposure groups. Together, the data from this aim suggests that maternal NP inhalation throughout pregnancy reduces uterine vascular flow and the surface area of fetal capillaries in the placenta, which may contribute to reduced placental glucose delivery and subsequent transfer to the fetus. Chapter 4 examined the effect of NP inhalation on placental glucose metabolism and cellular energy level. Although underpowered, the collected data show no difference in HK activity and significant increase in LDH activity, together indicating that the placenta does not transition to anerobic metabolism. Exposure also increased total cellular NAD (NAD<sup>+</sup> and NADH), suggesting a compensatory response of increasing redox cofactors to aid in energy generation. Separating the data by fetal sex, the potential for PFK activity in female placental labyrinth tissue was reduced, possibly due to a lower reliance on glucose metabolism. Additionally, total NAD was increased in female placentas. AMP concentrations were increased in

male placental labyrinth tissue, suggesting a compromised energy level. These data are evidence against our initial hypothesis of increased glycolytic activity. Additional data may help corroborate a sex-specific phenotype of metabolic stress in the placenta. Overall, these data support that inhaled NPs can travel to the placenta, and exposure is associated with a decrease in placental glucose metabolism and reduction in fetal blood glucose concentrations. It is possible that the identified reduction in fluid flow through the uterine artery and decrease in placental fetal blood capillary size could limit blood flow to the placenta affecting metabolism and limit nutrient transport to the fetal circulation.

The data support that inhaled NPs are retained in the lung and that a fraction is transferred to the systemic circulation allowing interaction with developing placental and fetal tissues. Based on the previous distribution literature exposing non-pregnant rodents to NP aerosols (Pujalté et al. 2017; Yin et al. 2014), and pregnant rodents to NPs by intravenous injection or oral routes (Hong et al. 2017a; Yamashita et al. 2011), direct particle deposition in the placenta and fetus after inhalation is highly likely. The confirmatory findings from our study are important to inform the toxicological effects of inhaled NPs at the feto-placental unit. In the field of nanotoxicology, there are three main mechanistic hypotheses put forth to explain toxicity after NP inhalation: 1) inflammation, 2) neural alterations, and 3) direct particle interactions (Hoet et al. 2004). While it is important to remember these are not mutually exclusive, our study adds to the body of literature that direct particle interactions occur with the placenta after inhalation of NPs during pregnancy.

Identification of direct NP interactions with the cells and organelles of the syncytium led to additional questions regarding the potential impact on placental nutrient transfer capacity. While our study specifically tested the function of glucose transfer, several others remain to be scrutinized. Firstly, the syncytium is a continuous epithelium meant to maximize surface area for nutrient-waste exchange. Based on its physiochemical properties, NPs can adhere and become internalized by

cellular membranes by energy-dependent processes (Lesniak et al. 2013). Adherence to the apical membrane can damage or compete with cell surface receptors critically involved in maternal-placental crosstalk, such as IGF-1 and IGF-2, (Harris et al. 2011), and important uptake and efflux xenobiotic transporters, such as P-gp, BCRP, and MRP1 (Hemauer et al. 2010). Therefore, the functions of receptor-mediated signaling of hormones or the uptake and efflux of drugs may be perturbed with NP inhalation. Secondly, the placenta must produce and secrete several hormones into the maternal circulation critical for the maintenance of healthy pregnancy, a process that requires mRNA transcription, translation, and membrane trafficking and release. Our study found NPs directly interacting with the rough endoplasmic reticulum, which may point to interference with the translation of the important peptide neurohormones (e.g., oxytocin, neuropeptides), growth factors (e.g., inhibin, activin, IGFs), and cytokines (e.g. interleukins, interferons) (Petraglia et al. 1996). These peptide hormones are critical chemical signals that communicate with maternal tissues to allow for maternal cardiovascular, metabolic, and immune adaptations (Sun and Sun 2022). Lastly, the interference with other nutrient uptake, metabolism, or transport that are important for fetal development remain to be investigated.

The identified significant reduction in fetal blood glucose (Chapter 3) suggests NP exposure reduces placental nutrient transport. There are several hypothesized mechanisms leading to this outcome, including direct NP-syncytiotrophoblast interactions, as well as indirect syncytiotrophoblast effects from NP interactions with other physiological systems (i.e., vascular, metabolic, immune). Hypotheses that involve direct NP interactions with syncytiotrophoblasts include physical DNA damage from NP contact that may lead to reduction in mRNA transcription including GLUT isoforms (Shukla et al. 2021). Additionally, physical NP contact can damage the rough endoplasmic reticulum and lead to reduced GLUT protein translation (Onoda et al. 2020). NPs have also been shown to make direct contact with phospholipid membrane-embedded channels and transporters resulting in reduced protein function (Foreman-Ortiz et al. 2020). Given the

abundance of GLUT1 and GLUT3 at the maternal-facing membrane, interactions with NPs may lead to disfiguration or damage leading to reduced capacity for glucose to diffuse through the transporter. Indirect theories describe the impact of NP exposure on physiological systems that may subsequently lead to reductions in placental nutrient transport. These include reduced vascular compliance leading to poor glucose availability to the placenta and fetus (Fournier et al. 2019b). Additionally, impeded placental development, which has been shown with inhalation of PM<sub>2.5</sub> in terms of thickness, diameter, and traverse diameter, could reduce placental surface area for nutrient uptake/transport (Soto et al. 2017). Other indirect theories include increased placental glucose metabolism, thereby reducing the amount of glucose to be delivered to the fetus.

The results from Chapter 3 do not support the theories of direct reduction of mRNA expression, protein translation, or protein localization at the proper apical and/or basolateral membranes. However, direct NP interactions with GLUTs and impact on function is yet to be explored. These data collected do not rule out DNA damage or endoplasmic reticulum stress through direct NP contact or oxidative damage from generated reactive oxygen species. These possibilities should be further examined given the direct NP contact with the nucleus and rough endoplasmic reticulum visualized in Chapter 2 with TEM. A TUNEL assay can help identify DNA damage by fluorescently labeling single or double stranded DNA breaks of the syncytiotrophoblast cells *in situ*. Additionally, to assess whether endoplasmic reticulum stress is activated in the syncytiotrophoblasts, the transcription of markers including BiP, ATF-6, and XBP-1 can be quantified with qPCR. These have previously been shown to be upregulated during endoplasmic reticulum stress after silver NP exposure in zebra fish (Christen et al. 2013). Overall, further experimentation is required to explore these other possible mechanisms of placental toxicity due to direct NP interactions.

The reduction in fluid flow across the uterine artery identified in Chapter 3, along with our previous data demonstrating that inhaled NPs cause uterine vascular dysfunction (Appendix 3) (Stapleton et al. 2013b), indicate that NP inhalation may lead to reduced uteroplacental perfusion and indirectly lead to reduced glucose delivery to the placenta. Chapter 4 also supports this conclusion. A decrease in placental glycolysis enzyme activity was identified, which may be due to less glucose-rich blood reaching the syncytium. Reduced glycolysis enzyme activity has been observed in other tissue types such as testes after poor tissue perfusion (Al-Maghrebi and Renno 2016). The mechanisms by which inhaled NPs beget uterine vascular dysfunction remain unknown. Additionally, the results from Chapter 3 show that the surface area of the fetal blood capillary space in the placenta is reduced by 28% with exposure, indicating a smaller region for glucose to be transported across. It is possible the reduction in surface area is due to restricted vascular nutrient delivery to support placental growth and development. Altogether, it is concluded that inhaled NPs translocate from the lung to the placenta and contribute to reduced placental blood flow and surface area for fetal nutrient uptake likely by a combination of both direct (i.e., NP interaction with DNA and ER) and indirect (i.e., uterine vascular dysfunction and reduced placental fetal blood capillary area) mechanisms. These findings warrant further investigation into the mechanisms of uterine vascular dysfunction and effects on placental function.

The placental glucose metabolism and energy status findings from Chapter 4 may be due to reductions in uterine vascular perfusion identified in Chapter 3. In other models of growth restriction, such as maternal hypoxia, placental glucose utilization is increased (Zamudio et al. 2010). In the hypoxia model, the placenta spares oxygen for fetal consumption and consumes more glucose to satisfy its own energy demands (Zamudio et al. 2010). Paradoxically, this metabolic paradigm restricts glucose availability for the fetus and impairs fetal growth and development. Our results were not in line with the initial hypothesis of increased placental glucose metabolism. We identified reductions in HK and PFK activity that would indicate reduced need for glycolytic

enzyme activity. This may be associated with less glucose reaching the placenta, such as in a model of reduced uteroplacental blood perfusion (RUPP). The RUPP model surgically ligates the uterine artery to recapitulate reduced uteroplacental perfusion to study placental and fetal outcomes. One RUPP experiment initiated on GD 14 and terminated on GD 19 that reduced uterine artery perfusion by 40%, significant ATP concentrations were found in placentas from the reduction in placental perfusion, possibly as part of a “demand reduction” response by turning down activity of ATP utilizers to spare energy and so that less glucose is required to drive cellular functions (McClements et al. 2022). In addition, RUPP placentas increased glycogen storage but had no change in Krebs Cycle metabolites, suggesting the placenta may depend less on glucose utilization. An accumulation of carnitine may support fatty acid use in oxidative pathways in place of glucose. These metabolic changes were also associated with downstream reduction in fetal heart glucose concentrations, to likely due to reduced glucose transport across the RUPP placenta (McClements et al. 2022). In this work, the decrease in glycolytic enzyme activity (Chapter 4), along with down regulation of GLUT4 (Chapter 3) and reduction in downstream fetal blood glucose (Chapter 3) suggest that there is a “placental response” model with NP exposure, like the RUPP study findings, where the placenta responds by turning down processes that require glucose to match decreased perfusion. It is important to bear in mind that the results from this dissertation were generated from enzyme activity assays, which determine enzymatic potential, and not the actual flux of glucose through the glycolytic pathway. Therefore, the critical next step would be to measure the glycolytic rate of the cells using a method such as the Seahorse XF Glycolytic Rate Assay Kit. In these experiments, fresh labyrinth tissue from repeat filtered air or nano-TiO<sub>2</sub> exposed dams (GD 4 to GD 19) can be added to individual plate wells for the assay protocol. This method specifically measures glycolytic activity by measuring proton efflux to give an accurate depiction of compensatory glycolytic activity when mitochondrial respiration is inhibited. This analysis would provide important data on the impact of gestational NP inhalation on placental basal glycolytic rate and mitochondrial function. Additionally, analysis of glucose-6-phosphatase, an enzyme

responsible for balancing the activity of HK for free glucose transport across the syncytial basolateral epithelium, should be assessed. This data would aid in determining placental capacity to meet fetal glucose demand. Overall, our enzyme activity data suggest the glycolysis enzyme changes may be due to reduced uteroplacental blood perfusion (Broere-Brown et al. 2016b; Rosenfeld 2015), in agreement with Chapter 3 findings of reduced uterine vascular fluid flow. Furthermore, these are the first data to infer that nutrient metabolism in the placenta is impacted with inhaled NP exposure. Further work to increase statistical power and assess glycolytic rate is required to corroborate these initial observations. Additionally, the potential metabolic mechanisms ruled out and identified from this work may inform future studies that aim to characterize the placental metabolic changes affected from NP inhalation.

The data presented in Chapter 4 also warrant further investigations into the sex-specific placental metabolic changes in response to maternal NP exposure. As previously discussed, the sex of the fetus largely determines placental behavior under normal conditions and in response to maternal environmental changes (Rosenfeld 2015; Saoi et al. 2020). Males fetuses are more susceptible to injury as a result of placental epigenetic programming to maximize fetal growth (Eriksson et al. 2010). Therefore, it was not surprising that evidence of sex-dependent changes of placental glycolytic enzyme activity and energy status in response to maternal NP inhalation were observed. The results indicate that male placentas were more susceptible to the effects of inhaled NPs on placental energy status and glucose transfer from findings in Chapter 3. Data from females did not indicate reduced energy status despite the significant decrease in PFK enzyme potential. Female fetuses also did not have a significant blood glucose reduction where male fetuses did (Chapter 3); therefore, female placentas maintained adequate ATP levels with lesser consequence to the fetus. Unfortunately, while statistical significance was identified, these studies remain statistically underpowered. Together, this information supports the hypothesis that changes to placental metabolism and energy status after maternal NP exposure may be sex specific. These data so far

may suggest the use of an alternate energy substrate to sustain ATP production by female placentas (Ferreira 2018). This could be assessed by analyzing the water-soluble (i.e., glycolytic intermediates, amino acids, nucleotides, Krebs Cycle intermediates) and lipid-soluble (i.e., fatty acids) metabolites present in female and male placentas with and without NP exposure using metabolomics. Alternatively, female placentas may be efficient at oxidative phosphorylation when challenged due to enhanced mitochondrial function at baseline (Cardinale et al. 2018). This can be analyzed by testing the effect of NP exposure on mitochondrial basal respiration, ATP-linked respiration, proton leak, spare respiratory capacity, and non-mitochondrial respiration with the Agilent Seahorse XF Cell Mito Stress Test Kit. These experiments should be conducted on isolated labyrinth tissue with sample size of  $\geq 6$  dams per group, one male and one female placenta per each dam. To date, there is an enormous gap in the literature with an emphasis on placental metabolism after maternal environmental exposures.

This dissertation tested the theory that reduced placental glucose transfer contributes to restricted fetal growth after maternal NP inhalation. FGR is defined as failure to meet full genetic growth potential due to placental insufficiency (Swanson and David 2015). Placental insufficiency can originate from conditions such as hypoxia (Bailey et al. 2019) or malnutrition (Bergmann et al. 2008). Alternatively, preeclampsia (Weiler et al. 2011) or maternal cigarette smoking (Reeves and Bernstein 2008) narrow the uterine vasculature and restrict of blood flow to the placenta and have been linked with FGR. Reduced uteroplacental perfusion creates malnutrition for the fetus by decreasing placental delivery of nutrient-rich blood (Swanson and David 2015). Janot et al., using the RUPP model, ligated the central part of each uterine artery on GD 16, 16.5, or 17 and found significant reductions in fetal and placental weights on GD 18.5 (Janot et al. 2014). Nüsken et al. also performed surgical ligation on GD 19, although at the most caudal points of the uterine artery, and identified significant fetal weight reductions at natural birth on GD 21 and 22 (Nüsken et al. 2008). In addition to the effects on fetal weight, McClements et al. used the RUPP model to study

fetal heart metabolic outcomes near term and identified significantly less glucose (McClements et al. 2022). The authors determined this was likely due to reduced glucose transport through the RUPP placenta because there were no changes to intermediates from the metabolism of glucose, adenosine, fatty acids, or amino acids (McClements et al. 2022). In a study by Leuder and Ogata, maternal uterine artery ligation resulted in reduced fetal weight and fetal plasma glucose levels at 24 and 48 hours after surgical intervention (Lueder and Ogata 1990). Additionally, they found at the 24 hour time point, placental and fetal tissues (i.e., fetal liver, fetal brain, fetal muscle) from the uterine ligation dams utilized significantly less glucose compared to controls (Lueder and Ogata 1990). Furthermore, Nüsken et al. used this model of FGR to investigate the offspring metabolic effects at 15 weeks of age, and found that the FGR offspring had increased body fat and impaired glucose tolerance (Nüsken et al. 2008). These studies demonstrate that interruptions to uterine artery blood flow by the RUPP intervention create a model to study impact on placental metabolism and glucose transfer to the fetus, and the effects on offspring growth and glucose homeostasis. Although in our studies reduced fetal weight was not found, the significant reductions found in uterine artery fluid flow (Chapter 3), placental glycolysis enzyme activity (Chapter 4), and fetal blood glucose concentrations (Chapter 3), agree with the RUPP model. Therefore, our model and the outcomes of these studies are like other models of reduced uteroplacental perfusion and fits in with the theory of reduced placental demand.

Our model of NP inhalation was found to reduce fluid flow through the uterine vasculature and fetal blood glucose, creating a fetal nutrient restriction that may set the stage for adult disease. As seen from the Dutch famine research, reduced fetal nutrition has been associated with adult glucose intolerance, cardiovascular diseases, obesity, and a shortened lifespan (Roseboom et al. 2006). Our laboratory's previous work has demonstrated that gestational nano-TiO<sub>2</sub> inhalation lead to epigenetic (Stapleton et al. 2018b) modifications, cardiovascular (Fournier et al. 2021; Hathaway et al. 2016; Stapleton et al. 2015a), and neurodevelopmental (Engler-Chiurazzi et al. 2016)

impairments in offspring. This dissertation identified that nano-TiO<sub>2</sub> inhalation is associated with placental and fetal particle deposition, reduced uterine vascular perfusion, and fetal blood glucose concentration. It is possible that the reduction in blood flow together with NPs entering fetal vasculature leads to immune and nervous system alterations that predisposes the fetus for cardiovascular disease. Previous research has shown strong associations between reduced uteroplacental perfusion and offspring cardiovascular impairments (Appendix 1). This could also suggest that the current public health crises (e.g., heart disease, obesity, type 2 diabetes) trace back to poor maternal air quality *in utero*. This DOHaD hypothesis was put forth by Dr. David Barker after a prospective study of individuals born from women that were pregnant during the Dutch famine stating that unfavorable intrauterine diseases, stressors, and exposures pre-program and predispose individuals to adult disease (Simmons 2009). Therefore, the developmental nutrient restriction after inhalation of environmental NP may apply under the DOHaD hypothesis.

There are limitations to be mentioned and improvements that can be made to this research going forward. While the scope of this study was limited to identify direct particle translocation, there are other theories to investigate. Of particular interest are inflammation and oxidative stress mechanisms at the placenta. Previous work has found placental oxidative damage after maternal TiO<sub>2</sub> exposure (Yamashita et al. 2011). The "spill over" theory suggests that inflammatory mediators generated in the lung may enter the blood stream and lead to systemic inflammation (Aragon et al. 2017). This theory has been investigated by comparing levels of cytokines in sputum and plasma from human subjects (Tkacova 2010). In our inhalation model, it is possible that inhaled NPs deposited in the alveoli induce an inflammatory and ROS reaction that also translocate to uteroplacental tissues. Our laboratory has previously demonstrated an acute significant increase in systemic cytokines IL-4 and IL-6 24-hours after whole-body nano-TiO<sub>2</sub> exposure during late-stage pregnancy (Stapleton et al. 2018c). It would be interesting to investigate whether these cytokines are also being expressed in the placenta, which could help connect the lung exposure with systemic

and placental inflammation. It would be important to note whether these effects persist with repeated exposure throughout pregnancy. An additional limitation is that concentrations of Ti were measured, and NPs were visualized in placental tissue, which supports but does not confirm the presence of inhaled nano-TiO<sub>2</sub> in the placenta. This technical limitation can be remedied by employing Raman Spectroscopy or SEM-EDX analysis. Another limitation to this study is that an assessment of fetal glucose homeostasis was not included. Fetal insulin and glucagon blood levels, pancreatic  $\beta$ -cell mass and function, and liver and skeletal expression of GLUT1 and GLUT4 would give more information on how the fetus is responding to reduced blood glucose concentrations. Additionally, adolescent and adult assessments of glucose tolerance after the intrauterine exposure would be critical to understand the long-term consequences. Together, these suggestions would strengthen the conclusions drawn from this work.

The *ex vivo* placental perfusion technique used in Chapter 3 was advantageous to test vascular fluid flow and glucose transfer from the maternal to the fetal circulation, as this physiology would be very difficult to scrutinize *in vivo*. In these experiments, the physiological saline solution was tailored to mimic maternal and fetal glucose concentrations and maternal oxygen tension to model concentration gradients *in situ*. These modifications were made to a previous methodology described in Appendix 2 and applied in Appendix 3 to follow maternal to fetal nanoparticle transport across the placenta (D'Errico et al. 2019; D'Errico et al. 2019a; Fournier et al. 2020). An important limitation to bear in mind for this methodology is that it is not a closed system. The cut and open radial arteries and uncannulated uterine veins may allow a portion of circulating fluid to escape into the vessel chamber bath. This makes it difficult to quantify the bi-directional fluid transfer across the placenta. However, considering this limitation the methodology can still be further optimized for use regarding placental metabolism, hemodynamics, and maternal-fetal transfer of nutrients, hormones, or xenobiotics. Next immediate steps could involve optimizing tissue oxygenation and identifying an approach to measure oxygen levels in the perfusate and tissue

during *ex vivo* perfusion. Once established, this method could be a powerful tool to study placental oxygen consumption and placental responses with challenged with varying oxygen tensions (e.g., hyperoxia, normoxia, hypoxia, anoxia) after NP exposure. This model could be relevant to study real-world air pollution exposures in tandem with conditions where maternal oxygenation is poor (e.g., maternal asthma, smoking, COPD, high altitude, acute/chronic respiratory tract infections, placental insufficiency, etc.).

Another limitation of this work is that only a single type of NP was used as the exposure test article. However, there are other types for which similar consequences on uteroplacental vascular function and fetal nutrition may be anticipated. Previous research using Sprague Dawley rats from our laboratory has demonstrated that gold (Appendix 3) (D'Errico et al. 2019a), and silver (Vidanapathirana et al. 2018), based NPs cause uterine vascular impairments and reduce fluid flow through the uterine artery. This evidence may indicate that metal-based NPs carry a risk for uteroplacental dysfunction, possibly due to the generation of ROS and scavenge the important vasodilator, nitric oxide (Slavin et al. 2017). Additionally, some evidence of uterine vascular dysfunction has also been found for non-metal-based NPs. One study identified that there was no impact to uteroplacental fluid flow after administration of a bolus of Rhodamine labeled 20 nm polystyrene beads into the uterine artery (Fournier et al. 2020). Furthermore, intravenous carbon-based polyvinylpyrrolidone (PVP) formulated fullerenes (C60) and intratracheally instilled carbon nanotubes both led to increased uterine vascular constriction in a pregnant Sprague Dawley rat model (Vidanapathirana et al. 2014a; Vidanapathirana et al. 2014b). It was shown that the vascular Rho pathway is involved with the PVP fullerene, but not the carbon nanotube exposure. These findings indicate that vascular perturbations are dependent on NP chemical composition. Therefore, full NP characterization is vital to the understanding of uteroplacental nanotoxicology.

### *Conclusion*

The objective of this dissertation was to improve our understanding of the effects of inhaled NPs on the placenta. The findings presented herein illustrate the extrapulmonary distribution of NPs to the placenta. Further, this research proposes that inhaled NPs lead to uterine vascular dysfunction with sex-dependent perturbations in placental glucose metabolism, placental energy homeostasis, and fetal blood glucose concentration. These data are significant as they improve our mechanistic understanding of human pregnancies that are affected after maternal NP exposure. Further, they highlight the importance of clean air for women during pregnancy to promote a healthy intrauterine environment for their offspring.

**APPENDIX 1: Developmental onset of cardiovascular disease- could the proof be in the placenta?**

JN D'Errico <sup>a</sup>, PA Stapleton<sup>a,b</sup>

**AFFILIATIONS:**

a. Department of Pharmacology and Toxicology, Ernest Mario School of Pharmacy, Rutgers University, Piscataway, NJ 08854, USA; b.Environmental and Occupational Health Sciences Institute, Piscataway, NJ 08854, USA

### **A-1.1 Abstract**

The Barker Hypothesis states change to the maternal environment may have significant impacts on fetal development, setting the stage for adult disease to occur. The development of the materno-fetal vasculature during implantation and maintenance during pregnancy is extremely precise, yet dynamic. Delays or dysfunction in the orchestration of anatomical remodeling, maintenance of blood pressure, or responsiveness to metabolic demand may have severe consequences to the developing fetus. While these intermissions may not be fatal to the developing fetus, an interruption, reduction, or an inability to meet fetal demand of blood flow during crucial stages of development may pre-dispose young to disease later in life. Maternal inability to meet fetal demand can be attributed to improper placental development and vascular support through morphological change or physiological function will significantly limit nutrient delivery and waste exchange to the developing fetus. Therefore, we present an overview of the uteroplacental vascular network, maternal cardiovascular adaptations that occur during pregnancy, placental blood flow, and common maternal comorbidities and/or exposures that may perturb maternal homeostasis and affect fetal development. Overall, we examine uterine microvasculature pathophysiology contributing to a hostile gestational environment and fetal predisposition to disease as it relates to the Barker Hypothesis.

### **A-1.2 Introduction**

Developmental Origins of Health and Disease is a concept proposed by Dr. David Barker that suggests change to the maternal environment and fetal milieu during gestation have significant impacts on health of the progeny in adulthood, later referred to as the *Barker Hypothesis* (Barker 1990; 1999). Many studies, including those conducted by Dr. David Barker, have associated small for development age at birth with the development of cardiovascular and/or metabolic disease later in life. Given cardiovascular disease is the leading cause of death worldwide, identification of all

risk factors is vital. The mechanisms connecting the *in utero* environment and maternal pathophysiology to the cardiovascular health of the next generation remain elusive.

One common development in a hostile gestational environment is the development of intrauterine growth restriction (IUGR). In this case, typically due to a reduction in placental and fetal perfusion; in these cases, babies are born small for gestational age. In response to poor health and nutrition in utero, the fetus may be reprogrammed to have a “thrifty phenotype” adapted to a perceived maternal low-nutrient environment (Barker et al. 2002; Simmons 2009). Offspring with IUGR tend to have altered glucose metabolism and insulin signaling despite a normal diet later in life (Thamotharan et al. 2007). Faced with ample available calories, these individuals develop obesity and other presentations of metabolic syndrome as adults due to alterations in homeostatic mechanisms that occurred during development. There is growing evidence that maternal health status can amend the fetal genome and imprint gene expression in subsequent developmental stages.

In this review, we will provide an overview of non-pregnant uterine vascular function and subsequent changes associated with fetal implantation and placentation, highlighting the importance of the macro and microvasculature with each state. Special attention will be given to the role of uterine endothelial function in adequate uteroplacental perfusion, and how dysfunction contributes to maternal and fetal disease. Further we discuss the maternal and fetal implications associated with changes to the maternal environment. These include disease (hypertension, obesity, diabetes), systemic inflammation, external stressors (noise pollution and sleep alterations), and environmental exposure (smoking, heavy metals, air pollution, and nanomaterials). Each of these variations to the maternal environment has fetal implications, which may act as a risk factor for the development of cardiovascular disease in adulthood. However, the mechanisms associated with the developmental onset of disease have not been elucidated.

### **A-1.3 Review**

## Overview of Uterine Circulation Before Pregnancy

From the outset, uterine arteries are extended bifurcation of the aorta shared with the ovary, and distally from the internal iliac artery; this redundancy is in place to prevent ischemia downstream in cases of occlusion (Osol and Moore 2014). Further, the uterine arteries branch to form arcuate networks, providing a consistent quality of oxygenated blood throughout the uterus in preparation to support implantation. These extend as smaller radial arteries penetrating the myometrium. The radial arteries then divide into daughter branches, identified as straight (basal) arterioles which feed the uterine muscle or coiled (spiral) arterioles spanning deeper across the myoendometrial junction also described as preplacental arterioles (Figure 1). In the non-pregnant uterus, the lineage of arteriolar vessels ends here. Capillaries meet and venules then drain and merge throughout the uterine layers ultimately meeting the inferior vena cava.

The rodent, commonly used as an animal model for reproductive studies, has a duplex or dual-horn uterus to maximize surface area for litter yielding, where the main uterine arteries run widely spaced from and alongside each horn. Where humans possess penetrating arcuate networks, rodents have secondary vessels that loop arcuate arteries back to the uterine artery to support a horn full of pups lengthwise, and tertiary vessels extending those loops down into the myometrium (Osol and Moore 2014).

The uterus is one of the few adult organs that undergoes routine vascular expansion and reduction, dictated by hormonal cycling of namely, estradiol and progesterone (Demir et al. 2010). Spiral arterioles are the most hormone-responsive vessels, whereupon stimulation during the estrogen-driven proliferative phase, undergo significant growth and coiling (Losordo and Isner 2001). Estradiol, VEGF/VEGFR and angiogenic factors collectively control arteriole proliferation (Bonagura et al. 2008). The spiral arterioles are destined to become the uteroplacental arteries, as they are the main supply and terminal extension to the endometrium.

During the first trimester of pregnancy the mammalian uterus undergoes extensive decidualization, a process initiated during the luteal phase of the reproductive cycle independent of

an implanted fetus to improve receptivity of the uterine endometrium. Decidualization involves morphological and physiological changes including infiltration of local immune cell populations and spiral arteriole remodeling. Ramified spiral arterioles from the proliferative phase are surrounded by uterine Natural Killer (uNK) cells, along with the presence of other immune cells, that appear to aid in the spiral arteriole remodeling and immunotolerance of invading fetal trophoblasts upon implantation (Tessier et al. 2015). In the absence of a conceptus, the richly vascularized bed facing the lumen is shed in response to falling levels of progesterone.

### **Implantation**

The success of implantation and maintenance through the first four weeks of human pregnancy (pre-placentation) is highly dependent upon the uterine preparation and overall health status of a female. Irregular cardiovascular, endocrine, and/or immune function threatens this process, with an emphasis on the requirement of reactive and responsive microvasculature for uterine priming. Implantation is a two-way interaction between the blastocyst and endometrial stromal cell-types. This cross-talk is accomplished by molecular cues such as paracrine factors regulated by estrogen and progesterone.

Decidualization involves the critical process of remodeling the spiral arterioles, the microvessels of the endometrium. The spiral arterioles from the proliferative phase of the reproductive cycle are now poised for invasion of fetal cells to establish the uteroplacental vessels, which will ultimately control maternal blood flow into the placenta. uNK cells and fetal extravillous trophoblasts target the extracellular matrix and smooth muscle of the spiral arterioles, promoting vasodilation to enhance nutrient delivery (Wallace et al. 2012). The trophoblasts further invade the arterioles and supplant the endothelium, assuming a phenotype as a pseudoendothelium (Damsky and Fisher 1998). Due to the hemochorial placentation of both humans and rodents, uterine microvasculature must also adapt to bring maternal blood into direct contact with fetal villous trophoblast during pregnancy (Robertson 1976); therefore, the terminal ends of the spiral arterioles

are held open, emptying into the lumen, which is remodeled to become the intervillous space of the placenta where maternal blood bathes the villous trophoblasts (Pijnenborg et al. 2011). The remodeling of the uterine microvessels and thus the establishment of the uteroplacental vasculature will initiate placentation and act as a conduit for nutrition for the developing fetus.

As the interface between the invasive trophoblasts and maternal spiral arterioles are responsible for placental perfusion, inadequate microvascular remodeling, perfusion, and/or reactivity have been associated with reduced placental blood flow and reproductive disorders, such as IUGR and preeclampsia (Furuya et al. 2008). Abnormal fat deposition, nutrient balance, oxidative stress and energy state have also been associated with higher rates of implantation failure and defective implantation leading to adverse consequences for pregnancy (Mathew et al. 2017; Mori et al. 2016b).

### **Changes/Development Throughout Pregnancy**

Throughout pregnancy uterine circulation undergoes significant restructuring to accommodate fetal demand for nutrients. Critical transformation events include: (1) luminal dilation; (2) trophoblast invasion of vessel media and endothelium; (3) deposition of fibrinoid material in place of vascular smooth muscle (Espinoza et al. 2006). Altogether, these changes achieve maximal delivery to intervillous space by increasing vessel diameter and decreasing reactivity to vasoconstricting agents.

During the first trimester of human pregnancy, invasive extravillous trophoblasts travel retrograde through spiral arterioles to serve as intraluminal plugs at the myometrial junction and permit slow release of plasma, but no true perfusion (Browne et al. 2015). At week 18 the low-pressure uteroplacental vessels are established by conversion of luminal plugs into circumferential stents (Brosens et al. 2002). About one third of spiral arterioles will be transformed into uteroplacental arterial openings into the intervillous space (Figure 1). Spiral arterioles at the center

of the placenta are more likely to be transformed into uteroplacental vessels over those located at the periphery (Brosens et al. 1967).

As pregnancy progresses, local changes initiate adaptive responses in the uterine vessels; adaptations of the uterine vessels occur by lengthening (axial) to accommodate the growing uterus and fetus and increase in diameter (circumferential) to, according to Poiseuille's law, exponentially increase flow. Experimentally, myometrial stretch alone is sufficient to induce vessel remodeling in the non-pregnant rat (Osol et al. 2012). Further, shear stress-induced activation of endothelial nitric oxide synthase (eNOS) becomes more sensitive (Ko et al. 2018; Osol et al. 2009). Precise mechanisms by which these phenomena occur are still unclear.

In addition to local uterine vascular changes, systemic hemodynamic accommodations are made by the mother during pregnancy. There is a significant increase in blood volume, increased cardiac output, elevated resting heart rate, decreased peripheral resistance, and decreased blood pressure (Fu 2018). Collectively, the physiological alterations made at the systemic level as well as the microcirculation level at the placenta dynamically meet the increasing need of blood to supply the fetus as pregnancy progresses. Readers interested in further information are referred to the following reviews (Mandala and Osol 2012; Osol and Mandala 2009).

### PLACENTAL BLOOD FLOW

The placenta is an incredibly unique, transient organ, utilized only during fetal gestation to transfer fresh nutrients to the fetus and waste to the mother. Therefore, the placenta has two circulations, receiving blood from the maternal vasculature [maternal-placental (uteroplacental)] and fetal systems [fetal-placental (fetoplacental)]. The counter-current pressure between the two systems drives perfusion and nutrient-waste exchange. Pressure in the uteroplacental system has been measured at 80-100 mmHg, 70 mmHg in spiral arterioles, and 10 mmHg in the intervillous space (Wang Y and S. 2010). This pressure gradient in combination with the low resistance arterioles permits efficient perfusion of intervillous space to ensure exchange of nutrients for waste.

The efficient exchange of blood gases and nutrients take place due to maternal blood in the intervillous space bathing the placental villi at a low pressure vs driving force. The reduction of maternal mean arterial pressures to the low flows required for proper placental function highlight the importance of the resistance vasculature within the uteroplacental system. Therefore, impairments to uterine microcirculation function and/or reactivity are a significant risk factor for adverse pregnancy outcomes.

Normal uteroplacental blood flow is achieved by the coordinated maternal hemodynamic accommodations, uterine vascular adaptations and invasion of trophoblasts. The doubling of the uterine artery diameter (circumferentially) enables an increase in blood flow to the uterus, directed at the placenta during fetal development (10 to 30 mL/min compared to  $\frac{1}{2}$  L/min) (Bullelli et al. 1986; Osol and Moore 2014). During the first trimester, spiral arterioles are lumenally obstructed by trophoblastic plugs, which then loosen and permit maternal blood flow into the intervillous space during the second and third trimesters (Osol and Moore 2014; Weiss et al. 2016). The venous system also undergo enlargement in diameter, increased distensibility and reduced elastin content which should enhance venous capacity (Osol and Mandala 2009).

The umbilical cord arises from embryonic cells and is the conduit between the fetus and placenta. It extends from the fetal umbilicus to the fetal-facing aspect of the placenta. In humans, the cord contains two arteries (umbilical arteries) and one vein (umbilical vein). As the umbilical vessels are of embryological/fetal origin, the anatomical terminology is similar to that of the pulmonary system, where the umbilical vein supplies the fetus with oxygenated, nutrient rich blood from the placenta, and the umbilical arteries return blood that is oxygen and nutrient-depleted. At the intersection of umbilical cord and placenta, each umbilical artery branches into at least eight stem arteries with average diameters of 1.5 mm (Wang Y and S. 2010). These first-order branches divide into four to eight horizontal vessels of the secondary order that have an average diameter of 1 mm. These arteries span at varying lengths and curve towards the center of the placenta as they begin branching into terminal third-order 0.1-0.6 mm villous branches that form capillary beds.

Villous capillaries fill an encasement created by another fetal trophoblast cell-type, and bring fetal blood into close proximity to maternal blood without direct intermingling. Gases and nutrients therefore have a two-cell layer barrier to traverse between blood circulations; the fetal villous trophoblast and the fetal endothelium. The blood pressure in the umbilical arteries leaving the fetal heart is about 50 mmHg, which falls to about 30 mmHg in the villous capillaries; whereas, umbilical vein pressure is about 20 mmHg (28).

#### UTEROPLACENTAL MICROVASCULAR FUNCTION

One of the defining characteristics of the microcirculation is to discuss the arterioles, capillaries, and venules within a tissue or organ of interest. Experimentally, this vasculature may then be challenged, cellular function evaluated, and reactivity assessed to identify impairments in blood flow to the tissue which may impact organ function. Physiological studies to identify the mechanisms associated with normal microvascular control, and by default microvasculopathy, continue. Microvascular perturbations that may affect organ perfusion (e.g. impaired remodeling or endothelial dysfunction) can limit blood flow within the tissue and impair the physiological function. The heart is a classical case, wherein reduced blood flow by either physical blockage or reduced arteriolar dilation may culminate in localized ischemia, reduced oxygenation and nutrient availability, and symptomatic angina. For simplicity within this review we will discuss hemodynamic control in yes or no terms, either the uterine microvasculature is capable of placental perfusion to meet fetal demand or it is not; in some cases, this may be associated with poor trophoblast invasion, inadequate spiral arteriolar remodeling, blunted arteriolar (radial, basal, or spiral) vasodilation responsiveness to chemical/mechanical stimuli, or heightened sensitivity to vasoconstrictive signaling molecules (Figure 1). Unfortunately, impaired uterine arteriolar function, implantation, placental perfusion, and the delivery of nutrients to the fetal compartment are much more complex, traditionally asymptomatic in the short term, and may propagate by affecting fetal cardiovascular health.

## PERTURBATIONS

### *Hypertension/Preeclampsia*

In general, hypertension is an abnormally high blood pressure which may be identified in an acute state after a physiological stressor (e.g. fight-or-flight) or in a chronic condition attributed to many lifestyle choices and family history. With respect to the microcirculation, chronic hypertension can result in systemic damage to the luminal endothelial lining and smooth muscle cells of blood vessels (Leitschuh and Chobanian 1987). Histological modifications lead to the weakening of the vessel wall and narrowing of the vessel lumen (Leitschuh and Chobanian 1987). These changes culminate in microvascular dysfunction and contribute to peripheral resistance, further propagating blood pressure dysregulation and inadequate blood delivery downstream. In the non-pregnant state, consequences of hypertension include myocardial infarction, strokes, and aneurysms (Kocemba et al. 1998).

Patients with hypertension prior to becoming pregnant tend to remain on their antihypertensive medications and are closely monitored by their physicians during pregnancy to limit maternal and fetal morbidity and mortality. During pregnancy major cardiovascular adaptations, including uterine microvascular remodeling, occur to increase uteroplacental blood flow. A hypertensive state during pregnancy is referred to as preeclampsia, is a consequence of failed uterine microvascular remodeling. This stoppage causes an increase of peripheral resistance sourcing from the uteroplacental vessels and, thus, a raise in maternal blood pressure. Along with preeclampsia is the release of placental hypoxic and oxidative stress factors that send additional signaling for a compensatory rise in maternal blood pressure. Moreover, the resulting local oxidative/nitrosative stress generated with poor perfusion has been shown to cause endothelial dysfunction of the microvessels providing blood to the pregnancy, leading to additional vessel narrowing and fetal risk (Sánchez-Aranguren et al. 2014).

The mechanisms associated with inappropriate uterine remodeling, culminating in poor uteroplacental perfusion and preeclampsia are currently being investigated (Fisher 2015); however, maternal inflammation, insulin resistance, metabolic syndromes and genetic predispositions participate independently or in association to increase risk (Eskenazi et al. 1991). Each of these risk factors has been identified within the literature to impact microvascular function in a variety of tissue beds, thereby limiting blood flow to downstream tissues (Romeo, ATVB, 2012); perfusion of the placenta is not uniquely impacted in this case, however tissue ischemia of the placenta can impair fetal development. Implications of preeclampsia involve maternal and fetal hazards including IUGR, placental abruption, and maternal and fetal death.

Poor uteroplacental blood flow, as seen with preeclampsia, may cause growth restriction to the fetus. Hypoperfusion of the placenta ablates nutrient and waste exchange, impeding maximal growth potential for the developing fetus which manifests by low birth weight. IUGR is associated with perinatal adverse events (prematurity, cerebral palsy, stillbirth, neonatal death) and a “preprogramming” for adult disease (obesity, hypertension, diabetes mellitus type 2) (Albu et al. 2014).

### *Metabolic Syndrome*

The substantial global prevalence of disorders involving perturbed energy utilization are increasing patient morbidity and mortality with cardiovascular disease. Metabolic Syndrome (MetS) is diagnosed as a collection of at least three of the following conditions: obesity, hypertension, hyperglycemia and dyslipidemia (Aguilar et al. 2015). It is postulated that the malutilization and storage of energy constituting these disorders is predisposing patients to microvascular disease by inducing endothelial dysfunction (Vykoukal and Davies 2011). This is believed to be caused by increased endothelial-derived NO quenching from elevated reactive oxygen species (ROS), adipose distribution and adipokine production, and endogenous corticosteroid production (Vykoukal and Davies 2011). Various cytokines (TNF- $\alpha$ , IL-6, IL-10)

that are elevated in MetS indirectly contribute to endothelial dysfunction by increasing Endothelin-1 secretion and inhibiting eNOS dysfunction (Vykoukal and Davies 2011). Adiponectin, having a vasoprotective activity, is reduced in obesity (Goldstein and Scalia 2004); while increased levels of leptin, deleterious to the cardiovascular system, lead to vascular calcification, vascular smooth muscle proliferation limiting expandability of vessel walls (Knudson et al. 2007). Excess circulating corticosteroids may also contribute to vasoconstriction (Ullian 1999).

MetS conditions in women who become pregnant are at higher risk to develop gestational diabetes mellitus (GDM) (Chu et al. 2007). Maternal insulin resistance is a normal process of human pregnancy and is critical to maintain maternal blood glucose to support the growing fetus, especially in the third trimester. Women with obesity enter pregnancy with preexisting insulin resistance that intensifies as pregnancy progresses (Friedman 2015). The placenta is most impacted by GDM through multiple mechanisms of reduced oxygen supply to the fetus and modifications in placental transport (Vambergue and Fajardy 2011). Interestingly, when assessed during pregnancy, one study found no differences in microvascular reactivity in women with or without GDM (Pontes et al. 2015). Further, obesity has an effect on uteroplacental remodeling. Increased levels of advanced glycation end products (AGEs) are significantly found within obese versus lean uterine cavities, which activated cellular stress pathways resulting in impaired decidualization, embryo implantation, and inhibited trophoblast invasion (Antoniotti et al. 2018). Uteroplacental micro and macrovascular endothelial dysfunction has also been associated with GDM and obesity during pregnancy. Several studies have identified abnormal eNOS expression and activity of the endothelial L-arginine/ nitric oxide signaling pathway (Leiva et al. 2011).

Exposure to adverse nutritional environment in utero permanently alters fetal metabolism and physiology with long term health consequences. Offspring of GDM are often born macrosomic as a result of the steeper maternal-to fetal concentration gradient of glucose across the placenta, a risk to the mother during delivery and to the fetus as glucose level plummet after birth. Fetal  $\beta$ -cell development is permanently altered during critical periods of development where organogenesis

aims to adapt to maternal environment (Simmons 2009; Vambergue and Fajardy 2011). Children who are born large for gestational age and were developmentally exposed to maternal diabetes or obesity are at increased risk to develop the constellation of conditions constituting MetS themselves (Boney et al. 2005).

### *Inflammation*

Acute and chronic inflammation may result in altered microvascular form and function. Unstressed endothelial cells serve as a nonreactive interface between circulation and tissue. Under inflammatory conditions, the endothelium of the microcirculation serves as a major contributor to a local response. Endothelial cells normally respond to neural, humoral, and endothelial-derived signals; therefore, in a pro-inflammatory environment, endothelial cells activate by thrusting selectins and integrins to the surface to signal the local recruitment of acute and chronic pro-inflammatory cells. Increased venular permeability is also a feature of the inflammatory process, under normal circumstances to allow for the immune cells and components to extravasate to the inflamed tissue (Pober and Sessa 2015). Molecularly, a pro-inflammatory environment may usurp the activity of eNOS to produce superoxide and thereby reducing the bioavailability of the endothelium-dependent vasodilator nitric oxide (Forstermann and Sessa 2012). Oxidative stress from inflammation may cause endothelial cells to increase production of the vasoconstrictive protein endothelin-1 (Marsden and Brenner 1992). Further, NO may be consumed as it reacts with oxidants, thereby limiting the bioavailability for vascular function (Incalza et al. 2018). Decreased endothelial-derived vasodilatory signals can inappropriately diminish perfusion to a specific tissue.

In healthy pregnancy, immune-mediator cells prevent excessive maternal inflammation and subsequent rejection of the invading fetal tissue (PrabhuDas et al.). However, in some cases interactions between the transformed decidual cell populations the fetal extravillous trophoblasts lead to failed spiral arteriole remodeling. Putative mechanisms include immune cell activation and subsequent secretion of cytokines and placental factors impeding trophoblast invasion,

angiogenesis, and in turn, placentation. Maternal inflammation (as demonstrated by LPS administration) has been associated with deficient trophoblast invasion, uteroplacental hemodynamic alterations, placental nitrosative stress, and spiral arteriole remodeling, possibly associated with an increased activated macrophage population identified at spiral arteries (Cotechini et al. 2014). An in vitro study confirmed that activated macrophages inhibit trophoblast motility and migration by secreting tumor necrosis factor (TNF) (Renaud et al. 2005; Todt et al. 1996). Mice with lipopolysaccharide-induced inflammation had a reversal of these effects with the administration of nitric oxide mimetic glyceryl trinitrate, indicating the role of inflammatory quenching of nitric oxide in perturbed uteroplacental circulation (Cotechini et al. 2014). Conclusively, maternal inflammation causes macrophage-derived TNF to inhibit spiral arteriole remodeling, and may thereby lead to the pathological processes of growth restriction sequelae. Further, cytokine-induced disassembly of cell-to-cell junctions at trophoblastic and endothelial cells in inflamed placental tissues may put the fetus at risk through an inability to maintain proper barrier function (Tossetta et al. 2014).

Fetal development may become compromised with abnormal maternal inflammation. Impaired placentation, uteroplacental perfusion, and homeostasis result and are shared characteristics of preeclampsia, IUGR and fetal demise. Indeed, it has been shown that women who have a history of miscarriage also have elevated levels of inflammation compared to non-pregnant women who went on to have healthy pregnancies (Wilson et al. 2004). Maternal inflammatory mediators (IL-6 and IL-8) have been associated with preterm delivery, low birth weight and respiratory insufficiency increasing fetal risk of long-term cardiac, metabolic and pulmonary deficiencies (Velten et al. 2012). Additionally, maternal inflammation in mid-pregnancy changes fetal neurodevelopment resulting in long-term behavioral deficits that may persist into adulthood (Goeden et al. 2016).

*Maternal Homeostasis (Noise Pollution and Circadian Rhythm Disruption)*

Homeostasis may become challenged under psychological and/or physiological stressors, where vessels need to undergo changes to restore equilibrium. The microvasculature plays a significant role in buffering fluctuations in blood pressure and blood flow to maintain a dynamic equilibrium. It has been hypothesized that stressors of ambient noise and sleep deprivation has adverse effects on human vascular health (Abrams 2015; Munzel et al. 2018). Noise pollution can cause high stress levels, sleep disturbances, among other harmful effects. Nighttime noise in particular has been observed to increase levels of stress hormones and vascular oxidative stress, thereby contributing to hypertension and diabetes (Munzel et al. 2018). Interestingly, one study reported impaired endothelial function in patients with or at risk for cardiovascular disease that appeared to be independent from annoyance or attitude towards nighttime aircraft noise (Schmidt et al. 2015). Noise-induced vascular damage appears to be mediated by activation of NADPH oxidase, which uncouples eNOS and activates inflammatory cells (Munzel et al. 2018). Sleep disorders in addition are associated with metabolic dysfunction and increased inflammation, which also contribute to endothelial cell dysfunction (Qiu et al. 2015). One group has identified that while sexually mature female mice are more susceptible to chronic stress, they exhibit a vasoprotective phenotype, wherein arteriolar reactivity is blunted, but not as severely as the male counterparts (Stanley et al. 2014). Unfortunately, there is a severe lack of research in this area; however available studies do implicate these environmental stressors in microvascular dysfunction and a reduced ability to achieve and maintain homeostasis.

Within the context of pregnancy, there is epidemiological evidence showing an association with noise pollution and gestational hypertension, low birth weight, and congenital malformations (Dzhambov et al. 2014; Yinon et al. 2006). One mouse study evaluating circadian rhythm disruption on pregnancy outcomes found no significant impact on gestation length, litter size and birth weight, suggesting there may be maternal compensatory mechanisms to maintain fetal growth during sleep disturbances (Varcoe et al. 2016). Further, non-pregnant female mice following an 8-week unpredictable chronic mild stress protocol demonstrate impaired arteriolar reactivity (Stanley

et al. 2014); while the estrous status of these mice is unknown, arteriolar dysfunction at crucial stages may affect trophoblast invasion and adequate placentation. Given the paucity of research evaluating noise, sleep disturbance and uteroplacental function, it is plausible that the increase in oxidative stress as a result of inflammation during pregnancy lends to uteroplacental microvascular dysfunction. In turn, it is plausible that these perturbations could increase susceptibility to the development of preeclampsia, IUGR, and other adverse fetal outcomes to ensue as a result. Further microvascular research in this space is urgently needed.

### *Environmental Exposure*

Accumulating evidence implicates environmental exposures to microvascular dysfunction and disease. To limit the overwhelming possibilities in this field, we will limit the scope in this review to nicotine, heavy metals as found in polluted drinking water, and air pollution/particulate matter. Nicotine is well known to have deleterious effects such as vasoconstriction and increased blood pressure, overall perturbing microvascular patency (Benowitz and Burbank 2016). Heavy metals such as cadmium alter microvascular permeability by disturbing junctional complexes that join adjacent endothelial cells (Prozialeck et al. 2008). Additionally, the particulate matter fraction of air pollution (of a diameter of 2.5  $\mu\text{m}$  and smaller;  $\text{PM}_{2.5}$ ) has been shown to escape the lung and reach distal organs through blood circulation (Brook et al. 2010). Proposed mechanisms for exposure to  $\text{PM}_{2.5}$  include high oxidative stress, hypercoagulability and inflammation that lend to cardiovascular outcomes (Brook 2008).

Smoking has also been linked to vasoconstriction of uteroplacental arteries, thereby reducing maternal blood flow into the intervillous space (Philipp et al. 1984). Further, nicotine increases free radicals within the placenta and exposes maternal and fetal systems to genetic and cellular oxidative damage (Mund et al. 2013). There is scarce data describing the effects other heavy metals on uteroplacental vasculature. However, the unifying factor is the ability for these metals to generate reactive oxygen and nitrogen species. With evidence that these metals occupy

and traverse the placenta, local oxidative stress may cause damage to trophoblastic and maternal endothelial cells, overall contributing to reduced placental function (Valko et al. 2005). Exposure to air pollution during gestation changes the morphology of multiple placental compartments including maternal spiral arteries, fetal capillaries and the interface of exchange. Moreover, these changes are found in association with low birth weights for exposed fetuses (Backes et al. 2013). Engineered nanomaterials have been primarily used as a surrogate for air pollution; however, more recently given an increase in manufacturing, biomedical applications, and nanotechnology there is risk of exposure to the pregnant population (Fournier et al. 2018; Stapleton 2016; Stapleton and Nurkiewicz 2014) . Maternal inhalation of ENM led to increased uterine vascular tone, smaller active diameter, and inappropriate response to an increase in luminal sheer stress (Stapleton et al. 2013b). Even a single exposure, 24-hours prior to assessment, caused significant impairment to endothelium-dependent dilation during late-stage pregnancy, indicating a reduced ability to react to vasodilatory mediators and limit maternal-fetal exchange (Stapleton et al. 2018c).

Environmental contaminants have the potential to directly and indirectly affect the placenta and fetus. Limited data show that fetal systems may be susceptible to maternal inhalation of particulate matter from direct translocation, as well as secondary inflammatory processes. Maternal smoking and nicotine leads to impaired fertility, type 2 diabetes, obesity, hypertension, neurobehavioral deficits and respiratory dysfunction in the offspring (Bruin et al. 2010). A large prospective study observed as smoking increased, placentas enlarged and developed microscopic lesions typical of under-perfusion from the uterine vasculature, which leads to low birth weight after maternal exposure (Naeye 1978). Heavy metal exposure leads to a myriad of fetal effects, from low birth weight to death due to toxicity (Wai et al. 2017). Heavy metals (mercury, lead, cadmium) are also well known to cross the placental barrier and cause both direct and indirect damage to the fetus and cause IUGR and perturbed neurodevelopment (Bose-O'Reilly et al. 2010; Potula and Kaye 2005; Stasenko et al. 2010). Maternal exposure to air pollution, results in abolished fetal endothelium-dependent reactivity which may predispose offspring to a myriad of adult

diseases (Backes et al. 2013; Stapleton et al. 2013b). Further, in our model, cardiac dysfunction is evident in surviving offspring including reduced coronary function, epicardial microvascular dysfunction, diminished cardiomyocyte contractility, and decreased mitochondrial energetics culminating in impaired metabolic function of the heart in adult offspring (Hathaway et al. 2017; Stapleton et al. 2018a; Stapleton et al. 2015d). This hypoperfusion along with toxicant accumulation in the placenta showed long lasting neurodevelopmental impairments, and low birth weight for the offspring. A robust understanding of fetal outcomes after various gestational exposures cause uteroplacental microvessel dysfunction has yet to be established.

#### **A-1.4 Conclusion**

Placental trophoblast invasion, remodeling of preplacental spiral arterioles, and fetal microvascular endothelial function are key for a successful pregnancy. The joining of maternal and fetal circulations is one of the most acutely demanding and complex processes set up to meet fetal nutritional needs. Uterine spiral arterioles are remodeled by embryonic cells to establish large vessels with low resistance. The importance of successful uterine microvascular remodeling is underscored by its failure resulting in pathologies which impact fetal development and impair fetal growth.

The effects of disease and environmental conditions on cardiovascular form and function have become increasingly understood and emphasized. Uterine microvasculature exhibits a rare example of adult cyclic angiogenesis where extensive remodeling prepares for optimal invasion and uteroplacental perfusion. This complex process is a critical set up for normal pregnancy and fetal development, with major pathological consequences if failed. The “Barker Hypothesis” suggests that fetal development within a hostile environment may underpin susceptibility to adult disease. While the available amount of literature is modest, internal and external variables such as maternal hypertension, obesity, diabetes, inflammation, or disruption of homeostasis derived from stressors or environmental exposure may impede the ability to distribute blood flow to the fetal

compartment. Further research in this area is urgently required to better understand the mechanisms of uterine microvascular disease creating a hostile gestational environment and the adult health risks involved for the offspring.

#### ACKNOWLEDGEMENTS

We thank Jane Salmon for her assistance in the preparation of Figure 1 and Dr. Sara Fournier for her critical review of the manuscript. This work was supported by the National Institute of Environmental Health Sciences (R00-ES024783), Rutgers Center for Environmental Exposures and Disease (P30-ES005022), and Rutgers Joint Graduate Program in Toxicology (T32-ES007148).

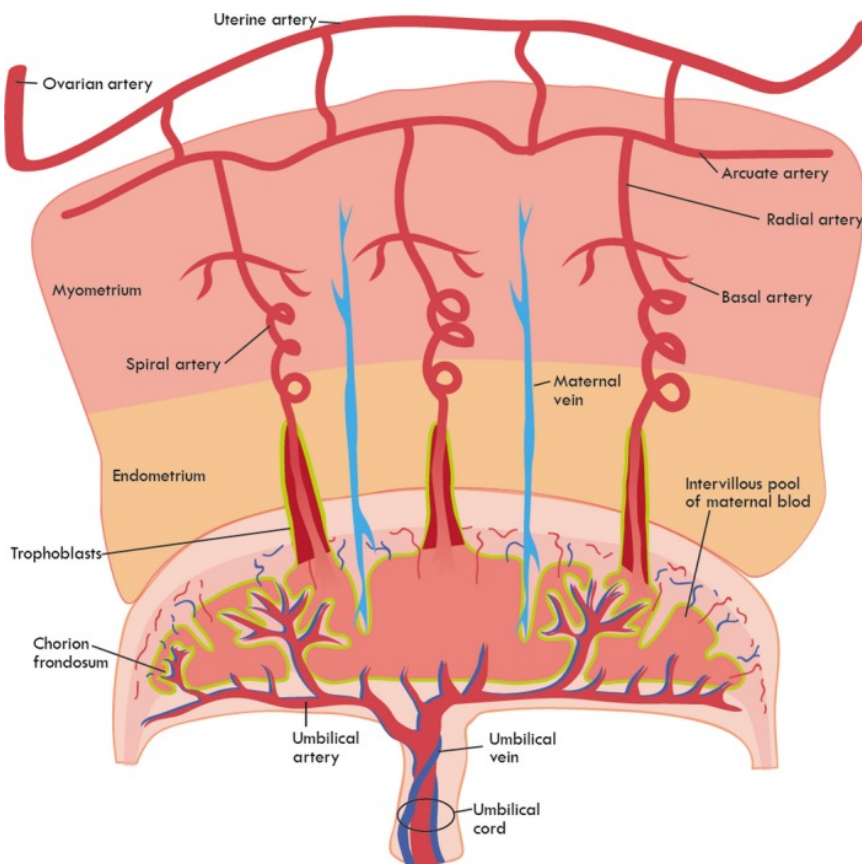


**Figure A-1.1: Schematic of utero-placental vasculature.** Development and responsiveness of the maternal-fetal macro- and microvasculature is crucial for proper placental perfusion, fetal development, and successful gestation. Perturbations to vascular maturity, trophoblast invasion, spiral arteriolar remodeling, or arteriolar (radial, basal, or spiral) reactivity, during pregnancy may limit placental perfusion and have dire consequences for the fetus.

#### References:

- Abrams RM. 2015. Sleep deprivation. *Obstetrics and gynecology clinics of North America*. 42(3):493-506.
- Aguilar M, Bhuket T, Torres S, Liu B, Wong RJ. 2015. Prevalence of the metabolic syndrome in the united states, 2003-2012. *Jama*. 313(19):1973-1974.
- Albu AR, Anca AF, Horhoianu VV, Horhoianu IA. 2014. Predictive factors for intrauterine growth restriction. *Journal of Medicine and Life*. 7(2):165-171.
- Antoniotti GS, Coughlan M, Salamonsen LA, Evans J. 2018. Obesity associated advanced glycation end products within the human uterine cavity adversely impact endometrial function and embryo implantation competence. *Human reproduction (Oxford, England)*. 33(4):654-665.

- Backes CH, Nelin T, Gorr MW, Wold LE. 2013. Early life exposure to air pollution: How bad is it? *Toxicology letters*. 216(1):47-53.
- Barker DJ. 1990. The fetal and infant origins of adult disease. *BMJ*. 301(6761):1111.
- Barker DJ. 1999. Fetal origins of cardiovascular disease. *Ann Med*. 31 Suppl 1:3-6.
- Barker DJ, Eriksson JG, Forsen T, Osmond C. 2002. Fetal origins of adult disease: Strength of effects and biological basis. *Int J Epidemiol*. 31(6):1235-1239.
- Benowitz NL, Burbank AD. 2016. Cardiovascular toxicity of nicotine: Implications for electronic cigarette use. *Trends in cardiovascular medicine*. 26(6):515-523.
- Bonagura TW, Pepe GJ, Enders AC, Albrecht ED. 2008. Suppression of extravillous trophoblast vascular endothelial growth factor expression and uterine spiral artery invasion by estrogen during early baboon pregnancy. *Endocrinology*. 149(10):5078-5087.
- Boney CM, Verma A, Tucker R, Vohr BR. 2005. Metabolic syndrome in childhood: Association with birth weight, maternal obesity, and gestational diabetes mellitus. *Pediatrics*. 115(3):e290-296.
- Bose-O'Reilly S, McCarty KM, Steckling N, Lettmeier B. 2010. Mercury exposure and children's health. *Current problems in pediatric and adolescent health care*. 40(8):186-215.
- Brook Robert D. 2008. Cardiovascular effects of air pollution. *Clinical Science*. 115(6):175.
- Brook RD, Rajagopalan S, Pope CA, 3rd, Brook JR, Bhatnagar A, Diez-Roux AV, Holguin F, Hong Y, Luepker RV, Mittleman MA et al. 2010. Particulate matter air pollution and cardiovascular disease: An update to the scientific statement from the American Heart Association. *Circulation*. 121(21):2331-2378.
- Brosens I, Robertson WB, Dixon HG. 1967. The physiological response of the vessels of the placental bed to normal pregnancy. *The Journal of pathology and bacteriology*. 93(2):569-579.
- Brosens JJ, Pijnenborg R, Brosens IA. 2002. The myometrial junctional zone spiral arteries in normal and abnormal pregnancies: A review of the literature. *American journal of obstetrics and gynecology*. 187(5):1416-1423.
- Browne VA, Julian CG, Toledo-Jaldin L, Cioffi-Ragan D, Vargas E, Moore LG. 2015. Uterine artery blood flow, fetal hypoxia and fetal growth. *Philosophical transactions of the Royal Society of London Series B, Biological sciences*. 370(1663):20140068.
- Bruin JE, Gerstein HC, Holloway AC. 2010. Long-term consequences of fetal and neonatal nicotine exposure: A critical review. *Toxicological sciences : an official journal of the Society of Toxicology*. 116(2):364-374.
- Bulletti C, Jasonni VM, Lubicz S, Flamigni C, Gurrupide E. 1986. Extracorporeal perfusion of the human uterus. *American journal of obstetrics and gynecology*. 154(3):683-688.
- Chu SY, Callaghan WM, Kim SY, Schmid CH, Lau J, England LJ, Dietz PM. 2007. Maternal obesity and risk of gestational diabetes mellitus. *Diabetes care*. 30(8):2070-2076.
- Cotechini T, Komisarenko M, Sperou A, Macdonald-Goodfellow S, Adams MA, Graham CH. 2014. Inflammation in rat pregnancy inhibits spiral artery remodeling leading to fetal growth restriction and features of preeclampsia. *The Journal of Experimental Medicine*. 211(1):165-179.
- Damsky CH, Fisher SJ. 1998. Trophoblast pseudo-vasculogenesis: Faking it with endothelial adhesion receptors. *Current opinion in cell biology*. 10(5):660-666.
- Demir R, Yaba A, Huppertz B. 2010. Vasculogenesis and angiogenesis in the endometrium during menstrual cycle and implantation. *Acta histochemica*. 112(3):203-214.
- Dzhambov AM, Dimitrova DD, Dimitrakova ED. 2014. Noise exposure during pregnancy, birth outcomes and fetal development: Meta-analyses using quality effects model. *Folia medica*. 56(3):204-214.

- Eskenazi B, Fenster L, Sidney S. 1991. A multivariate analysis of risk factors for preeclampsia. *Jama*. 266(2):237-241.
- Espinoza J, Romero R, Mee Kim Y, Kusanovic JP, Hassan S, Erez O, Gotsch F, Than NG, Papp Z, Jai Kim C. 2006. Normal and abnormal transformation of the spiral arteries during pregnancy. *Journal of perinatal medicine*. 34(6):447-458.
- Fisher SJ. 2015. Why is placentation abnormal in preeclampsia? *American journal of obstetrics and gynecology*. 213(4 Suppl):S115-122.
- Forstermann U, Sessa WC. 2012. Nitric oxide synthases: Regulation and function. *European heart journal*. 33(7):829-837, 837a-837d.
- Fournier SB, D'Errico JN, Stapleton PA. 2018. Engineered nanomaterial applications in perinatal therapeutics. *Pharmacol Res*. 130:36-43.
- Friedman JE. 2015. Obesity and gestational diabetes mellitus pathways for programming in mouse, monkey, and man—where do we go next? The 2014 norbert freinkel award lecture. *Diabetes care*. 38(8):1402-1411.
- Fu Q. 2018. Hemodynamic and electrocardiographic aspects of uncomplicated singleton pregnancy. *Advances in experimental medicine and biology*. 1065:413-431.
- Furuya M, Ishida J, Aoki I, Fukamizu A. 2008. Pathophysiology of placentation abnormalities in pregnancy-induced hypertension. *Vascular Health and Risk Management*. 4(6):1301-1313.
- Goeden N, Velasquez J, Arnold KA, Chan Y, Lund BT, Anderson GM, Bonnin A. 2016. Maternal inflammation disrupts fetal neurodevelopment via increased placental output of serotonin to the fetal brain. *The Journal of Neuroscience*. 36(22):6041-6049.
- Goldstein BJ, Scalia R. 2004. Adiponectin: A novel adipokine linking adipocytes and vascular function. *The Journal of clinical endocrinology and metabolism*. 89(6):2563-2568.
- Hathaway QA, Nichols CE, Shepherd DL, Stapleton PA, McLaughlin SL, Stricker JC, Rellick SL, Pinti MV, Abukabda AB, McBride CR et al. 2017. Maternal-engineered nanomaterial exposure disrupts progeny cardiac function and bioenergetics. *Am J Physiol Heart Circ Physiol*. 312(3):H446-H458.
- Incalza MA, D'Oria R, Natalicchio A, Perrini S, Laviola L, Giorgino F. 2018. Oxidative stress and reactive oxygen species in endothelial dysfunction associated with cardiovascular and metabolic diseases. *Vascular pharmacology*. 100:1-19.
- Knudson JD, Dick GM, Tune JD. 2007. Adipokines and coronary vasomotor dysfunction. *Experimental Biology and Medicine*. 232(6):727-736.
- Ko NL, John L, Gelinne A, Mandala M, Osol G. 2018. Venoarterial communication mediates arterial wall shear stress-induced maternal uterine vascular remodeling during pregnancy. *American journal of physiology Heart and circulatory physiology*.
- Kocemba J, Kawecka-Jaszcz K, Gryglewska B, Grodzicki T. 1998. Isolated systolic hypertension: Pathophysiology, consequences and therapeutic benefits. *Journal of human hypertension*. 12(9):621-626.
- Leitschuh M, Chobanian A. 1987. Vascular changes in hypertension. *The Medical clinics of North America*. 71(5):827-841.
- Leiva A, Pardo F, Ramírez MA, Farías M, Casanello P, Sobrevia L. 2011. Fetoplacental vascular endothelial dysfunction as an early phenomenon in the programming of human adult diseases in subjects born from gestational diabetes mellitus or obesity in pregnancy. *Experimental diabetes research*. 2011:349286-349286.
- Losordo DW, Isner JM. 2001. Estrogen and angiogenesis: A review. *Arteriosclerosis, thrombosis, and vascular biology*. 21(1):6-12.

- Mandala M, Osol G. 2012. Physiological remodelling of the maternal uterine circulation during pregnancy. *Basic & clinical pharmacology & toxicology*. 110(1):12-18.
- Marsden PA, Brenner BM. 1992. Transcriptional regulation of the endothelin-1 gene by tn $\alpha$ . *The American journal of physiology*. 262(4 Pt 1):C854-861.
- Mathew H, Castracane VD, Mantzoros C. 2017. Adipose tissue and reproductive health. *Metabolism: clinical and experimental*.
- Mori M, Bogdan A, Balassa T, Csabai T, Szekeres-Bartho J. 2016. The decidua—the maternal bed embracing the embryo—maintains the pregnancy. *Seminars in Immunopathology*. 38(6):635-649.
- Mund M, Louwen F, Klingelhofer D, Gerber A. 2013. Smoking and pregnancy — a review on the first major environmental risk factor of the unborn. *International Journal of Environmental Research and Public Health*. 10(12):6485-6499.
- Munzel T, Schmidt FP, Steven S, Herzog J, Daiber A, Sorensen M. 2018. Environmental noise and the cardiovascular system. *Journal of the American College of Cardiology*. 71(6):688-697.
- Naeye RL. 1978. Effects of maternal cigarette smoking on the fetus and placenta. *British journal of obstetrics and gynaecology*. 85(10):732-737.
- Osol G, Barron C, Gokina N, Mandala M. 2009. Inhibition of nitric oxide synthases abrogates pregnancy-induced uterine vascular expansive remodeling. *Journal of vascular research*. 46(5):478-486.
- Osol G, Barron C, Mandala M. 2012. Uterine distension differentially affects remodelling and distensibility of the uterine vasculature in non-pregnant rats. *Reproduction, fertility, and development*. 24(6):835-842.
- Osol G, Mandala M. 2009. Maternal uterine vascular remodeling during pregnancy. *Physiology (Bethesda, Md)*. 24:58-71.
- Osol G, Moore LG. 2014. Maternal uterine vascular remodeling during pregnancy. *Microcirculation*. 21(1):38-47.
- Philipp K, Pateisky N, Endler M. 1984. Effects of smoking on uteroplacental blood flow. *Gynecologic and obstetric investigation*. 17(4):179-182.
- Pijnenborg R, Vercruyse L, Brosens I. 2011. Deep placentation. *Best practice & research Clinical obstetrics & gynaecology*. 25(3):273-285.
- Pober JS, Sessa WC. 2015. Inflammation and the blood microvascular system. *Cold Spring Harbor Perspectives in Biology*. 7(1):a016345.
- Pontes IEA, Afra KF, Silva JR, Borges PSN, Clough GF, Alves JGB. 2015. Microvascular reactivity in women with gestational diabetes mellitus studied during pregnancy. *Diabetology & Metabolic Syndrome*. 7:27.
- Potula V, Kaye W. 2005. Report from the cdc. Is lead exposure a risk factor for bone loss? *Journal of women's health (2002)*. 14(6):461-464.
- PrabhuDas M, Bonney E, Caron K, doi:10.1038/ni.3131. ea-. Immune mechanisms at the maternal-fetal interface: Perspectives and challenges. *Nature Immunology*. 16(4):328-334.
- Prozialeck WC, Edwards JR, Nebert DW, Woods JM, Barchowsky A, Atchison WD. 2008. The vascular system as a target of metal toxicity. *Toxicological sciences : an official journal of the Society of Toxicology*. 102(2):207-218.
- Qiu C, Sanchez SE, Gelaye B, Enquobahrie DA, Ananth CV, Williams MA. 2015. Maternal sleep duration and complaints of vital exhaustion during pregnancy is associated with placental abruption. *The journal of maternal-fetal & neonatal medicine : the official journal of the European Association of Perinatal Medicine, the Federation of Asia and Oceania Perinatal Societies, the International Society of Perinatal Obstetricians*. 28(3):350-355.

- Renaud SJ, Postovit LM, Macdonald-Goodfellow SK, McDonald GT, Caldwell JD, Graham CH. 2005. Activated macrophages inhibit human cytotrophoblast invasiveness in vitro. *Biology of reproduction*. 73(2):237-243.
- Robertson WB. 1976. Uteroplacental vasculature. *Journal of clinical pathology Supplement (Royal College of Pathologists)*. 10:9-17.
- Sánchez-Aranguren LC, Prada CE, Riaño-Medina CE, Lopez M. 2014. Endothelial dysfunction and preeclampsia: Role of oxidative stress. *Frontiers in Physiology*. 5:372.
- Schmidt F, Kolle K, Kreuder K, Schnorbus B, Wild P, Hechtner M, Binder H, Gori T, Munzel T. 2015. Nighttime aircraft noise impairs endothelial function and increases blood pressure in patients with or at high risk for coronary artery disease. *Clinical research in cardiology : official journal of the German Cardiac Society*. 104(1):23-30.
- Simmons RA. 2009. Developmental origins of adult disease. *Pediatric Clinics of North America*. 56(3):449-Contents.
- Stanley SC, Brooks SD, Butcher JT, d'Audiffret AC, Frisbee SJ, Frisbee JC. 2014. Protective effect of sex on chronic stress- and depressive behavior-induced vascular dysfunction in balb/cj mice. *Journal of applied physiology (Bethesda, Md : 1985)*. 117(9):959-970.
- Stapleton PA. 2016. Gestational nanomaterial exposures: Microvascular implications during pregnancy, fetal development and adulthood. *J Physiol*. 594(8):2161-2173.
- Stapleton PA, Hathaway QA, Nichols CE, Abukabda AB, Pinti MV, Shepherd DL, McBride CR, Yi J, Castranova VC, Hollander JM et al. 2018a. Maternal engineered nanomaterial inhalation during gestation alters the fetal transcriptome. *Part Fibre Toxicol*. 15(1):3.
- Stapleton PA, McBride CR, Yi J, Abukabda AB, Nurkiewicz TR. 2018b. Estrous cycle-dependent modulation of in vivo microvascular dysfunction after nanomaterial inhalation. *Reproductive toxicology (Elmsford, NY)*. 78:20-28.
- Stapleton PA, Minarchick VC, Yi J, Engels K, McBride CR, Nurkiewicz TR. 2013. Maternal engineered nanomaterial exposure and fetal microvascular function: Does the barker hypothesis apply? *American journal of obstetrics and gynecology*. 209(3):227.e221-211.
- Stapleton PA, Nichols CE, Yi J, McBride CR, Minarchick VC, Shepherd DL, Hollander JM, Nurkiewicz TR. 2015. Microvascular and mitochondrial dysfunction in the female f1 generation after gestational tio2 nanoparticle exposure. *Nanotoxicology*. 9(8):941-951.
- Stapleton PA, Nurkiewicz TR. 2014. Maternal nanomaterial exposure: A double threat to maternal uterine health and fetal development? *Nanomedicine (Lond)*. 9(7):929-931.
- Stasenko S, Bradford EM, Piasek M, Henson MC, Varnai VM, Jurasovic J, Kusec V. 2010. Metals in human placenta: Focus on the effects of cadmium on steroid hormones and leptin. *Journal of applied toxicology : JAT*. 30(3):242-253.
- Tessier DR, Yockell-Lelievre J, Gruslin A. 2015. Uterine spiral artery remodeling: The role of uterine natural killer cells and extravillous trophoblasts in normal and high-risk human pregnancies. *American journal of reproductive immunology (New York, NY : 1989)*. 74(1):1-11.
- Thamotharan M, Garg M, Oak S, Rogers LM, Pan G, Sangiorgi F, Lee PW, Devaskar SU. 2007. Transgenerational inheritance of the insulin-resistant phenotype in embryo-transferred intrauterine growth-restricted adult female rat offspring. *American journal of physiology Endocrinology and metabolism*. 292(5):E1270-1279.
- Todt JC, Yang Y, Lei J, Lauria MR, Sorokin Y, Cotton DB, Yelian FD. 1996. Effects of tumor necrosis factor-alpha on human trophoblast cell adhesion and motility. *American journal of reproductive immunology (New York, NY : 1989)*. 36(2):65-71.

- Tossetta G, Paolinelli F, Avellini C, Salvolini E, Ciarmela P, Lorenzi T, Emanuelli M, Toti P, Giuliani R, Gesuita R et al. 2014. Il-1beta and tgf-beta weaken the placental barrier through destruction of tight junctions: An in vivo and in vitro study. *Placenta*. 35(7):509-516.
- Ullian ME. 1999. The role of corticosteroids in the regulation of vascular tone. *Cardiovascular research*. 41(1):55-64.
- Valko M, Morris H, Cronin MT. 2005. Metals, toxicity and oxidative stress. *Current medicinal chemistry*. 12(10):1161-1208.
- Vambergue A, Fajardy I. 2011. Consequences of gestational and pregestational diabetes on placental function and birth weight. *World Journal of Diabetes*. 2(11):196-203.
- Varcoe TJ, Voultios A, Gatford KL, Kennaway DJ. 2016. The impact of prenatal circadian rhythm disruption on pregnancy outcomes and long-term metabolic health of mice progeny. *Chronobiology international*. 33(9):1171-1181.
- Velten M, Britt RD, Heyob KM, Welty SE, Eiberger B, Tipple TE, Rogers LK. 2012. Prenatal inflammation exacerbates hyperoxia-induced functional and structural changes in adult mice. *American Journal of Physiology - Regulatory, Integrative and Comparative Physiology*. 303(3):R279-R290.
- Vykoukal D, Davies MG. 2011. Vascular biology of metabolic syndrome. *Journal of vascular surgery : official publication, the Society for Vascular Surgery [and] International Society for Cardiovascular Surgery, North American Chapter*. 54(3):819-831.
- Wai KM, Mar O, Kosaka S, Umemura M, Watanabe C. 2017. Prenatal heavy metal exposure and adverse birth outcomes in myanmar: A birth-cohort study. *International Journal of Environmental Research and Public Health*. 14(11):1339.
- Wallace AE, Fraser R, Cartwright JE. 2012. Extravillous trophoblast and decidual natural killer cells: A remodelling partnership. *Human reproduction update*. 18(4):458-471.
- Wang Y, S. Z. 2010. *Vascular biology of the placenta*. San Rafael CA: Morcan and Claypool Life Sciences.
- Weiss G, Sundl M, Glasner A, Huppertz B, Moser G. 2016. The trophoblast plug during early pregnancy: A deeper insight. *Histochemistry and cell biology*. 146(6):749-756.
- Wilson R, Jenkins C, Miller H, McInnes IB, Moore J, McLean MA, Walker JJ. 2004. Abnormal cytokine levels in non-pregnant women with a history of recurrent miscarriage. *European Journal of Obstetrics & Gynecology and Reproductive Biology*. 115(1):51-54.
- Yinon D, Lowenstein L, Suraya S, Beloosesky R, Zmora O, Malhotra A, Pillar G. 2006. Pre-eclampsia is associated with sleep-disordered breathing and endothelial dysfunction. *The European respiratory journal : official journal of the European Society for Clinical Respiratory Physiology*. 27(2):328-333.

**APPENDIX 2: *Ex vivo* perfusion of the rodent placenta**

JN D'Errico<sup>a</sup>, SB Fournier<sup>b</sup>, PA Stapleton<sup>a,b</sup>

**AFFILIATIONS:**

a. Department of Pharmacology and Toxicology, Ernest Mario School of Pharmacy, Rutgers University, 160 Frelinghuysen Rd., Piscataway, NJ 08854, USA; b. Environmental and Occupational Health Sciences Institute, 170 Frelinghuysen Rd., Piscataway, NJ 08854, USA

### A-2.1 Abstract

The placenta is a key organ during pregnancy that serves as a barrier to fetal xenobiotic exposure and mediates the exchange of nutrients for waste. Here is described an assay to perfuse an isolated rat placenta and evaluate maternal-to-fetal translocation of xenobiotics *ex vivo*. In addition, the evaluation of physiological processes such as fluid flow to the fetus and placental metabolism may be conducted with this methodology. This technique is suitable for evaluating maternal-to-fetal kinetics of pharmaceutical candidates or environmental contaminants. In contrast to current alternative approaches, this methodology allows the evaluation of isolated maternal-fetal vasculature, with systemic neural or immune involvement removed, allowing any observed changes of physiological function to be attributable to local factors within the isolated tissue.

### A-2.2 Introduction

By maintaining morphological structure and physiological responsiveness, organ perfusion has been an accepted system- or tissue-based approach for analyzing metabolic function. These perfusion techniques allow for the *ex vivo* examination of intact tissue responses to a variety of pharmacological and mechanical stimuli. Perfusion of human placenta was initially described in 1958 to identify the hormonal effects on metabolic activity of the citric acid cycle; having previously been identified in tissue homogenates, Drs. Troen and Gordon recognized the need to clarify endocrine activity using a novel physiological approach (Troen and Gordon 1958). In the same era, single-perfusion (maternal-to-fetal or fetal-to-maternal) strategies were described in large (Alexander et al. 1955a; Alexander et al. 1955b) and small (Dancis and Money 1960) animal models to understand the placental transfer of sugars, salts, and antipyrine drug transfer. *In vivo* and *ex vivo* dual-perfusion (coordinated maternal and fetal perfusion) techniques were described to further characterize placental transfer using *in vivo* (London et al. 1963) and *ex vivo* (Bond et al. 2006; Goeden and Bonnin 2013; Stulc et al. 1990) methodologies. Technological advancements in

transmission and scanning electron microscopy allowed researchers to verify the structural and functional integrity of human placental tissues after perfusion (Illsley et al. 1985).

While perfusion of human placental tissues and individual cotyledon are most relevant, the rapid development of pharmacological agents and environmental contaminants necessitates the use of an animal perfusion model for early screening of xenobiotic transfer across the placental barrier. This placental perfusion methodology allows for evaluation of transfer across the placental barrier using more easily attainable and physiologically relevant rat placenta. In addition, fluid flow across the placental barrier over a period of time after an exposure can be evaluated by measuring the volume of perfusate coming from the umbilical artery. By virtue of allowing placental perfusion from both the maternal and fetal circulations, this dual-flow whole organ approach can be advantageous compared to current *in vitro* and *in vivo* approaches. This methodology would allow administration of a xenobiotic through the maternal aspect to be measured from perfusate emerging across the placenta through the umbilical vein, or vice versa. The preparation depicted here will describe the transfer of 20 nm polystyrene, a common nanoplastic used in food and medical products, from the maternal uterine artery to the fetal compartment and an associated decrease in fluid flow across the placenta to illustrate use in multiple physiological, pharmacological, and toxicological settings, to assess placental transfer, metabolism, and physiological alterations affecting maternal and/or fetal flow.

#### ETHICS STATEMENT:

All experimental procedures were approved by the Institutional Animal Care and Use Committee of Rutgers University.

#### **A-2.3 Protocol**

## 1. Preparation before the experiment

### 1.1 Modify the vessel chamber. (Figure 1A and B)

1.1.1 Move the thermistor sensor from beneath the clip and bent to hang free in the perfusion bath.

1.1.2 Install two 4-inch blunt-tip stainless steel needles with standard luer connection hubs, one 25-gauge and one 23-gauge secured beneath the thermistor clip and added a 3-way stopcock to allow for cannulation of the umbilical vasculature.

Note: The luer connections of different gauge sizes are color coded. This is advantageous to ease in vessel identification below, during and after the experiment.

1.2 Install 70-100  $\mu\text{m}$  glass micropipettes. For further information on these procedures, please review the following manuscripts (Butcher et al. 2012; Davis et al. 1995). The tip diameter commonly used in these experiments is 70-100  $\mu\text{m}$ .

Note: Tip diameters smaller than this may puncture the vascular wall during cannulation and larger may add difficulty to the cannulation process.

1.3 Prepare ties from sterile nylon suture (for proximal and distal ends of the uterine artery) and from black braided silk non-sterile suture (for the umbilical vessels). Single ties are made by looping suture as to initiate a square knot or tie a shoe. They are commonly made and kept in a petri dish filled with a small layer of rubber to help by working on a sticky background.

1.4 Prepare 2,000 mL (2 liters) of physiological salt solution (PSS) at a pH of  $7.40 \pm 0.02$  and pH confirm by submerging the electrode of a pH meter into the solution. If the pH of the solution slightly higher than 7.4, slowly add a few drops of acid (1 N sodium chloride) or base (1 M hydrochloric acid) to the solution into the solution and wait at least 20 seconds

before reading the adjusted pH measurement on the meter. Store PSS until ready for use in the refrigerator to reduce contamination. The recipe for PSS is as follows: PSS (in mmol/l): 129.8 NaCl, 5.4 KCl, 0.5 NaH<sub>2</sub>PO<sub>4</sub>, 0.83 MgSO<sub>4</sub>, 19 NaHCO<sub>3</sub>, 1.8 CaCl<sub>2</sub>, and 5.5 glucose.

1.5 Label microcentrifuge tubes for “maternal” and “fetal” effluent collection for each time point i.e. “MBaseline, M10, M20” and so forth to the 180 minute timepoint. Prepare the same for "F" for fetal effluents.

1.6 Calibrate the system, including circulating bath temperature and blood pressure monitors associated with maintaining uterine (80 mmHg) and umbilical (50 mmHg) perfusate pressures.

## 2. Day of the Experiment

2.1 All supporting perfusion system equipment must be turned on to check for proper function.

Remove the PSS from refrigeration and warm to room temperature. The PSS will be used as the perfusate and superfusate.

2.2 Place a small bubbling stone to deliver a gas mixture into the superfusate reservoir.

Commonly used mixtures include 21% O<sub>2</sub>, 8% O<sub>2</sub>, 3% O<sub>2</sub>, and 0% O<sub>2</sub>. Turn gas on to provide small bubbles to the superfusate solution. Adjust the delivery of gas to avoid splashing.

2.3 Arrange the animal dissecting station by checking anesthetic, arranging surgical equipment, and preparing suture ties. Prepare the dissecting chamber (if available) by collecting dissecting pins, turning on the chiller (or retrieving ice), and filling the dissecting chamber with cold PSS.

2.4 Gently fill all chambers, needles, pipettes, tubing, and reservoirs with warmed PSS, carefully watching for and eliminating air bubbles by suctioning out with a fine tip transfer pipette. Turn all 3-way stopcocks with “off” facing the direction of the pipette to secure fluid within the pipette.

2.5 Place a single tie on each of the two glass pipettes in preparation for uterine cannulation and the two blunt tip needles designated for umbilical cannulation. Secure ties to the pipettes and blunt tip needles in order to prevent loss during chamber movements (**Figure 1C**).

### 3. Placental Harvesting

3.1 Anesthetize a pregnant female rat on gestational day 19 with 5% isoflurane for about 4 minutes or until the animal exhibits labored breathing. Move animal to the nose cone and administer 2.5-3% isoflurane as maintenance anesthesia. Confirm unconsciousness by lack of toe pinch reflex.

3.2 Identify and isolate the uterine horn (right or left) of choice by lifting out and spreading out long-ways outside of the rat carcass. By using a braided silk suture, tie off the uterine artery at the ovary end and vaginal end of the horn. Include the ovary inside of the suture with the uterine horn. Using a surgical scissor, excise away the uterine horn by making cuts on the proximal side of the ovary tie and distal side of the vaginal tie, leaving your uterine horn tied off with the sutures on both ends. Transfer the uterine horn into a dissecting dish filled with cold PSS. Whether the right or left horn is chosen, maintain that same side for selection in each experiment for consistency.

- 3.3 Pin the uterine horn in the with the ovary side to the left and vaginal side to the right to visualize the uterine vasculature. Select a maternal-placenta-fetal unit central to the horn and ligate the uterine artery and vein with surgical scissors.
- 3.4 The entirety of the placental unit including the uterine muscle, placenta, amniotic sac, fetal pup, umbilical cord, and the supporting vasculature may be cut and removed. The uterine muscle can be retracted by pulling it to the side, it is important to leave it intact, but pull away from covering the fetal pup.
- 3.5 Using fine forceps and scissors, remove the amniotic membrane from the fetal surface of the placenta, taking care to avoid the umbilical cord.
- 3.6 Unravel and ligate the umbilical cord to separate the fetal pup.
- 3.7 Identify the umbilical artery (thicker vessel) and vein (thinner vessel). Mark the umbilical vein for easy identification by cutting it slightly shorter than the umbilical artery.
- 3.8 Gently separate the umbilical artery and vein from each other.

#### 4. Placental Perfusion

- 4.1 Maintaining the correct orientation of uterine artery anatomical blood flow, place the placental unit (comprised of the uterine vasculature, uterine muscle, placenta, and umbilical cord) into the modified isolated vessel chamber filled with warmed, oxygenated PSS.

4.2 Using a pair of fine forceps in each hand, cannulate the proximal and distal ends of the uterine artery onto the glass pipette.

4.3 Tightly secure the uterine artery using the sterile nylon suture tie previously secured onto the pipette.

Note: Two-tie loops may be necessary; however, a single tie loop allows for greater adjustment.

4.4 Cannulate the umbilical artery (fetal-to-maternal blood flow) onto the 23-gauge (larger) needle and securing with black braided silk suture.

4.5 Cannulate and secure the umbilical vein (maternal-to-fetal blood flow) onto the 25-gauge (smaller) blunt needle and secure with black braided silk suture.

4.6 Move to the placental perfusion station and backfill all stopcocks and tubing to prevent air bubbles. Connect all tubing (Figure 2).

4.7 Place small weigh boats under distal cannulation of maternal uterine artery and needle cannulation of fetal umbilical vein to catch the effluent that emerges for each 10-minute time point. Suction up effluent by pipette and save in corresponding labeled microcentrifuge tube.

4.8 Turn on peristaltic pump and slowly increase flow to 80 mm Hg for perfusate through uterine artery and watch for leaks around the chamber. Turn on the peristaltic pump to initiate flow into the uterine artery and open the stopcock to permit fluid flow. Note: If

the peristaltic pump is running at a high speed, re-evaluate the proximal uterine cannulation and tie for fluid leaks. If identified, they must be remedied.

4.9 Turn the stopcock to permit fluid flow into the umbilical artery. Set the pressure to approximately 50 mmHg, which can be implemented with a peristaltic pump or gravity-fed system (as depicted here) (Figure 3).

4.10 Check all reservoirs to confirm fluid volume.

## 5. Mock Experiment

5.1 After cannulation and starting the PSS perfusion, allow tissues equilibrate for 30-minutes to allow vasculature to adjust to new fluid flow.

5.2 After equilibration, establish baseline perfusion by collecting effluents from both weigh boats in microcentrifuge tubes and measuring volume of fluid that emerged through the uterine artery and umbilical vein.

5.3 Sample collection is initiated after equilibration at 10-minute intervals by collecting the effluents from the distal uterine artery and umbilical vein.

Note: These effluent samples will allow for measurement of contaminants within the fluid (either xenobiotic, pharmacologic, or metabolite) and provide the rate of fluid flow through the uterine artery or across the placenta and into the fetal compartment (Figure 5).

5.4 In this experiment, a 900  $\mu\text{L}$  bolus dose of 20 nm rhodamine-labeled polystyrene nanoparticles ( $8 \times 10^{14}$  particles/mL) suspended in 0.01% surfactant is administered to the line perfusing the uterine artery to identify the time course passage of xenobiotic nanoparticles across the placental barrier.

5.5 After bolus infusion, samples were collected from the distal uterine artery and fetal umbilical vein effluent (Figure 6) every 10 min for a total of 180 min after infusion.

## 6. Cleaning the Equipment

6.1 After each experiment, remove the placental unit from the pipettes. All sutures may be saved to be reused in future experiments. The placental tissue may be saved for additional histological or mechanistic studies.

6.2 Clean all tubing and cannulas of the perfusion system with 70% ethanol followed by distilled water and vacuum dry.

Note: If tubing or pipettes begin to discolor or appear damaged, replace prior to the next experiment. Further, after an experimental cohort is complete (e.g. all studies pertaining to a single contaminant), replace all tubing within the chamber to prevent cross contamination.

### **A-2.4 Representative Results**

Figure 4 shows the proof-of-principle experiments using Evan's blue dye, allowing us to test the system and visualize appropriate fluid and placental barrier function and to prevent containment transfer into the fetal compartment.

Figure 6 shows data for the mock experiment described in this protocol. Effluent samples from the distal end of the uterine artery and fetal umbilical vein were measured at each 10-minute segment to evaluate fluid flow over time after the bolus dose was administered to the maternal uterine artery

(Figure 6). A reduced fluid transfer to the fetal compartment within 10 minutes after polystyrene infusion was identified. To quantify polystyrene transfer into the fetal compartment under the time course in which it occurs, 25  $\mu$ L of perfused fluid from each time point was placed into a 96 well plate in duplicate to measure sample fluorescence. Fluorescence is determined by spectroscopy read at 546/575 nm (ex/em) using a fluorescent microplate reader. Polystyrene transfer to the fetal compartment occurred within 10 minutes and peaked at 20 minutes and continued for 90 minutes (Figure 6B).

A subset of perfused placental tissues were saved for histopathology and morphological assessments. The tissues were formalin-fixed and hematoxylin and eosin stained and reviewed by a board certified veterinary pathologist. These experts identified no structural abnormalities in placentas perfused by only PSS, nor PSS with the bolus dose of rhodamine-labeled polystyrene.

### **A-2.5 Discussion**

This perfusion methodology allows for rapid assessment of placental barrier and physiological function of the uterine vasculature and trophoblast layer. Cannulation and perfusion of the proximal to distal ends of the maternal uterine artery simulates the physiology of maternal blood flow through this major vessel responsible for sending blood to the developing fetus. This methodology allows for physiological evaluation of the isolated maternal, placental and umbilical vasculature, and therefore changes in physiology may be identified as vascular pathology; the immune and neural innervations are removed in the ex-vivo procedure. To ensure proper evaluation, it is therefore critical to cannulate these vessels carefully as to not create any tears or punctures in the vessel walls, and to remove air bubbles. Gas emboli may cause damage to microcirculation or obstruct blood vessels. By maintaining the vascular connections between the uterus, placenta and fetus during dissection, the evaluation of fluid and translocation to the fetus can be observed. With the

administration of a xenobiotic, in this case 20 nm polystyrene, kinetics to the distal end of the uterine artery and through the placenta to the fetal compartment can be evaluated by analysis of effluents over a time course of 180 minutes.

While described is a dual-perfusion model and monitored transfer of particles and fluid from the maternal to the fetal compartment, assessments can also be made in reverse from the fetal to the maternal compartment. One limitation to the methodology described here is that the distal uterine vein was not cannulated or sampled. In future studies, especially those focused on fetal-to-maternal transfer, it will be important to cannulate and sample this vessel. The collections taken from this mock experiment were used to assess xenobiotic transfer; however, a wide array of assessments pertaining to endocrine and molecular placental functions or fetal nutrition may be performed.

The strengths of this preparation far outweigh minor limitations. These studies maintain physiological structure and integrity of a whole organ to assess experimental conditions. *Ex vivo* placental perfusion is a scientific progression from cellular based *in vitro* to whole animal exposures to properly determine reproductive risk assessment. This may be considered a valuable technique for studies evaluating placental pharmacologic drug disposition, pharmacokinetics, toxicology, physiology, and maternal-fetal medicine.

#### DISCLOSURES:

The authors report no financial or any other conflict of interest regarding the publication of this article.

#### ACKNOWLEDGEMENTS

This work was supported by the National Institute of Environmental Health Sciences (R00-ES024783), Rutgers Center for Environmental Exposures and Disease (P30-ES005022), and Rutgers Joint Graduate Program in Toxicology (T32-ES007148). We would also like to thank Drs.

Michael Goedken, Marianne Polunas, and Pedro Louro for their technical expertise and Dr. Adam Goodwill for his assistance in designing our perfusion schematic (Figure 5).

**FIGURES:**

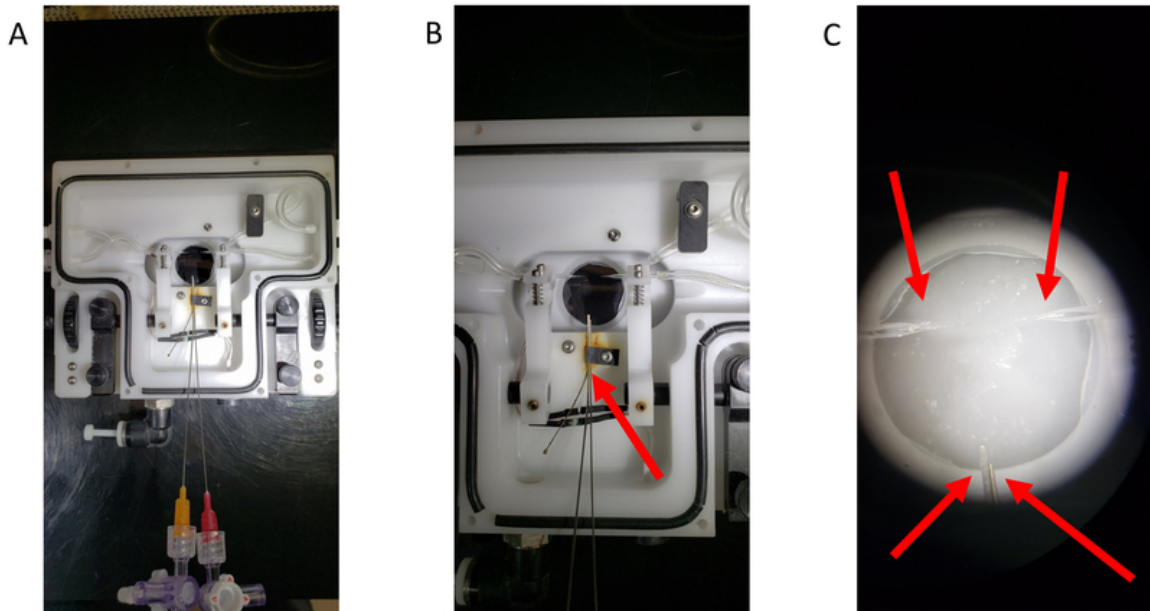


**Figure A-2.1:** This figure represents the modified single vessel chamber. (A) An overview of the modified chamber. (B) A close up of the blunt-tip needles secured within the vessel chamber. The red arrow indicates the thermistor clip that has been altered to hold the needles in place for umbilical cannulation. (C) A representative image of the 4 cannula prepared for tissue cannulation with a single fine ophthalmic ties loosely ties to each. Red arrow point to each of the ties.

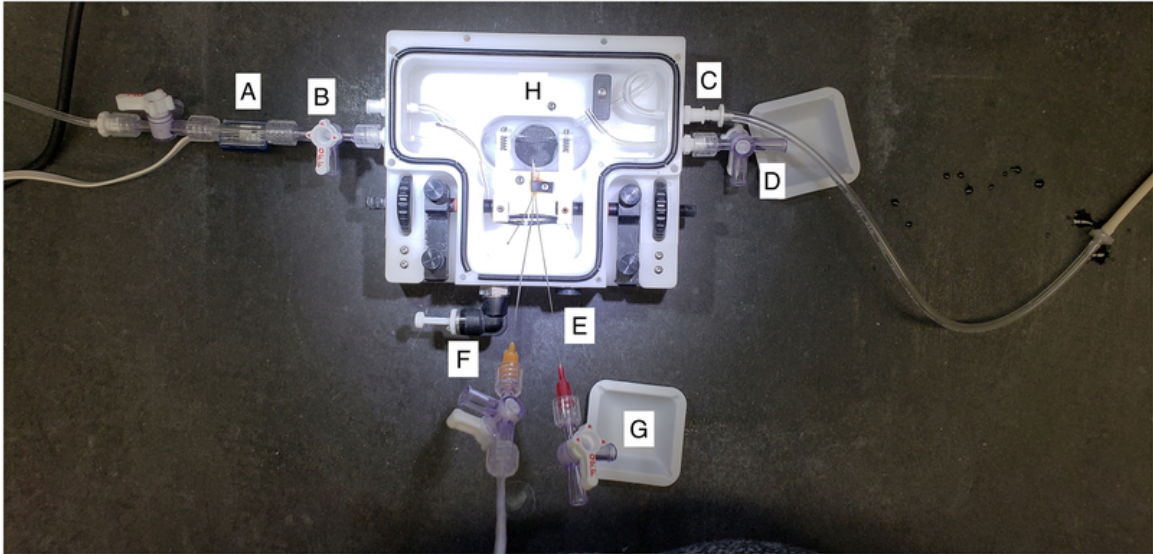


**Figure A-2.2: A closer view of the placental perfusion chamber.** (A) This represents the tubing attached to the pressure transducer and cannulated proximal maternal uterine artery, or the “inflow”. Pressure is set to a constant 80 mmHg as defined by the literature. (B) This represents the chamber drain port for the superfusate surrounding the placental tissue during perfusion. (C) This represents the chamber inflow of superfusate to bathe the placenta with warmed PSS during perfusion. (D) This represents the distal maternal uterine port, where effluent from the uterine perfusion may be collected. (E) This represents the temperature port, where the vessel chamber can be attached to a thermometer and heater to maintain a consistent temperature throughout the experiment. (F) This represents the umbilical artery cannulation. The umbilical artery is pressurized to 50 mmHg to allow for countercurrent flow at the level of the placenta. (G) This represents the umbilical vein effluent collection. Fluid that flows toward the fetal compartment during perfusion will be collected here. (H) This is the center of the perfusion system, where the placenta is cannulated and remains throughout perfusion.

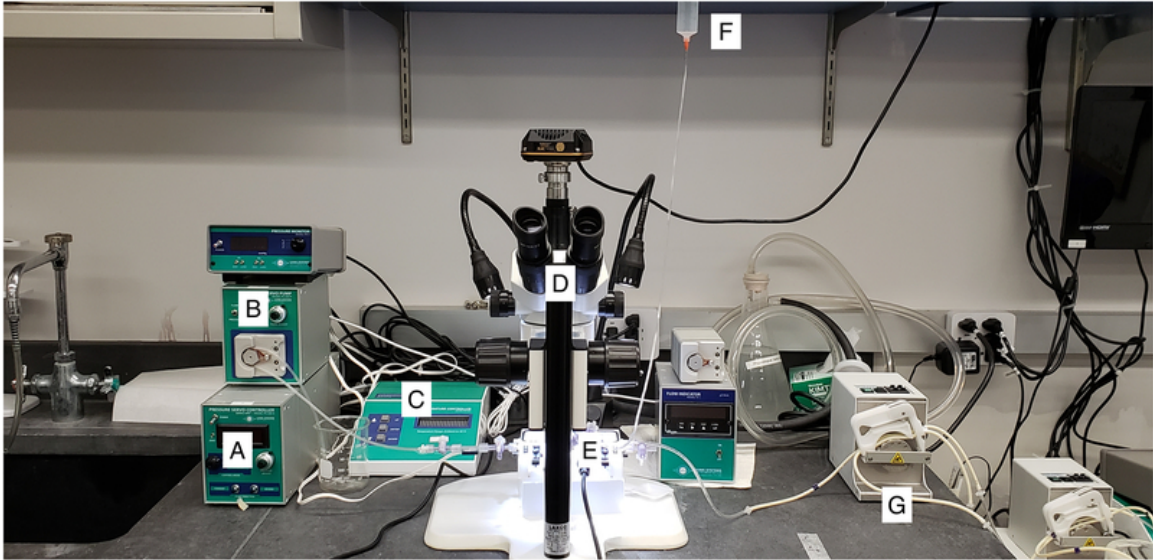


**Figure A-2.3: A view of the placental perfusion system.** (A and B) Represents the Pressure control system to monitor and maintain 80 mmHg of perfusate through uterine artery. The equipment shown here is made by Living Systems Instrumentation, however other companies also make similar equipment, or the system may be gravity fed. (C) This represents the thermo-regulation of the perfusion chamber. (D) Microscope. (E) Perfusion Chamber. (F) Gravity fed umbilical artery perfusion, set at 50 mmHg. (G) Peristaltic pump to fill and drain placental superfusate PSS.

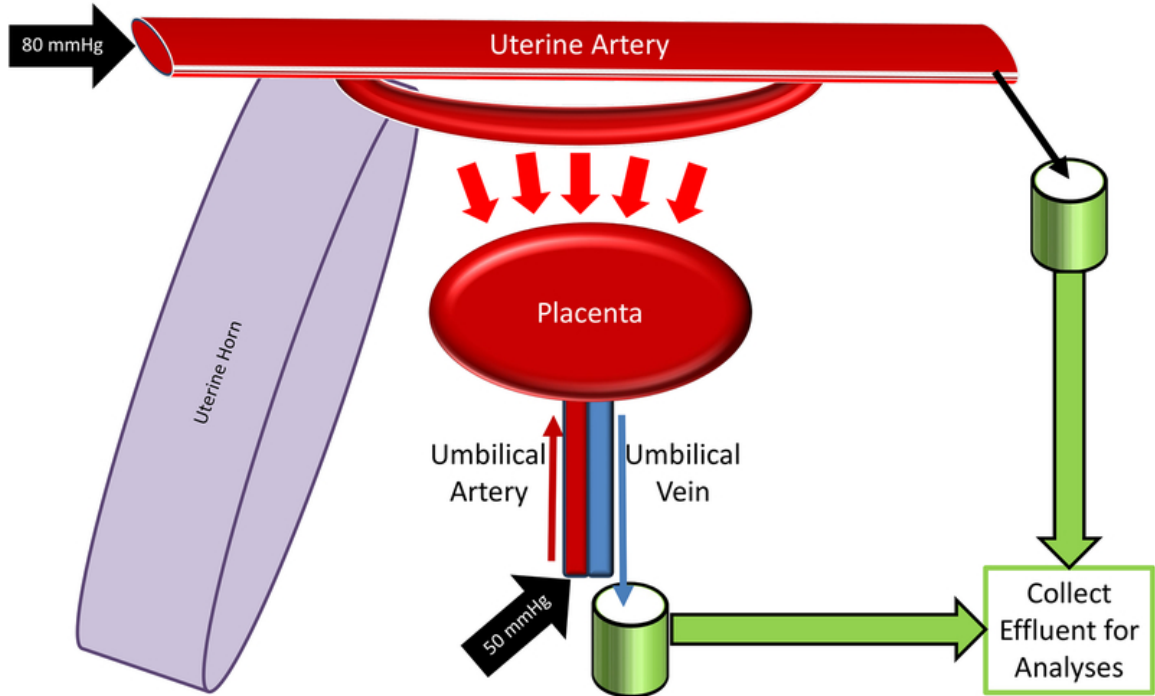
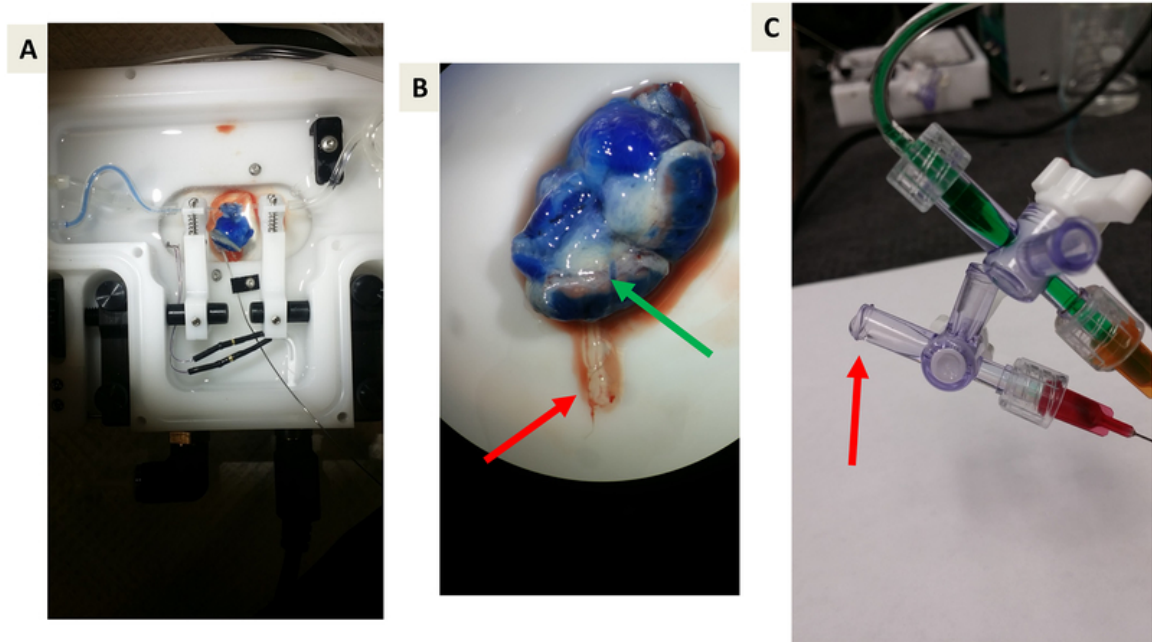
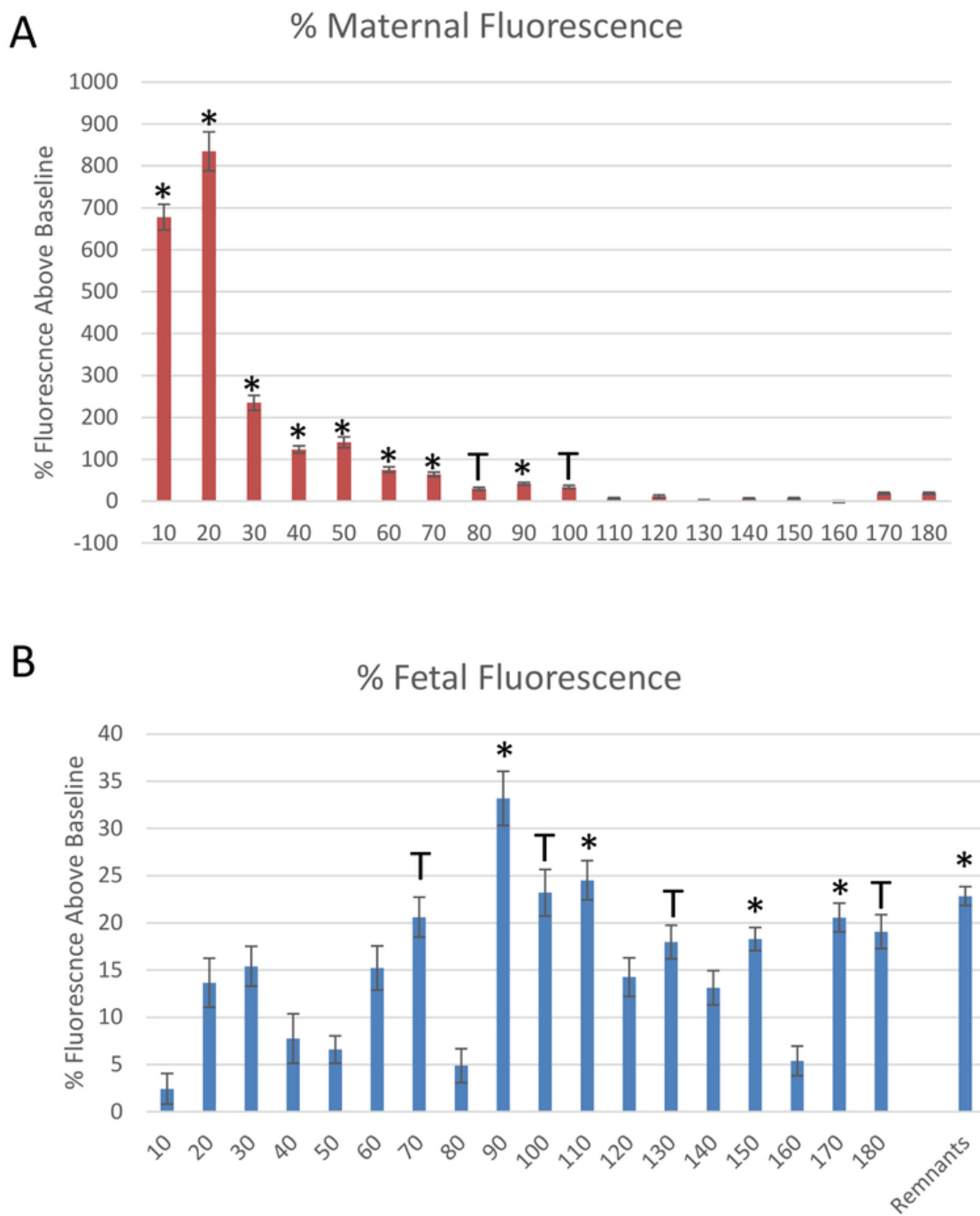


Figure A-2.5: Schematic of placental perfusion system.



**Figure A-2.5: Representative images of proof-of-principle experiments using Evan's blue dye.** (A and B) Proof-of-principle that Evan's blue will perfuse the uterine vasculature, uterine muscle, and placenta but will not cross the placental barrier due to albumin binding. Green Arrow indicates blue venous drain from the placenta back to maternal circulation. Red arrows indicate umbilical vein effluent toward the fetal compartment. Note the lack of blue dye. (C) Representative image of collecting effluent draining from the umbilical vein. Red arrow indicates drop formation prior to collection.



**Figure A-2.6: Data derived from the mock experiment.** Rhodamine-labeled polystyrene (PS-R) ENM fluorescence measurements normalized to baseline fluorescence through collection of the (A) uterine artery and (B) fetal umbilical vein effluent. Mean normalized to baseline fluorescence  $\pm$  SE. \*:p<0.05 and T:p<0.1 via ANOVA.

**REFERENCES**

- Alexander DP, Andrews RD, Huggett AS, Nixon DA, Widdas WF. 1955a. The placental transfer of sugars in the sheep: Studies with radioactive sugar. *J Physiol.* 129(2):352-366.
- Alexander DP, Huggett AS, Nixon DA, Widdas WF. 1955b. The placental transfer of sugars in the sheep: The influence of concentration gradient upon the rates of hexose formation as shown in umbilical perfusion of the placenta. *J Physiol.* 129(2):367-383.
- Bond H, Baker B, Boyd RD, Cowley E, Glazier JD, Jones CJ, Sibley CP, Ward BS, Husain SM. 2006. Artificial perfusion of the fetal circulation of the in situ mouse placenta: Methodology and validation. *Placenta.* 27 Suppl A:S69-75.
- Butcher JT, Goodwill AG, Frisbee JC. 2012. The ex vivo isolated skeletal microvessel preparation for investigation of vascular reactivity. *J Vis Exp.* (62).
- Dancis J, Money WL. 1960. Transfer of sodium and iodo-antipyrine across guinea pig placenta with an in situ perfusion technique. *Am J Obstet Gynecol.* 80:215-220.
- Davis MJ, Kuo L, Chilian WM, Muller JM. 1995. Isolated, perfused microvessels. In: Barker JH, Anderson GL, Menger MD, editors. *Clinically applied microcirculation research.* 1 ed. Boca Raton: CRC Press. p. 435-456.
- Goeden N, Bonnin A. 2013. Ex vivo perfusion of mid-to-late-gestation mouse placenta for maternal-fetal interaction studies during pregnancy. *Nature protocols.* 8(1):66-74.
- Illsley NP, Fox H, Van der Veen F, Chawner L, Penfold P. 1985. Human placental ultrastructure after in vitro dual perfusion. *Placenta.* 6(1):23-32.
- London WT, Money WL, Rawson RW. 1963. Placental transport of i-131-labeled thyroxine and triiodothyronine in the guinea pig. *Endocrinology.* 73:205-209.
- Stulc J, Stulcova B, Svihovec J. 1990. Transport of calcium across the dually perfused placenta of the rat. *J Physiol.* 420:295-311.
- Troen P, Gordon EE. 1958. Perfusion studies of the human placenta. I. Effect of estradiol and human chorionic gonadotropin on citric acid metabolism. *J Clin Invest.* 37(11):1516-1523.

**APPENDIX 3: Identification and quantification of gold engineered nanomaterials  
and impaired fluid transfer across the rat placenta via *ex vivo* perfusion**

JN D'Errico<sup>a</sup>, C Doherty<sup>b</sup>, SB Fournier<sup>b</sup>, N Renkel<sup>b</sup>, S Kallontzi<sup>c</sup>, M Goedken<sup>d</sup>, L Fabris<sup>c</sup>, B  
Buckley<sup>b</sup>, PA Stapleton<sup>a,b</sup>

**AFFILIATIONS:**

a. Department of Pharmacology and Toxicology, Ernest Mario School of Pharmacy, Rutgers University, 160 Frelinghuysen Rd., Piscataway, NJ 08854, USA; b. Environmental and Occupational Health Sciences Institute, 170 Frelinghuysen Rd., Piscataway, NJ 08854, USA; c. Department of Material Science and Engineering, School of Engineering, Rutgers University, 607 Taylor Rd., Piscataway, NJ 08854, USA; d. Research Pathology Services, Rutgers University, Piscataway, NJ 08854, USA.

### **A-3.1 Abstract**

Development and implementation of products incorporating nanoparticles are occurring at a rapid pace. These particles are widely utilized in domestic, occupational, and biomedical applications. Currently, it is unclear if pregnant women will be able to take advantage of the potential biomedical nanoproducts out of concerns associated with placental transfer and fetal interactions. We recently developed an *ex vivo* rat placental perfusion technique to allow for the evaluation of xenobiotic transfer and placental physiological perturbations. In this study, a segment of the uterine horn and associated placenta was isolated from pregnant (gestational day 20) Sprague-Dawley rats and placed into a modified pressure myography vessel chamber. The proximal and distal ends of the maternal uterine artery and the vessels of the umbilical cord were cannulated, secured, and perfused with physiological salt solution (PSS). The proximal uterine artery and umbilical artery were pressurized at 80 mmHg and 50 mmHg, respectively, to allow countercurrent flow through the placenta. After equilibration, a single 900  $\mu$ L bolus dose of 20 nm gold engineered nanoparticles (Au-ENM) was introduced into the proximal maternal artery. Distal uterine and umbilical vein effluents were collected every 10 minutes for 180 minutes to measure placental fluid dynamics. The quantification of Au-ENM transfer was conducted via inductively coupled plasma mass spectrometry (ICP-MS). Overall, we were able to measure Au-ENM within uterine and umbilical effluent with 20 minutes of material infusion. This novel methodology may be widely incorporated into studies of pharmacology, toxicology, and placental physiology.

### **A-3.2 Introduction**

Treatment of a woman during pregnancy is a delicate balance between maternal therapy and fetal risk. Maternal exposure to xenobiotic pharmaceuticals, particles, or chemicals during gestation can lead to spontaneous abortion, fetal malformations, and developmental onset of disease (Rasmussen 2012; Thorpe et al. 2013). Central to this unique environment is the placenta, a temporary organ that functions as a barrier to prevent passage of unwanted xenobiotics and that transfers nutrients

in exchange for waste. Therefore, it is critical to understand the passage of pharmaceuticals and xenobiotic particles from the maternal to the fetal compartment.

Development and implementation of products incorporating nanoparticles are occurring at a rapid pace. These pervasive particles are widely utilized, with many domestic, occupational, and biomedical applications. Gold nanoparticles (Au-ENM) have demonstrated a great potential in biosensing, imaging, and theranostic applications (Cabuzu et al. 2015; Elahi et al. 2018; Khlebtsov et al. 2013). Gold nanoparticles are given as an intravenous injection in the clinic for the purpose of contrast imaging for diagnostic procedures (Cheheltani et al. 2016; Mahan and Doiron 2018). These applications can be expanded by modifying the physicochemical properties of the material (e.g., material, size, shape, inclusion of functionalized groups) making them more useful, but in turn altering the biological interactions, pharmacological function, and toxicological relevance (D'Errico and Stapleton 2018; Elahi et al. 2018; Fournier et al. 2018). Increasing biomedical applications and consumer use products have led to domestic unintentional exposures, including during pregnancy (Fournier et al. 2018; Hougaard et al. 2015b; Stapleton 2016; Stapleton and Nurkiewicz 2014). Therefore, understanding ENM behavior and prenatal and perinatal outcomes of ENM exposure is paramount.

Few studies have comprehensively evaluated ENM translocation from the maternal blood and deposition within the placenta and fetus after intravenous injection during pregnancy (Campagnolo et al. 2013; Semmler-Behnke et al. 2014; Snyder et al. 2015; Sweeney et al. 2018; Yamashita et al. 2011; Zhang et al. 2015). Using ENM with a wide variety of physiochemical properties, previous studies have demonstrated translocation to the embryo of gold (Semmler-Behnke et al. 2014), silica (Yamashita et al. 2011), titanium-dioxide (Yamashita et al. 2011), functionalized-mesoporous silica (Sweeney et al. 2018), and functionalized carbon in the forms of pegylated (PEG) single-walled carbon nanotubes (Campagnolo et al. 2013) and radiolabeled fullerenes (Snyder et al. 2015).

However, it is unclear from these studies how quickly ENM passage occurs from the maternal circulation to the fetal compartment and if this transport acutely impairs normal placental function with respect to blood flow and nutrient delivery.

Experiments using *ex vivo* human placental perfusion of a single cotyledon to investigate passage of functionalized Au-ENM (3-4 nm) to the fetal compartment after 6 hours of infusion identified passage of PEG-Au-ENM but no passage of carboxylated-Au-ENM (Aengenheister et al. 2018a). Interestingly, recirculating human placental perfusion studies of 10, 15, and 30 nm PEG-Au-ENM demonstrates no transfer to fetal effluent (Myllynen et al. 2008). Similar experiments to evaluate size-dependent passage of fluorescent polystyrene ENM have been conducted (Wick et al. 2010). These *ex vivo* studies identified passage of ENM 50 to 300 nm in diameter across the placenta in both maternal-to-fetal and fetal-to-maternal directions without compromising cellular survival (Graffmueller et al. 2015a; Wick et al. 2010). ENM modifications, including non-uniformity of particle size and/or surface modifications designed to increase material biomedical functionality or prevent particle agglomeration will alter the kinetics of ENM transfer across the human placenta (Graffmueller et al. 2015b). Investigations using human tissue are exceedingly valuable, but have limitations. These studies are technically demanding, require specialized equipment, and are limited by tissue access. Investigations of disease or pre-term xenobiotic transfer using human tissue may not be possible given ethical considerations. Investigators (Aengenheister et al. 2018b; Sastry 1999; Stapleton and Nurkiewicz 2014) have called for the need of additional studies focused of placental transfer of ENM and for confirmation of the physiochemical properties of ENM used within toxicological studies.

The mouse is the most commonly used animal model to study the placenta, and *ex vivo* mouse placental perfusion techniques have been established (Goeden and Bonnin 2013; Goeden et al. 2017). Use of this species as a model is beneficial for physiological and mechanistic studies due to

genetic manipulation capabilities. While the mouse model exhibits the same hemochorial placentation classification and analogous cell types, there are distinct differences to humans. Mouse placentas do not have trophoblastic cells that invade the myometrium or spiral arterioles of the maternal uterus (Rosenfeld 2015). Rat placentas show more similarities to humans at the site of maternal-fetal interface and do reflect the deep uterine vascular invasion and remodeling (Soares et al. 2017). Therefore, *ex vivo* rat placental perfusion is advantageous for toxicological and pharmacological investigations, as the test article maternal-fetal kinetics can be more relevant for extrapolation to humans.

We recently developed a novel *in situ* rat placental perfusion methodology for toxicological studies (D'Errico et al. 2019b). Without morphological or physiological impairment, this methodology permits the measurement of fluid transport across the placenta in addition to maternal/fetal kinetics of the xenobiotic. Previous descriptions of isolated rat placenta have reported solute transfer solely from the fetus to the maternal blood (Bond et al. 2006; Nishimura et al. 2012). Use of the dually-perfused isolated rat placenta has led to the assessments of phosphate, calcium, and chloride solute transport across the placenta (Stulc and Stulcova 1996; Stulc et al. 1996; Stulc et al. 1990), cyclosporine transfer (Pavek et al. 2001), barrier activity (Pavek et al. 2003), and in some cases, to reporting physiological adaptations of the placenta to environmental changes (e.g. hypoxia) (Kafka et al. 2012). However, none of these studies have been completed with a pharmacological or toxicological focus to assess the passage of xenobiotic particles from the maternal circulation to the developing fetus (Goeden and Bonnin 2013). Therefore, the purpose of this study was to identify the transfer of Au-ENM from the maternal to fetal compartment, record the time course of this transfer, and assess the placental physiological reactivity after Au-ENM infusion. While previous work has demonstrated nanoparticle translocation to the fetal compartment after 24 hours, we hypothesize that transfer from the maternal circulation, across the placental barrier, and into the

fetal compartment occurs within minutes. We further hypothesize that this transfer will impair placental hemodynamics and reduce blood flow to the developing fetus.

### **A-3.3 Materials and Methods**

#### *Animals*

Sprague Dawley rats were purchased time-pregnant from Charles River Laboratories (Kingston, NY). Animals were delivered at least 48-hours before use and acclimated within the AAALAC accredited facilities at Rutgers University with food and water available *ad libitum*. Animal sacrifice and placental perfusions took place at full term on GD 20. All procedures were approved by the Institutional Animal Care and Use Committee of Rutgers University.

#### *ENM Characterization*

Stock solution of 20 nm naïve gold nanoparticle spheres (gold ENM;  $7 \times 10^{11}$  particles/mL; GP01-20-100; NanoCS, New York, NY) was suspended in 0.01% sodium citrate and sonicated for 15 minutes prior to measurement. The average agglomerate size was identified as  $49.89 \text{ nm} \pm 0.16$  via dynamic light scattering (DLS) techniques using Zetasizer Nano ZS by Malvern. The size of the nanoparticles was measured with Non-Invasive Backscatter optics (NIBS) using a 4 mW, 633 nm laser. The ENM  $\zeta$ -potential was also measured via Zetasizer Nano ZS.

#### *Placental Isolation*

Under isoflurane general anesthesia (5% induction and 2% maintenance), the central placental unit of the right uterine horn was isolated, excised and transferred into cold physiological salt solution (PSS). Briefly, the uterine vasculature was ligated, and the placental unit with uterine muscle, placenta, amniotic sac, fetal pup, umbilical cord, and the supporting vasculature removed. Prior to extracting the fetus, uterine muscle was retracted, amniotic membranes removed, umbilical cord

unraveled, umbilical vasculature identified and separated, as previously published (D'Errico et al. 2019b).

#### *Placental Perfusion*

The placental unit was placed within a modified isolated vessel chamber (Living Systems Instrumentation, Burlington, VT) (Figure 1) filled with warmed, oxygenated, circulating PSS. The proximal and distal ends of the uterine artery were cannulated with glass pipettes measuring 75-100  $\mu\text{m}$  at the tips and secured using 11-0 nylon suture (Alcon). The umbilical artery and vein were cannulated using 4-inch 26 g blunt needles and secured with 11-0 nylon suture. The uterine artery was perfused via a peristaltic pump with PSS at 80 mmHg and perfusate was collected from the distal end. The umbilical artery was perfused with gravity-fed PSS at 50 mmHg and fetal effluent was collected from the umbilical vein cannula. Steps for this procedure can be accessed in further detail in our previous technical publication (D'Errico et al. 2019b). After cannulation and 20-minute equilibration, baseline perfusion effluent was collected for 10 minutes prior to ENM infusion and sample collection continued to occur in 10-minute intervals for a total of 180 minutes. Further, fluid that remained in the 4" pipette cannulating the umbilical vein was also collected and identified as residual effluent (R).

#### *Engineered Nanomaterial Exposure*

1 mL of 20 nm naïve Au-ENM spheres was prepared by sonicating the ENM in stock solution for 2 minutes. A single bolus dose of 0.9 mL stock solution (5775.94 ng/mL) was administered and infused into the proximal uterine artery through a 3-way stopcock. Distal maternal and fetal umbilical effluents were collected every 10 minutes for 180 minutes for analysis.

#### *Histology and Pathology Assessments*

After perfusion, placentas were fixed in a 10% neutral buffered formalin prior to processing and paraffin embedding. Haematoxylin and eosin (H&E) stained sections were assessed by an ACVP board-certified veterinary pathologist.

#### *Material Visualization*

Histological placental sections were visualized via transmitted darkfield hyperspectral images and data captured using CytoViva darkfield optics at 60x magnification with oil objective. Hyperspectral imaging provides a spectral analysis permitting differentiation between particles. Dual Mode Fluorescence (DMF) images were captured with Texas Red excitation filter and triple pass emission filter to allow for visualization of fluorescent and non-fluorescent particles simultaneously. Data was processed using ENVI 4.8 (CytoViva, Auburn, AL).

#### *Sample Preparation for ICP-MS analysis*

Au-ENM perfusion effluent was prepared by dissolving ~50-200  $\mu\text{L}$  of sample in aqua regia (3:1, [HCl] : [HNO<sub>3</sub>]). No difference was found between ambient temperature digestion and microwave digestion for the Au-ENM in physiological salt solution (PSS). Therefore, all subsequent samples were digested at ambient temperature in acid-cleaned polypropylene centrifuge tubes. Control samples (i.e. PSS spiked with Au-ENM) were digested alongside the perfused samples to monitor Au recovery and matrix effects.

Tissue samples (~0.2 g) were weighed into 50 mL polypropylene centrifuge tubes and homogenized by ultra-sonicating in 1 mL of concentrated HNO<sub>3</sub>. The samples were allowed to react and degas overnight and subsequently digested using a CEM MARS X microwave digestion system, applying the following procedure (Table 1).

Control samples (i.e. tissue not treated with Au-ENM perfusion) were digested alongside the perfused samples and spiked with Au to monitor recovery and matrix effects. All digested samples were diluted to 3% HCl:1% HNO<sub>3</sub> in preparation for analysis by ICP-MS.

#### *Measurement with ICP-MS*

Au concentrations were measured at mass 197 on a Nu AttoM high resolution ICP-MS, at low resolution (300). The operating conditions were as follows: RF power of 1550 W, carrier gas flow of 1.00 L/min Ar, and nebulizer gas flow of ~36 psi Ar. Three replicates of <sup>197</sup>Au were measured in deflector jump mode with 200 μs peak dwell time, 500 sweeps, and 10 cycles.

Standards were prepared daily with Au concentrations ranging from 0.001 - 5 ppb, in 3% HCl:1% HNO<sub>3</sub>. Sample concentrations were determined using a linear regression through at least five standards, with a correlation coefficient > 0.999 for all runs. Matrix matched quality control standards were repeatedly measured after every sixth sample to account for instrument drift and monitor reproducibility. Quality control standards reproduced with RSD <5% (n=2-7 depending on number of samples in the batch).

To reduce Au memory effect, a washout solution containing 3% HCl:1% HNO<sub>3</sub> + 0.2% L-cysteine was used following each sample for 3 minutes to mobilize remnant Au, then followed with clean 3% HCl:1% HNO<sub>3</sub>. Au memory effect was further monitored by bracketing samples with clean acid carryover (3% HCl:1% HNO<sub>3</sub>) following the washout, and detection limit was reduced to 0.001 ppb for effluent analyses and 0.005 ppb for tissue analyses.

#### *Fluid Flow Across the Placenta*

After equilibration, effluent was collected at 10-minute intervals from the maternal and fetal segments for 180 minutes. This fluid was weighed to quantify the rate of fluid that passage through

the uterine artery or placenta and umbilical vein and identify any decreases in fluid flow within the system attributed to ENM infusion.

#### *Statistics*

Au-ENM transport at baseline and through the maternal and fetal effluents was analyzed by each time point compared to control measurements with Student's T-test. Significance was set at  $p < 0.05$  and a trend (T) was identified as  $p < 0.1$ . SEM is reported.

### **A-3.4 Results**

Initial verification of the model was necessary to confirm that all histological and morphological membranes remain intact during *ex vivo* perfusion of the placenta. Samples were reviewed by a veterinary pathologist and no pathological damage was identified (Figure 2a), indicating that translocation within the system is due to normal physiological function of the placenta. Figure 2b identifies the passage of Au-ENM through hyperspectral analysis and darkfield microscopy. The hyperspectral analysis provides a spectral response associated with Au-ENM exposure (red) compared to control (white) and image of the reflectance of the Au-ENM deposition within the placental tissue.

Au-ENM transfer to maternal vasculature was confirmed with significant translocation across the uterine artery within 20 minutes after Au-ENM infusion (Figure 3a). This significance remains for all 180 minutes after bolus material infusion. Further, significant concentrations of Au-ENM were detected in the fetal compartment within 20 minutes of uterine artery infusion (Figure 3b). These results confirmed Au-ENM passage from maternal-fetal tissues to the fetal compartment.

This model was used not only to calculate the amount of material passaging through the system, but to document the physiological response within the *ex vivo* system. In this respect, there was no significant decrease in maternal artery fluid flow after Au-ENM infusion (Figure 4a).

However, there were significant reductions in fluid flow across the placenta and to the umbilical vein and fetal compartment after Au-ENM uterine infusion (Figure 4b). While calculated significance varied in the time post-material infusion, any reduction in blood flow to the developing fetal pup could have serious consequences to fetal growth, nutrient delivery, and waste exchange.

Finally, we quantified total Au-ENM transfer during the placental perfusion within the maternal effluents, uterine muscle and vasculature, placenta and fetal umbilical effluent. From the total Au-ENM that was recovered, there was an average of 77.8% found in the maternal effluent, 17.4% within the uterine muscle and vasculature, 6.17% placenta and 0.065% within the fetal effluent (Figure 5).

### **A-3.5 Discussion**

Using novel techniques and methodology, these studies identified a time course of *ex vivo* material transfer and quantified a reduction of fluid flow across the placenta after ENM infusion into the maternal uterine artery. Through the development and implementation of this novel *ex vivo* placental perfusion technique we were able to quantify Au-ENM 3 hours after material infusion. In preparation for ICP-MS analyses, improvements to tissue preparation and material extraction methodologies were also developed. To our knowledge, this is the first application of rodent placental perfusion to directly assess the physiological implication to fluid transport and placental barrier function after naïve Au-ENM exposure.

The changes to fluid flow quantified within this system lend validity to measurements previously made within our laboratory identifying hemodynamic abnormalities in uterine basal arterioles 24-hours after a single inhalation exposure to nanosized titanium dioxide (TiO<sub>2</sub>) aerosols using intravital microscopy to visualize the intact uterine vasculature (Stapleton et al. 2018c). After chronic inhalation exposure to TiO<sub>2</sub> ENM aerosols we identified endothelium-dependent dysfunction in isolated radial arterioles compared to control (Stapleton et al. 2013a). Maternal ENM exposures during pregnancy have significant implications to fetal development and fetal health (Hougaard et al. 2015b). These include reduced maternal weight gain, fetal number, fetal weight, neonatal weight (Hougaard et al. 2013; Stapleton et al. 2013a), and increased reabsorption sites (Fournier et al. 2019b). Furthermore, uterine and umbilical vascular dysfunction is evident after both chronic and acute maternal exposure to ENM during pregnancy, limiting resources to developing fetal pups downstream (Fournier et al. 2019b; Stapleton et al. 2018c; Stapleton et al. 2013a; Vidanapathirana et al. 2014a). Fetal exposure during gestation culminates in reduced fetal health including impaired neonatal growth, epigenetic modifications, coronary and vascular dysfunction, metabolic complications, pulmonary impairments, and neurodevelopmental changes (Blum et al. 2012b; Engler-Chiurazzi et al. 2016; Hathaway et al. 2017; Notter et al. 2018; Paul et al. 2017; Stapleton et al. 2018a; Stapleton et al. 2013a; Umezawa et al. 2018). These effects may be attributed to maternal inflammation (Stapleton et al. 2018c), neurological impacts (Stapleton et al. 2015b), maternal physiological adaptations associated with exposure (Hougaard et al. 2010; Hougaard et al. 2013; Stapleton et al. 2013a), and/or direct engineered nanomaterial translocation to the fetus (Austin et al. 2016; Austin et al. 2012; Campagnolo et al. 2017a).

While the results associated with material and fluid transfer to the fetal compartment include some trending differences, we would contend that the identification of any xenobiotic material within the fetal compartment and any reduction of blood flow would have physiological implications to uterine health and could have long lasting effects on fetal development. If offspring were to survive,

this exposure may be a platform for the developmental onset of future adult disease. While not all post-infusion time points reached statistical significance, even subtle hemodynamic changes may be detrimental to fetal growth. Taken together, these studies indicate a reduction in blood flow from the uterine circulation to the fetal compartment after maternal ENM exposure. This reduction in blood puts the developing fetus at risk of ischemia, hypoxia, hyponutrition, intrauterine growth restriction, and death.

One drawback of the *ex vivo* rat placental perfusion is a partial loss of the original dose administered in two ways. Because we did not cannulate the maternal uterine vein, this remains an opening for loss of dose through the maternal venous system. There is also additional loss to be accounted for within the plastic tubing and glass pipette cannulas, as Au may stick to these surfaces while passing through the system. Future work should include maternal uterine vein cannulation to capture test article that is sent back through venous circulation.

Other groups have initiated *ex vivo* rodent perfusion studies to evaluate microvascular function of the placenta after dam ENM inhalation (Abukabda et al. 2019). These studies have focused on uterine vascular reactivity post-exposure, providing further evidence of uteroplacental dysfunction after maternal ENM exposure. The distinctions of our methodology involve the umbilical vasculature cannulations, cross-perfusion of the placenta, and toxicological assessment of the fetal compartment. One study to date evaluates maternal-fetal transfer after chronic nose-only ENM exposure (Campagnolo et al. 2017a); however, it is unclear if this is a cumulative outcome or if ENM transfer to and deposition within the fetus may occur after a single exposure.

Human placental perfusion studies are performed using a single cotyledon, due to variability of deposition within the tissue, the physiological function of the entire organ should be considered.

Further, human tissue has logistical considerations with respect to access and previous exposure(s) during gestation (Aengenheister et al. 2018a; Grafmueller et al. 2015a; Myllynen et al. 2008; Wick et al. 2010). The improvement of analytical techniques in the last decade may account for differences between laboratories. For example, the study examining PEG-Au-ENM using human cotyledon perfusion by Myllynen (2008) found no material transfer; whereas PEG-Au-ENM was identified by Aengenheister (2018) using similar methodology. As these techniques continue to advance, measurements of the transfer of material associated with real-world dosages will become readily available.

*In vitro* toxicological studies of placental transport focus on the use of immortal trophoblasts (BeWo cells) and are limited to the confines of a cell culture model including the use of immortal cell lines, high treatment dosages, and lack a physiological system (tissue support, fluid flows) (Aengenheister et al. 2018b; Muller et al. 2018; Myllynen et al. 2008; Tang et al. 2018). On the other hand, *in vivo* studies have traditionally used high doses of a single intravenously injected ENM to track movement and material deposition (Campagnolo et al. 2013; Semmler-Behnke et al. 2014; Snyder et al. 2015; Sweeney et al. 2018; Yamashita et al. 2011). Fortunately, more sensitive analytical techniques have become available to help identify and quantify these materials.

Overall, these studies highlight the rapid transport of Au-ENM from the maternal uterine vasculature to the fetal compartment. These data are vital for future development of biomedical products using Au-ENM as a vehicle or functionalized backbone. These studies provide a platform for the development of perinatal therapies targeted for fetal treatment and a methodology to assess the likelihood of fetal avoidance during drug development. Manipulation of the Au-ENM physiochemical properties and addition of functionalized groups will allow for the design of targeted therapies for placental interaction or for avoidance of cellular uptake within the uteroplacental system (D'Errico and Stapleton 2018; Fournier et al. 2018). In addition, using an *ex*

*vivo* rodent model with many pups per pregnancy would allow for multiple studies to be completed with a single animal. Future studies using this *ex vivo* methodology will not only identify xenobiotic transfer, but also include biochemical assessments of the maternal and fetal effluents to quantify changes to placental function, identify markers and gender-specific adaptations of placental stress, decreases in oxygen tension, and vasoactive metabolites to assess perinatal health.

#### ACKNOWLEDGEMENTS

This work was supported by the National Institute of Environmental Health Sciences (R00-ES024783), Rutgers Center for Environmental Exposures and Disease (P30-ES005022), and Rutgers Joint Graduate Program in Toxicology (T32-ES007148). Thank you to Adam Goodwill for assistance in designing Figure 1. Thank you to CytoViva, Inc for their assistance with Figure 2B.

**FIGURES:**

## Figure 1 – Perfusion Schematic

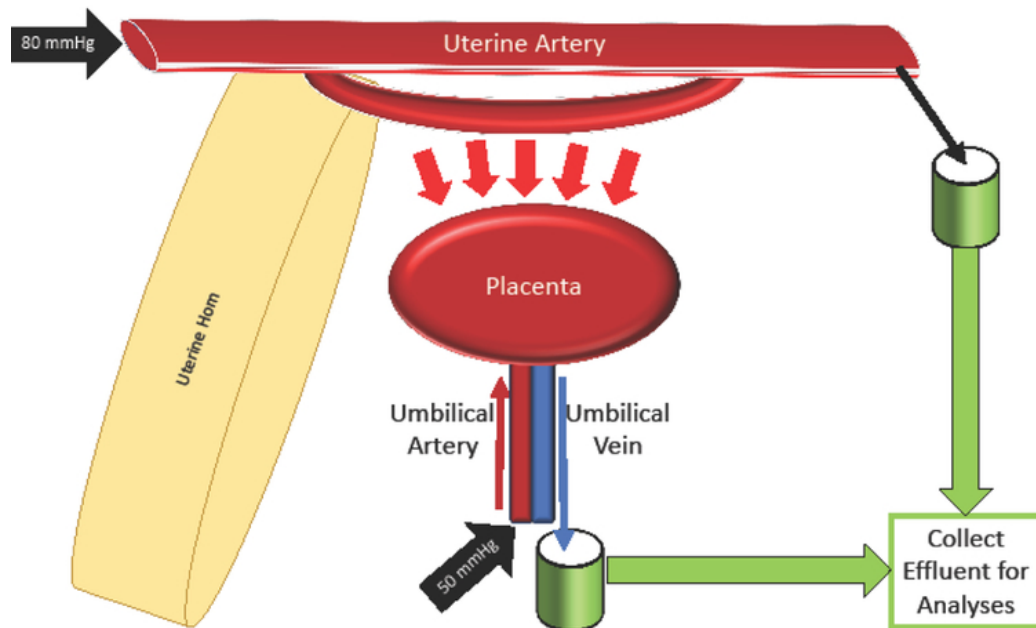


**Figure A-3.1: Schematic of placental perfusion methodology.** Isolation of the uterine horn and placental until permits cannulation of the proximal uterine artery and umbilical vein; perfusion of these arteries allows for perfusion and countercurrent flow within the placenta. Cannulation of the distal uterine artery and umbilical artery allow for effluent collection for biochemical and physiological analyses.

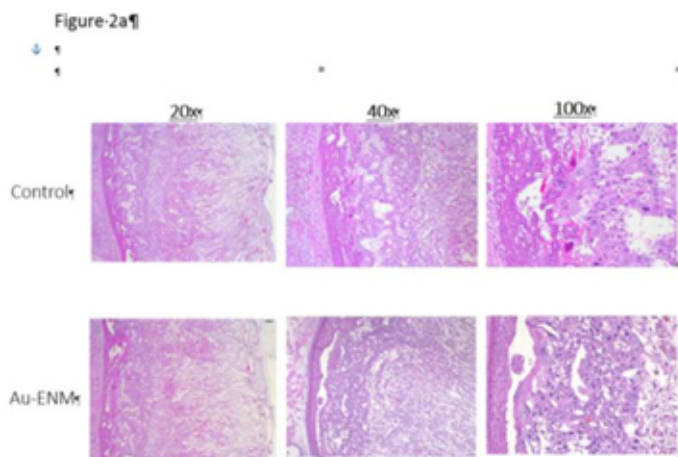
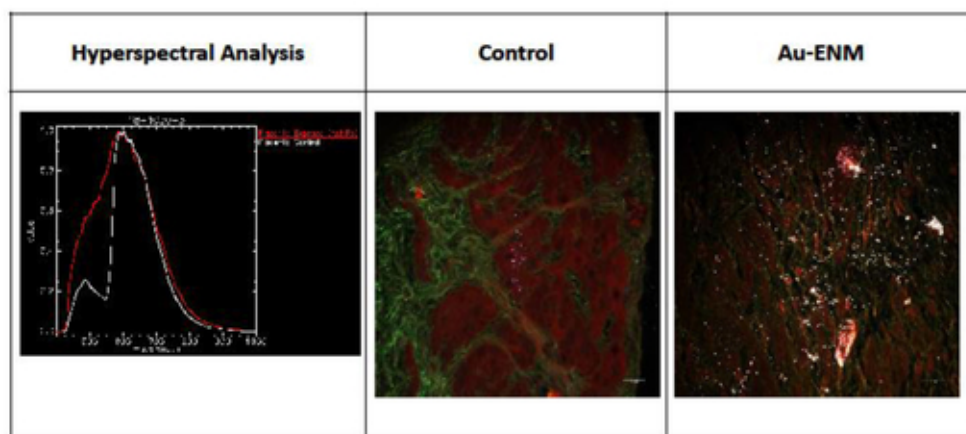


Figure 2b – CytoViva



**Figure A-3.2: Representative images of placental morphology after *ex vivo* perfusion.** (A) There was no identifiable histopathology associated with Au-ENM exposure or perfusion pressures in any of the samples (n=3). (B) Identification and visualization of Au-ENM particle deposition within the placenta after material infusion and placental perfusion using enhanced hyperspectral microscopy (CytoViva, Inc). While xenobiotic particles were identified in the control samples, these particles exhibit a different hyperspectral waveform compared to the Au-ENM samples.

## Figure 3 – Gold Transport

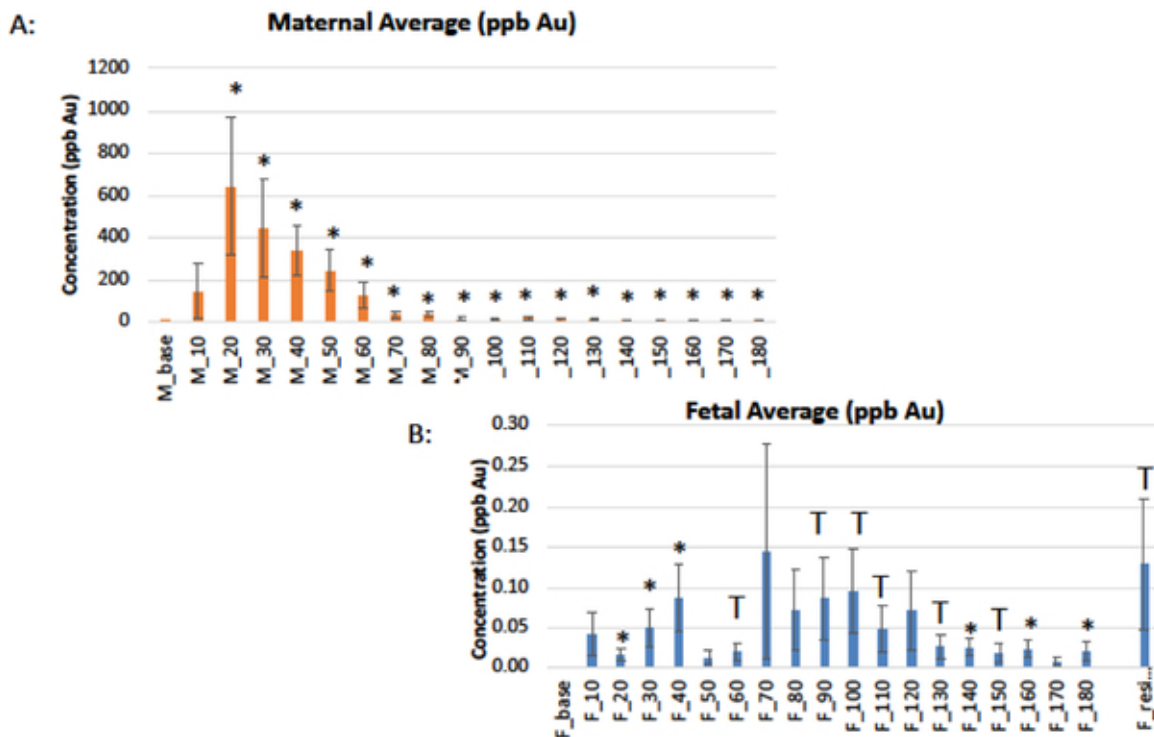
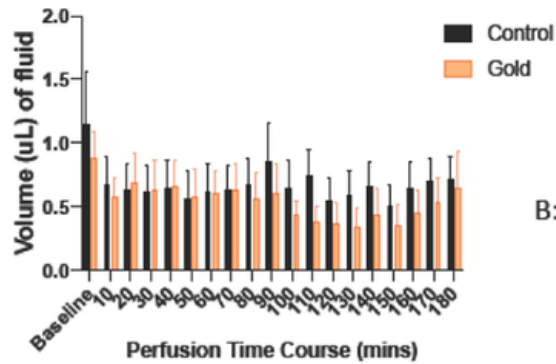


Figure A-3.3: Quantification of Au-ENM concentration within the (A) uterine artery effluents and (B) fetal umbilical vein effluents over a 180-minute time course via ICP-MS analyses, normalized and compared to baseline. \* $p < 0.05$ ;  $\text{T}p < 0.1$ . (n=11)

## Figure 4 –Fluid Flow

A: Fluid Flow Across Uterine Artery  
After Au-ENM Bolus Dose



B: Fluid Flow to the Fetal Compartment  
After Au-ENM Bolus Dose

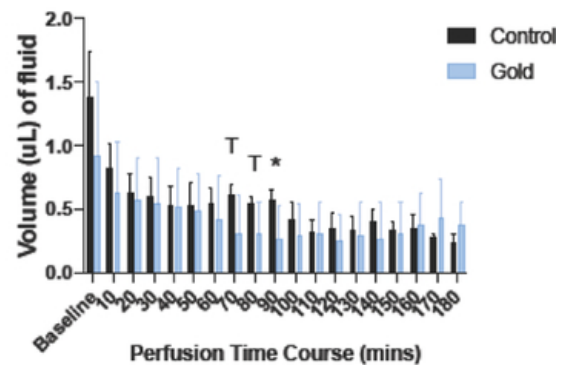
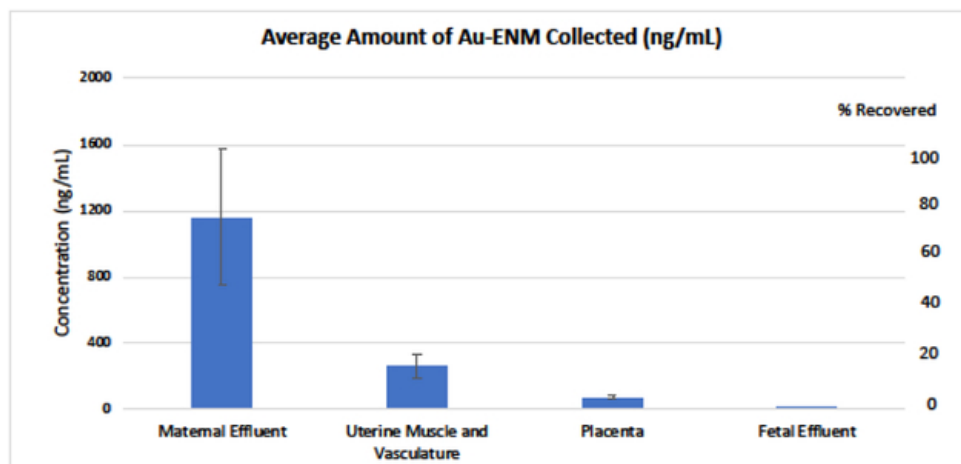


Figure A-3.4: Measurement of (A) maternal fluid flow across the uterine artery or (B) fluid flow across the placenta to the fetal compartment after Au-ENM infusion. \* $p < 0.05$ ; <sup>T</sup> $p < 0.1$ , compared to control values. (n=11)

## Figure 5 – Total Gold Transfer



**Figure A-3.5: Total Au-ENM transfer after the perfusion experiment was complete via ICP-MS analyses.** These represent the distribution of Au-ENM within the maternal effluents (time course samples pooled), uterine muscle and vasculature, placenta, and fetal effluents (time course samples pooled). Data is represented as quantified deposition (left) and percentage of material collected (right).

**APPENDIX 4: Considering intrauterine location in a model of fetal growth restriction after maternal titanium dioxide nanoparticle inhalation**

JN D'Errico<sup>a</sup>, SB Fournier<sup>b</sup>, PA Stapleton<sup>a,b</sup>

**AFFILIATIONS:**

a. Department of Pharmacology and Toxicology, Ernest Mario School of Pharmacy, Rutgers University, 160 Frelinghuysen Rd., Piscataway, NJ 08854, USA; b. Environmental and Occupational Health Sciences Institute, 170 Frelinghuysen Rd., Piscataway, NJ 08854, USA

#### A-4.1 Abstract

Fetal growth restriction (FGR) is a condition with several underlying etiologies including gestational disease (e.g., preeclampsia, gestational diabetes) and xenobiotic exposure (e.g., environmental contaminants, pharmaceuticals, recreational drugs). Rodent models allow study of FGR pathogenesis. However, given the multiparous rodent pregnancy, fetal growth variability within uterine horns may arise. To ascertain whether intrauterine position is a determinant of fetal growth, we redesigned fetal weight analysis to include litter size and maternal weight. Our FGR model is produced by exposing pregnant Sprague Dawley rats to aerosolized nano-TiO<sub>2</sub> at  $9.44 \pm 0.26 \text{ mg/m}^3$  on gestational day (GD) 4, GD 12 or GD 17 or  $9.53 \pm 1.01 \text{ mg/m}^3$  between GD 4-GD 19. In this study fetal weight data was reorganized by intrauterine location [i.e., right/left uterine horn and ovarian/middle/vaginal position] and normalized by maternal weight and number of feti per uterine horn. A significant difference in fetal weight in the middle location in controls ( $0.061 \text{ g} \pm 0.001$  vs.  $0.055 \text{ g} \pm 0.002$ ), GD 4 ( $0.033 \text{ g} \pm 0.003$  vs.  $0.049 \text{ g} \pm 0.004$ ), and GD 17 ( $0.047 \text{ g} \pm 0.002$  vs.  $0.038 \text{ g} \pm 0.002$ ) exposed animals was identified. Additionally, GD 4 exposure produced significantly smaller feti in the right uterine horn at the ovarian end ( $0.052 \text{ g} \pm 0.003$  vs.  $0.029 \text{ g} \pm 0.003$ ) and middle of the right uterine horn ( $0.060 \text{ g} \pm 0.001$  vs.  $0.033 \text{ g} \pm 0.003$ ). GD 17 exposure produced significantly smaller feti in the left uterine horn middle location ( $0.055 \text{ g} \pm 0.002$  vs.  $0.033 \pm 0.002$ ). Placental weights were unaffected, and placental efficiency was reduced in the right uterine horn middle location after GD 17 exposure ( $5.74 \text{ g} \pm 0.16$  vs.  $5.09 \text{ g} \pm 0.14$ ). These findings identified: 1) differences in fetal weight of controls between the right and left horns in the middle position, and 2) differential effects of single whole-body pulmonary exposure to titanium dioxide nanoparticles on fetal weight by position and window of maternal exposure. In conclusion, these results indicate that consideration for intrauterine position, maternal weight, and number of feti per

horn provides a more sensitive assessment of FGR from rodent reproductive and developmental studies.

**Abbreviations List:**

DART- Developmental and Reproductive Toxicology

FGR- Fetal Growth Restriction

GD- Gestational Day

GLUT- Glucose Transporter Protein

IUP- Intrauterine Position

Nano TiO<sub>2</sub> – Titanium Dioxide nanoparticles

R/L CE- Right/Left Cervical End

R/L MD- Right/Left Middle

R/L NCE- Right/Left Next-to Cervical End

R/L NOE- Right/Left Next-to Ovarian End

R/L OE- Right/Left Ovarian End

SD- Sprague Dawley

SMPS- Scanning Mobility Particle Sizer

**A-4.2 Introduction:**

Fetal growth restriction (FGR) is a pathology where the full *in utero* growth potential for a fetus is not met during the period of gestation (Wollmann 1998). In the clinical terms, this is identified as birth weight below the 10<sup>th</sup> percentile on a singleton growth curve (Bamfo and Odibo 2011). Concerningly, a FGR diagnosis is commonly accompanied by other immediate health concerns of perinatal death and neonatal complications. Surviving newborns face an increased likelihood of

developing cardiovascular disease, asthma, type 2 diabetes, and metabolic disorders later in life (BARKER 2006; Curhan et al. 1996; Hales et al. 1991; Leon et al. 1998; Martyn et al. 1995; Xu et al. 2014). Because of these associations with short- and long-term health conditions, FGR is a condition of concern for obstetric, pediatric, and primary care practitioners as well as reproductive and developmental scientists. Although a large body of work has identified several genetic and environmental etiologies of FGR, it is clear that many have yet to be uncovered (Sharma et al. 2016; Wollmann 1998). Recently, accumulating evidence has suggested that pregnant women environmentally exposed to components of air pollution (e.g., fine/ultrafine fractions of particulate matter) or occupationally exposed to nanoparticles are at increased risk for FGR (Bekkar et al. 2020; Manangama et al. 2019; Rogers and Dunlop 2006).

Laboratory studies have helped to unveil the molecular mechanisms and potential therapeutics of common gestational diseases and disorders. These may include models of preeclampsia, gestational diabetes, genetic abnormalities, infections, and maternal environmental exposures (e.g., high altitude, phthalates, heavy metals, and ultrafine particles), each likely to result in the development of FGR (Arce et al. 2012; Bailey et al. 2019; Chen et al. 2020a; Morales-Rubio et al. 2019; Shen et al. 2017; Tachibana et al. 2019; Tunster et al. 2014; Xu et al. 2016; Yamashita et al. 2003). It is estimated that 95% of the animals used in these studies are multiparous rodents, including mice and rats (Vandamme 2014). While these models have proven beneficial for understanding FGR and developmental and reproductive science, the nature of rodent uterine anatomy and placentation has inherent differences from humans.

A cornerstone of Developmental and Reproductive Toxicology (DART) studies is fetal weight evaluation. This involves calculating the average weight of a litter per dam, and subsequently averaging litter weights per experimental group, which for our purposes we will refer to as the “traditional” approach (Lazic and Essioux 2013). This traditional approach may detect a significant

impact on fetal body weight, but without consideration for variability between feti in specific uterine locations, right and left uterine horns, litter size, or maternal body weight. Studies utilizing a fetal pig model have shown that there is intra-litter variability in fetal growth, in that implantation in the middle of a uterine horn produces smaller feti than those deposited at the ends of the uterine horn (e.g., near the ovary or vagina) (Jang et al. 2014; Perry and Rowell 1969). Furthermore, human studies identify that feti which implant on the lateral aspects of the uterus are more likely to be smaller and are at a higher risk for the development of preeclampsia, miscarriage, or preterm birth compared with feti that implant in anterior or posterior positionings (Gonser et al. 1996; Kalanithi et al. 2007; Magann et al. 2007). Particularly hazardous implantation sites that are low in the uterine body can result in placental growth that partially or entirely covers the cervix, a condition known as placenta previa (Balayla et al. 2019). The uterine tissue around the cervix does not have a strong blood supply and is not well perfused; therefore, fetal implantations diagnosed with placenta previa are at heightened risk for placental ischemia, placental hypoxia, and reduced fetal growth (Harper et al. 2010). This evidence that implantation site is a factor in fetal growth underscores a need to account for intrauterine position in laboratory DART studies, especially when considering pregnancies that result in multiple offspring. Unfortunately, few rodent investigations have examined whether intrauterine position influences fetal body weight at term, thereby contributing to study variability.

The number of feti in a litter is negatively correlated with birth weight (Ishikawa et al. 2006; McLaurin and Mactutus 2015; Romero et al. 1992). Romero and colleagues reported an inverse relationship between fetal weight and litter size in Sprague Dawley (SD) rats, and emphasized that if this relationship is not taken into account when toxicity on fetal weight is analyzed there is a potential to mask a decrease in fetal weight due to litter size reduction (Romero et al. 1992). Importantly, the number of feti deposited within the right and left uterine horns respectively, not total litter size, determines the influence of the intrauterine position effect; therefore, experimental

outcomes should be evaluated on a per-horn basis (McLaurin and Mactutus 2015; Raz et al. 2012). Lastly, maternal weight may be an important consideration, as smaller dams may have less energy reserve per fetus to produce feti of a similar weight compared to a larger female (Thame et al. 2015).

The impact of environmental exposure during pregnancy affecting intrauterine positional growth has received little attention. Our model of maternal exposure to titanium dioxide nanoparticle (nano-TiO<sub>2</sub>) aerosols during gestation has identified impairments in gestational health (Fournier et al. 2019b; Stapleton et al. 2013b). Utilizing this model, we have previously reported effects on fetal reabsorption and placental and fetal weight depending on the window(s) of gestational exposure (Fournier et al. 2019b; Stapleton et al. 2013b). Therefore, the purpose of this study was to develop a stepwise method of analysis to organize and normalize fetal growth to more accurately assess FGR in our model. We evaluated fetal weight in a gravid SD rat model under control conditions and after maternal exposure to nano-TiO<sub>2</sub> aerosols by position, maternal GD 20 weight, and number of feti per uterine horn. To ascertain whether exposure caused FGR in a particular uterine location and if the timing of the exposure generated a different outcome, the analysis was conducted with data from four different exposure scenarios: single exposure on gestational day (GD) 4, GD 12, or GD 17, and repeat exposures occurring between GD 4 and GD 19. This challenges the traditional methods and serves useful for future investigations of fetal growth.

### **A-4.3 Materials and Methods**

#### *Animals*

Timed-pregnant SD rats were purchased from Charles River Laboratories (Kingston, NY). Animals were single housed in an AAALAC-approved Rutgers University vivarium where they were

allowed access to Purina 5053 chow and water *ad libitum*. Animals arrived on GD 2 or GD 3. After a 24-hour acclimation period, animals were randomly assigned to control (n=21), filtered-air control (n=6), or nano-TiO<sub>2</sub> exposed groups (n=6-9). Nano-TiO<sub>2</sub> groups received a single exposure on GD 4, GD 12, or GD 17 as described previously (Fournier et al. 2019b) or repeat exposures between GD 4 and GD 19 to aerosolized TiO<sub>2</sub> nanoparticles via whole-body inhalation. Control animals were exposed to filtered air via whole-body inhalation. Naïve animals were not subjected to the inhalation facility. All procedures were approved by the Institutional Animal Care and Use Committee at Rutgers University.

#### *Particle characterization*

Powdered titanium dioxide was purchased from Evonik (Aeroxide TiO<sub>2</sub>, Parsippany, NJ). Previous characterization of the material determined a composition to be primarily anatase (80%) and rutile (20%) (Fournier et al. 2019b). Primary particle size was determined to be 21 nm with a mean surface area of 48.08 mg<sup>2</sup>/g (Fournier et al. 2019b).

#### *Inhalation exposure to aerosolized titanium dioxide nanoparticles*

The nano-TiO<sub>2</sub> preparation and aerosol exposure has been detailed from one other study previously published (Fournier et al. 2019b). Briefly, animals were administered whole-body inhalation exposures in a custom rodent inhalation facility (IEStechno, Morgantown, WV). The size distribution and relative mass of the particle aerosols were monitored in real time with a Scanning Mobility Particle Sizer (SMPS, TSI, Shoreview, MN). Aerosols were collected on a 47-nm PTFE membrane filter for gravimetric sampling to confirm concentration. The exposures were carried out for 4-hr on single days (i.e., GD 4, GD 12, GD 17) or took place repeatedly 5 days/week from GD

4 through GD 19. Average aerosol concentrations were measured at  $9.44 \pm 0.26 \text{ mg/m}^3$  and  $9.53 \pm 1.01 \text{ mg/m}^3$  for 4-hr single and repeat exposures, respectively.

#### *Cesarean procedure and data collection*

On GD 20 animals were anesthetized via isoflurane inhalation (i.e., 5% induction, 3% maintenance) and positioned supine. Surgical scissors were used to create a Y-shaped incision through the abdomen to expose the uterus. The left and right gravid uterine horns were identified, removed, and individually pinned to a dissecting dish positioned with the ovary to the left and the vaginal end to the right.

Using a surgical scissor, the uterine muscle was cut lengthwise to reveal placentas, amniotic sacs, and feti. The fetus from the ovary-most end was designated as fetus number 1 (Figure 1). Moving towards the vaginal end, each fetus was numbered, removed from its amniotic sac, and weighed. Associated placentas were weighed, and wet weights were recorded.

#### *Protocol for intrauterine position analysis*

The inclusion criteria in this analysis required a uterine horn to have at least 5 feti. Dams that had less than 5 feti in the litter were excluded from analysis (Table 1). Right or left uterine horns that had less than 5 feti were also excluded from analysis. Data from horns that met inclusion criteria were organized by intrauterine position [i.e., right/left ovary end (R/L OE), right/left next to ovary end (R/L NOE), right/left middle (R/L MD), right/left next to cervical end (R/L NCE) and right/left cervical end (R/L CE)] (Figure 1). Feti in the middle of uterine horns with more than 5 feti were averaged for the “middle” category.

Existing literature has shown that maternal horn size and litter size can influence the intrauterine position effect in the Sprague Dawley rat (McLaurin and Mactutus 2015; Raz et al. 2012). To correct for differences in maternal weight and litter size, each fetal weight was normalized to the number of feti within that horn by the following equation:

$$\text{Fetal Weight} / (\text{Maternal GD 20 weight} / \text{Number of feti in horn})$$

#### *Calculation of placental efficiency*

Placental efficiency, a ratio of fetal weight to placental weight, is often used as a proxy measurement of placental function in human and laboratory animal studies (Hayward et al. 2016). Placental efficiency was calculated by dividing the raw fetal weight by its respective raw placental weight that were measured on GD 20.

#### *Statistical Analysis*

A Grubb's test was employed to remove any outliers from the data set before further analysis. Student's t test was then used to compare fetal weights using the traditional approach. Fetal weights were also analyzed by arranging and normalizing according to our developed protocol, the individual intrauterine positions from each group were compared between the right and left horn using a two-way ANOVA and Sidak's multiple comparisons test. The nano-TiO<sub>2</sub> exposed group was compared with controls by position for the right and left horn using a two-way ANOVA and Sidak's multiple comparison test. Placental weights and placental efficiencies, calculated as a ratio of fetal weight to placental weight, were evaluated with a similar approach using raw unnormalized values. Effect sizes were calculated and included as Supplemental Figure 1. Statistical analysis was

conducted with GraphPad Prism 8.0 (San Diego, CA, USA). Data is reported as mean  $\pm$  standard error. Statistical significance was set to  $p < 0.05$  and is indicated with an asterisk (\*).

#### **A-4.4 Results**

##### *Traditional analysis of fetal weight*

Fetal body weight was compared between control dams exposed to filtered air in our inhalation exposure facility and naïve animal that never entered the facility using both the traditional and developed approaches. As in previous assessments, no statistical differences were observed (data not shown) between control filtered air exposed or naïve groups (Fournier et al. 2019b). Therefore, in this study, all assessments compared each nano-TiO<sub>2</sub> exposed group to a group naïve animals identified as “control”.

Fetal body weights were compared using the traditional approach of averaging fetal weight by litter and then by treatment group (Table 1). No significant differences and thus no FGR was found using this approach.

##### *Intrauterine position on fetal body weight*

Fetal weights were compared using our developed approach by organizing data by intrauterine position and normalizing by maternal weight at necropsy (GD 20) and number of feti per horn. In controls, average of total fetal weights from the left horn ( $0.053\text{g} \pm 0.001$ ) were smaller than those in the right horn ( $0.058\text{g} \pm 0.001$ ) ( $p=0.08$ ). When the overall right and left horn were compared for exposure groups, repeat and GD 17 exposure resulted in significantly smaller feti in the left horn ( $p=0.02$  and  $0.01$ , respectively). GD 4 exposure resulted in significantly smaller feti in the

right horn ( $p < 0.0001$ ) (Figure 2A). GD 4 and GD 17 also produced significantly smaller pups ( $p < 0.0001$  each) in the right horn, as compared to control growth in the right horn (Figure 2B). Comparisons for the left horn produced significantly smaller pups on GD 17 ( $p < 0.0001$ ) (Figure 2B).

When positional outcomes (Figure 1) were included in the analyses, fetal weights were significantly smaller in the LMD position compared with the RMD position in controls (LMD  $0.054\text{g} \pm 0.002$  vs. RMD  $0.060\text{g} \pm 0.001$ ) (Figure 3A). The fetuses with the lowest weight in control dams were in the LOE and LNOE positions.

When analyzing fetal body weights, exposure to a single inhalation of nano-TiO<sub>2</sub> during pregnancy had a differential effect on fetal weight by intrauterine location based on the timing of exposure. Dams that were repeatedly exposed had no position that was significantly impacted (Figure 3B). Dams exposed on GD 4 had significantly smaller fetal weight in the RMD location compared with the LMD location ( $0.033\text{g} \pm 0.003$  vs.  $0.049\text{g} \pm 0.004$ , respectively) (Figure 3C). Exposure on GD 12 resulted in no significant differences between intrauterine locations within and between right and left horns (Figure 3D). Dams exposed on GD 17 had significantly smaller fetuses on the LOE ( $0.036\text{g} \pm 0.005$  vs.  $0.051\text{g} \pm 0.002$ ) and the LMD ( $0.038\text{g} \pm 0.002$  vs.  $0.047\text{g} \pm 0.002$ ) locations (Figure 3E).

When comparing fetal weights between exposure groups on a per-location basis, exposure on GD 4 had a statistically significant impact on the ROE ( $0.052\text{g} \pm 0.003$  vs.  $0.029\text{g} \pm 0.003$ ), RNOE ( $0.053\text{g} \pm 0.004$  vs.  $0.029\text{g} \pm 0.003$ ), the RMD ( $0.060\text{g} \pm 0.001$  vs.  $0.033\text{g} \pm 0.003$ ) and the RNCE ( $0.055\text{g} \pm 0.004$  vs.  $0.034\text{g} \pm 0.003$ ) locations as compared to control (Figure 4). No significance was found between control and repeated exposed or control and GD 12 exposed groups at any

intrauterine location. Exposure on GD 17 had a statistically significant impact, compared to control, on the LMD location ( $p=0.003$ ).

#### *Intrauterine position effect on placental weight*

When analyzing for placental weight under control conditions, there was no significant impact on placental weight within and between the right and left uterine horns in control animals (Figure 5A). Placental weights were not impacted within or between intrauterine locations in the right and left uterine horns with repeated or single exposures to nano-TiO<sub>2</sub> (Figure 5B-E). Comparison of raw placental weights at each intrauterine location between each experimental group and the control group showed no significance differences (Figure 6).

#### *Intrauterine position effect on placental efficiency*

When analyzing for placental efficiency, the ratio of fetal weight to placental weight, under control conditions, there was no difference in either horn or at any location (Figure 7A). Placental efficiency was not impacted within and between intrauterine locations in the right and left uterine horns with repeated (Figure 7B) or single (Figure 7C-E) exposures to nano-TiO<sub>2</sub> aerosols. When comparing placental efficiency between each experimental group and the control group no significance was found with the exception of a single exposure on GD 17 resulting in a significant reduction in placental efficiency at the RMD location ( $5.09 \pm 0.14$  vs.  $5.74 \pm 0.16$ ) (Figure 8).

### **A-4.5 Discussion**

In this study, data from controls and experimental exposures to nano-TiO<sub>2</sub> were evaluated in a manner that challenges the traditional dogma of litter data analysis. Herein, we were able to account

for intrauterine position, number of feti per horn and maternal weight. When evaluating this dataset using traditional methods, we did not detect significant differences or more than 10% reduction in fetal growth between treatment groups. However, upon further evaluation using our revised approach we observed that under control conditions, feti implanted in the left uterine horn tended to be smaller in body weight at term compared with feti implanted in the right uterine horn. These analyses also demonstrated significant FGR in exposed animals compared with controls, separated by uterine horn and intrauterine position, outcomes that were lost with traditional approaches. This imbalance of fetal growth between the uterine horns was exacerbated after either repeated maternal exposure to nano-TiO<sub>2</sub> aerosols during gestation or a single exposure early (GD 4) or in late (GD 17) pregnancy. The most severe FGR in terms of magnitude of impact and locations affected were apparent from a single maternal exposure on GD 4 in the middle position of the right uterine horn. The middle position of the right uterine horn was also impacted with respect to other endpoints including increased placental weight, reduced fetal weight, and decreased placental efficiency after a single exposure late in gestation, on GD 17. Interestingly, there was no significant positional impact after repeated maternal nano-TiO<sub>2</sub> exposure compared to control in this cohort. Overall, this study demonstrates both critical windows of maternal exposure early and late in gestation and the risks associated with anatomical positioning of implanted fetus in the right horn. Moreover, this information was not gleaned using a traditional approach to data analysis, where no impact on fetal weight was detected.

Observations from control conditions are in agreement with findings from other studies, in that despite anatomical similarities, the right horn produced larger feti suggesting a more favorable environment than the left (Lan et al. 2010; Wiebold and Becker 1987). This observation has also held from human studies, where there is a tendency for right ovary ovulation and implantation on the right side of the reproductive tract (Fukuda et al. 2000; Kawakami et al. 1993). The anatomical or physiological reasons behind this phenomenon are not understood. Moreover, when comparing

each designated position between horns, a significant difference was found in the middle position. Others have reported the middle of the uterine horn to be impacted when considering intrauterine position in pigs (Jang et al. 2014; Perry and Rowell 1969) and mice (Raz et al. 2012). Interestingly, rat studies have a species-specific effect where fetal growth is largest in the middle of each uterine horn (Jensh et al. 1970; Padmanabhan and Singh 1981). This phenomenon may be explained by middle placentas receiving dual-artery blood supply from ovarian and uterine arteries (Avni et al. 2012). Our findings from the control group of animals are in agreement with these observations. In our experimental groups we observed feti in middle positions were also most susceptible to reduced body weight after exposure on GD 4 and GD 17 (Figure 3c and 3e). These findings suggest differences in fetal growth between intrauterine implantation positions under control conditions and after maternal exposure that may be applicable to DART studies.

When comparing between right and left horns (Figure 2) and specific intrauterine position within (Figure 3) after a single or repeated nano-TiO<sub>2</sub> inhalation, the patterns of fetal growth were dependent on the timing of exposure during pregnancy. After a single exposure on GD 4, smaller feti were found in the right horn compared with the left, oppositional to all other findings (Figure 2a). Additionally, the middle position in GD 4 (Figure 3c) as well as GD 17 (Figure 3e) exposure fetal weights were impacted between horns (Figure 3). GD 17 exposed dams had an additional effect on the body weight of feti on the left horn (Figure 2b), and specifically in the ovarian end position (Figure 3e). Animals exposed repeatedly or on GD 12 did not present significant outcomes. These findings are also similar to other studies evaluating the gestational timing of maternal particulate inhalation exposures on FGR, wherein the outcome is dependent upon the pregnancy window(s) of exposure (Blatt et al. 2015; DeFranco et al. 2015).

The resulting FGR outcomes with maternal inhalation of nano-TiO<sub>2</sub> may be associated with vascular dysfunction of the maternal uterine vascular tree. Previous studies have demonstrated a

blunted relaxation and increased vascular smooth muscle contractility of the uterine artery following a single maternal exposure during early, mid, and late pregnancy (Fournier et al. 2019b). Uterine microvascular dysfunction of the radial arteries has been identified in correlation with reduced fetal growth after repeated maternal nano-TiO<sub>2</sub> inhalation in previous studies (Stapleton et al. 2013b). Further, impaired basal arteriolar dilation was identified in late-stage pregnancy *in vivo* 24-hr after a single exposure to nano-TiO<sub>2</sub> aerosols (Stapleton et al. 2018c), unfortunately fetal growth was not evaluated in this study. The variability in fetal weight by location may be attributed to differences in perfusion of the uterine tissue, as previously demonstrated by arterial spin labeling MRI imaging in mice uterine vasculature (Raz et al. 2012). Dual-perfusion to the placental-fetal unit is delivered cranially from the ovarian artery and caudally from the uterine artery (Figure 1). In theory, there should be no change to blood quality or oxygenation between the ovarian, middle, or vaginal segments of the uterine horn (Burbank 2012). However, as evidenced by human placental position studies and control animal data, balanced perfusion throughout the uterus may not be the case (Garris et al. 1983; Jang et al. 2014; Kalanithi et al. 2007; McLaurin and Mactutus 2015; Zia 2013). Raz and colleagues suggested feti at extreme ends of a uterine horn receive more nutrient- and volume- rich blood conveying a growth advantage over the middle positions in a normal pregnancy (Raz et al. 2012). They also suggest that this dual perfusion model may provide a survival advantage to fetus implanted in the middle of the uterine horn in cases of arterial perturbation (Raz et al. 2012). Other studies have shown nonuniformity in hematocrit dispersal, pressure gradients, and blood flow at vascular bifurcations, which may also occur at branching along the uterine arteries (Kalsho and Kassab 2004; Sriram et al. 2014). During disease states, instances of non-uniformity or non-equitable blood distribution are exacerbated (Butcher et al. 2014; Frisbee et al. 2016); this may also be the case after environmental exposure as evidenced in Figure 2A. More research of blood distribution through the uterus and perturbations to uterine perfusion after maternal xenobiotic exposures is needed. Other potential mechanisms of toxicity may include: 1) impaired uterine angiogenesis (Bosquiazzo et al. 2010; Pereira et al. 2015), 2)

increased uterine/spiral artery rarefaction (Baykal et al. 2004), 3) decreased quality of blood oxygenation or nutrition (Zamudio et al. 2010), 5) impaired placental function/nutrient transfer (Vrijer et al. 2004), 6) altered placental metabolism (Challis et al. 2000; Vaughan and Fowden 2016), and 7) nano-TiO<sub>2</sub> translocation culminating in physical blockade within the placenta (Ho et al. 2017; Zhang et al. 2018a).

The placenta regulates the interface between maternal and fetal systems and is often implicated in cases of FGR as a reduction in placental efficiency. Interestingly, with the exception of GD 17 in the RMD position, neither placental weight nor efficiency were impacted. A change in placental weight may indicate placental stress and/or adaptation to the maternal milieu (Furukawa et al. 2011; Ouyang et al. 2013). Decreased placental efficiency ratios are associated with the development of chronic disease in later life, such as cardiovascular disease, diabetes, and other metabolic diseases (Martyn et al. 1996). Although we did not observe changes in placental weights and placental efficiency ratios that aligned with every pinpointed FGR location, placental oxidative stress balance and nutrient transfer may be perturbed at the molecular level (Huang et al. 2018; Zygula et al. 2020). Other environmental exposures, such as cadmium, are known to cause changes at the transcriptional level to the glucose transport proteins (GLUTs), impairing fetal glucose transfer (Xu et al. 2016). Alternatively, physical sedimentation of particles within the placenta may be causing physical blockage of fetal nutrient transfer (D'Errico et al. 2019a; Fournier et al. 2020). Additional studies are required to understand potential placental molecular mechanisms that link exposure to nano-TiO<sub>2</sub> to FGR outcomes.

The etiologies, pathogenesis, and potential therapies for FGR pregnancies have yet to be elucidated. Although many maternal factors (e.g., age, BMI, nutritional status, infections, cardiovascular, immune, pulmonary or thyroid disorders), administered medications (e.g., anticoagulants, steroids, beta blockers, anticonvulsants, and tranquilizers (Redmond 1979)), and social behaviors (e.g.,

smoking, drinking, and substance abuse (Carter et al. 2013; Garrison et al. 2016; Sabra et al. 2017; Vogt Isaksen 2004)) have been documented with human FGR studies, it is estimated that a large portion of FGR cases are of an unknown etiology. Domestic, occupational, or environmental exposures may play a large or confounding role in the initiation of FGR.

There are some limitations to our analyses in this study. While we focused on the effect of intrauterine growth positioning on fetal growth, the pathogenesis of FGR may also be influenced by fetal sex, a variable not assessed in these studies. Fetal sex plays a role in macronutrient uptake through the placenta, and thus sex-dependent differences in response to a growth-hindering intrauterine environment may occur (Mukhopadhyay et al. 2018). It has been hypothesized that male feti demonstrate a higher demand for nutrients for a rapid rate of growth; whereas, female feti are more frugal with nutrient uptake from the mother (Alur 2019b). Thus, because of this higher demand male feti may be more vulnerable to reduced growth if the maternal intrauterine condition is perturbed; in contrast, female feti may be more responsive to changes in the intrauterine environment, modifying growth to nutritional availability (Alur 2019b). Some studies that have stratified their fetal growth data by sex identified male-specific growth restriction after maternal conditions, such as gestational phthalate exposure (Zhao et al. 2014) and hypoxia (Thompson et al. 2020), have found evidence to support that FGR may be sex-dependent. Therefore, when conducting any assessment for fetal growth, stratifying data by fetal sex will be important to reveal sex dependent FGR. Future studies should include this variable in their analyses. Second, maternal body weight pre-pregnancy (Zhao et al. 2018) and gestational weight gain (Ludwig and Currie 2010; Sato and Miyasaka 2019) have been shown to correlate with fetal growth. Studies show larger females deliver larger feti, reasonably a result of more nutrition available for fetal growth. In this study maternal body weight on GD 20 was recorded and used in normalization calculations. Future studies should utilize maternal weight gain throughout pregnancy (e.g., maternal weight prior to

implantation and at sacrifice or delivery) to have a better representation of exposure effects and nutritional concentrations available for fetal growth.

The overall goal of DART is to use information gained from animal studies to identify hazardous substances for a developing fetus. It is of utmost importance that reliable results are generated from these investigations; disregard for disparities associated with intrauterine positioning may lead to future studies riddled with variability. Therefore, clarity on the intrauterine positioning of feti such as those utilized and analyzed in these studies is paramount. Herein, we presented evidence of anatomical intrauterine positional effects after maternal exposure to nano-TiO<sub>2</sub> aerosols, thereby challenging common DART dogma. Reconsidering the way in which these data are evaluated may reduce study variability and allow for more refined conclusions of hazard to fetal growth to be drawn.

#### ACKNOWLEDGEMENTS

We would like to thank Ms. Chelsea Cary and Ms. Talia Seymore for their critical reading and review of the manuscript. This work was supported by the National Institute of Environmental Health Sciences (R00-ES024783; R01-ES031285), Rutgers Center for Environmental Exposures and Disease (P30-ES005022), and Rutgers Joint Graduate Program in Toxicology (T32-ES007148).

## FIGURES:

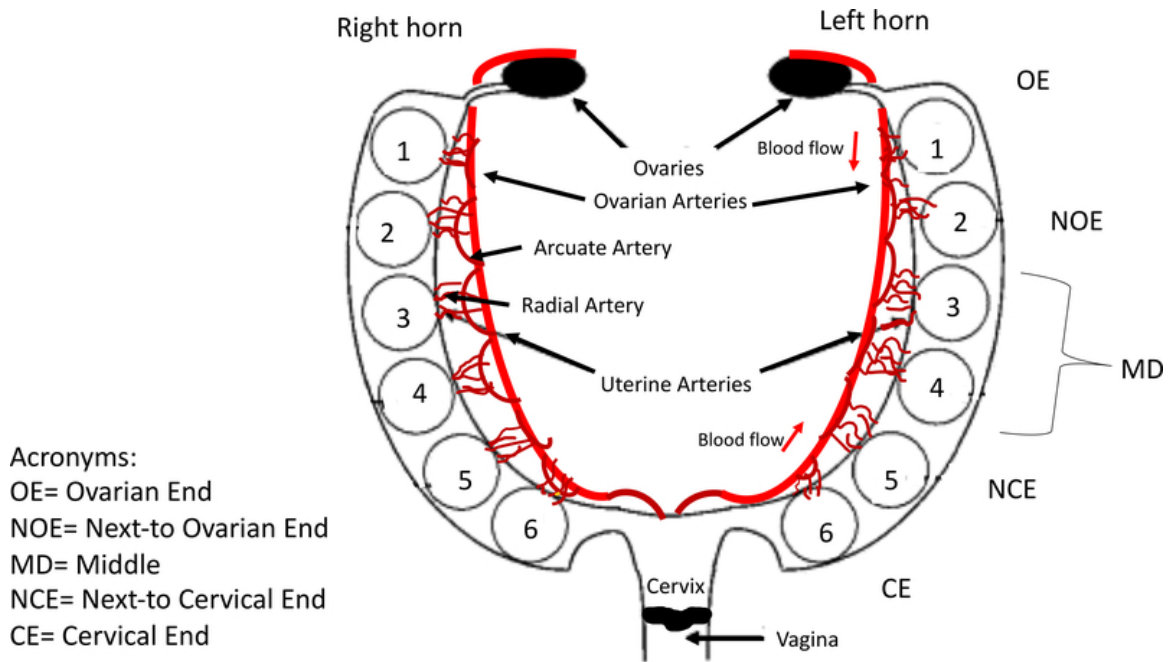


**Figure A-4.1. Schematic of rodent uterine horn anatomy from the ventral aspect and acronym key.** Feti are numbered within each horn from the ovary end (OE) as fetus 1 to the cervical end (CE) as fetus 6. Anatomy of major uterine and ovarian arteries and associated arcuate and radial artery branching is displayed.

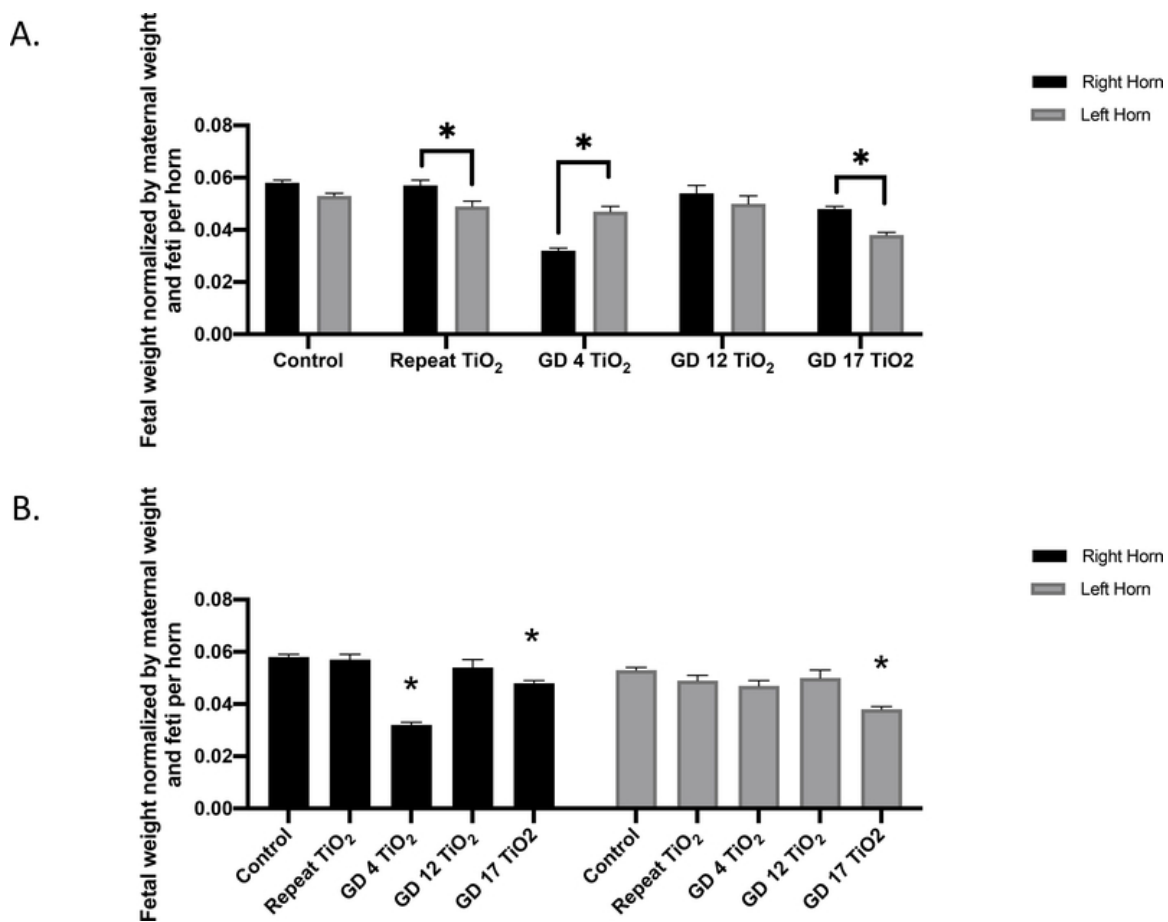


**Figure A-4.2. Fetal weight normalized by maternal weight on GD 20 and number of fetuses per uterine horn.** (A) Normalized fetal weights comparing the right and left horn within each exposure timing condition. This analysis identifies differing fetal growth between the uterine horns within the same experimental condition. (B) Normalized fetal weight of the right and left horns for each exposure group compared to control. This analysis identifies fetal growth impaired by maternal exposure to nano-TiO<sub>2</sub> during gestation. Significance is set to  $p < 0.05$  and values are shown as mean  $\pm$  SEM.

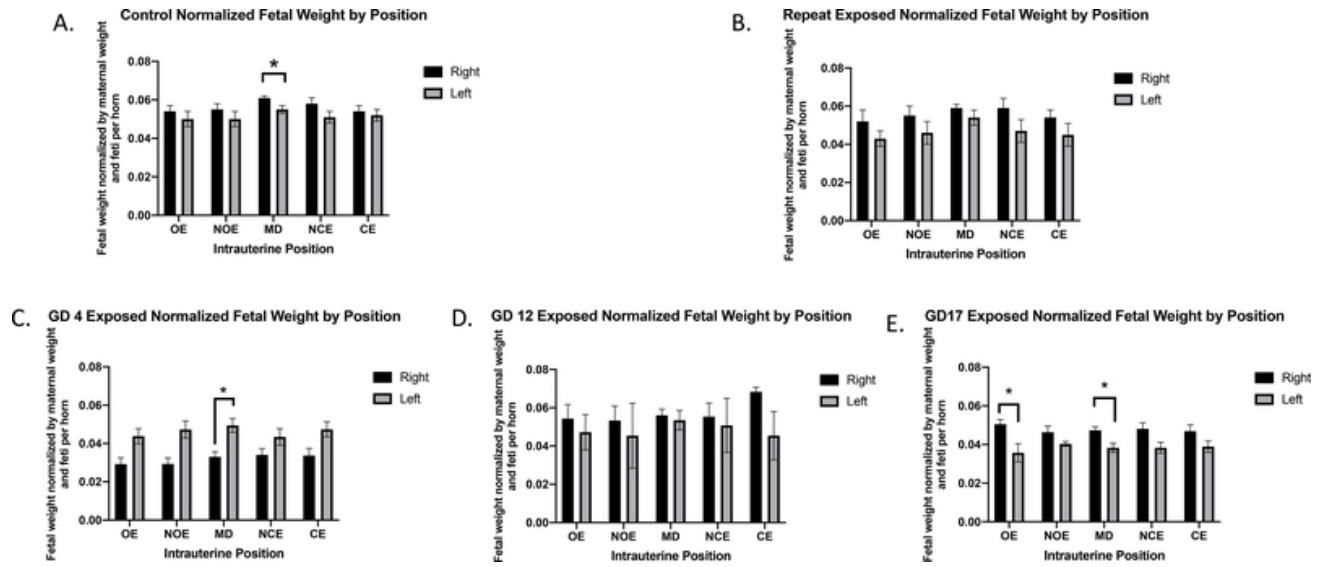


**Figure A-4.3. Fetal weight normalized by maternal weight on GD 20 and number of feti per horn.** Data is analyzed by anatomical uterine position to identify differences between right and left uterine horns in (A) control and (B-E) exposure groups. Significance is set to  $p < 0.05$  and values are shown as mean  $\pm$  SEM.

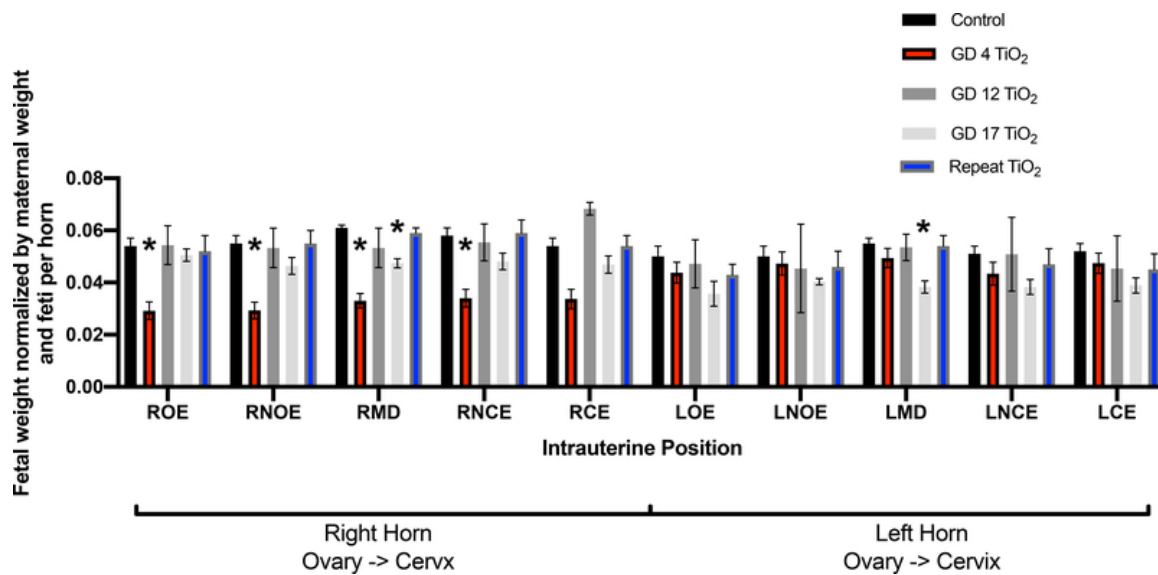


**Figure A-4.4. Fetal weight normalized by maternal weight on GD 20 and number of fetu per horn.** This analysis pinpoints intrauterine positions which are susceptible to growth reduction after certain timing of exposure(s) compared to controls. Significance is set to  $p < 0.05$ , indicated as \*, and values are shown as mean  $\pm$  SEM.

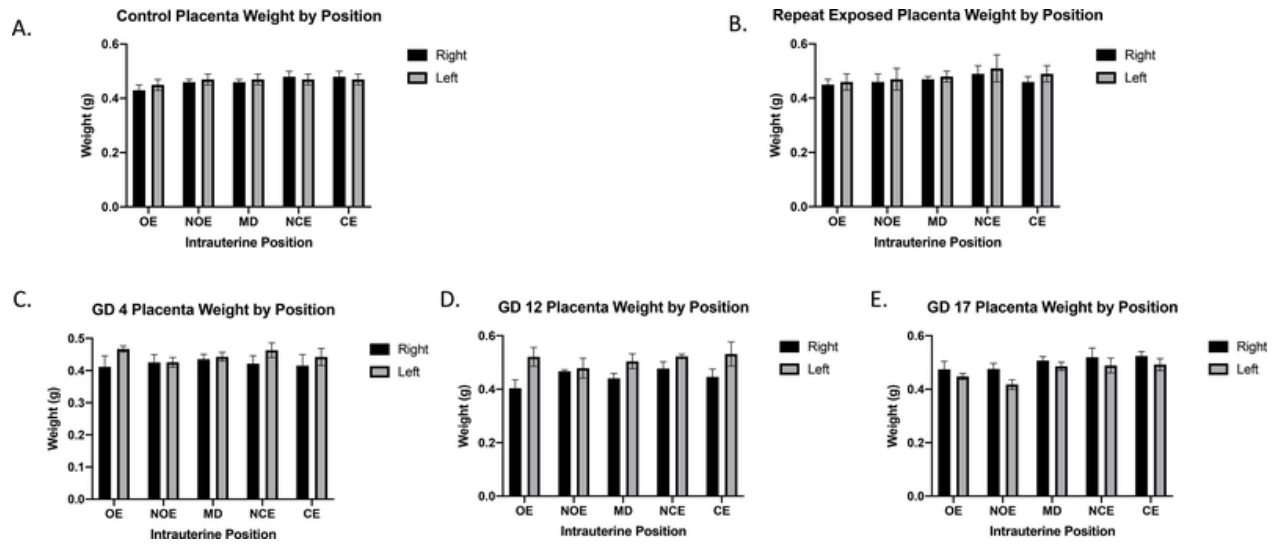


**Figure A-4.5. Raw placental weights (g).** Data is analyzed by anatomical uterine position to identify differences between right and left uterine horns in (A) control and (B-D) exposure conditions.

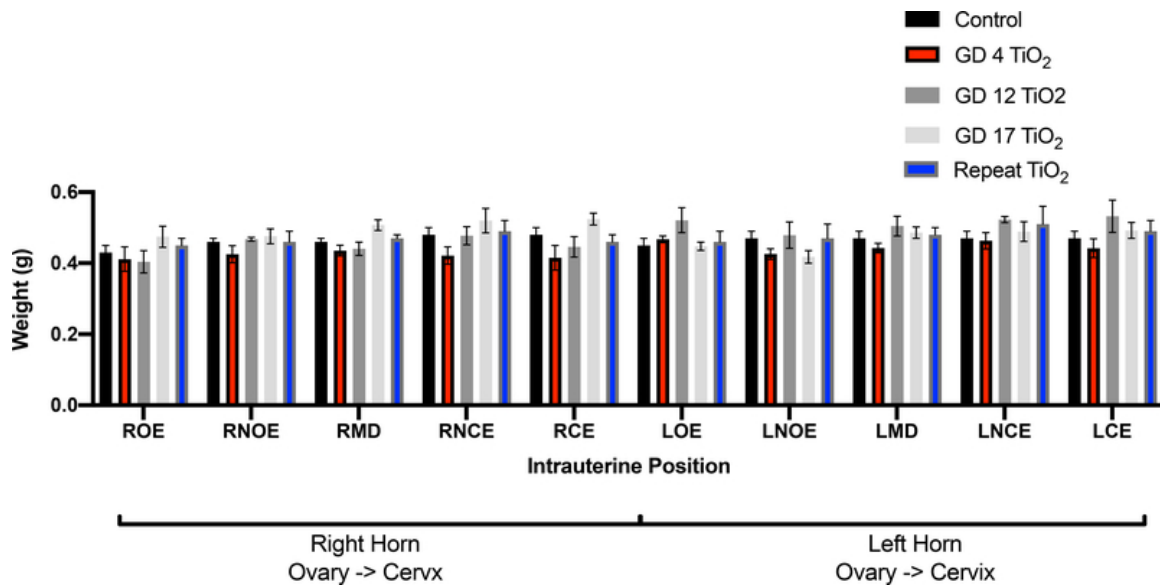


**Figure A-4.6. Raw placental weight (g) at each intrauterine position for control and exposure groups.** This analysis pinpoints intrauterine positions which are susceptible to placental weight change after certain timing of exposure(s) compared to controls.

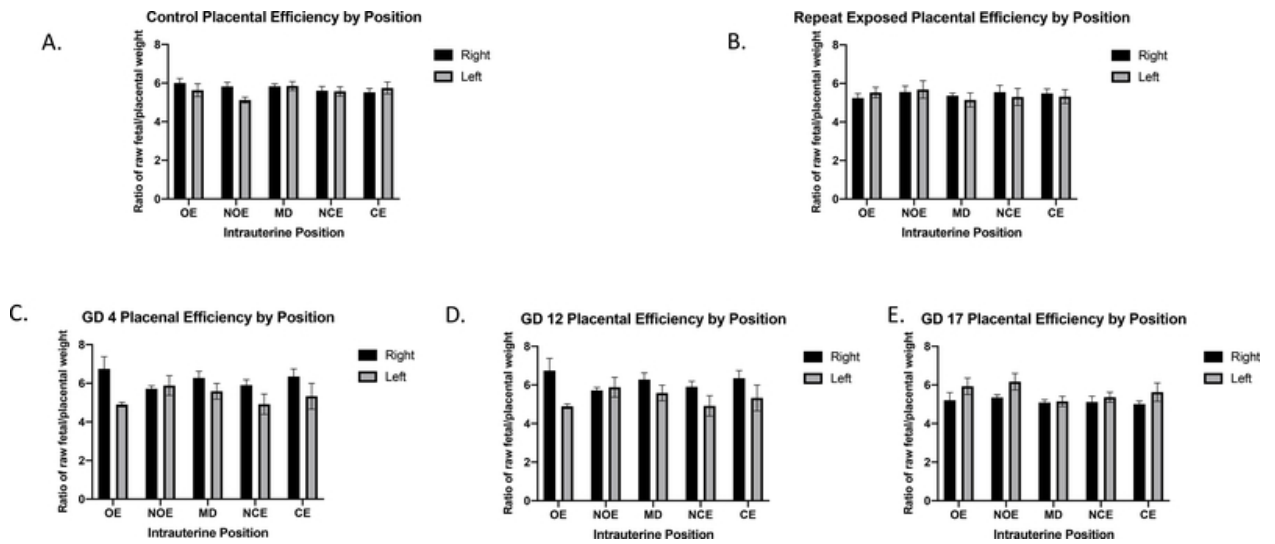


**Figure A-4.7. Placental efficiency calculated by fetal weight/placental weight.** Data is analyzed by anatomical uterine position to identify differences between right and left uterine horns in control and exposure groups.

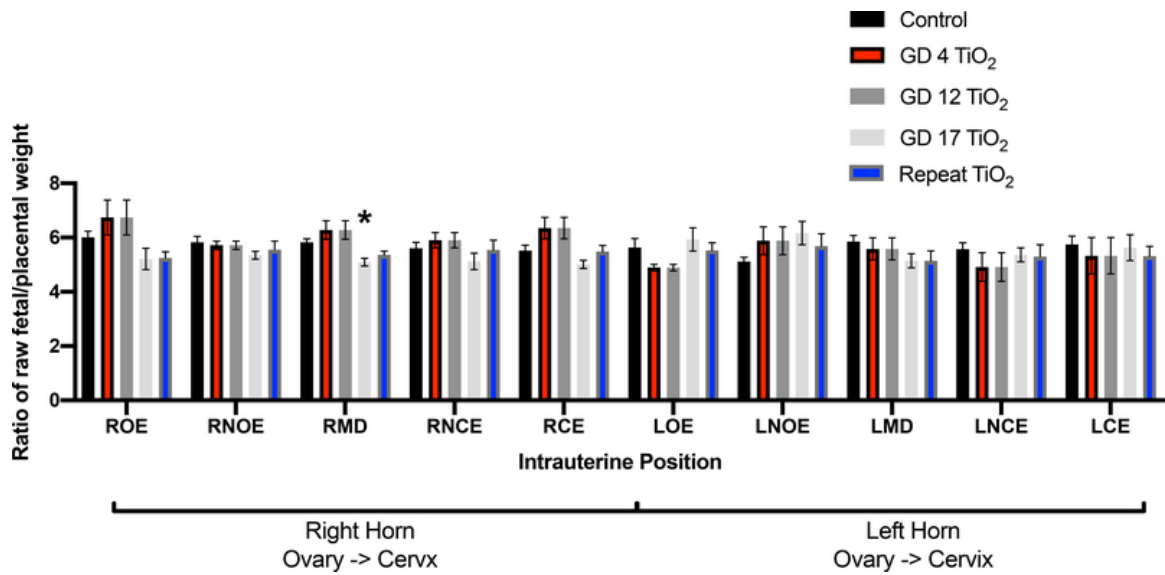


**Figure A-4.8. Placental efficiency, calculated by fetal weight/placental weight, for control and exposure groups.** This analysis pinpoints intrauterine positions which are susceptible to reduced placental efficiency after certain timing of exposure(s) compared to controls. Significance is set to  $p < 0.05$ , indicated as \*, and values are shown as mean  $\pm$  SEM.

Supplemental  
Table 1.

		Traditional, T-Test	P-value	Effect Size (Cohen's d)		
		Repeat	0.13	0.57	Effect Level Threshold: Small= 0.2 Medium= 0.5 Large= 0.8	
		GD 4	0.15	0.66		
		GD 12	0.87	0.07		
		GD 17	0.55	0.24		
IUP, 2-Way ANOVA	DF	F	P-value	Effect Size		
<b>Control (Left and Right Horn)</b>						
IUP	4	F (4, 207) = 0.2387	0.02	0.05	Effect Level Threshold: Small= 0.01 Medium= 0.059 Large= 0.138	
<b>Repeat</b>						
IUP	4	F (4, 97) = 1.675	0.16	0.01		
<b>GD 4</b>						
IUP	4	F (4, 51) = 0.3500	0.84	0.02		
<b>GD 12</b>						
IUP	4	F (4, 43) = 0.2270	0.92	0.02		
<b>GD 17</b>						
IUP	4	F (4,64) = 0.01026	0.99	0.0005		
<b>Exposure and IUP</b>						
IUP	9	F (9, 451) = 1.488	0.15	0.02		
<b>Exposure and Horn</b>						
Timing of Exposure	4	F (1, 503) = 4.086	0.004	0.1818		

**Supplemental Table A-4.1: Table of effect sizes for traditional analysis approach (T-Test) and for our developed method (2-Way ANOVA).**

## References:

- Alur P. 2019. Sex differences in nutrition, growth, and metabolism in preterm infants. *Frontiers in Pediatrics*. 7(22).
- Arce RM, Caron KM, Barros SP, Offenbacher S. 2012. Toll-like receptor 4 mediates intrauterine growth restriction after systemic campylobacter rectus infection in mice. *Mol Oral Microbiol*. 27(5):373-381.
- Avni R, Raz T, Biton IE, Kalchenko V, Garbow JR, Neeman M. 2012. Unique in utero identification of fetuses in multifetal mouse pregnancies by placental bidirectional arterial spin labeling mri. *Magn Reson Med*. 68(2):560-570.
- Bailey BA, Donnelly M, Bol K, Moore LG, Julian CG. 2019. High altitude continues to reduce birth weights in colorado. *Matern Child Health J*. 23(11):1573-1580.
- Balayla J, Desilets J, Shrem G. 2019. Placenta previa and the risk of intrauterine growth restriction (iugr): A systematic review and meta-analysis. *Journal of perinatal medicine*. 47(6):577-584.
- Bamfo JEAK, Odibo AO. 2011. Diagnosis and management of fetal growth restriction. *Journal of pregnancy*. 2011:640715-640715.
- BARKER DJP. 2006. Adult consequences of fetal growth restriction. *Clinical obstetrics and gynecology*. 49(2):270-283.
- Baykal C, Sargon MF, Esinler I, Onderoğlu S, Onderoğlu L. 2004. Placental microcirculation of intrauterine growth retarded fetuses: Scanning electron microscopy of placental vascular casts. *Arch Gynecol Obstet*. 270(2):99-103.
- Bekkar B, Pacheco S, Basu R, DeNicola N. 2020. Association of air pollution and heat exposure with preterm birth, low birth weight, and stillbirth in the us: A systematic review. *JAMA Network Open*. 3(6):e208243-e208243.
- Blatt K, Moore E, Chen A, Van Hook J, DeFranco EA. 2015. Association of reported trimester-specific smoking cessation with fetal growth restriction. *Obstetrics and gynecology*. 125(6):1452-1459.
- Bosquiazzo VL, Varayoud J, Muñoz-de-Toro M, Luque EH, Ramos JG. 2010. Effects of neonatal exposure to bisphenol a on steroid regulation of vascular endothelial growth factor expression and endothelial cell proliferation in the adult rat uterus. *Biology of reproduction*. 82(1):86-95.
- Burbank F. 2012. Hemodynamic changes in the uterus and its blood vessels in pregnancy\*.
- Butcher JT, Stanley SC, Brooks SD, Chantler PD, Wu F, Frisbee JC. 2014. Impact of increased intramuscular perfusion heterogeneity on skeletal muscle microvascular hematocrit in the metabolic syndrome. *Microcirculation (New York, NY : 1994)*. 21(8):677-687.
- Carter RC, Jacobson JL, Sokol RJ, Avison MJ, Jacobson SW. 2013. Fetal alcohol-related growth restriction from birth through young adulthood and moderating effects of maternal prepregnancy weight. *Alcohol Clin Exp Res*. 37(3):452-462.
- Challis DE, Pfarrer CD, Ritchie JW, Koren G, Adamson SL. 2000. Glucose metabolism is elevated and vascular resistance and maternofetal transfer is normal in perfused placental cotyledons from severely growth-restricted fetuses. *Pediatric research*. 47(3):309-315.
- Chen B, Hong W, Yang P, Tang Y, Zhao Y, Aguilar ZP, Xu H. 2020. Nano zinc oxide induced fetal mice growth restriction, based on oxide stress and endoplasmic reticulum stress. *Nanomaterials (Basel)*. 10(2):259.
- Curhan GC, Willett WC, Rimm EB, Spiegelman D, Ascherio AL, Stampfer MJ. 1996. Birth weight and adult hypertension, diabetes mellitus, and obesity in us men. *Circulation*. 94(12):3246-3250.

- D'Errico JN, Doherty C, Fournier SB, Renkel N, Kallontzi S, Goedken M, Fabris L, Buckley B, Stapleton PA. 2019. Identification and quantification of gold engineered nanomaterials and impaired fluid transfer across the rat placenta via ex vivo perfusion. *Biomedicine & Pharmacotherapy*. 117:109148.
- DeFranco E, Hall E, Hossain M, Chen A, Haynes EN, Jones D, Ren S, Lu L, Muglia L. 2015. Air pollution and stillbirth risk: Exposure to airborne particulate matter during pregnancy is associated with fetal death. *PLoS One*. 10(3):e0120594.
- Fournier SB, D'Errico JN, Adler DS, Kollontzi S, Goedken MJ, Fabris L, Yurkow EJ, Stapleton PA. 2020. Nanopolystyrene translocation and fetal deposition after acute lung exposure during late-stage pregnancy. *Part Fibre Toxicol*. 17(1):55.
- Fournier SB, Kallontzi S, Fabris L, Love C, Stapleton PA. 2019. Effect of gestational age on maternofetal vascular function following single maternal engineered nanoparticle exposure. *Cardiovascular toxicology*.
- Frisbee JC, Goodwill AG, Frisbee SJ, Butcher JT, Wu F, Chantler PD. 2016. Microvascular perfusion heterogeneity contributes to peripheral vascular disease in metabolic syndrome. *J Physiol*. 594(8):2233-2243.
- Fukuda M, Fukuda K, Andersen CY, Byskov AG. 2000. Right-sided ovulation favours pregnancy more than left-sided ovulation. *Human Reproduction*. 15(9):1921-1926.
- Furukawa S, Hayashi S, Usuda K, Abe M, Hagio S, Ogawa I. 2011. Toxicological pathology in the rat placenta. *Journal of toxicologic pathology*. 24(2):95-111.
- Garris DR, Blankenship LT, Whitehead DS. 1983. Regional variations in uterine blood flow in the guinea pig: Relationship to pregnancy site distribution. *Gynecologic and obstetric investigation*. 15(1):33-40.
- Garrison L, Leeman L, Savich RD, Gutierrez H, Rayburn WF, Bakhireva LN. 2016. Fetal growth outcomes in a cohort of polydrug- and opioid-dependent patients. *J Reprod Med*. 61(7-8):311-319.
- Gonser M, Tillack N, Pfeiffer KH, Mielke G. 1996. [placental location and incidence of pre-eclampsia]. *Ultraschall Med*. 17(5):236-238.
- Hales CN, Barker DJ, Clark PM, Cox LJ, Fall C, Osmond C, Winter PD. 1991. Fetal and infant growth and impaired glucose tolerance at age 64. *BMJ*. 303(6809):1019-1022.
- Harper LM, Odibo AO, Macones GA, Crane JP, Cahill AG. 2010. Effect of placenta previa on fetal growth. *American journal of obstetrics and gynecology*. 203(4):330.e331-330.e3305.
- Hayward CE, Lean S, Sibley CP, Jones RL, Wareing M, Greenwood SL, Dilworth MR. 2016. Placental adaptation: What can we learn from birthweight:Placental weight ratio? *Frontiers in physiology*. 7:28-28.
- Ho D, Leong JW, Crew RC, Norret M, House MJ, Mark PJ, Waddell BJ, Iyer KS, Keelan JA. 2017. Maternal-placental-fetal biodistribution of multimodal polymeric nanoparticles in a pregnant rat model in mid and late gestation. *Scientific reports*. 7(1):2866-2866.
- Huang X, Anderle P, Hostettler L, Baumann MU, Surbek DV, Ontsouka EC, Albrecht C. 2018. Identification of placental nutrient transporters associated with intrauterine growth restriction and pre-eclampsia. *BMC Genomics*. 19(1):173.
- Ishikawa H, Seki R, Yokonishi S, Yamauchi T, Yokoyama K. 2006. Relationship between fetal weight, placental growth and litter size in mice from mid- to late-gestation. *Reproductive Toxicology*. 21(3):267-270.
- Jang YD, Ma YL, Lindemann MD. 2014. Intrauterine position affects fetal weight and crown-rump length throughout gestation. *J Anim Sci*. 92(10):4400-4406.
- Jensh RP, Brent RL, Barr M, Jr. 1970. The litter effect as a variable in teratologic studies of the albino rat. *Am J Anat*. 128(2):185-191.

- Kalanithi LEG, Illuzzi JL, Nossov VB, Frisbæk Y, Abdel-Razeq S, Copel JA, Norwitz ER. 2007. Intrauterine growth restriction and placental location. *Journal of Ultrasound in Medicine*. 26(11):1481-1489.
- Kalsho G, Kassab GS. 2004. Bifurcation asymmetry of the porcine coronary vasculature and its implications on coronary flow heterogeneity. *American Journal of Physiology-Heart and Circulatory Physiology*. 287(6):H2493-H2500.
- Kawakami Y-u, Andoh K, Mizunuma H, Yamada K, Itoh M, Ibuki Y. 1993. Assessment of the implantation site by transvaginal ultrasonography. *Fertility and Sterility*. 59(5):1003-1006.
- Lan KC, Huang FJ, Lin YC, Kung FT, Lan TH, Chang SY. 2010. Significantly superior response in the right ovary compared with the left ovary after stimulation with follicle-stimulating hormone in a pituitary down-regulation regimen. *Fertil Steril*. 93(7):2269-2273.
- Lazic SE, Essioux L. 2013. Improving basic and translational science by accounting for litter-to-litter variation in animal models. *BMC neuroscience*. 14:37-37.
- Leon DA, Lithell HO, Vagero D, Koupilova I, Mohsen R, Berglund L, Lithell UB, McKeigue PM. 1998. Reduced fetal growth rate and increased risk of death from ischaemic heart disease: Cohort study of 15 000 swedish men and women born 1915-29. *BMJ*. 317(7153):241-245.
- Ludwig DS, Currie J. 2010. The association between pregnancy weight gain and birthweight: A within-family comparison. *Lancet (London, England)*. 376(9745):984-990.
- Magann EF, Doherty DA, Turner K, Lanneau GS, Jr., Morrison JC, Newnham JP. 2007. Second trimester placental location as a predictor of an adverse pregnancy outcome. *J Perinatol*. 27(1):9-14.
- Manangama G, Migault L, Audignon-Durand S, Gramond C, Zaros C, Bouvier G, Brochard P, Sentilhes L, Lacourt A, Delva F. 2019. Maternal occupational exposures to nanoscale particles and small for gestational age outcome in the french longitudinal study of children. *Environment international*. 122:322-329.
- Martyn CN, Barker DJ, Jaspersen S, Greenwald S, Osmond C, Berry C. 1995. Growth in utero, adult blood pressure, and arterial compliance. *Br Heart J*. 73(2):116-121.
- Martyn CN, Barker DJP, Osmond C. 1996. Mothers' pelvic size, fetal growth, and death from stroke and coronary heart disease in men in the uk. *The Lancet*. 348(9037):1264-1268.
- McLaurin KA, Mactutus CF. 2015. Polytocus focus: Uterine position effect is dependent upon horn size. *Int J Dev Neurosci*. 40:85-91.
- Morales-Rubio RA, Alvarado-Cruz I, Manzano-León N, Andrade-Oliva M-d-I-A, Uribe-Ramirez M, Quintanilla-Vega B, Osornio-Vargas Á, De Vizcaya-Ruiz A. 2019. In utero exposure to ultrafine particles promotes placental stress-induced programming of renin-angiotensin system-related elements in the offspring results in altered blood pressure in adult mice. *Particle and Fibre Toxicology*. 16(1):7.
- Mukhopadhyay A, Thomas T, Bosch RJ, Dwarkanath P, Thomas A, Duggan CP, Kurpad AV. 2018. Fetal sex modifies the effect of maternal macronutrient intake on the incidence of small-for-gestational-age births: A prospective observational cohort study. *The American Journal of Clinical Nutrition*. 108(4):814-820.
- Ouyang F, Parker M, Cerda S, Pearson C, Fu L, Gillman MW, Zuckerman B, Wang X. 2013. Placental weight mediates the effects of prenatal factors on fetal growth: The extent differs by preterm status. *Obesity (Silver Spring)*. 21(3):609-620.
- Padmanabhan R, Singh S. 1981. Effect of intrauterine position on foetal weight in cf rats. *Indian J Med Res*. 73:134-139.
- Pereira RD, De Long NE, Wang RC, Yazdi FT, Holloway AC, Raha S. 2015. Angiogenesis in the placenta: The role of reactive oxygen species signaling. *BioMed research international*. 2015:814543-814543.

- Perry JS, Rowell JG. 1969. Variations in foetal weight and vascular supply along the uterine horn of the pig. *Journal of reproduction and fertility*. 19(3):527-534.
- Raz T, Avni R, Addadi Y, Cohen Y, Jaffa AJ, Hemmings B, Garbow JR, Neeman M. 2012. The hemodynamic basis for positional- and inter-fetal dependent effects in dual arterial supply of mouse pregnancies. *PLOS ONE*. 7(12):e52273.
- Redmond GP. 1979. Effect of drugs on intrauterine growth. *Clin Perinatol*. 6(1):5-19.
- Rogers JF, Dunlop AL. 2006. Air pollution and very low birth weight infants: A target population? *Pediatrics*. 118(1):156-164.
- Romero A, Villamayor F, Grau MT, Sacristán A, Ortiz JA. 1992. Relationship between fetal weight and litter size in rats: Application to reproductive toxicology studies. *Reproductive toxicology (Elmsford, NY)*. 6(5):453-456.
- Sabra S, Gratacós E, Gómez Roig MD. 2017. Smoking-induced changes in the maternal immune, endocrine, and metabolic pathways and their impact on fetal growth: A topical review. *Fetal Diagnosis and Therapy*. 41(4):241-250.
- Sato N, Miyasaka N. 2019. Stratified analysis of the correlation between gestational weight gain and birth weight for gestational age: A retrospective single-center cohort study in japan. *BMC Pregnancy Childbirth*. 19(1):402.
- Sharma D, Shastri S, Sharma P. 2016. Intrauterine growth restriction: Antenatal and postnatal aspects. *Clin Med Insights Pediatr*. 10:67-83.
- Shen R, Zhao LL, Yu Z, Zhang C, Chen YH, Wang H, Zhang ZH, Xu DX. 2017. Maternal di-(2-ethylhexyl) phthalate exposure during pregnancy causes fetal growth restriction in a stage-specific but gender-independent manner. *Reproductive toxicology (Elmsford, NY)*. 67:117-124.
- Sriram K, Intaglietta M, Tartakovsky DM. 2014. Hematocrit dispersion in asymmetrically bifurcating vascular networks. *American Journal of Physiology-Heart and Circulatory Physiology*. 307(11):H1576-H1586.
- Stapleton PA, McBride CR, Yi J, Abukabda AB, Nurkiewicz TR. 2018. Estrous cycle-dependent modulation of in vivo microvascular dysfunction after nanomaterial inhalation. *Reproductive toxicology (Elmsford, NY)*. 78:20-28.
- Stapleton PA, Minarchick VC, Yi J, Engels K, McBride CR, Nurkiewicz TR. 2013. Maternal engineered nanomaterial exposure and fetal microvascular function: Does the barker hypothesis apply? *American journal of obstetrics and gynecology*. 209(3):227.e221-211.
- Tachibana R, Umekawa T, Yoshikawa K, Owa T, Magawa S, Furuhashi F, Tsuji M, Maki S, Shimada K, Kaneda MK et al. 2019. Tadalafil treatment in mice for preeclampsia with fetal growth restriction has neuro-benefic effects in offspring through modulating prenatal hypoxic conditions. *Scientific reports*. 9(1):234-234.
- Thame M, Osmond C, Trotman H. 2015. Fetal growth and birth size is associated with maternal anthropometry and body composition. *Matern Child Nutr*. 11(4):574-582.
- Thompson LP, Turan S, Aberdeen GW. 2020. Sex differences and the effects of intrauterine hypoxia on growth and in vivo heart function of fetal guinea pigs. *American Journal of Physiology-Regulatory, Integrative and Comparative Physiology*. 319(3):R243-R254.
- Tunster SJ, Van De Pette M, John RM. 2014. Isolating the role of elevated phlda2 in asymmetric late fetal growth restriction in mice. *Dis Model Mech*. 7(10):1185-1191.
- Vandamme TF. 2014. Use of rodents as models of human diseases. *J Pharm Bioallied Sci*. 6(1):2-9.
- Vaughan OR, Fowden AL. 2016. Placental metabolism: Substrate requirements and the response to stress. *Reprod Domest Anim*. 51 Suppl 2:25-35.

- Vogt Isaksen C. 2004. Maternal smoking, intrauterine growth restriction, and placental apoptosis. *Pediatr Dev Pathol.* 7(5):433-442.
- Vrijer Bd, Regnault TRH, Wilkening RB, Meschia G, Battaglia FC. 2004. Placental uptake and transport of acp, a neutral nonmetabolizable amino acid, in an ovine model of fetal growth restriction. *American Journal of Physiology-Endocrinology and Metabolism.* 287(6):E1114-E1124.
- Wiebold JL, Becker WC. 1987. Inequality in function of the right and left ovaries and uterine horns of the mouse. *Journal of reproduction and fertility.* 79(1):125-134.
- Wollmann HA. 1998. Intrauterine growth restriction: Definition and etiology. *Hormone Research in Paediatrics.* 49(suppl 2)(Suppl. 2):1-6.
- Xu P, Wu Z, Xi Y, Wang L. 2016. Epigenetic regulation of placental glucose transporters mediates maternal cadmium-induced fetal growth restriction. *Toxicology.* 372:34-41.
- Xu X-F, Li Y-J, Sheng Y-J, Liu J-L, Tang L-F, Chen Z-M. 2014. Effect of low birth weight on childhood asthma: A meta-analysis. *BMC Pediatr.* 14:275-275.
- Yamashita H, Shao J, Qiao L, Pagliassotti M, Friedman JE. 2003. Effect of spontaneous gestational diabetes on fetal and postnatal hepatic insulin resistance in *lepr(db/+)* mice. *Pediatric research.* 53(3):411-418.
- Zamudio S, Torricos T, Fik E, Oyala M, Echalar L, Pullockaran J, Tutino E, Martin B, Belliappa S, Balanza E et al. 2010. Hypoglycemia and the origin of hypoxia-induced reduction in human fetal growth. *PLoS One.* 5(1):e8551.
- Zhang B, Tan L, Yu Y, Wang B, Chen Z, Han J, Li M, Chen J, Xiao T, Ambati BK et al. 2018. Placenta-specific drug delivery by trophoblast-targeted nanoparticles in mice. *Theranostics.* 8(10):2765-2781.
- Zhao R, Xu L, Wu ML, Huang SH, Cao XJ. 2018. Maternal pre-pregnancy body mass index, gestational weight gain influence birth weight. *Women Birth.* 31(1):e20-e25.
- Zhao Y, Chen L, Li L-x, Xie C-m, Li D, Shi H-j, Zhang Y-h. 2014. Gender-specific relationship between prenatal exposure to phthalates and intrauterine growth restriction. *Pediatric research.* 76(4):401-408.
- Zia S. 2013. Placental location and pregnancy outcome. *Journal of the Turkish German Gynecological Association.* 14(4):190-193.
- Zygula A, Kosinski P, Wroczynski P, Makarewicz-Wujec M, Pietrzak B, Wielgos M, Giebultowicz J. 2020. Oxidative stress markers differ in two placental dysfunction pathologies: Pregnancy-induced hypertension and intrauterine growth restriction. *Oxidative Medicine and Cellular Longevity.* 2020:1323891.

## REFERENCES

- Abukabda AB, Bowdridge EC, McBride CR, Batchelor TP, Goldsmith WT, Garner KL, Friend S, Nurkiewicz TR. 2019. Maternal titanium dioxide nanomaterial inhalation exposure compromises placental hemodynamics. *Toxicology and applied pharmacology*. 367:51-61.
- Aengenheister L, Dietrich D, Sadeghpour A, Manser P, Diener L, Wichser A, Karst U, Wick P, Buerki-Thurnherr T. 2018a. Gold nanoparticle distribution in advanced in vitro and ex vivo human placental barrier models. *J Nanobiotechnology*. 16(1):79.
- Aengenheister L, Keevend K, Muoth C, Schonenberger R, Diener L, Wick P, Buerki-Thurnherr T. 2018b. An advanced human in vitro co-culture model for translocation studies across the placental barrier. *Sci Rep*. 8(1):5388.
- Austin CA, Hinkley GK, Mishra AR, Zhang Q, Umbreit TH, Betz MW, B EW, Casey BJ, Francke-Carroll S, Hussain SM et al. 2016. Distribution and accumulation of 10 nm silver nanoparticles in maternal tissues and visceral yolk sac of pregnant mice, and a potential effect on embryo growth. *Nanotoxicology*. 10(6):654-661.
- Austin CA, Umbreit TH, Brown KM, Barber DS, Dair BJ, Francke-Carroll S, Feswick A, Saint-Louis MA, Hikawa H, Siebein KN et al. 2012. Distribution of silver nanoparticles in pregnant mice and developing embryos. *Nanotoxicology*. 6:912-922.
- Blum JL, Xiong JQ, Hoffman C, Zelikoff JT. 2012. Cadmium associated with inhaled cadmium oxide nanoparticles impacts fetal and neonatal development and growth. *Toxicol Sci*.
- Bond H, Baker B, Boyd RD, Cowley E, Glazier JD, Jones CJ, Sibley CP, Ward BS, Husain SM. 2006. Artificial perfusion of the fetal circulation of the in situ mouse placenta: Methodology and validation. *Placenta*. 27 Suppl A:S69-75.
- Cabuzu D, Cirja A, Puiu R, Grumezescu AM. 2015. Biomedical applications of gold nanoparticles. *Curr Top Med Chem*. 15(16):1605-1613.
- Campagnolo L, Massimiani M, Palmieri G, Bernardini R, Sacchetti C, Bergamaschi A, Vecchione L, Magrini A, Bottini M, Pietroiusti A. 2013. Biodistribution and toxicity of pegylated single wall carbon nanotubes in pregnant mice. *Part Fibre Toxicol*. 10:21.
- Campagnolo L, Massimiani M, Vecchione L, Piccirilli D, Toschi N, Magrini A, Bonanno E, Scimeca M, Castagnozzi L, Buonanno G et al. 2017. Silver nanoparticles inhaled during pregnancy reach and affect the placenta and the foetus. *Nanotoxicology*. 11(5):687-698.
- Cheheltani R, Ezzibdeh RM, Chhour P, Pulaparathi K, Kim J, Jurcova M, Hsu JC, Blundell C, Litt HI, Ferrari VA et al. 2016. Tunable, biodegradable gold nanoparticles as contrast agents for computed tomography and photoacoustic imaging. *Biomaterials*. 102:87-97.
- D'Errico JN, Stapleton PA. 2018. Developmental onset of cardiovascular disease - could the proof be in the placenta? *Microcirculation*. e12526.
- D'Errico JN, Fournier SB, Stapleton PA. 2019. *Ex vivo* perfusion of the rodent placenta. *J Vis Exp*. (147):e59412.
- Elahi N, Kamali M, Baghersad MH. 2018. Recent biomedical applications of gold nanoparticles: A review. *Talanta*. 184:537-556.
- Engler-Chiurazzi EB, Stapleton PA, Stalnaker JJ, Ren X, Hu H, Nurkiewicz TR, McBride CR, Yi J, Engels K, Simpkins JW. 2016. Impacts of prenatal nanomaterial exposure on male adult sprague-dawley rat behavior and cognition. *Journal of toxicology and environmental health Part A*. 79(11):447-452.

- Fournier SB, D'Errico JN, Stapleton PA. 2018. Engineered nanomaterial applications in perinatal therapeutics. *Pharmacol Res.* 130:36-43.
- Fournier SB, Kallontzi S, Fabris L, Love C, Stapleton PA. 2019. Effect of gestational age on maternofetal vascular function following single maternal engineered nanoparticle exposure. *Cardiovascular toxicology.*
- Goeden N, Bonnin A. 2013. Ex vivo perfusion of mid-to-late-gestation mouse placenta for maternal-fetal interaction studies during pregnancy. *Nature protocols.* 8(1):66-74.
- Goeden N, Notarangelo FM, Pocivavsek A, Beggiato S, Bonnin A, Schwarcz R. 2017. Prenatal dynamics of kynurenine pathway metabolism in mice: Focus on kynurenic acid. *Developmental neuroscience.* 39(6):519-528.
- Grafmueller S, Manser P, Diener L, Diener PA, Maeder-Althaus X, Maurizi L, Jochum W, Krug HF, Buerki-Thurnherr T, von Mandach U et al. 2015a. Bidirectional transfer study of polystyrene nanoparticles across the placental barrier in an ex vivo human placental perfusion model. *Environ Health Perspect.* 123(12):1280-1286.
- Grafmueller S, Manser P, Diener L, Maurizi L, Diener PA, Hofmann H, Jochum W, Krug HF, Buerki-Thurnherr T, von Mandach U et al. 2015b. Transfer studies of polystyrene nanoparticles in the ex vivo human placenta perfusion model: Key sources of artifacts. *Sci Technol Adv Mater.* 16(4):044602.
- Hathaway QA, Nichols CE, Shepherd DL, Stapleton PA, McLaughlin SL, Stricker JC, Rellick SL, Pinti MV, Abukabda AB, McBride CR et al. 2017. Maternal-engineered nanomaterial exposure disrupts progeny cardiac function and bioenergetics. *Am J Physiol Heart Circ Physiol.* 312(3):H446-H458.
- Hougaard KS, Campagnolo L, Chavatte-Palmer P, Tarrade A, Rousseau-Ralliard D, Valentino S, Park MV, de Jong WH, Wolterink G, Piersma AH et al. 2015. A perspective on the developmental toxicity of inhaled nanoparticles. *Reprod Toxicol.* 56:118-140.
- Hougaard KS, Jackson P, Jensen KA, Sloth JJ, Loschner K, Larsen EH, Birkedal RK, Vibenholt A, Boisen AM, Wallin H et al. 2010. Effects of prenatal exposure to surface-coated nanosized titanium dioxide (uv-titan). A study in mice. *Part Fibre Toxicol.* 7:16.
- Hougaard KS, Jackson P, Kyjovska ZO, Birkedal RK, De Temmerman PJ, Brunelli A, Verleysen E, Madsen AM, Saber AT, Pojana G et al. 2013. Effects of lung exposure to carbon nanotubes on female fertility and pregnancy. A study in mice. *Reprod Toxicol.* 41:86-97.
- Kafka P, Vajnerova O, Herget J, Hampl V. 2012. Rho-kinase inhibition attenuates acute hypoxic fetoplacental vasoconstriction in the rat. *Physiol Res.* 61 Suppl 2:S43-48.
- Khlebtsov N, Bogatyrev V, Dykman L, Khlebtsov B, Staroverov S, Shirokov A, Matora L, Khanadeev V, Pylaev T, Tsyganova N et al. 2013. Analytical and theranostic applications of gold nanoparticles and multifunctional nanocomposites. *Theranostics.* 3(3):167-180.
- Mahan MM, Doiron AL. 2018. Gold nanoparticles as x-ray, ct, and multimodal imaging contrast agents: Formulation, targeting, and methodology. *Journal of Nanomaterials.* 2018:15.
- Muller EK, Grafe C, Wiekhorst F, Bergemann C, Weidner A, Dutz S, Clement JH. 2018. Magnetic nanoparticles interact and pass an in vitro co-culture blood-placenta barrier model. *Nanomaterials (Basel).* 8(2).
- Myllynen PK, Loughran MJ, Howard CV, Sormunen R, Walsh AA, Vahakangas KH. 2008. Kinetics of gold nanoparticles in the human placenta. *Reprod Toxicol.* 26(2):130-137.
- Nishimura T, Chishu T, Tomi M, Nakamura R, Sato K, Kose N, Sai Y, Nakashima E. 2012. Mechanism of nucleoside uptake in rat placenta and induction of placental cnt2 in experimental diabetes. *Drug Metab Pharmacokinet.* 27(4):439-446.

- Notter T, Aengenheister L, Weber-Stadlbauer U, Naegeli H, Wick P, Meyer U, Buerki-Thurnherr T. 2018. Prenatal exposure to tio<sub>2</sub> nanoparticles in mice causes behavioral deficits with relevance to autism spectrum disorder and beyond. *Transl Psychiatry*. 8(1):193.
- Paul E, Franco-Montoya ML, Paineau E, Angeletti B, Vibhushan S, Ridoux A, Tiendrebeogo A, Salome M, Hesse B, Vantelon D et al. 2017. Pulmonary exposure to metallic nanomaterials during pregnancy irreversibly impairs lung development of the offspring. *Nanotoxicology*. 11(4):484-495.
- Pavek P, Fendrich Z, Staud F, Malakova J, Brozmanova H, Laznicek M, Semecky V, Grundmann M, Palicka V. 2001. Influence of p-glycoprotein on the transplacental passage of cyclosporine. *J Pharm Sci*. 90(10):1583-1592.
- Pavek P, Staud F, Fendrich Z, Sklenarova H, Libra A, Novotna M, Kopecky M, Nobilis M, Semecky V. 2003. Examination of the functional activity of p-glycoprotein in the rat placental barrier using rhodamine 123. *J Pharmacol Exp Ther*. 305(3):1239-1250.
- Rasmussen SA. 2012. Human teratogens update 2011: Can we ensure safety during pregnancy? *Birth Defects Res A Clin Mol Teratol*. 94(3):123-128.
- Rosenfeld CS. 2015. Sex-specific placental responses in fetal development. *Endocrinology*. 156(10):3422-3434.
- Sastry BV. 1999. Techniques to study human placental transport. *Advanced drug delivery reviews*. 38(1):17-39.
- Semmler-Behnke M, Lipka J, Wenk A, Hirn S, Schaffler M, Tian F, Schmid G, Oberdorster G, Kreyling WG. 2014. Size dependent translocation and fetal accumulation of gold nanoparticles from maternal blood in the rat. *Part Fibre Toxicol*. 11:33.
- Snyder RW, Fennell TR, Wingard CJ, Mortensen NP, Holland NA, Shannahan JH, Pathmasiri W, Lewin AH, Sumner SC. 2015. Distribution and biomarker of carbon-14 labeled fullerene c<sub>60</sub> ([<sup>14</sup>C]<sub>60</sub>) in pregnant and lactating rats and their offspring after maternal intravenous exposure. *J Appl Toxicol*. 35(12):1438-1451.
- Soares MJ, Iqbal K, Kozai K. 2017. Hypoxia and placental development. *Birth defects research*. 109(17):1309-1329.
- Stapleton PA. 2016. Gestational nanomaterial exposures: Microvascular implications during pregnancy, fetal development and adulthood. *J Physiol*. 594(8):2161-2173.
- Stapleton PA, Abukabda AB, Hardy SL, Nurkiewicz TR. 2015. Xenobiotic pulmonary exposure and systemic cardiovascular response via neurological links. *Am J Physiol Heart Circ Physiol*. 309(10):H1609-1620.
- Stapleton PA, Hathaway QA, Nichols CE, Abukabda AB, Pinti MV, Shepherd DL, McBride CR, Yi J, Castranova VC, Hollander JM et al. 2018a. Maternal engineered nanomaterial inhalation during gestation alters the fetal transcriptome. *Part Fibre Toxicol*. 15(1):3.
- Stapleton PA, McBride CR, Yi J, Abukabda AB, Nurkiewicz TR. 2018b. Estrous cycle-dependent modulation of in vivo microvascular dysfunction after nanomaterial inhalation. *Reproductive toxicology (Elmsford, NY)*. 78:20-28.
- Stapleton PA, Minarchick VC, Yi J, Engels K, McBride CR, Nurkiewicz TR. 2013. Maternal engineered nanomaterial exposure and fetal microvascular function: Does the barker hypothesis apply? *Am J Obstet Gynecol*.
- Stapleton PA, Nurkiewicz TR. 2014. Maternal nanomaterial exposure: A double threat to maternal uterine health and fetal development? *Nanomedicine (Lond)*. 9(7):929-931.
- Stulc J, Stulcova B. 1996. Placental transfer of phosphate in anaesthetized rats. *Placenta*. 17(7):487-493.
- Stulc J, Stulcova B, Husain S, Sibley CP. 1996. Transfer of Cl<sup>-</sup> across placenta of anesthetized rat. *Am J Physiol*. 271(5 Pt 2):R1107-1114.

- Stulc J, Stulcova B, Svihovec J. 1990. Transport of calcium across the dually perfused placenta of the rat. *J Physiol.* 420:295-311.
- Sweeney S, Adamcakova-Dodd A, Thorne PS, Assouline JG. 2018. Multifunctional nanoparticles for real-time evaluation of toxicity during fetal development. *PLoS One.* 13(2):e0192474.
- Tang H, Jiang Z, He H, Li X, Hu H, Zhang N, Dai Y, Zhou Z. 2018. Uptake and transport of pullulan acetate nanoparticles in the bewo b30 placental barrier cell model. *Int J Nanomedicine.* 13:4073-4082.
- Thorpe PG, Gilboa SM, Hernandez-Diaz S, Lind J, Cragan JD, Briggs G, Kweder S, Friedman JM, Mitchell AA, Honein MA et al. 2013. Medications in the first trimester of pregnancy: Most common exposures and critical gaps in understanding fetal risk. *Pharmacoepidemiol Drug Saf.* 22(9):1013-1018.
- Umezawa M, Onoda A, Korshunova I, Jensen ACO, Koponen IK, Jensen KA, Khodosevich K, Vogel U, Hougaard KS. 2018. Maternal inhalation of carbon black nanoparticles induces neurodevelopmental changes in mouse offspring. *Part Fibre Toxicol.* 15(1):36.
- Vidanapathirana AK, Thompson LC, Mann EE, Odom JT, Holland NA, Sumner SJ, Han L, Lewin AH, Fennell TR, Brown JM et al. 2014. Pvp formulated fullerene (c60) increases rho-kinase dependent vascular tissue contractility in pregnant sprague dawley rats. *Reproductive toxicology (Elmsford, NY).* 49:86-100.
- Wick P, Malek A, Manser P, Meili D, Maeder-Althaus X, Diener L, Diener PA, Zisch A, Krug HF, von Mandach U. 2010. Barrier capacity of human placenta for nanosized materials. *Environ Health Perspect.* 118(3):432-436.
- Yamashita K, Yoshioka Y, Higashisaka K, Mimura K, Morishita Y, Nozaki M, Yoshida T, Ogura T, Nabeshi H, Nagano K et al. 2011. Silica and titanium dioxide nanoparticles cause pregnancy complications in mice. *Nat Nanotechnol.* 6(5):321-328.
- Zhang XF, Park JH, Choi YJ, Kang MH, Gurunathan S, Kim JH. 2015. Silver nanoparticles cause complications in pregnant mice. *Int J Nanomedicine.* 10:7057-7071.

## References

- Abrams RM. 2015. Sleep deprivation. *Obstetrics and gynecology clinics of North America*. 42(3):493-506.
- Abu Zeid EH, Alam RTM, Abd El-Hameed NE. 2017. Impact of titanium dioxide on androgen receptors, seminal vesicles and thyroid hormones of male rats: Possible protective trial with aged garlic extract. *Andrologia*. 49(5):e12651.
- Abukabda AB, Bowdridge EC, McBride CR, Batchelor TP, Goldsmith WT, Garner KL, Friend S, Nurkiewicz TR. 2019. Maternal titanium dioxide nanomaterial inhalation exposure compromises placental hemodynamics. *Toxicology and applied pharmacology*. 367:51-61.
- Abukabda AB, Stapleton PA, McBride CR, Yi J, Nurkiewicz TR. 2017. Heterogeneous vascular bed responses to pulmonary titanium dioxide nanoparticle exposure. *Front Cardiovasc Med*. 4:33.
- Abusalah A, Gavana M, Haidich AB, Smyrnakis E, Papadakis N, Papanikolaou A, Benos A. 2012. Low birth weight and prenatal exposure to indoor pollution from tobacco smoke and wood fuel smoke: A matched case-control study in gaza strip. *Matern Child Health J*. 16(8):1718-1727.
- Adachi K, Yamada N, Yamamoto K, Yoshida Y, Yamamoto O. 2010. In vivo effect of industrial titanium dioxide nanoparticles experimentally exposed to hairless rat skin. *Nanotoxicology*. 4(3):296-306.
- Adachi K, Yamada N, Yoshida Y, Yamamoto O. 2013. Subchronic exposure of titanium dioxide nanoparticles to hairless rat skin. *Exp Dermatol*. 22(4):278-283.
- Adeva-Andany MM, González-Lucán M, Donapetry-García C, Fernández-Fernández C, Ameneiros-Rodríguez E. 2016. Glycogen metabolism in humans. *BBA Clin*. 5:85-100.
- Aengenheister L, Dietrich D, Sadeghpour A, Manser P, Diener L, Wichser A, Karst U, Wick P, Buerki-Thurnherr T. 2018a. Gold nanoparticle distribution in advanced in vitro and ex vivo human placental barrier models. *J Nanobiotechnology*. 16(1):79.
- Aengenheister L, Dugershaw BB, Manser P, Wichser A, Schoenenberger R, Wick P, Hesler M, Kohl Y, Straskraba S, Suter MJ et al. 2019. Investigating the accumulation and translocation of titanium dioxide nanoparticles with different surface modifications in static and dynamic human placental transfer models. *Eur J Pharm Biopharm*. 142:488-497.
- Aengenheister L, Keevend K, Muoth C, Schoenenberger R, Diener L, Wick P, Buerki-Thurnherr T. 2018b. An advanced human in vitro co-culture model for translocation studies across the placental barrier. *Sci Rep*. 8(1):5388.
- Aguilar M, Bhuket T, Torres S, Liu B, Wong RJ. 2015. Prevalence of the metabolic syndrome in the united states, 2003-2012. *Jama*. 313(19):1973-1974.

- Aiko Y, Askew DJ, Aramaki S, Myoga M, Tomonaga C, Hachisuga T, Suga R, Kawamoto T, Tsuji M, Shibata E. 2014. Differential levels of amino acid transporters system I and asct2, and the mtor protein in placenta of preeclampsia and iugr. *BMC Pregnancy and Childbirth*. 14(1):181.
- Akison LK, Nitert MD, Clifton VL, Moritz KM, Simmons DG. 2017. Review: Alterations in placental glycogen deposition in complicated pregnancies: Current preclinical and clinical evidence. *Placenta*. 54:52-58.
- Al Shoyaib A, Archie SR, Karamyan VT. 2019. Intraperitoneal route of drug administration: Should it be used in experimental animal studies? *Pharm Res*. 37(1):12-12.
- Al-Maghrebi M, Renno WM. 2016. Altered expression profile of glycolytic enzymes during testicular ischemia reperfusion injury is associated with the p53/tigar pathway: Effect of fructose 1,6-diphosphate. *PeerJ*. 4:e2195.
- Alberry M, Soothill P. 2007. Management of fetal growth restriction. *Arch Dis Child Fetal Neonatal Ed*. 92(1):F62-F67.
- Albu AR, Anca AF, Horhoianu VV, Horhoianu IA. 2014. Predictive factors for intrauterine growth restriction. *Journal of Medicine and Life*. 7(2):165-171.
- Alexander DP, Andrews RD, Huggett AS, Nixon DA, Widdas WF. 1955a. The placental transfer of sugars in the sheep: Studies with radioactive sugar. *J Physiol*. 129(2):352-366.
- Alexander DP, Huggett AS, Nixon DA, Widdas WF. 1955b. The placental transfer of sugars in the sheep: The influence of concentration gradient upon the rates of hexose formation as shown in umbilical perfusion of the placenta. *J Physiol*. 129(2):367-383.
- Almeida-Val VMF, Oliveira AR, de Nazaré Paula da Silva M, Ferreira-Nozawa MS, Araújo RM, Val AL, Nozawa SR. 2011. Anoxia- and hypoxia-induced expression of Ldh-a\* in the Amazon oscar, *Astronotus crassipinis*. *Genet Mol Biol*. 34(2):315-322.
- Alur P. 2019a. Sex differences in nutrition, growth, and metabolism in preterm infants. *Front Pediatr*. 7:22.
- Alur P. 2019b. Sex differences in nutrition, growth, and metabolism in preterm infants. *Frontiers in Pediatrics*. 7(22).
- Angiolini E, Coan PM, Sandovici I, Iwajomo OH, Peck G, Burton GJ, Sibley CP, Reik W, Fowden AL, Constância M. 2011. Developmental adaptations to increased fetal nutrient demand in mouse genetic models of igf2-mediated overgrowth. *Faseb J*. 25(5):1737-1745.
- Antoniotto GS, Coughlan M, Salamonsen LA, Evans J. 2018. Obesity associated advanced glycation end products within the human uterine cavity adversely impact endometrial function and embryo implantation competence. *Human reproduction (Oxford, England)*. 33(4):654-665.
- Aragon MJ, Topper L, Tyler CR, Sanchez B, Zychowski K, Young T, Herbert G, Hall P, Erdely A, Eye T et al. 2017. Serum-borne bioactivity caused by pulmonary multiwalled carbon nanotubes induces neuroinflammation via blood-brain barrier impairment. *Proceedings of the National Academy of Sciences*. 114(10):E1968-E1976.
- Arce RM, Caron KM, Barros SP, Offenbacher S. 2012. Toll-like receptor 4 mediates intrauterine growth restriction after systemic *Campylobacter rectus* infection in mice. *Mol Oral Microbiol*. 27(5):373-381.
- Armengaud JB, Zydorczyk C, Siddeek B, Peyter AC, Simeoni U. 2021. Intrauterine growth restriction: Clinical consequences on health and disease at adulthood. *Reproductive Toxicology*. 99:168-176.
- Austin CA, Hinkley GK, Mishra AR, Zhang Q, Umbreit TH, Betz MW, B EW, Casey BJ, Francke-Carroll S, Hussain SM et al. 2016. Distribution and accumulation of 10 nm silver nanoparticles in

- maternal tissues and visceral yolk sac of pregnant mice, and a potential effect on embryo growth. *Nanotoxicology*. 10(6):654-661.
- Austin CA, Umbreit TH, Brown KM, Barber DS, Dair BJ, Francke-Carroll S, Feswick A, Saint-Louis MA, Hikawa H, Siebein KN et al. 2012. Distribution of silver nanoparticles in pregnant mice and developing embryos. *Nanotoxicology*. 6:912-922.
- Avni R, Raz T, Biton IE, Kalchenko V, Garbow JR, Neeman M. 2012. Unique in utero identification of fetuses in multifetal mouse pregnancies by placental bidirectional arterial spin labeling mri. *Magn Reson Med*. 68(2):560-570.
- Aztatzi-Aguilar OG, Uribe-Ramírez M, Narvárez-Morales J, De Vizcaya-Ruiz A, Barbier O. 2016. Early kidney damage induced by subchronic exposure to pm2.5 in rats. *Particle and fibre toxicology*. 13(1):68.
- Bachler G, Losert S, Umehara Y, von Goetz N, Rodriguez-Lorenzo L, Petri-Fink A, Rothen-Rutishauser B, Hungerbuehler K. 2015. Translocation of gold nanoparticles across the lung epithelial tissue barrier: Combining in vitro and in silico methods to substitute in vivo experiments. *Particle and fibre toxicology*. 12:18-18.
- Backes CH, Nelin T, Gorr MW, Wold LE. 2013. Early life exposure to air pollution: How bad is it? *Toxicology letters*. 216(1):47-53.
- Bailey BA, Donnelly M, Bol K, Moore LG, Julian CG. 2019. High altitude continues to reduce birth weights in colorado. *Matern Child Health J*. 23(11):1573-1580.
- Baisch BL, Corson NM, Wade-Mercer P, Gelein R, Kennell AJ, Oberdörster G, Elder A. 2014. Equivalent titanium dioxide nanoparticle deposition by intratracheal instillation and whole body inhalation: The effect of dose rate on acute respiratory tract inflammation. *Particle and fibre toxicology*. 11(1):5.
- Balayla J, Desilets J, Shrem G. 2019. Placenta previa and the risk of intrauterine growth restriction (iugr): A systematic review and meta-analysis. *Journal of perinatal medicine*. 47(6):577-584.
- Bamfo JEAK, Odibo AO. 2011. Diagnosis and management of fetal growth restriction. *Journal of pregnancy*. 2011:640715-640715.
- Bara A, Manduca A, Bernabeu A, Borsoi M, Serviado M, Lassalle O, Murphy M, Wager-Miller J, Mackie K, Pelissier-Alicot A-L et al. 2018. Sex-dependent effects of in utero cannabinoid exposure on cortical function. *eLife*. 7:e36234.
- Barash V, Shafir E. 1990. Mobilization of placental glycogen in diabetic rats. *Placenta*. 11(6):515-521.
- Barker DJ. 1990. The fetal and infant origins of adult disease. *BMJ*. 301(6761):1111.
- Barker DJ. 1999. Fetal origins of cardiovascular disease. *Ann Med*. 31 Suppl 1:3-6.
- Barker DJ, Eriksson JG, Forsen T, Osmond C. 2002. Fetal origins of adult disease: Strength of effects and biological basis. *Int J Epidemiol*. 31(6):1235-1239.
- BARKER DJP. 2006. Adult consequences of fetal growth restriction. *Clinical obstetrics and gynecology*. 49(2):270-283.
- Barua S, Mitragotri S. 2014. Challenges associated with penetration of nanoparticles across cell and tissue barriers: A review of current status and future prospects. *Nano Today*. 9(2):223-243.
- Baumann MU, Deborde S, Illsley NP. 2002. Placental glucose transfer and fetal growth. *Endocrine*. 19(1):13-22.
- Baumann MU, Schneider H, Malek A, Palta V, Surbek DV, Sager R, Zamudio S, Illsley NP. 2014. Regulation of human trophoblast glut1 glucose transporter by insulin-like growth factor i (igf-i). *PLoS one*. 9(8):e106037-e106037.

- Baykal C, Sargon MF, Esinler I, Onderoğlu S, Onderoğlu L. 2004. Placental microcirculation of intrauterine growth retarded fetuses: Scanning electron microscopy of placental vascular casts. *Arch Gynecol Obstet.* 270(2):99-103.
- Bekkar B, Pacheco S, Basu R, DeNicola N. 2020. Association of air pollution and heat exposure with preterm birth, low birth weight, and stillbirth in the us: A systematic review. *JAMA Network Open.* 3(6):e208243-e208243.
- Belfiore F, Iannello S, Rabuazzo AM, Campione R. 1989. Increased hexokinase/glucose-6-phosphatase ratio in the diabetic kidney as index of glucose overutilization. *Clin Physiol Biochem.* 7(5):223-228.
- Bell AW, Ehrhardt RA. 2002. Regulation of placental nutrient transport and implications for fetal growth. *Nutrition Research Reviews.* 15(2):211-230.
- Benowitz NL, Burbank AD. 2016. Cardiovascular toxicity of nicotine: Implications for electronic cigarette use. *Trends in cardiovascular medicine.* 26(6):515-523.
- Bergmann RL, Bergmann KE, Dudenhausen JW. 2008. Undernutrition and growth restriction in pregnancy. *Nestle Nutr Workshop Ser Pediatr Program.* 61:103-121.
- Biola-Clier M, Gaillard JC, Rabilloud T, Armengaud J, Carriere M. 2020. Titanium dioxide nanoparticles alter the cellular phosphoproteome in a549 cells. *Nanomaterials (Basel).* 10(2).
- Blackford JA, Jr., Jones W, Dey RD, Castranova V. 1997. Comparison of inducible nitric oxide synthase gene expression and lung inflammation following intratracheal instillation of silica, coal, carbonyl iron, or titanium dioxide in rats. *J Toxicol Environ Health.* 51(3):203-218.
- Blatt K, Moore E, Chen A, Van Hook J, DeFranco EA. 2015. Association of reported trimester-specific smoking cessation with fetal growth restriction. *Obstetrics and gynecology.* 125(6):1452-1459.
- Blaznik U, Krušič S, Hribar M, Kušar A, Žmitek K, Pravst I. 2021. Use of food additive titanium dioxide (e171) before the introduction of regulatory restrictions due to concern for genotoxicity. *Foods.* 10(8):1910.
- Bloxam DL, Bullen BE, Walters BN, Lao TT. 1987. Placental glycolysis and energy metabolism in preeclampsia. *American journal of obstetrics and gynecology.* 157(1):97-101.
- Blum JL, Chen L-C, Zelikoff JT. 2017. Exposure to ambient particulate matter during specific gestational periods produces adverse obstetric consequences in mice. *Environmental Health Perspectives.* 125(7):077020.
- Blum JL, Xiong JQ, Hoffman C, Zelikoff JT. 2012a. Cadmium associated with inhaled cadmium oxide nanoparticles impacts fetal and neonatal development and growth. *Toxicological sciences : an official journal of the Society of Toxicology.* 126(2):478-486.
- Blum JL, Xiong JQ, Hoffman C, Zelikoff JT. 2012b. Cadmium associated with inhaled cadmium oxide nanoparticles impacts fetal and neonatal development and growth. *Toxicol Sci.*
- Boguenet M, Bouet P-E, Spiers A, Reynier P, May-Panloup P. 2021. Mitochondria: Their role in spermatozoa and in male infertility. *Human reproduction update.* 27(4):697-719.
- Bonagura TW, Pepe GJ, Enders AC, Albrecht ED. 2008. Suppression of extravillous trophoblast vascular endothelial growth factor expression and uterine spiral artery invasion by estrogen during early baboon pregnancy. *Endocrinology.* 149(10):5078-5087.
- Bond H, Baker B, Boyd RD, Cowley E, Glazier JD, Jones CJ, Sibley CP, Ward BS, Husain SM. 2006. Artificial perfusion of the fetal circulation of the in situ mouse placenta: Methodology and validation. *Placenta.* 27 Suppl A:S69-75.

- Boney CM, Verma A, Tucker R, Vohr BR. 2005. Metabolic syndrome in childhood: Association with birth weight, maternal obesity, and gestational diabetes mellitus. *Pediatrics*. 115(3):e290-296.
- Bongaerts E, Nawrot TS, Van Pee T, Ameloot M, Bové H. 2020. Translocation of (ultra)fine particles and nanoparticles across the placenta; a systematic review on the evidence of in vitro, ex vivo, and in vivo studies. *Part Fibre Toxicol*. 17(1):56.
- Bose-O'Reilly S, McCarty KM, Steckling N, Lettmeier B. 2010. Mercury exposure and children's health. *Current problems in pediatric and adolescent health care*. 40(8):186-215.
- Bosquiazzo VL, Varayoud J, Muñoz-de-Toro M, Luque EH, Ramos JG. 2010. Effects of neonatal exposure to bisphenol a on steroid regulation of vascular endothelial growth factor expression and endothelial cell proliferation in the adult rat uterus. *Biology of reproduction*. 82(1):86-95.
- Bowdridge EC, Abukabda AB, Engles KJ, McBride CR, Batchelor TP, Goldsmith WT, Garner KL, Friend S, Nurkiewicz TR. 2019. Maternal engineered nanomaterial inhalation during gestation disrupts vascular kisspeptin reactivity. *Toxicological sciences : an official journal of the Society of Toxicology*. 169(2):524-533.
- Braakhuis HM, Gosens I, Krystek P, Boere JAF, Cassee FR, Fokkens PHB, Post JA, van Loveren H, Park MVDZ. 2014. Particle size dependent deposition and pulmonary inflammation after short-term inhalation of silver nanoparticles. *Particle and Fibre Toxicology*. 11(1):49.
- Broere-Brown ZA, Baan E, Schalekamp-Timmermans S, Verburg BO, Jaddoe VW, Steegers EA. 2016a. Sex-specific differences in fetal and infant growth patterns: A prospective population-based cohort study. *Biol Sex Differ*. 7:65.
- Broere-Brown ZA, Baan E, Schalekamp-Timmermans S, Verburg BO, Jaddoe VWV, Steegers EAP. 2016b. Sex-specific differences in fetal and infant growth patterns: A prospective population-based cohort study. *Biology of Sex Differences*. 7(1):65.
- Brook Robert D. 2008. Cardiovascular effects of air pollution. *Clinical Science*. 115(6):175.
- Brook RD, Rajagopalan S, Pope CA, 3rd, Brook JR, Bhatnagar A, Diez-Roux AV, Holguin F, Hong Y, Luepker RV, Mittleman MA et al. 2010. Particulate matter air pollution and cardiovascular disease: An update to the scientific statement from the american heart association. *Circulation*. 121(21):2331-2378.
- Brosens I, Robertson WB, Dixon HG. 1967. The physiological response of the vessels of the placental bed to normal pregnancy. *The Journal of pathology and bacteriology*. 93(2):569-579.
- Brosens JJ, Pijnenborg R, Brosens IA. 2002. The myometrial junctional zone spiral arteries in normal and abnormal pregnancies: A review of the literature. *American journal of obstetrics and gynecology*. 187(5):1416-1423.
- Brosnan JT. 1999. Comments on metabolic needs for glucose and the role of gluconeogenesis. *Eur J Clin Nutr*. 53 Suppl 1:S107-111.
- Brown JS, Zeman KL, Bennett WD. 2002. Ultrafine particle deposition and clearance in the healthy and obstructed lung. *American journal of respiratory and critical care medicine*. 166(9):1240-1247.
- Browne VA, Julian CG, Toledo-Jaldin L, Cioffi-Ragan D, Vargas E, Moore LG. 2015. Uterine artery blood flow, fetal hypoxia and fetal growth. *Philosophical transactions of the Royal Society of London Series B, Biological sciences*. 370(1663):20140068.
- Bruin JE, Gerstein HC, Holloway AC. 2010. Long-term consequences of fetal and neonatal nicotine exposure: A critical review. *Toxicological sciences : an official journal of the Society of Toxicology*. 116(2):364-374.

- Bulletti C, Jasonni VM, Lubicz S, Flamigni C, Gurpide E. 1986. Extracorporeal perfusion of the human uterus. *American journal of obstetrics and gynecology*. 154(3):683-688.
- Burbank F. 2012. Hemodynamic changes in the uterus and its blood vessels in pregnancy\*.
- Burch WM. 2002. Passage of inhaled particles into the blood circulation in humans. *Circulation*. 106(20):e141-142; author reply e141-142.
- Burton GJ, Fowden AL. 2015. The placenta: A multifaceted, transient organ. *Philosophical transactions of the Royal Society of London Series B, Biological sciences*. 370(1663):20140066-20140066.
- Butcher JT, Goodwill AG, Frisbee JC. 2012. The ex vivo isolated skeletal microvessel preparation for investigation of vascular reactivity. *J Vis Exp*. (62).
- Butcher JT, Stanley SC, Brooks SD, Chantler PD, Wu F, Frisbee JC. 2014. Impact of increased intramuscular perfusion heterogeneity on skeletal muscle microvascular hematocrit in the metabolic syndrome. *Microcirculation (New York, NY : 1994)*. 21(8):677-687.
- Butte NF. 2000. Carbohydrate and lipid metabolism in pregnancy: Normal compared with gestational diabetes mellitus. *The American Journal of Clinical Nutrition*. 71(5):1256s-1261s.
- Cabuzu D, Cirja A, Puiu R, Grumezescu AM. 2015. Biomedical applications of gold nanoparticles. *Curr Top Med Chem*. 15(16):1605-1613.
- Campagnolo L, Massimiani M, Palmieri G, Bernardini R, Sacchetti C, Bergamaschi A, Vecchione L, Magrini A, Bottini M, Pietroiusti A. 2013. Biodistribution and toxicity of pegylated single wall carbon nanotubes in pregnant mice. *Part Fibre Toxicol*. 10:21.
- Campagnolo L, Massimiani M, Vecchione L, Piccirilli D, Toschi N, Magrini A, Bonanno E, Scimeca M, Castagnozzi L, Buonanno G et al. 2017a. Silver nanoparticles inhaled during pregnancy reach and affect the placenta and the foetus. *Nanotoxicology*. 11(5):687-698.
- Campagnolo L, Massimiani M, Vecchione L, Piccirilli D, Toschi N, Magrini A, Bonanno E, Scimeca M, Castagnozzi L, Buonanno G et al. 2017b. Silver nanoparticles inhaled during pregnancy reach and affect the placenta and the foetus. *Nanotoxicology*. 11(5):687-698.
- Cantó C, Menzies KJ, Auwerx J. 2015. Nad(+) metabolism and the control of energy homeostasis: A balancing act between mitochondria and the nucleus. *Cell Metab*. 22(1):31-53.
- Cao X, Hua X, Wang X, Chen L. 2017. Exposure of pregnant mice to triclosan impairs placental development and nutrient transport. *Scientific Reports*. 7(1):44803.
- Cardinale DA, Larsen FJ, Schiffer TA, Morales-Alamo D, Ekblom B, Calbet JAL, Holmberg H-C, Boushel R. 2018. Superior intrinsic mitochondrial respiration in women than in men. *Frontiers in physiology*. 9:1133-1133.
- Carter AM. 1989. Factors affecting gas transfer across the placenta and the oxygen supply to the fetus. *J Dev Physiol*. 12(6):305-322.
- Carter AM. 2000. Placental oxygen consumption. Part i: In vivo studies--a review. *Placenta*. 21 Suppl A:S31-37.
- Carter JE, Weber G. 1966. Glucose-6-phosphatase-like activity in the human placenta, fetal liver, and decidual tissue. *American Journal of Obstetrics & Gynecology*. 95(7):914-924.
- Carter RC, Jacobson JL, Sokol RJ, Avison MJ, Jacobson SW. 2013. Fetal alcohol-related growth restriction from birth through young adulthood and moderating effects of maternal prepregnancy weight. *Alcohol Clin Exp Res*. 37(3):452-462.
- Cesta MF. 2006. Normal structure, function, and histology of the spleen. *Toxicol Pathol*. 34(5):455-465.
- Cetin I, Barberis B, Brusati V, Brighina E, Mandia L, Arighi A, Radaelli T, Biondetti P, Bresolin N, Pardi G et al. 2011. Lactate detection in the brain of growth-restricted fetuses with

- magnetic resonance spectroscopy. *American journal of obstetrics and gynecology*. 205(4):350.e351-357.
- Cetin I, Taricco E, Mandò C, Radaelli T, Boito S, Nuzzo AM, Giussani DA. 2020. Fetal oxygen and glucose consumption in human pregnancy complicated by fetal growth restriction. *Hypertension*. 75(3):748-754.
- Challis DE, Pfarrer CD, Ritchie JW, Koren G, Adamson SL. 2000. Glucose metabolism is elevated and vascular resistance and maternofetal transfer is normal in perfused placental cotyledons from severely growth-restricted fetuses. *Pediatric research*. 47(3):309-315.
- Challis J, Newnham J, Petraglia F, Yeganegi M, Bocking A. 2013. Fetal sex and preterm birth. *Placenta*. 34(2):95-99.
- Chang Y-L, Chao A-S, Chang S-D, Cheng P-J. 2021. Placental glucose transporter 1 and 3 gene expression in monochorionic twin pregnancies with selective fetal growth restriction. *BMC Pregnancy and Childbirth*. 21(1):260.
- Chassen SS, Ferchaud-Roucher V, Palmer C, Li C, Jansson T, Nathanielsz PW, Powell TL. 2020. Placental fatty acid transport across late gestation in a baboon model of intrauterine growth restriction. *J Physiol*. 598(12):2469-2489.
- Chavatte-Palmer P, Tarrade A. 2016. Placentation in different mammalian species. *Ann Endocrinol (Paris)*. 77(2):67-74.
- Che L, Xu M, Yang Z, Xu S, Che L, Lin Y, Fang Z, Feng B, Li J, Chen D et al. 2016. Detection of placental proteomes at different uterine positions in large white and meishan gilts on gestational day 90. *PLOS ONE*. 11(12):e0167799.
- Cheeseman C, Long W. 2015. Structure of, and functional insight into the glut family of membrane transporters. *Cell Health and Cytoskeleton*. 7:167.
- Cheheltani R, Ezzibdeh RM, Chhour P, Pulaparathi K, Kim J, Jurcova M, Hsu JC, Blundell C, Litt HI, Ferrari VA et al. 2016. Tunable, biodegradable gold nanoparticles as contrast agents for computed tomography and photoacoustic imaging. *Biomaterials*. 102:87-97.
- Chen B, Hong W, Yang P, Tang Y, Zhao Y, Aguilar ZP, Xu H. 2020a. Nano zinc oxide induced fetal mice growth restriction, based on oxide stress and endoplasmic reticulum stress. *Nanomaterials (Basel)*. 10(2):259.
- Chen B, Huang S, He J, He Q, Chen S, Liu X, Peng S, Luo D, Duan Y. 2020b. Sex-specific influence of prenatal air pollutant exposure on neonatal neurobehavioral development and the sensitive window. *Chemosphere*. 254:126824.
- Christen V, Capelle M, Fent K. 2013. Silver nanoparticles induce endoplasmic reticulum stress response in zebrafish. *Toxicology and applied pharmacology*. 272(2):519-528.
- Chu SY, Callaghan WM, Kim SY, Schmid CH, Lau J, England LJ, Dietz PM. 2007. Maternal obesity and risk of gestational diabetes mellitus. *Diabetes care*. 30(8):2070-2076.
- Coan PM, Ferguson-Smith AC, Burton GJ. 2004. Developmental dynamics of the definitive mouse placenta assessed by stereology<sup>1</sup>. *Biology of reproduction*. 70(6):1806-1813.
- Cohen AJ, Brauer M, Burnett R, Anderson HR, Frostad J, Estep K, Balakrishnan K, Brunekreef B, Dandona L, Dandona R et al. 2017. Estimates and 25-year trends of the global burden of disease attributable to ambient air pollution: An analysis of data from the global burden of diseases study 2015. *Lancet*. 389(10082):1907-1918.
- Cole C, Shyr T, Ou-Yang H. 2016. Metal oxide sunscreens protect skin by absorption, not by reflection or scattering. *Photodermatology, photoimmunology & photomedicine*. 32(1):5-10.
- Colella M, Frérot A, Novais ARB, Baud O. 2018. Neonatal and long-term consequences of fetal growth restriction. *Curr Pediatr Rev*. 14(4):212-218.

- Costa MA. 2016. The endocrine function of human placenta: An overview. *Reproductive biomedicine online*. 32(1):14-43.
- Cotechini T, Komisarenko M, Sperou A, Macdonald-Goodfellow S, Adams MA, Graham CH. 2014. Inflammation in rat pregnancy inhibits spiral artery remodeling leading to fetal growth restriction and features of preeclampsia. *The Journal of Experimental Medicine*. 211(1):165-179.
- Crosera M, Prodi A, Mauro M, Pelin M, Florio C, Bellomo F, Adami G, Apostoli P, De Palma G, Bovenzi M et al. 2015. Titanium dioxide nanoparticle penetration into the skin and effects on hacat cells. *International journal of environmental research and public health*. 12(8):9282-9297.
- Cueni LN, Detmar M. 2008. The lymphatic system in health and disease. *Lymphat Res Biol*. 6(3-4):109-122.
- Cui Z-H, Wu F, Jiang H. 2016. First-principles study of relative stability of rutile and anatase  $\text{TiO}_2$  using the random phase approximation. *Physical Chemistry Chemical Physics*. 18(43):29914-29922.
- Curhan GC, Willett WC, Rimm EB, Spiegelman D, Ascherio AL, Stampfer MJ. 1996. Birth weight and adult hypertension, diabetes mellitus, and obesity in us men. *Circulation*. 94(12):3246-3250.
- D'Errico JN, Fournier SB, Stapleton PA. 2019. Ex vivo perfusion of the rodent placenta. *J Vis Exp*. (147).
- D'Errico JN, Fournier SB, Stapleton PA. 2021. Considering intrauterine location in a model of fetal growth restriction after maternal titanium dioxide nanoparticle inhalation. *Frontiers in Toxicology*. 3(11).
- D'Errico JN, Stapleton PA. 2018. Developmental onset of cardiovascular disease - could the proof be in the placenta? *Microcirculation*. e12526.
- D'Errico JN, Doherty C, Fournier SB, Renkel N, Kallontzi S, Goedken M, Fabris L, Buckley B, Stapleton PA. 2019a. Identification and quantification of gold engineered nanomaterials and impaired fluid transfer across the rat placenta via ex vivo perfusion. *Biomedicine & Pharmacotherapy*. 117:109148.
- D'Errico JN, Fournier SB, Stapleton PA. 2019b. Ex vivo perfusion of the rodent placenta. *J Vis Exp*. (147):e59412.
- D'Errico JN, Fournier SB, Stapleton PA. Forthcoming 2019c. Ex vivo perfusion of the rodent placenta. *Journal of Video Experiments*.
- Dahlerup BR, Egsmose EL, Siersma V, Mortensen EL, Hedegaard M, Knudsen LE, Mathiesen L. 2018. Maternal stress and placental function, a study using questionnaires and biomarkers at birth. *PLoS one*. 13(11):e0207184-e0207184.
- Damsky CH, Fisher SJ. 1998. Trophoblast pseudo-vasculogenesis: Faking it with endothelial adhesion receptors. *Current opinion in cell biology*. 10(5):660-666.
- Dancis J, Money WL. 1960. Transfer of sodium and iodo-antipyrine across guinea pig placenta with an in situ perfusion technique. *Am J Obstet Gynecol*. 80:215-220.
- Daneman R, Prat A. 2015. The blood-brain barrier. *Cold Spring Harbor perspectives in biology*. 7(1):a020412-a020412.
- Davis MJ, Kuo L, Chilian WM, Muller JM. 1995. Isolated, perfused microvessels. In: Barker JH, Anderson GL, Menger MD, editors. *Clinically applied microcirculation research*. 1 ed. Boca Raton: CRC Press. p. 435-456.
- DeFranco E, Hall E, Hossain M, Chen A, Haynes EN, Jones D, Ren S, Lu L, Muglia L. 2015. Air pollution and stillbirth risk: Exposure to airborne particulate matter during pregnancy is associated with fetal death. *PLoS One*. 10(3):e0120594.

- Delgado Alvarado E, Peña-Juárez M, Perez-Perez C, Pérez E, Gonzalez-Calderon JA. 2019. Improvement in the dispersion of tio<sub>2</sub> particles inside chitosan-methyl cellulose films by the use of silane coupling agent. *Journal of the Mexican Chemical Society*. 63.
- Demir R, Yaba A, Huppertz B. 2010. Vasculogenesis and angiogenesis in the endometrium during menstrual cycle and implantation. *Acta histochemica*. 112(3):203-214.
- Desai V, Kowshik M. 2009. Antimicrobial activity of titanium dioxide nanoparticles synthesized by sol-gel technique. *Research Journal of Microbiology*. 4:97-103.
- Deysenroth MA, Rosa MJ, Eliot MN, Kelsey KT, Kloog I, Schwartz JD, Wellenius GA, Peng S, Hao K, Marsit CJ et al. 2021. Placental gene networks at the interface between maternal pm<sub>2.5</sub> exposure early in gestation and reduced infant birthweight. *Environmental Research*. 199:111342.
- Di Cianni G, Miccoli R, Volpe L, Lencioni C, Del Prato S. 2003. Intermediate metabolism in normal pregnancy and in gestational diabetes. *Diabetes Metab Res Rev*. 19(4):259-270.
- Di Renzo GC, Rosati A, Sarti RD, Cruciani L, Cutuli AM. 2007. Does fetal sex affect pregnancy outcome? *Gend Med*. 4(1):19-30.
- Díaz P, Powell TL, Jansson T. 2014. The role of placental nutrient sensing in maternal-fetal resource allocation. *Biology of reproduction*. 91(4):82-82.
- Dréno B, Alexis A, Chuberre B, Marinovich M. 2019. Safety of titanium dioxide nanoparticles in cosmetics. *J Eur Acad Dermatol Venereol*. 33 Suppl 7:34-46.
- Ducray AD, Felser A, Zielinski J, Bittner A, Bürgi JV, Nuoffer J-M, Frenz M, Mevissen M. 2017. Effects of silica nanoparticle exposure on mitochondrial function during neuronal differentiation. *Journal of Nanobiotechnology*. 15(1):49.
- Dunlop W. 1981. Serial changes in renal haemodynamics during normal human pregnancy. *British journal of obstetrics and gynaecology*. 88(1):1-9.
- Dzhambov AM, Dimitrova DD, Dimitrakova ED. 2014. Noise exposure during pregnancy, birth outcomes and fetal development: Meta-analyses using quality effects model. *Folia medica*. 56(3):204-214.
- El-Sayed YS, Shimizu R, Onoda A, Takeda K, Umezawa M. 2015. Carbon black nanoparticle exposure during middle and late fetal development induces immune activation in male offspring mice. *Toxicology*. 327:53-61.
- Elahi N, Kamali M, Baghersad MH. 2018. Recent biomedical applications of gold nanoparticles: A review. *Talanta*. 184:537-556.
- Elder A, Gelein R, Silva V, Feikert T, Opanashuk L, Carter J, Potter R, Maynard A, Ito Y, Finkelstein J et al. 2006. Translocation of inhaled ultrafine manganese oxide particles to the central nervous system. *Environ Health Perspect*. 114(8):1172-1178.
- Engler-Chiurazzi EB, Stapleton PA, Stalnaker JJ, Ren X, Hu H, Nurkiewicz TR, McBride CR, Yi J, Engels K, Simpkins JW. 2016. Impacts of prenatal nanomaterial exposure on male adult sprague-dawley rat behavior and cognition. *Journal of toxicology and environmental health Part A*. 79(11):447-452.
- Ericsson A, Hamark B, Powell TL, Jansson T. 2005. Glucose transporter isoform 4 is expressed in the syncytiotrophoblast of first trimester human placenta. *Human reproduction (Oxford, England)*. 20(2):521-530.
- Eriksson JG, Kajantie E, Osmond C, Thornburg K, Barker DJ. 2010. Boys live dangerously in the womb. *Am J Hum Biol*. 22(3):330-335.
- Eskenazi B, Fenster L, Sidney S. 1991. A multivariate analysis of risk factors for preeclampsia. *Jama*. 266(2):237-241.

- Espinoza J, Romero R, Mee Kim Y, Kusanovic JP, Hassan S, Erez O, Gotsch F, Than NG, Papp Z, Jai Kim C. 2006. Normal and abnormal transformation of the spiral arteries during pregnancy. *Journal of perinatal medicine*. 34(6):447-458.
- Even MD, Laughlin MH, Krause GF, vom Saal FS. 1994. Differences in blood flow to uterine segments and placentae in relation to sex, intrauterine location and side in pregnant rats. *Reproduction*. 102(1):245-252.
- Fazlollahi F, Kim YH, Sipos A, Hamm-Alvarez SF, Borok Z, Kim K-J, Crandall ED. 2013. Nanoparticle translocation across mouse alveolar epithelial cell monolayers: Species-specific mechanisms. *Nanomedicine: Nanotechnology, Biology and Medicine*. 9(6):786-794.
- Ferreira LF. 2018. Mitochondrial basis for sex-differences in metabolism and exercise performance. *American journal of physiology Regulatory, integrative and comparative physiology*. 314(6):R848-R849.
- Fisher SJ. 2015. Why is placentation abnormal in preeclampsia? *American journal of obstetrics and gynecology*. 213(4 Suppl):S115-122.
- Flores-Riveros JR, McLenithan JC, Ezaki O, Lane MD. 1993. Insulin down-regulates expression of the insulin-responsive glucose transporter (glut4) gene: Effects on transcription and mrna turnover. *Proceedings of the National Academy of Sciences of the United States of America*. 90(2):512-516.
- Foreman-Ortiz IU, Liang D, Laudadio ED, Calderin JD, Wu M, Keshri P, Zhang X, Schwartz MP, Hamers RJ, Rotello VM et al. 2020. Anionic nanoparticle-induced perturbation to phospholipid membranes affects ion channel function. *Proceedings of the National Academy of Sciences*. 117(45):27854-27861.
- Forstermann U, Sessa WC. 2012. Nitric oxide synthases: Regulation and function. *European heart journal*. 33(7):829-837, 837a-837d.
- Fournier SB, D'Errico JN, Adler DS, Kollontzi S, Goedken MJ, Fabris L, Yurkow EJ, Stapleton PA. 2020. Nanopolystyrene translocation and fetal deposition after acute lung exposure during late-stage pregnancy. *Part Fibre Toxicol*. 17(1):55.
- Fournier SB, D'Errico JN, Stapleton PA. 2018. Engineered nanomaterial applications in perinatal therapeutics. *Pharmacol Res*. 130:36-43.
- Fournier SB, Kallontzi S, Fabris L, Love C, Stapleton PA. 2019a. Effect of gestational age on maternofetal vascular function following single maternal engineered nanoparticle exposure. *Cardiovascular toxicology*.
- Fournier SB, Kallontzi S, Fabris L, Love C, Stapleton PA. 2019b. Effect of gestational age on maternofetal vascular function following single maternal engineered nanoparticle exposure. *Cardiovascular toxicology*.
- Fournier SB, Lam V, Goedken MJ, Fabris L, Stapleton PA. 2021. Development of coronary dysfunction in adult progeny after maternal engineered nanomaterial inhalation during gestation. *Sci Rep*. 11(1):19374.
- Fowden AL. 2003. The insulin-like growth factors and feto-placental growth. *Placenta*. 24(8-9):803-812.
- Friedman JE. 2015. Obesity and gestational diabetes mellitus pathways for programming in mouse, monkey, and man—where do we go next? The 2014 norbert freinkel award lecture. *Diabetes care*. 38(8):1402-1411.
- Frisbee JC, Goodwill AG, Frisbee SJ, Butcher JT, Wu F, Chantler PD. 2016. Microvascular perfusion heterogeneity contributes to peripheral vascular disease in metabolic syndrome. *J Physiol*. 594(8):2233-2243.
- Fröhlich E. 2002. [structure and function of blood-tissue barriers]. *Dtsch Med Wochenschr*. 127(49):2629-2634.

- Fu Q. 2018. Hemodynamic and electrocardiographic aspects of uncomplicated singleton pregnancy. *Advances in experimental medicine and biology*. 1065:413-431.
- Fukuda M, Fukuda K, Andersen CY, Byskov AG. 2000. Right-sided ovulation favours pregnancy more than left-sided ovulation. *Human Reproduction*. 15(9):1921-1926.
- Furukawa S, Hayashi S, Usuda K, Abe M, Hagio S, Ogawa I. 2011. Toxicological pathology in the rat placenta. *Journal of toxicologic pathology*. 24(2):95-111.
- Furukawa S, Kuroda Y, Sugiyama A. 2014. A comparison of the histological structure of the placenta in experimental animals. *Journal of toxicologic pathology*. 27(1):11-18.
- Furukawa S, Tsuji N, Sugiyama A. 2019. Morphology and physiology of rat placenta for toxicological evaluation. *Journal of toxicologic pathology*. 32(1):1-17.
- Furuya M, Ishida J, Aoki I, Fukamizu A. 2008. Pathophysiology of placentation abnormalities in pregnancy-induced hypertension. *Vascular Health and Risk Management*. 4(6):1301-1313.
- Gabbe SG, Demers LM, Greep RO, Villee CA. 1972. The effects of hypoxia on placental glycogen metabolism. *American journal of obstetrics and gynecology*. 114(4):540-545.
- Gabory A, Ferry L, Fajardy I, Jouneau L, Gothié JD, Vigé A, Fleur C, Mayeur S, Gallou-Kabani C, Gross MS et al. 2012. Maternal diets trigger sex-specific divergent trajectories of gene expression and epigenetic systems in mouse placenta. *PLoS One*. 7(11):e47986.
- Gaccioli F, Lager S. 2016. Placental nutrient transport and intrauterine growth restriction. *Frontiers in Physiology*. 7(40).
- Gao L, Lv C, Xu C, Li Y, Cui X, Gu H, Ni X. 2012. Differential regulation of glucose transporters mediated by crh receptor type 1 and type 2 in human placental trophoblasts. *Endocrinology*. 153(3):1464-1471.
- Gao Y, Gopee NV, Howard PC, Yu LR. 2011. Proteomic analysis of early response lymph node proteins in mice treated with titanium dioxide nanoparticles. *J Proteomics*. 74(12):2745-2759.
- Garris DR, Blankenship LT, Whitehead DS. 1983. Regional variations in uterine blood flow in the guinea pig: Relationship to pregnancy site distribution. *Gynecologic and obstetric investigation*. 15(1):33-40.
- Garrison L, Leeman L, Savich RD, Gutierrez H, Rayburn WF, Bakhireva LN. 2016. Fetal growth outcomes in a cohort of polydrug- and opioid-dependent patients. *J Reprod Med*. 61(7-8):311-319.
- Gaté L, Disdier C, Cosnier F, Gagnaire F, Devoy J, Saba W, Brun E, Chalansonnet M, Mabondzo A. 2017. Biopersistence and translocation to extrapulmonary organs of titanium dioxide nanoparticles after subacute inhalation exposure to aerosol in adult and elderly rats. *Toxicology letters*. 265:61-69.
- Gatoo MA, Naseem S, Arfat MY, Mahmood Dar A, Qasim K, Zubair S. 2014. Physicochemical properties of nanomaterials: Implication in associated toxic manifestations. *BioMed Research International*. 2014:498420.
- Geiser M, Casaulta M, Kupferschmid B, Schulz H, Semmler-Behnke M, Kreyling W. 2008a. The role of macrophages in the clearance of inhaled ultrafine titanium dioxide particles. *Am J Respir Cell Mol Biol*. 38(3):371-376.
- Geiser M, Casaulta M, Kupferschmid B, Schulz H, Semmler-Behnke M, Kreyling W. 2008b. The role of macrophages in the clearance of inhaled ultrafine titanium dioxide particles. *Am J Respir Cell Mol Biol*. 38(3):371-376.
- Geiser M, Rothen-Rutishauser B, Kapp N, Schurch S, Kreyling W, Schulz H, Semmler M, Im Hof V, Heyder J, Gehr P. 2005. Ultrafine particles cross cellular membranes by nonphagocytic mechanisms in lungs and in cultured cells. *Environ Health Perspect*. 113(11):1555-1560.

- Geurtsen ML, van Soest EEL, Voerman E, Steegers EAP, Jaddoe VVW, Gaillard R. 2019. High maternal early-pregnancy blood glucose levels are associated with altered fetal growth and increased risk of adverse birth outcomes. *Diabetologia*. 62(10):1880-1890.
- Gewolb IH, Barrett C, Warshaw JB. 1983. Placental growth and glycogen metabolism in streptozotocin diabetic rats. *Pediatric research*. 17(7):587-591.
- Goeden N, Bonnin A. 2013. Ex vivo perfusion of mid-to-late-gestation mouse placenta for maternal-fetal interaction studies during pregnancy. *Nature protocols*. 8(1):66-74.
- Goeden N, Notarangelo FM, Pocivavsek A, Beggiato S, Bonnin A, Schwarcz R. 2017. Prenatal dynamics of kynurenine pathway metabolism in mice: Focus on kynurenic acid. *Developmental neuroscience*. 39(6):519-528.
- Goeden N, Velasquez J, Arnold KA, Chan Y, Lund BT, Anderson GM, Bonnin A. 2016. Maternal inflammation disrupts fetal neurodevelopment via increased placental output of serotonin to the fetal brain. *The Journal of Neuroscience*. 36(22):6041-6049.
- Goldstein BJ, Scalia R. 2004. Adiponectin: A novel adipokine linking adipocytes and vascular function. *The Journal of clinical endocrinology and metabolism*. 89(6):2563-2568.
- Gonser M, Tillack N, Pfeiffer KH, Mielke G. 1996. [placental location and incidence of pre-eclampsia]. *Ultraschall Med*. 17(5):236-238.
- Grafmueller S, Manser P, Diener L, Diener PA, Maeder-Althaus X, Maurizi L, Jochum W, Krug HF, Buerki-Thurnherr T, von Mandach U et al. 2015a. Bidirectional transfer study of polystyrene nanoparticles across the placental barrier in an ex vivo human placental perfusion model. *Environ Health Perspect*. 123(12):1280-1286.
- Grafmueller S, Manser P, Diener L, Maurizi L, Diener PA, Hofmann H, Jochum W, Krug HF, Buerki-Thurnherr T, von Mandach U et al. 2015b. Transfer studies of polystyrene nanoparticles in the ex vivo human placenta perfusion model: Key sources of artifacts. *Sci Technol Adv Mater*. 16(4):044602.
- Grassian VH, O'Shaughnessy PT, Adamcakova-Dodd A, Pettibone JM, Thorne PS. 2007. Inhalation exposure study of titanium dioxide nanoparticles with a primary particle size of 2 to 5 nm. *Environmental health perspectives*. 115(3):397-402.
- Gray LR, Tompkins SC, Taylor EB. 2014. Regulation of pyruvate metabolism and human disease. *Cell Mol Life Sci*. 71(14):2577-2604.
- Griffiths SK, Campbell JP. 2015. Placental structure, function and drug transfer. *Continuing Education in Anaesthesia Critical Care & Pain*. 15(2):84-89.
- Gu W, Jones CT, Harding JE. 1987. Metabolism of glucose by fetus and placenta of sheep. The effects of normal fluctuations in uterine blood flow. *J Dev Physiol*. 9(4):369-389.
- Habishi F. 2016. Ilmenite for pigment and metal production. *Interdisciplinary Journal of Chemistry*. 1:28-33.
- Hahn T, Barth S, Graf R, Engelmann M, Beslagic D, Reul JM, Holsboer F, Dohr G, Desoye G. 1999. Placental glucose transporter expression is regulated by glucocorticoids. *The Journal of clinical endocrinology and metabolism*. 84(4):1445-1452.
- Hales CN, Barker DJ, Clark PM, Cox LJ, Fall C, Osmond C, Winter PD. 1991. Fetal and infant growth and impaired glucose tolerance at age 64. *BMJ*. 303(6809):1019-1022.
- Hammond SA, Carew AC, Helbing CC. 2013. Evaluation of the effects of titanium dioxide nanoparticles on cultured rana catesbeiana tailfin tissue. *Front Genet*. 4:251-251.
- Harper LM, Odibo AO, Macones GA, Crane JP, Cahill AG. 2010. Effect of placenta previa on fetal growth. *American journal of obstetrics and gynecology*. 203(4):330.e331-330.e3305.
- Harris LK, Crocker IP, Baker PN, Aplin JD, Westwood M. 2011. Igf2 actions on trophoblast in human placenta are regulated by the insulin-like growth factor 2 receptor, which can function as both a signaling and clearance receptor1. *Biology of reproduction*. 84(3):440-446.

- Hathaway Q, Nichols C, Shepherd D, Stapleton P, McLaughlin S, Stricker J, Rellick S, Pinti M, Abukabda A, McBride C et al. 2016. Maternal-engineered nanomaterial exposure disrupts progeny cardiac function and bioenergetics. *American Journal of Physiology Heart and Circulatory Physiology*. 312(3):446-458.
- Hathaway QA, Nichols CE, Shepherd DL, Stapleton PA, McLaughlin SL, Stricker JC, Rellick SL, Pinti MV, Abukabda AB, McBride CR et al. 2017. Maternal-engineered nanomaterial exposure disrupts progeny cardiac function and bioenergetics. *American journal of physiology Heart and circulatory physiology*. 312(3):H446-h458.
- Hay WW. 1991a. Energy and substrate requirements of the placenta and fetus. *Proceedings of the Nutrition Society*. 50(2):321-336.
- Hay WW, Jr. 1991b. Energy and substrate requirements of the placenta and fetus. *Proc Nutr Soc*. 50(2):321-336.
- Hay WW, Jr. 1994. Placental transport of nutrients to the fetus. *Horm Res*. 42(4-5):215-222.
- Hay WW, Jr. 2006. Placental-fetal glucose exchange and fetal glucose metabolism. *Trans Am Clin Climatol Assoc*. 117:321-340.
- Hayward CE, Lean S, Sibley CP, Jones RL, Wareing M, Greenwood SL, Dilworth MR. 2016. Placental adaptation: What can we learn from birthweight:Placental weight ratio? *Frontiers in physiology*. 7:28-28.
- Hemauer SJ, Patrikeeva SL, Nanovskaya TN, Hankins GDV, Ahmed MS. 2010. Role of human placental apical membrane transporters in the efflux of glyburide, rosiglitazone, and metformin. *American journal of obstetrics and gynecology*. 202(4):383.e381-383.e3837.
- Herbert A, Ng H, Jessup W, Kockx M, Cartland S, Thomas SR, Hogg PJ, Wargon O. 2011. Hypoxia regulates the production and activity of glucose transporter-1 and indoleamine 2,3-dioxygenase in monocyte-derived endothelial-like cells: Possible relevance to infantile haemangioma pathogenesis. *Br J Dermatol*. 164(2):308-315.
- Ho D, Leong JW, Crew RC, Norret M, House MJ, Mark PJ, Waddell BJ, Iyer KS, Keelan JA. 2017. Maternal-placental-fetal biodistribution of multimodal polymeric nanoparticles in a pregnant rat model in mid and late gestation. *Scientific reports*. 7(1):2866-2866.
- Hoet PH, Brüske-Hohlfeld I, Salata OV. 2004. Nanoparticles - known and unknown health risks. *Journal of nanobiotechnology*. 2(1):12-12.
- Holman GD. 2020. Structure, function and regulation of mammalian glucose transporters of the slc2 family. *Pflügers Archiv - European Journal of Physiology*. 472(9):1155-1175.
- Hong F, Zhou Y, Zhao X, Sheng L, Wang L. 2017a. Maternal exposure to nanosized titanium dioxide suppresses embryonic development in mice. *International journal of nanomedicine*. 12:6197-6204.
- Hong F, Zhou Y, Zhao X, Sheng L, Wang L. 2017b. Maternal exposure to nanosized titanium dioxide suppresses embryonic development in mice. *International journal of nanomedicine*. 12:6197-6204.
- Hougaard K, Campagnolo L, Palmer P, Tarrade A, Ralliard D. 2015a. A perspective on the developmental toxicity of inhaled nanoparticles. *Reproductive Toxicology*. 56:118-140.
- Hougaard KS, Campagnolo L, Chavatte-Palmer P, Tarrade A, Rousseau-Ralliard D, Valentino S, Park MV, de Jong WH, Wolterink G, Piersma AH et al. 2015b. A perspective on the developmental toxicity of inhaled nanoparticles. *Reprod Toxicol*. 56:118-140.
- Hougaard KS, Jackson P, Jensen KA, Sloth JJ, Loschner K, Larsen EH, Birkedal RK, Vibenholt A, Boisen AM, Wallin H et al. 2010. Effects of prenatal exposure to surface-coated nanosized titanium dioxide (uv-titan). A study in mice. *Part Fibre Toxicol*. 7:16.

- Hougaard KS, Jackson P, Kyjovska ZO, Birkedal RK, De Temmerman PJ, Brunelli A, Verleysen E, Madsen AM, Saber AT, Pojana G et al. 2013. Effects of lung exposure to carbon nanotubes on female fertility and pregnancy. A study in mice. *Reprod Toxicol*. 41:86-97.
- Huang S, Chueh PJ, Lin YW, Shih TS, Chuang SM. 2009. Disturbed mitotic progression and genome segregation are involved in cell transformation mediated by nano-tio2 long-term exposure. *Toxicology and applied pharmacology*. 241(2):182-194.
- Huang X, Anderle P, Hostettler L, Baumann MU, Surbek DV, Ontsouka EC, Albrecht C. 2018. Identification of placental nutrient transporters associated with intrauterine growth restriction and pre-eclampsia. *BMC Genomics*. 19(1):173.
- Hunziker RD, Gambel P, Wegmann TG. 1984. Placenta as a selective barrier to cellular traffic. *Journal of immunology (Baltimore, Md : 1950)*. 133(2):667-671.
- Illsley NP, Aarnoudse JG, Penfold P, Bardsley SE, Coade SB, Stacey TE, Hytten FE. 1984. Mechanical and metabolic viability of a placental perfusion system in vitro under oxygenated and anoxic conditions. *Placenta*. 5(3):213-225.
- Illsley NP, Baumann MU. 2020. Human placental glucose transport in fetoplacental growth and metabolism. *Biochim Biophys Acta Mol Basis Dis*. 1866(2):165359-165359.
- Illsley NP, Caniggia I, Zamudio S. 2010a. Placental metabolic reprogramming: Do changes in the mix of energy-generating substrates modulate fetal growth? *Int J Dev Biol*. 54(2-3):409-419.
- Illsley NP, Caniggia I, Zamudio S. 2010b. Placental metabolic reprogramming: Do changes in the mix of energy-generating substrates modulate fetal growth? *Int J Dev Biol*. 54(2-3):409-419.
- Illsley NP, Fox H, Van der Veen F, Chawner L, Penfold P. 1985. Human placental ultrastructure after in vitro dual perfusion. *Placenta*. 6(1):23-32.
- Incalza MA, D'Oria R, Natalicchio A, Perrini S, Laviola L, Giorgino F. 2018. Oxidative stress and reactive oxygen species in endothelial dysfunction associated with cardiovascular and metabolic diseases. *Vascular pharmacology*. 100:1-19.
- Ingemarsson I. 2003. Gender aspects of preterm birth. *BJOG : an international journal of obstetrics and gynaecology*. 110 Suppl 20:34-38.
- Ishikawa H, Seki R, Yokonishi S, Yamauchi T, Yokoyama K. 2006. Relationship between fetal weight, placental growth and litter size in mice from mid- to late-gestation. *Reproductive Toxicology*. 21(3):267-270.
- James-Allan LB, Arbet J, Teal SB, Powell TL, Jansson T. 2019a. Insulin stimulates glut4 trafficking to the syncytiotrophoblast basal plasma membrane in the human placenta. *The Journal of Clinical Endocrinology & Metabolism*. 104(9):4225-4238.
- James-Allan LB, Arbet J, Teal SB, Powell TL, Jansson T. 2019b. Insulin stimulates glut4 trafficking to the syncytiotrophoblast basal plasma membrane in the human placenta. *The Journal of clinical endocrinology and metabolism*. 104(9):4225-4238.
- Jang YD, Ma YL, Lindemann MD. 2014. Intrauterine position affects fetal weight and crown-rump length throughout gestation. *J Anim Sci*. 92(10):4400-4406.
- Janot M, Cortes-Dubly M-L, Rodriguez S, Huynh-Do U. 2014. Bilateral uterine vessel ligation as a model of intrauterine growth restriction in mice. *Reproductive biology and endocrinology : RB&E*. 12:62-62.
- Janssen BG, Munters E, Pieters N, Smeets K, Cox B, Cuypers A, Fierens F, Penders J, Vangronsveld J, Gyselaers W et al. 2012. Placental mitochondrial DNA content and particulate air pollution during in utero life. *Environmental health perspectives*. 120(9):1346-1352.
- Jansson T, Aye IL, Goberdhan DC. 2012. The emerging role of mtorc1 signaling in placental nutrient-sensing. *Placenta*. 33 Suppl 2(Suppl 2):e23-29.

- Jansson T, Wennergren M, Illsley NP. 1993. Glucose transporter protein expression in human placenta throughout gestation and in intrauterine growth retardation. *The Journal of Clinical Endocrinology & Metabolism*. 77(6):1554-1562.
- Janzen C, Lei MYY, Cho J, Sullivan P, Shin BC, Devaskar SU. 2013. Placental glucose transporter 3 (glut3) is up-regulated in human pregnancies complicated by late-onset intrauterine growth restriction. *Placenta*. 34(11):1072-1078.
- Jensh RP, Brent RL, Barr M, Jr. 1970. The litter effect as a variable in teratologic studies of the albino rat. *Am J Anat*. 128(2):185-191.
- Ji L, Brkic J, Liu M, Fu G, Peng C, Wang YL. 2013. Placental trophoblast cell differentiation: Physiological regulation and pathological relevance to preeclampsia. *Molecular aspects of medicine*. 34(5):981-1023.
- Johansson M, Karlsson L, Wennergren M, Jansson T, Powell TL. 2003. Activity and protein expression of na<sup>+</sup>/k<sup>+</sup> atpase are reduced in microvillous syncytiotrophoblast plasma membranes isolated from pregnancies complicated by intrauterine growth restriction. *The Journal of Clinical Endocrinology & Metabolism*. 88(6):2831-2837.
- Jorge JRP, Barão VA, Delben JA, Faverani LP, Queiroz TP, Assunção WG. 2013. Titanium in dentistry: Historical development, state of the art and future perspectives. *J Indian Prosthodont Soc*. 13(2):71-77.
- Jurašin DD, Čurlin M, Capjak I, Crnković T, Lovrić M, Babič M, Horák D, Vinković Vrček I, Gajović S. 2016. Surface coating affects behavior of metallic nanoparticles in a biological environment. *Beilstein journal of nanotechnology*. 7:246-262.
- Kaestner KH, Flores-Riveros JR, McLenithan JC, Janicot M, Lane MD. 1991. Transcriptional repression of the mouse insulin-responsive glucose transporter (glut4) gene by camp. *Proceedings of the National Academy of Sciences*. 88(5):1933-1937.
- Kafka P, Vajnerova O, Herget J, Hampl V. 2012. Rho-kinase inhibition attenuates acute hypoxic fetoplacental vasoconstriction in the rat. *Physiol Res*. 61 Suppl 2:S43-48.
- Kaiglová A, Reichrtová E, Adamcáková A, Wsólová L. 2001. Lactate dehydrogenase activity in human placenta following exposure to environmental pollutants. *Physiol Res*. 50(5):525-528.
- Kalanithi LEG, Illuzzi JL, Nossov VB, Frisbæk Y, Abdel-Razeq S, Copel JA, Norwitz ER. 2007. Intrauterine growth restriction and placental location. *Journal of Ultrasound in Medicine*. 26(11):1481-1489.
- Kalhan S, Parimi P. 2000. Gluconeogenesis in the fetus and neonate. *Seminars in perinatology*. 24(2):94-106.
- Kalsho G, Kassab GS. 2004. Bifurcation asymmetry of the porcine coronary vasculature and its implications on coronary flow heterogeneity. *American Journal of Physiology-Heart and Circulatory Physiology*. 287(6):H2493-H2500.
- Kamai EM, McElrath TF, Ferguson KK. 2019. Fetal growth in environmental epidemiology: Mechanisms, limitations, and a review of associations with biomarkers of non-persistent chemical exposures during pregnancy. *Environmental Health*. 18(1):43.
- Kan H, Wu Z, Lin Y-C, Chen T-H, Cumpston JL, Kashon ML, Leonard S, Munson AE, Castranova V. 2014. The role of nodose ganglia in the regulation of cardiovascular function following pulmonary exposure to ultrafine titanium dioxide. *Nanotoxicology*. 8(4):447-454.
- Kawakami Y-u, Andoh K, Mizunuma H, Yamada K, Itoh M, Ibuki Y. 1993. Assessment of the implantation site by transvaginal ultrasonography. *Fertility and Sterility*. 59(5):1003-1006.
- Kawashima A, Koide K, Ventura W, Hori K, Takenaka S, Maruyama D, Matsuoka R, Ichizuka K, Sekizawa A. 2014. Effects of maternal smoking on the placental expression of genes

- related to angiogenesis and apoptosis during the first trimester. *PLoS one*. 9(8):e106140-e106140.
- Kellum JA. 2000. Determinants of blood pH in health and disease. *Critical care (London, England)*. 4(1):6-14.
- Keshavarzian E, Ghalati PF, Abouali O, Ahmadi G, Bagheri MH. 2012. Micro/nano-particle deposition in the airway of a 6-year-old child from nostril to the third generation.
- Khan AO, Di Maio A, Guggenheim EJ, Chetwynd AJ, Pencross D, Tang S, Belinga-Desaunay M-FA, Thomas SG, Rappoport JZ, Lynch I. 2020. Surface chemistry-dependent evolution of the nanomaterial corona on tio2 nanomaterials following uptake and sub-cellular localization. *Nanomaterials*. 10(3):401.
- Khlebtsov N, Bogatyrev V, Dykman L, Khlebtsov B, Staroverov S, Shirokov A, Matora L, Khanadeev V, Pylaev T, Tsyganova N et al. 2013. Analytical and theranostic applications of gold nanoparticles and multifunctional nanocomposites. *Theranostics*. 3(3):167-180.
- Khoja SM, Salem AM. 1991. Regulation of 6-phosphofructo-1-kinase in the placenta and small intestine of pregnant streptozotocin-induced diabetic rats. *Diabetes Res Clin Pract*. 13(1-2):85-94.
- Kim H-T, Loftus JP, Mann S, Wakshlag JJ. 2018. Evaluation of arsenic, cadmium, lead and mercury contamination in over-the-counter available dry dog foods with different animal ingredients (red meat, poultry, and fish). *Front Vet Sci*. 5:264-264.
- Knudsen L, Ochs M. 2018. The micromechanics of lung alveoli: Structure and function of surfactant and tissue components. *Histochemistry and cell biology*. 150(6):661-676.
- Knudson JD, Dick GM, Tune JD. 2007. Adipokines and coronary vasomotor dysfunction. *Experimental Biology and Medicine*. 232(6):727-736.
- Ko NL, John L, Gelinne A, Mandala M, Osol G. 2018. Venoarterial communication mediates arterial wall shear stress-induced maternal uterine vascular remodeling during pregnancy. *American journal of physiology Heart and circulatory physiology*.
- Kocemba J, Kawecka-Jaszcz K, Gryglewska B, Grodzicki T. 1998. Isolated systolic hypertension: Pathophysiology, consequences and therapeutic benefits. *Journal of human hypertension*. 12(9):621-626.
- Kopac T. 2021. Protein corona, understanding the nanoparticle–protein interactions and future perspectives: A critical review. *International Journal of Biological Macromolecules*. 169:290-301.
- Kourtis IC, Hirosue S, de Titta A, Kontos S, Stegmann T, Hubbell JA, Swartz MA. 2013. Peripherally administered nanoparticles target monocytic myeloid cells, secondary lymphoid organs and tumors in mice. *PLOS ONE*. 8(4):e61646.
- Kwon H-S, Ryu MH, Carlsten C. 2020. Ultrafine particles: Unique physicochemical properties relevant to health and disease. *Experimental & molecular medicine*. 52(3):318-328.
- Kwon S, Yang Y-S, Yang H-S, Lee J, Kang M-S, Lee B-S, Lee K, Song C-W. 2012. Nasal and pulmonary toxicity of titanium dioxide nanoparticles in rats. *Toxicological research*. 28(4):217-224.
- Lambot N, Lybaert P, Boom A, Delogne-Desnoeck J, Vanbellinghen AM, Graff G, Lebrun P, Meuris S. 2006. Evidence for a clathrin-mediated recycling of albumin in human term placenta. *Biology of reproduction*. 75(1):90-97.
- Lammel T, Mackevica A, Johansson BR, Sturve J. 2019. Endocytosis, intracellular fate, accumulation, and agglomeration of titanium dioxide (tio2) nanoparticles in the rainbow trout liver cell line rtl-w1. *Environmental Science and Pollution Research*. 26(15):15354-15372.

- Lan KC, Huang FJ, Lin YC, Kung FT, Lan TH, Chang SY. 2010. Significantly superior response in the right ovary compared with the left ovary after stimulation with follicle-stimulating hormone in a pituitary down-regulation regimen. *Fertil Steril*. 93(7):2269-2273.
- Lanone S, Rogerieux F, Geys J, Dupont A, Maillot-Marechal E, Boczkowski J, Lacroix G, Hoet P. 2009. Comparative toxicity of 24 manufactured nanoparticles in human alveolar epithelial and macrophage cell lines. *Particle and Fibre Toxicology*. 6(1):14.
- Lappas M, Andrikopoulos S, Permezel M. 2012. Hypoxanthine-xanthine oxidase down-regulates glut1 transcription via sirt1 resulting in decreased glucose uptake in human placenta. *The Journal of endocrinology*. 213(1):49-57.
- Lazic SE, Essioux L. 2013. Improving basic and translational science by accounting for litter-to-litter variation in animal models. *BMC neuroscience*. 14:37-37.
- LeBlanc AJ, Moseley AM, Chen BT, Frazer D, Castranova V, Nurkiewicz TR. 2010. Nanoparticle inhalation impairs coronary microvascular reactivity via a local reactive oxygen species-dependent mechanism. *Cardiovascular toxicology*. 10(1):27-36.
- Lee J, Jeong J-S, Kim SY, Park M-K, Choi S-D, Kim U-J, Park K, Jeong EJ, Nam S-Y, Yu W-J. 2019. Titanium dioxide nanoparticles oral exposure to pregnant rats and its distribution. *Particle and Fibre Toxicology*. 16(1):31.
- Lee MJ, Lee SJ, Yun SJ, Jang JY, Kang H, Kim K, Choi IH, Park S. 2016. Silver nanoparticles affect glucose metabolism in hepatoma cells through production of reactive oxygen species. *Int J Nanomedicine*. 11:55-68.
- Leitschuh M, Chobanian A. 1987. Vascular changes in hypertension. *The Medical clinics of North America*. 71(5):827-841.
- Leiva A, Pardo F, Ramírez MA, Farías M, Casanello P, Sobrevia L. 2011. Fetoplacental vascular endothelial dysfunction as an early phenomenon in the programming of human adult diseases in subjects born from gestational diabetes mellitus or obesity in pregnancy. *Experimental diabetes research*. 2011:349286-349286.
- Lenzen S. 2014. A fresh view of glycolysis and glucokinase regulation: History and current status. *The Journal of biological chemistry*. 289(18):12189-12194.
- Leon DA, Lithell HO, Vagero D, Koupilova I, Mohsen R, Berglund L, Lithell UB, McKeigue PM. 1998. Reduced fetal growth rate and increased risk of death from ischaemic heart disease: Cohort study of 15 000 swedish men and women born 1915-29. *BMJ*. 317(7153):241-245.
- Lesniak A, Salvati A, Santos-Martinez MJ, Radomski MW, Dawson KA, Åberg C. 2013. Nanoparticle adhesion to the cell membrane and its effect on nanoparticle uptake efficiency. *J Am Chem Soc*. 135(4):1438-1444.
- Leverve X, Batandier C, Fontaine E. 2007. Choosing the right substrate. *Novartis Found Symp*. 280:108-121; discussion 121-107, 160-104.
- Li X, Li A, Zhang W, Liu X, Liang Y, Yao X, Song M. 2019. A pilot study of mothers and infants reveals fetal sex differences in the placental transfer efficiency of heavy metals. *Ecotoxicology and Environmental Safety*. 186:109755.
- Liang G, Pu Y, Yin L, Liu R, Ye B, Su Y, Li Y. 2009. Influence of different sizes of titanium dioxide nanoparticles on hepatic and renal functions in rats with correlation to oxidative stress. *Journal of Toxicology and Environmental Health, Part A*. 72(11-12):740-745.
- Liu NM, Miyashita L, Maher BA, McPhail G, Jones CJP, Barratt B, Thangaratinam S, Karloukovski V, Ahmed IA, Aslam Z et al. 2021. Evidence for the presence of air pollution nanoparticles in placental tissue cells. *Sci Total Environ*. 751:142235.
- Liu S, Xu L, Zhang T, Ren G, Yang Z. 2010. Oxidative stress and apoptosis induced by nanosized titanium dioxide in pc12 cells. *Toxicology*. 267(1-3):172-177.

- Liu Y, Wang L, Wang F, Li C. 2016. Effect of fine particulate matter (pm2.5) on rat placenta pathology and perinatal outcomes. *Med Sci Monit.* 22:3274-3280.
- Löndahl J, Möller W, Pagels JH, Kreyling WG, Swietlicki E, Schmid O. 2014. Measurement techniques for respiratory tract deposition of airborne nanoparticles: A critical review. *Journal of aerosol medicine and pulmonary drug delivery.* 27(4):229-254.
- Löndahl J, Swietlicki E, Rissler J, Bengtsson A, Boman C, Blomberg A, Sandström T. 2012. Experimental determination of the respiratory tract deposition of diesel combustion particles in patients with chronic obstructive pulmonary disease. *Particle and Fibre Toxicology.* 9(1):30.
- London WT, Money WL, Rawson RW. 1963. Placental transport of i-131-labeled thyroxine and triiodothyronine in the guinea pig. *Endocrinology.* 73:205-209.
- Longo LD. 1983. Maternal blood volume and cardiac output during pregnancy: A hypothesis of endocrinologic control. *The American journal of physiology.* 245(5 Pt 1):R720-729.
- Losordo DW, Isner JM. 2001. Estrogen and angiogenesis: A review. *Arteriosclerosis, thrombosis, and vascular biology.* 21(1):6-12.
- Ludwig DS, Currie J. 2010. The association between pregnancy weight gain and birthweight: A within-family comparison. *Lancet (London, England).* 376(9745):984-990.
- Lueder FL, Ogata ES. 1990. Uterine artery ligation in the maternal rat alters fetal tissue glucose utilization. *Pediatric research.* 28(5):464-468.
- Lumey LH, Ravelli ACJ, Wiessing LG, Koppe JG, Treffers PE, Stein ZA. 1993. The dutch famine birth cohort study: Design, validation of exposure, and selected characteristics of subjects after 43 years follow-up. *Paediatric and perinatal epidemiology.* 7(4):354-367.
- Luo Y, Benali A, Shulenburg L, Krogel JT, Heinonen O, Kent PRC. 2016. Phase stability of tio2polymorphs from diffusion quantum monte carlo. *New Journal of Physics.* 18(11):113049.
- Lv H, Tong J, Yang J, Lv S, Li WP, Zhang C, Chen ZJ. 2018. Dysregulated pseudogene hk2p1 may contribute to preeclampsia as a competing endogenous rna for hexokinase 2 by impairing decidualization. *Hypertension.* 71(4):648-658.
- Ma L, Zhao J, Wang J, Liu J, Duan Y, Liu H, Li N, Yan J, Ruan J, Wang H et al. 2009. The acute liver injury in mice caused by nano-anatase tio2. *Nanoscale Research Letters.* 4(11):1275.
- Ma-Hock L, Burkhardt S, Strauss V, Gamer AO, Wiench K, van Ravenzwaay B, Landsiedel R. 2009. Development of a short-term inhalation test in the rat using nano-titanium dioxide as a model substance. *Inhal Toxicol.* 21(2):102-118.
- Magann EF, Doherty DA, Turner K, Lanneau GS, Jr., Morrison JC, Newnham JP. 2007. Second trimester placental location as a predictor of an adverse pregnancy outcome. *J Perinatol.* 27(1):9-14.
- Mahan MM, Doiron AL. 2018. Gold nanoparticles as x-ray, ct, and multimodal imaging contrast agents: Formulation, targeting, and methodology. *Journal of Nanomaterials.* 2018:15.
- Malhotra A, Allison BJ, Castillo-Melendez M, Jenkin G, Polglase GR, Miller SL. 2019. Neonatal morbidities of fetal growth restriction: Pathophysiology and impact. *Frontiers in Endocrinology.* 10(55).
- Manangama G, Migault L, Audignon-Durand S, Gramond C, Zaros C, Bouvier G, Brochard P, Sentilhes L, Lacourt A, Delva F. 2019. Maternal occupational exposures to nanoscale particles and small for gestational age outcome in the french longitudinal study of children. *Environment international.* 122:322-329.
- Mandala M, Osol G. 2012. Physiological remodelling of the maternal uterine circulation during pregnancy. *Basic & clinical pharmacology & toxicology.* 110(1):12-18.

- Mao J, Zhang X, Sieli PT, Falduto MT, Torres KE, Rosenfeld CS. 2010. Contrasting effects of different maternal diets on sexually dimorphic gene expression in the murine placenta. *Proceedings of the National Academy of Sciences*. 107(12):5557-5562.
- Mao Z, Li Y, Dong T, Zhang L, Zhang Y, Li S, Hu H, Sun C, Xia Y. 2019. Exposure to titanium dioxide nanoparticles during pregnancy changed maternal gut microbiota and increased blood glucose of rat. *Nanoscale Res Lett*. 14(1):26.
- Maria Edesina Aguiar MCBOS, Angela Maria V. M. D. Lima, Maria Auxiliadora M.L. Machado, Maria M. Conceicao, Elaine S. Azevedo. 1980. Hexokinase activity and isozyme pattern in human placenta: A population study. *Biochemical Medicine*. 24:190-193.
- Marsden PA, Brenner BM. 1992. Transcriptional regulation of the endothelin-1 gene by tn $\alpha$ . *The American journal of physiology*. 262(4 Pt 1):C854-861.
- Martínez-Reyes I, Chandel NS. 2020. Mitochondrial tca cycle metabolites control physiology and disease. *Nature Communications*. 11(1):102.
- Martyn CN, Barker DJ, Jespersen S, Greenwald S, Osmond C, Berry C. 1995. Growth in utero, adult blood pressure, and arterial compliance. *Br Heart J*. 73(2):116-121.
- Martyn CN, Barker DJP, Osmond C. 1996. Mothers' pelvic size, fetal growth, and death from stroke and coronary heart disease in men in the uk. *The Lancet*. 348(9037):1264-1268.
- Masoumy EP, Sawyer AA, Sharma S, Patel JA, Gordon PMK, Regnault TRH, Matuszewski B, Weintraub NL, Richardson B, Thompson JA et al. 2018. The lifelong impact of fetal growth restriction on cardiac development. *Pediatric research*. 84(4):537-544.
- Mathew H, Castracane VD, Mantzoros C. 2017. Adipose tissue and reproductive health. *Metabolism: clinical and experimental*.
- McClements L, Richards C, Patel N, Chen H, Sesperez K, Bubb KJ, Karlstaedt A, Aksentijevic D. 2022. Impact of reduced uterine perfusion pressure model of preeclampsia on metabolism of placenta, maternal and fetal hearts. *Scientific Reports*. 12(1):1111.
- McIntyre KR, Hayward CE, Sibley CP, Greenwood SL, Dilworth MR. 2019. Evidence of adaptation of maternofetal transport of glutamine relative to placental size in normal mice, and in those with fetal growth restriction. *J Physiol*. 597(19):4975-4990.
- McLaurin KA, Mactutus CF. 2015. Polytocus focus: Uterine position effect is dependent upon horn size. *Int J Dev Neurosci*. 40:85-91.
- Miao W, Zhu B, Xiao X, Li Y, Dirbaba NB, Zhou B, Wu H. 2015. Effects of titanium dioxide nanoparticles on lead bioconcentration and toxicity on thyroid endocrine system and neuronal development in zebrafish larvae. *Aquat Toxicol*. 161:117-126.
- Michelsen TM, Holme AM, Holm MB, Roland MC, Haugen G, Powell TL, Jansson T, Henriksen T. 2018. Uteroplacental glucose uptake and fetal glucose consumption: A quantitative study in human pregnancies. *The Journal of Clinical Endocrinology & Metabolism*. 104(3):873-882.
- Miller MR, Raftis JB, Langrish JP, McLean SG, Samutrtai P, Connell SP, Wilson S, Vesey AT, Fokkens PHB, Boere AJF et al. 2017. Inhaled nanoparticles accumulate at sites of vascular disease. *ACS nano*. 11(5):4542-4552.
- Miller SL, Huppi PS, Mallard C. 2016. The consequences of fetal growth restriction on brain structure and neurodevelopmental outcome. *J Physiol*. 594(4):807-823.
- Miura N, Ohtani K, Hasegawa T, Yoshioka H, Hwang G-W. 2019. Biphasic adverse effect of titanium nanoparticles on testicular function in mice. *Scientific Reports*. 9(1):14373.
- Molina-Reyes J, Romero-Moran A, Uribe-Vargas H, Lopez-Ruiz B, Sanchez-Salas JL, Ortega E, Ponce A, Morales-Sanchez A, Lopez-Huerta F, Zuñiga-Islas C. 2020. Study on the photocatalytic activity of titanium dioxide nanostructures: Nanoparticles, nanotubes and ultra-thin films. *Catalysis Today*. 341:2-12.

- Möller W, Häussinger K, Ziegler-Heitbrock L, Heyder J. 2006. Mucociliary and long-term particle clearance in airways of patients with immotile cilia. *Respir Res.* 7(1):10-10.
- Montaner P, Dominguez R, Corcoy R. 2002. Self-monitored blood glucose in pregnant women without gestational diabetes mellitus. *Diabetes care.* 25(11):2104.
- Morales-Rubio RA, Alvarado-Cruz I, Manzano-León N, Andrade-Oliva M-d-I-A, Uribe-Ramirez M, Quintanilla-Vega B, Osornio-Vargas Á, De Vizcaya-Ruiz A. 2019. In utero exposure to ultrafine particles promotes placental stress-induced programming of renin-angiotensin system-related elements in the offspring results in altered blood pressure in adult mice. *Particle and Fibre Toxicology.* 16(1):7.
- Mori M, Bogdan A, Balassa T, Csabai T, Szekeres-Bartho J. 2016a. The decidua-the maternal bed embracing the embryo-maintains the pregnancy. *Seminars in immunopathology.* 38(6):635-649.
- Mori M, Bogdan A, Balassa T, Csabai T, Szekeres-Bartho J. 2016b. The decidua—the maternal bed embracing the embryo—maintains the pregnancy. *Seminars in Immunopathology.* 38(6):635-649.
- Morimoto Y, Izumi H, Yoshiura Y, Tomonaga T, Lee BW, Okada T, Oyabu T, Myojo T, Kawai K, Yatera K et al. 2016. Comparison of pulmonary inflammatory responses following intratracheal instillation and inhalation of nanoparticles. *Nanotoxicology.* 10(5):607-618.
- Mozafari M, Khoradmehr A, Danafar A, Miresmaeili M, Kalantar SM. 2020. Toxic effects of maternal exposure to silver nanoparticles on mice fetal development during pregnancy. *Birth defects research.* 112(1):81-92.
- Mueckler M, Weng W, Kruse M. 1994. Glutamine 161 of glut1 glucose transporter is critical for transport activity and exofacial ligand binding. *J Biol Chem.* 269(32):20533-20538.
- Mühlfeld C, Geiser M, Kapp N, Gehr P, Rothen-Rutishauser B. 2007. Re-evaluation of pulmonary titanium dioxide nanoparticle distribution using the "relative deposition index": Evidence for clearance through microvasculature. *Particle and fibre toxicology.* 4:7.
- Mukhopadhyay A, Thomas T, Bosch RJ, Dwarkanath P, Thomas A, Duggan CP, Kurpad AV. 2018. Fetal sex modifies the effect of maternal macronutrient intake on the incidence of small-for-gestational-age births: A prospective observational cohort study. *The American Journal of Clinical Nutrition.* 108(4):814-820.
- Muller EK, Grafe C, Wiekhorst F, Bergemann C, Weidner A, Dutz S, Clement JH. 2018. Magnetic nanoparticles interact and pass an in vitro co-culture blood-placenta barrier model. *Nanomaterials (Basel).* 8(2).
- Mund M, Louwen F, Klingelhoef D, Gerber A. 2013. Smoking and pregnancy — a review on the first major environmental risk factor of the unborn. *International Journal of Environmental Research and Public Health.* 10(12):6485-6499.
- Munzel T, Schmidt FP, Steven S, Herzog J, Daiber A, Sorensen M. 2018. Environmental noise and the cardiovascular system. *Journal of the American College of Cardiology.* 71(6):688-697.
- Murray AJ. 2012. Oxygen delivery and fetal-placental growth: Beyond a question of supply and demand? *Placenta.* 33 Suppl 2:e16-22.
- Musial J, Krakowiak R, Mlynarczyk DT, Goslinski T, Stanisz BJ. 2020. Titanium dioxide nanoparticles in food and personal care products-what do we know about their safety? *Nanomaterials (Basel).* 10(6):1110.
- Myllynen PK, Loughran MJ, Howard CV, Sormunen R, Walsh AA, Vahakangas KH. 2008. Kinetics of gold nanoparticles in the human placenta. *Reprod Toxicol.* 26(2):130-137.
- Nadra K, Anghel SI, Joye E, Tan NS, Basu-Modak S, Trono D, Wahli W, Desvergne B. 2006. Differentiation of trophoblast giant cells and their metabolic functions are dependent on peroxisome proliferator-activated receptor beta/delta. *Mol Cell Biol.* 26(8):3266-3281.

- Naeye RL. 1978. Effects of maternal cigarette smoking on the fetus and placenta. *British journal of obstetrics and gynaecology*. 85(10):732-737.
- Nakai A, Sekiya I, Oya A, Koshino T, Araki T. 2002. Assessment of the hepatic arterial and portal venous blood flows during pregnancy with doppler ultrasonography. *Arch Gynecol Obstet*. 266(1):25-29.
- Nakajima H. 1995. [phosphofructokinase (pfc)]. *Nihon Rinsho*. 53(5):1241-1246.
- Napso T, Yong HEJ, Lopez-Tello J, Sferruzzi-Perri AN. 2018. The role of placental hormones in mediating maternal adaptations to support pregnancy and lactation. *Front Physiol*. 9:1091.
- Nedder M, Boland S, Devineau S, Zerrad-Saadi A, Rogozarski J, Lai-Kuen R, Baya I, Guibourdenche J, Vibert F, Chissey A et al. 2020. Uptake of cerium dioxide nanoparticles and impact on viability, differentiation and functions of primary trophoblast cells from human placenta. *Nanomaterials (Basel)*. 10(7).
- Nemmar A, Hoet PH, Vanquickenborne B, Dinsdale D, Thomeer M, Hoylaerts MF, Vanbilloen H, Mortelmans L, Nemery B. 2002. Passage of inhaled particles into the blood circulation in humans. *Circulation*. 105(4):411-414.
- Newbern D, Freemark M. 2011. Placental hormones and the control of maternal metabolism and fetal growth. *Curr Opin Endocrinol Diabetes Obes*. 18(6):409-416.
- Ng S-W, Norwitz GA, Pavlicev M, Tilburgs T, Simón C, Norwitz ER. 2020. Endometrial decidualization: The primary driver of pregnancy health. *International journal of molecular sciences*. 21(11):4092.
- Nishimura T, Chishu T, Tomi M, Nakamura R, Sato K, Kose N, Sai Y, Nakashima E. 2012. Mechanism of nucleoside uptake in rat placenta and induction of placental cnt2 in experimental diabetes. *Drug Metab Pharmacokinet*. 27(4):439-446.
- Nobles CJ, Grantz KL, Liu D, Williams A, Ouidir M, Seeni I, Sherman S, Mendola P. 2019. Ambient air pollution and fetal growth restriction: Physician diagnosis of fetal growth restriction versus population-based small-for-gestational age. *Sci Total Environ*. 650(Pt 2):2641-2647.
- Norlén F, Gustavsson P, Wiebert P, Rylander L, Westgren M, Plato N, Albin M, Selander J. 2019. Occupational exposure to organic particles and combustion products during pregnancy and birth outcome in a nationwide cohort study in sweden. *Occup Environ Med*. 76(8):537-544.
- Notter T, Aengenheister L, Weber-Stadlbauer U, Naegeli H, Wick P, Meyer U, Buerki-Thurnherr T. 2018. Prenatal exposure to tio2 nanoparticles in mice causes behavioral deficits with relevance to autism spectrum disorder and beyond. *Transl Psychiatry*. 8(1):193.
- Nurkiewicz TR, Porter DW, Hubbs AF, Cumpston JL, Chen BT, Frazer DG, Castranova V. 2008. Nanoparticle inhalation augments particle-dependent systemic microvascular dysfunction. *Part Fibre Toxicol*. 5:1.
- Nüsken K-D, Dötsch Jr, Rauh M, Rascher W, Schneider H. 2008. Uteroplacental insufficiency after bilateral uterine artery ligation in the rat: Impact on postnatal glucose and lipid metabolism and evidence for metabolic programming of the offspring by sham operation. *Endocrinology*. 149(3):1056-1063.
- Onoda A, Kawasaki T, Tsukiyama K, Takeda K, Umezawa M. 2020. Carbon nanoparticles induce endoplasmic reticulum stress around blood vessels with accumulation of misfolded proteins in the developing brain of offspring. *Scientific Reports*. 10(1):10028.
- Osol G, Barron C, Gokina N, Mandala M. 2009. Inhibition of nitric oxide synthases abrogates pregnancy-induced uterine vascular expansive remodeling. *Journal of vascular research*. 46(5):478-486.

- Osol G, Barron C, Mandala M. 2012. Uterine distension differentially affects remodelling and distensibility of the uterine vasculature in non-pregnant rats. *Reproduction, fertility, and development*. 24(6):835-842.
- Osol G, Mandala M. 2009. Maternal uterine vascular remodeling during pregnancy. *Physiology (Bethesda, Md)*. 24:58-71.
- Osol G, Moore LG. 2014. Maternal uterine vascular remodeling during pregnancy. *Microcirculation*. 21(1):38-47.
- Ouyang F, Parker M, Cerda S, Pearson C, Fu L, Gillman MW, Zuckerman B, Wang X. 2013. Placental weight mediates the effects of prenatal factors on fetal growth: The extent differs by preterm status. *Obesity (Silver Spring)*. 21(3):609-620.
- Oyabu T, Morimoto Y, Izumi H, Yoshiura Y, Tomonaga T, Lee B-W, Okada T, Myojo T, Shimada M, Kubo M et al. 2016. Comparison between whole-body inhalation and nose-only inhalation on the deposition and health effects of nanoparticles. *Environ Health Prev Med*. 21(1):42-48.
- Padmanabhan R, Singh S. 1981. Effect of intrauterine position on foetal weight in cf rats. *Indian J Med Res*. 73:134-139.
- Park S, Lee YK, Jung M, Kim KH, Chung N, Ahn EK, Lim Y, Lee KH. 2007. Cellular toxicity of various inhalable metal nanoparticles on human alveolar epithelial cells. *Inhal Toxicol*. 19 Suppl 1:59-65.
- Paul E, Franco-Montoya ML, Paineau E, Angeletti B, Vibhushan S, Ridoux A, Tiendrebeogo A, Salome M, Hesse B, Vantelon D et al. 2017. Pulmonary exposure to metallic nanomaterials during pregnancy irreversibly impairs lung development of the offspring. *Nanotoxicology*. 11(4):484-495.
- Pavek P, Fendrich Z, Staud F, Malakova J, Brozmanova H, Laznicek M, Semecky V, Grundmann M, Palicka V. 2001. Influence of p-glycoprotein on the transplacental passage of cyclosporine. *J Pharm Sci*. 90(10):1583-1592.
- Pavek P, Staud F, Fendrich Z, Sklenarova H, Libra A, Novotna M, Kopecky M, Nobilis M, Semecky V. 2003. Examination of the functional activity of p-glycoprotein in the rat placental barrier using rhodamine 123. *J Pharmacol Exp Ther*. 305(3):1239-1250.
- Pereira RD, De Long NE, Wang RC, Yazdi FT, Holloway AC, Raha S. 2015. Angiogenesis in the placenta: The role of reactive oxygen species signaling. *BioMed research international*. 2015:814543-814543.
- Perry JS, Rowell JG. 1969. Variations in foetal weight and vascular supply along the uterine horn of the pig. *Journal of reproduction and fertility*. 19(3):527-534.
- Petraglia F, Florio P, Nappi C, Genazzani AR. 1996. Peptide signaling in human placenta and membranes: Autocrine, paracrine, and endocrine mechanisms. *Endocrine reviews*. 17(2):156-186.
- Philipp K, Pateisky N, Endler M. 1984. Effects of smoking on uteroplacental blood flow. *Gynecologic and obstetric investigation*. 17(4):179-182.
- Piccinno F, Gottschalk F, Seeger S, Nowack B. 2012. Industrial production quantities and uses of ten engineered nanomaterials in europe and the world. *Journal of Nanoparticle Research*. 14(9):1109.
- Picut CA, Swanson CL, Parker RF, Scully KL, Parker GA. 2009. The metrial gland in the rat and its similarities to granular cell tumors. *Toxicol Pathol*. 37(4):474-480.
- Pietroiusti A, Massimiani M, Fenoglio I, Colonna M, Valentini F, Palleschi G, Camaioni A, Magrini A, Siracusa G, Bergamaschi A et al. 2011. Low doses of pristine and oxidized single-wall carbon nanotubes affect mammalian embryonic development. *ACS Nano*. 5(6):4624-4633.

- Pijnenborg R, Vercruyse L, Brosens I. 2011. Deep placentation. Best practice & research Clinical obstetrics & gynaecology. 25(3):273-285.
- Pintican D, Poienar AA, Strilciuc S, Miha D. 2019. Effects of maternal smoking on human placental vascularization: A systematic review. Taiwanese Journal of Obstetrics and Gynecology. 58(4):454-459.
- Pober JS, Sessa WC. 2015. Inflammation and the blood microvascular system. Cold Spring Harbor Perspectives in Biology. 7(1):a016345.
- Pontes IEA, Afra KF, Silva JR, Borges PSN, Clough GF, Alves JGB. 2015. Microvascular reactivity in women with gestational diabetes mellitus studied during pregnancy. Diabetology & Metabolic Syndrome. 7:27.
- Potula V, Kaye W. 2005. Report from the cdc. Is lead exposure a risk factor for bone loss? Journal of women's health (2002). 14(6):461-464.
- PrabhuDas M, Bonney E, Caron K, doi:10.1038/ni.3131. ea-. Immune mechanisms at the maternal-fetal interface: Perspectives and challenges. Nature Immunology. 16(4):328-334.
- Tabulated molar extinction coefficient for hemoglobin in water. 1998. [accessed]. <https://omlc.org/spectra/hemoglobin/summary.html>.
- Prozialeck WC, Edwards JR, Nebert DW, Woods JM, Barchowsky A, Atchison WD. 2008. The vascular system as a target of metal toxicity. Toxicological sciences : an official journal of the Society of Toxicology. 102(2):207-218.
- Pujalté I, Dieme D, Haddad S, Serventi AM, Bouchard M. 2017. Toxicokinetics of titanium dioxide (tio<sub>2</sub>) nanoparticles after inhalation in rats. Toxicology letters. 265:77-85.
- Qi W, Bi J, Zhang X, Wang J, Wang J, Liu P, Li Z, Wu W. 2014. Damaging effects of multi-walled carbon nanotubes on pregnant mice with different pregnancy times. Sci Rep. 4:4352.
- Qiu C, Sanchez SE, Gelaye B, Enquobahrie DA, Ananth CV, Williams MA. 2015. Maternal sleep duration and complaints of vital exhaustion during pregnancy is associated with placental abruption. The journal of maternal-fetal & neonatal medicine : the official journal of the European Association of Perinatal Medicine, the Federation of Asia and Oceania Perinatal Societies, the International Society of Perinatal Obstetricians. 28(3):350-355.
- Ramos-Delgado NA, Gracia-Pinilla MÁ, Mangalaraja RV, O'Shea K, Dionysiou DD. 2016. Industrial synthesis and characterization of nanophotocatalysts materials: Titania. Nanotechnology Reviews. 5(5):467-479.
- Rasmussen SA. 2012. Human teratogens update 2011: Can we ensure safety during pregnancy? Birth Defects Res A Clin Mol Teratol. 94(3):123-128.
- Raz T, Avni R, Addadi Y, Cohen Y, Jaffa AJ, Hemmings B, Garbow JR, Neeman M. 2012. The hemodynamic basis for positional- and inter-fetal dependent effects in dual arterial supply of mouse pregnancies. PLOS ONE. 7(12):e52273.
- Reckzeh ES, Waldmann H. 2020. Small-molecule inhibition of glucose transporters glut-1-4. Chembiochem. 21(1-2):45-52.
- Redmond GP. 1979. Effect of drugs on intrauterine growth. Clin Perinatol. 6(1):5-19.
- Reeves S, Bernstein I. 2008. Effects of maternal tobacco-smoke exposure on fetal growth and neonatal size. Expert Rev Obstet Gynecol. 3(6):719-730.
- Renaud SJ, Postovit LM, Macdonald-Goodfellow SK, McDonald GT, Caldwell JD, Graham CH. 2005. Activated macrophages inhibit human cytotrophoblast invasiveness in vitro. Biology of reproduction. 73(2):237-243.
- Reyes-Caballero H, Rao X, Sun Q, Warmoes MO, Lin P, Sussan TE, Park B, Fan TWM, Maiseyeu A, Rajagopalan S et al. 2019. Air pollution-derived particulate matter dysregulates hepatic krebs cycle, glucose and lipid metabolism in mice. Scientific reports. 9(1):17423-17423.

- Rizzoni D, Muiesan ML, Porteri E, Ciuceis CD, Boari GEM, Salvetti M, Paini A, Rosei EA. 2009. Vascular remodeling, macro- and microvessels: Therapeutic implications. *Blood Pressure*. 18(5):242-246.
- Roberts DJ, Miyamoto S. 2015. Hexokinase ii integrates energy metabolism and cellular protection: Akting on mitochondria and torcing to autophagy. *Cell Death Differ*. 22(2):248-257.
- Robertson WB. 1976. Uteroplacental vasculature. *Journal of clinical pathology Supplement (Royal College of Pathologists)*. 10:9-17.
- Rogers JF, Dunlop AL. 2006. Air pollution and very low birth weight infants: A target population? *Pediatrics*. 118(1):156-164.
- Roland MC, Friis CM, Voldner N, Godang K, Bollerslev J, Haugen G, Henriksen T. 2012. Fetal growth versus birthweight: The role of placenta versus other determinants. *PLoS One*. 7(6):e39324.
- Romero A, Villamayor F, Grau MT, Sacristán A, Ortiz JA. 1992. Relationship between fetal weight and litter size in rats: Application to reproductive toxicology studies. *Reproductive toxicology (Elmsford, NY)*. 6(5):453-456.
- Roseboom T, de Rooij S, Painter R. 2006. The dutch famine and its long-term consequences for adult health. *Early Hum Dev*. 82(8):485-491.
- Rosenfeld CS. 2012. Effects of maternal diet and exposure to bisphenol a on sexually dimorphic responses in conceptuses and offspring. *Reprod Domest Anim*. 47 Suppl 4:23-30.
- Rosenfeld CS. 2015. Sex-specific placental responses in fetal development. *Endocrinology*. 156(10):3422-3434.
- Rossi S, Savi M, Mazzola M, Pinelli S, Alinovi R, Gennaccaro L, Pagliaro A, Meraviglia V, Galetti M, Lozano-Garcia O et al. 2019. Subchronic exposure to titanium dioxide nanoparticles modifies cardiac structure and performance in spontaneously hypertensive rats. *Particle and fibre toxicology*. 16(1):25-25.
- Rudge CV, Röllin HB, Nogueira CM, Thomassen Y, Rudge MC, Odland J. 2009. The placenta as a barrier for toxic and essential elements in paired maternal and cord blood samples of south african delivering women. *Journal of environmental monitoring : JEM*. 11(7):1322-1330.
- Rueda-Clausen CF, Morton JS, Lopaschuk GD, Davidge ST. 2010. Long-term effects of intrauterine growth restriction on cardiac metabolism and susceptibility to ischaemia/reperfusion. *Cardiovascular research*. 90(2):285-294.
- Sabra S, Gratacós E, Gómez Roig MD. 2017. Smoking-induced changes in the maternal immune, endocrine, and metabolic pathways and their impact on fetal growth: A topical review. *Fetal Diagnosis and Therapy*. 41(4):241-250.
- Sadiq HF, Demello DE, Devaskar SU. 1998. The effect of intrauterine growth restriction upon fetal and postnatal hepatic glucose transporter and glucokinase proteins. *Pediatric research*. 43(1):91-100.
- Sánchez-Aranguren LC, Prada CE, Riaño-Medina CE, Lopez M. 2014. Endothelial dysfunction and preeclampsia: Role of oxidative stress. *Frontiers in Physiology*. 5:372.
- Sandoo A, van Zanten JJ, Metsios GS, Carroll D, Kitas GD. 2010. The endothelium and its role in regulating vascular tone. *The open cardiovascular medicine journal*. 4:302-312.
- Sang X, Zheng L, Sun Q, Li N, Cui Y, Hu R, Gao G, Cheng Z, Cheng J, Gui S et al. 2012. The chronic spleen injury of mice following long-term exposure to titanium dioxide nanoparticles. *J Biomed Mater Res A*. 100(4):894-902.

- Saoi M, Kennedy KM, Gohir W, Sloboda DM, Britz-McKibbin P. 2020. Placental metabolomics for assessment of sex-specific differences in fetal development during normal gestation. *Scientific Reports*. 10(1):9399.
- Sastry B. 1991. Placental toxicology: Tobacco smoke, abused drugs, multiple chemical interactions, and placental function. *Reproduction, Fertility and Development*. 3(4):355-372.
- Sastry BV. 1999. Techniques to study human placental transport. *Advanced drug delivery reviews*. 38(1):17-39.
- Sato N, Miyasaka N. 2019. Stratified analysis of the correlation between gestational weight gain and birth weight for gestational age: A retrospective single-center cohort study in Japan. *BMC Pregnancy Childbirth*. 19(1):402.
- Schleh C, Holzwarth U, Hirn S, Wenk A, Simonelli F, Schäffler M, Möller W, Gibson N, Kreyling WG. 2013. Biodistribution of inhaled gold nanoparticles in mice and the influence of surfactant protein D. *Journal of aerosol medicine and pulmonary drug delivery*. 26(1):24-30.
- Schmidt F, Kolle K, Kreuder K, Schnorbus B, Wild P, Hechtner M, Binder H, Gori T, Munzel T. 2015. Nighttime aircraft noise impairs endothelial function and increases blood pressure in patients with or at high risk for coronary artery disease. *Clinical research in cardiology : official journal of the German Cardiac Society*. 104(1):23-30.
- Schneider JS, Anderson DW, Kidd SK, Sobolewski M, Cory-Slechta DA. 2016. Sex-dependent effects of lead and prenatal stress on post-translational histone modifications in frontal cortex and hippocampus in the early postnatal brain. *Neurotoxicology*. 54:65-71.
- Scholl TO, Sowers M, Chen X, Lenders C. 2001. Maternal glucose concentration influences fetal growth, gestation, and pregnancy complications. *American Journal of Epidemiology*. 154(6):514-520.
- Semmler-Behnke M, Lipka J, Wenk A, Hirn S, Schaffler M, Tian F, Schmid G, Oberdorster G, Kreyling WG. 2014. Size dependent translocation and fetal accumulation of gold nanoparticles from maternal blood in the rat. *Part Fibre Toxicol*. 11:33.
- Semmler-Behnke M, Takenaka S, Fertsch S, Wenk A, Seitz J, Mayer P, Oberdorster G, Kreyling WG. 2007. Efficient elimination of inhaled nanoparticles from the alveolar region: Evidence for interstitial uptake and subsequent reentrainment onto airways epithelium. *Environ Health Perspect*. 115(5):728-733.
- Shao X, Cheng H, Zhou J, Zhang J, Zhu Y, Yang C, Di Narzo A, Yu J, Shen Y, Li Y et al. 2020. Prenatal exposure to ambient air multi-pollutants significantly impairs intrauterine fetal development trajectory. *Ecotoxicology and environmental safety*. 201:110726-110726.
- Sharma D, Shastri S, Sharma P. 2016. Intrauterine growth restriction: Antenatal and postnatal aspects. *Clin Med Insights Pediatr*. 10:67-83.
- Shen R, Zhao LL, Yu Z, Zhang C, Chen YH, Wang H, Zhang ZH, Xu DX. 2017. Maternal di-(2-ethylhexyl) phthalate exposure during pregnancy causes fetal growth restriction in a stage-specific but gender-independent manner. *Reproductive toxicology (Elmsford, NY)*. 67:117-124.
- Sheng L, Wang L, Sang X, Zhao X, Hong J, Cheng S, Yu X, Liu D, Xu B, Hu R et al. 2014. Nano-sized titanium dioxide-induced splenic toxicity: A biological pathway explored using microarray technology. *J Hazard Mater*. 278:180-188.
- Shi H, Magaye R, Castranova V, Zhao J. 2013. Titanium dioxide nanoparticles: A review of current toxicological data. *Particle and Fibre Toxicology*. 10(1):15.
- Shukla RK, Badiye A, Vajpayee K, Kapoor N. 2021. Genotoxic potential of nanoparticles: Structural and functional modifications in DNA. *Front Genet*. 12:728250-728250.

- Simmons DG, Cross JC. 2005. Determinants of trophoblast lineage and cell subtype specification in the mouse placenta. *Developmental biology*. 284(1):12-24.
- Simmons RA. 2009. Developmental origins of adult disease. *Pediatric Clinics of North America*. 56(3):449-Contents.
- Simmons RA, Templeton LJ, Gertz SJ. 2001. Intrauterine growth retardation leads to the development of type 2 diabetes in the rat. *Diabetes*. 50(10):2279.
- Skocaj M, Filipic M, Petkovic J, Novak S. 2011. Titanium dioxide in our everyday life; is it safe? *Radiol Oncol*. 45(4):227-247.
- Slavin YN, Asnis J, Häfeli UO, Bach H. 2017. Metal nanoparticles: Understanding the mechanisms behind antibacterial activity. *Journal of Nanobiotechnology*. 15(1):65.
- Smijs TG, Pavel S. 2011. Titanium dioxide and zinc oxide nanoparticles in sunscreens: Focus on their safety and effectiveness. *Nanotechnol Sci Appl*. 4:95-112.
- Smith CH, Moe AJ, Ganapathy V. 1992. Nutrient transport pathways across the epithelium of the placenta. *Annu Rev Nutr*. 12:183-206.
- Snyder RW, Fennell TR, Wingard CJ, Mortensen NP, Holland NA, Shannahan JH, Pathmasiri W, Lewin AH, Sumner SC. 2015. Distribution and biomarker of carbon-14 labeled fullerene c60 ([<sup>14</sup>C]c60) in pregnant and lactating rats and their offspring after maternal intravenous exposure. *J Appl Toxicol*. 35(12):1438-1451.
- Soares MJ. 2004. The prolactin and growth hormone families: Pregnancy-specific hormones/cytokines at the maternal-fetal interface. *Reproductive biology and endocrinology : RB&E*. 2:51-51.
- Soares MJ, Chakraborty D, Karim Rumi MA, Konno T, Renaud SJ. 2012. Rat placentation: An experimental model for investigating the hemochorial maternal-fetal interface. *Placenta*. 33(4):233-243.
- Soares MJ, Iqbal K, Kozai K. 2017. Hypoxia and placental development. *Birth defects research*. 109(17):1309-1329.
- Soma-Pillay P, Nelson-Piercy C, Tolppanen H, Mebazaa A. 2016. Physiological changes in pregnancy. *Cardiovasc J Afr*. 27(2):89-94.
- Sonagra AD, Biradar SM, K D, Murthy D S J. 2014. Normal pregnancy- a state of insulin resistance. *J Clin Diagn Res*. 8(11):CC01-CC03.
- Song B, Liu J, Feng X, Wei L, Shao L. 2015. A review on potential neurotoxicity of titanium dioxide nanoparticles. *Nanoscale research letters*. 10(1):1042-1042.
- Soto SF, Melo JO, Marchesi GD, Lopes KL, Veras MM, Oliveira IB, Souza RM, de Castro I, Furukawa LNS, Saldiva PHN et al. 2017. Exposure to fine particulate matter in the air alters placental structure and the renin-angiotensin system. *PLoS One*. 12(8):e0183314.
- Sriram K, Intaglietta M, Tartakovsky DM. 2014. Hematocrit dispersion in asymmetrically bifurcating vascular networks. *American Journal of Physiology-Heart and Circulatory Physiology*. 307(11):H1576-H1586.
- Stanley SC, Brooks SD, Butcher JT, d'Audiffret AC, Frisbee SJ, Frisbee JC. 2014. Protective effect of sex on chronic stress- and depressive behavior-induced vascular dysfunction in balb/cj mice. *Journal of applied physiology (Bethesda, Md : 1985)*. 117(9):959-970.
- Stapleton P, McBride C, Yi J, Abukabda A, Nurkiewics T. 2017. Estrous cycle dependent modulation of in vivo microvascular dysfunction after nanomaterial inhalation.
- Stapleton P, Nichols C, Yi J, McBride C, Minarchick V, Shepherd D, Hollander J, Nurkiewics T. 2015a. Microvascular and mitochondrial dysfunction in the female f1 generation after gestational tio2 nanoparticle exposure. *Nanotoxicology*. 9(8):929-931.
- Stapleton PA. 2016. Gestational nanomaterial exposures: Microvascular implications during pregnancy, fetal development and adulthood. *J Physiol*. 594(8):2161-2173.

- Stapleton PA, Abukabda AB, Hardy SL, Nurkiewicz TR. 2015b. Xenobiotic pulmonary exposure and systemic cardiovascular response via neurological links. *Am J Physiol Heart Circ Physiol*. 309(10):H1609-1620.
- Stapleton PA, Hathaway QA, Nichols CE, Abukabda AB, Pinti MV, Shepherd DL, McBride CR, Yi J, Castranova VC, Hollander JM et al. 2018a. Maternal engineered nanomaterial inhalation during gestation alters the fetal transcriptome. *Part Fibre Toxicol*. 15(1):3.
- Stapleton PA, Hathaway QA, Nichols CE, Abukabda AB, Pinti MV, Shepherd DL, McBride CR, Yi J, Castranova VC, Hollander JM et al. 2018b. Maternal engineered nanomaterial inhalation during gestation alters the fetal transcriptome. *Particle and Fibre Toxicology*. 15(1):3.
- Stapleton PA, McBride CR, Yi J, Abukabda AB, Nurkiewicz TR. 2018c. Estrous cycle-dependent modulation of in vivo microvascular dysfunction after nanomaterial inhalation. *Reproductive toxicology (Elmsford, NY)*. 78:20-28.
- Stapleton PA, McBride CR, Yi J, Nurkiewicz TR. 2015c. Uterine microvascular sensitivity to nanomaterial inhalation: An in vivo assessment. *Toxicology and applied pharmacology*. 288(3):420-428.
- Stapleton PA, Minarchick VC, Yi J, Engels K, McBride CR, Nurkiewicz TR. 2013a. Maternal engineered nanomaterial exposure and fetal microvascular function: Does the barker hypothesis apply? *Am J Obstet Gynecol*.
- Stapleton PA, Minarchick VC, Yi J, Engels K, McBride CR, Nurkiewicz TR. 2013b. Maternal engineered nanomaterial exposure and fetal microvascular function: Does the barker hypothesis apply? *American journal of obstetrics and gynecology*. 209(3):227.e221-211.
- Stapleton PA, Nichols CE, Yi J, McBride CR, Minarchick VC, Shepherd DL, Hollander JM, Nurkiewicz TR. 2015d. Microvascular and mitochondrial dysfunction in the female f1 generation after gestational tio2 nanoparticle exposure. *Nanotoxicology*. 9(8):941-951.
- Stapleton PA, Nichols CE, Yi J, McBride CR, Minarchick VC, Shepherd DL, Hollander JM, Nurkiewicz TR. 2015e. Microvascular and mitochondrial dysfunction in the female f1 generation after gestational tio2 nanoparticle exposure. *Nanotoxicology*. 9(8):941-951.
- Stapleton PA, Nurkiewicz TR. 2014. Maternal nanomaterial exposure: A double threat to maternal uterine health and fetal development? *Nanomedicine (Lond)*. 9(7):929-931.
- Stasenko S, Bradford EM, Piasek M, Henson MC, Varnai VM, Jurasovic J, Kusec V. 2010. Metals in human placenta: Focus on the effects of cadmium on steroid hormones and leptin. *Journal of applied toxicology : JAT*. 30(3):242-253.
- Strobel C, Torrano AA, Herrmann R, Malissek M, Bräuchle C, Reller A, Treuel L, Hilger I. 2013. Effects of the physicochemical properties of titanium dioxide nanoparticles, commonly used as sun protection agents, on microvascular endothelial cells. *Journal of Nanoparticle Research*. 16(1):2130.
- Stulc J, Stulcova B. 1996. Placental transfer of phosphate in anaesthetized rats. *Placenta*. 17(7):487-493.
- Stulc J, Stulcova B, Husain S, Sibley CP. 1996. Transfer of cl- across placenta of anesthetized rat. *Am J Physiol*. 271(5 Pt 2):R1107-1114.
- Stulc J, Stulcova B, Svihovec J. 1990. Transport of calcium across the dually perfused placenta of the rat. *J Physiol*. 420:295-311.
- Su J, Wang L. 2012. Research advances in neonatal hypoglycemic brain injury. *Transl Pediatr*. 1(2):108-115.
- Sun J, Sun J. 2022. How neuroactive factors mediates immune responses during pregnancy: An interdisciplinary view. *Neuropeptides*. 91:102213.
- Sunada K, Watanabe T, Hashimoto K. 2003. Studies on photokilling of bacteria on tio2 thin film. *Journal of Photochemistry and Photobiology A: Chemistry*. 156(1):227-233.

- Swanson AM, David AL. 2015. Animal models of fetal growth restriction: Considerations for translational medicine. *Placenta*. 36(6):623-630.
- Sweeney S, Adamcakova-Dodd A, Thorne PS, Assouline JG. 2018. Multifunctional nanoparticles for real-time evaluation of toxicity during fetal development. *PLoS One*. 13(2):e0192474.
- Tachibana R, Umekawa T, Yoshikawa K, Owa T, Magawa S, Furuhashi F, Tsuji M, Maki S, Shimada K, Kaneda MK et al. 2019. Tadalafil treatment in mice for preeclampsia with fetal growth restriction has neuro-benefic effects in offspring through modulating prenatal hypoxic conditions. *Scientific reports*. 9(1):234-234.
- Tang H, Jiang Z, He H, Li X, Hu H, Zhang N, Dai Y, Zhou Z. 2018. Uptake and transport of pullulan acetate nanoparticles in the bewo b30 placental barrier cell model. *Int J Nanomedicine*. 13:4073-4082.
- Tapia VL, Vasquez BV, Vu B, Liu Y, Steenland K, Gonzales GF. 2020. Association between maternal exposure to particulate matter (pm2.5) and adverse pregnancy outcomes in lima, peru. *Journal of Exposure Science & Environmental Epidemiology*. 30(4):689-697.
- Tassinari R, Cubadda F, Moracci G, Aureli F, D'Amato M, Valeri M, De Berardis B, Raggi A, Mantovani A, Passeri D et al. 2014. Oral, short-term exposure to titanium dioxide nanoparticles in sprague-dawley rat: Focus on reproductive and endocrine systems and spleen. *Nanotoxicology*. 8(6):654-662.
- Teng C, Jia J, Wang Z, Yan B. 2020. Oral co-exposures to zinc oxide nanoparticles and cdcl(2) induced maternal-fetal pollutant transfer and embryotoxicity by damaging placental barriers. *Ecotoxicol Environ Saf*. 189:109956.
- TeSlaa T, Teitell MA. 2014. Techniques to monitor glycolysis. *Methods Enzymol*. 542:91-114.
- Tessier DR, Yockell-Lelievre J, Gruslin A. 2015. Uterine spiral artery remodeling: The role of uterine natural killer cells and extravillous trophoblasts in normal and high-risk human pregnancies. *American journal of reproductive immunology (New York, NY : 1989)*. 74(1):1-11.
- Thame M, Osmond C, Trotman H. 2015. Fetal growth and birth size is associated with maternal anthropometry and body composition. *Matern Child Nutr*. 11(4):574-582.
- Thamotharan M, Garg M, Oak S, Rogers LM, Pan G, Sangiorgi F, Lee PW, Devaskar SU. 2007. Transgenerational inheritance of the insulin-resistant phenotype in embryo-transferred intrauterine growth-restricted adult female rat offspring. *American journal of physiology Endocrinology and metabolism*. 292(5):E1270-1279.
- Thompson LP, Pence L, Pinkas G, Song H, Telugu BP. 2016. Placental hypoxia during early pregnancy causes maternal hypertension and placental insufficiency in the hypoxic guinea pig model. *Biology of reproduction*. 95(6):128-128.
- Thompson LP, Turan S, Aberdeen GW. 2020. Sex differences and the effects of intrauterine hypoxia on growth and in vivo heart function of fetal guinea pigs. *American Journal of Physiology-Regulatory, Integrative and Comparative Physiology*. 319(3):R243-R254.
- Thorley AJ, Ruenaroengsak P, Potter TE, Tetley TD. 2014. Critical determinants of uptake and translocation of nanoparticles by the human pulmonary alveolar epithelium. *ACS Nano*. 8(11):11778-11789.
- Thorpe PG, Gilboa SM, Hernandez-Diaz S, Lind J, Cragan JD, Briggs G, Kweder S, Friedman JM, Mitchell AA, Honein MA et al. 2013. Medications in the first trimester of pregnancy: Most common exposures and critical gaps in understanding fetal risk. *Pharmacoepidemiol Drug Saf*. 22(9):1013-1018.
- Tkacova R. 2010. Systemic inflammation in chronic obstructive pulmonary disease: May adipose tissue play a role? Review of the literature and future perspectives. *Mediators Inflamm*. 2010:585989-585989.

- Todt JC, Yang Y, Lei J, Lauria MR, Sorokin Y, Cotton DB, Yelian FD. 1996. Effects of tumor necrosis factor-alpha on human trophoblast cell adhesion and motility. *American journal of reproductive immunology (New York, NY : 1989)*. 36(2):65-71.
- Tossetta G, Paolinelli F, Avellini C, Salvolini E, Ciarmela P, Lorenzi T, Emanuelli M, Toti P, Giuliani R, Gesuita R et al. 2014. Il-1beta and tgf-beta weaken the placental barrier through destruction of tight junctions: An in vivo and in vitro study. *Placenta*. 35(7):509-516.
- Troen P, Gordon EE. 1958. Perfusion studies of the human placenta. I. Effect of estradiol and human chorionic gonadotropin on citric acid metabolism. *J Clin Invest*. 37(11):1516-1523.
- Tucci P, Porta G, Agostini M, Dinsdale D, Iavicoli I, Cain K, Finazzi-Agró A, Melino G, Willis A. 2013. Metabolic effects of tio<sub>2</sub> nanoparticles, a common component of sunscreens and cosmetics, on human keratinocytes. *Cell Death & Disease*. 4(3):e549-e549.
- Tunster SJ, Van De Pette M, John RM. 2014. Isolating the role of elevated phlda2 in asymmetric late fetal growth restriction in mice. *Dis Model Mech*. 7(10):1185-1191.
- Tunster SJ, Watson ED, Fowden AL, Burton GJ. 2020. Placental glycogen stores and fetal growth: Insights from genetic mouse models. *Reproduction*. 159(6):R213-r235.
- Ullian ME. 1999. The role of corticosteroids in the regulation of vascular tone. *Cardiovascular research*. 41(1):55-64.
- Umezawa M, Onoda A, Korshunova I, Jensen ACO, Koponen IK, Jensen KA, Khodosevich K, Vogel U, Hougaard KS. 2018. Maternal inhalation of carbon black nanoparticles induces neurodevelopmental changes in mouse offspring. *Part Fibre Toxicol*. 15(1):36.
- Umezawa M, Tainaka H, Kawashima N, Shimizu M, Takeda K. 2012. Effect of fetal exposure to titanium dioxide nanoparticle on brain development - brain region information. *The Journal of toxicological sciences*. 37(6):1247-1252.
- Uyuklu M, Canpolat M, Meiselman HJ, Baskurt OK. 2011. Wavelength selection in measuring red blood cell aggregation based on light transmittance. *J Biomed Opt*. 16(11):117006-117006.
- Valentini X, Rugira P, Frau A, Tagliatti V, Conotte R, Laurent S, Colet J-M, Nonclercq D. 2019. Hepatic and renal toxicity induced by tio<sub>2</sub> nanoparticles in rats: A morphological and metabolomic study. *Journal of Toxicology*. 2019:5767012.
- Valko M, Morris H, Cronin MT. 2005. Metals, toxicity and oxidative stress. *Current medicinal chemistry*. 12(10):1161-1208.
- Vambergue A, Fajardy I. 2011. Consequences of gestational and pregestational diabetes on placental function and birth weight. *World Journal of Diabetes*. 2(11):196-203.
- van den Hooven EH, Pierik FH, de Kluizenaar Y, Hofman A, van Ratingen SW, Zandveld PY, Russcher H, Lindemans J, Miedema HM, Steegers EA et al. 2012. Air pollution exposure and markers of placental growth and function: The generation r study. *Environ Health Perspect*. 120(12):1753-1759.
- Van Gronigen Case G, Storey KM, Parmeley LE, Schulz LC. 2021. Effects of maternal nutrient restriction during the periconceptual period on placental development in the mouse. *PLOS ONE*. 16(1):e0244971.
- van schaftingen E, Gerin I. 2002. The glucose-6-phosphatase system. *Biochemical Journal*. 362(3):513-532.
- Vandamme TF. 2014. Use of rodents as models of human diseases. *J Pharm Bioallied Sci*. 6(1):2-9.
- Varcoe TJ, Voultzios A, Gatford KL, Kennaway DJ. 2016. The impact of prenatal circadian rhythm disruption on pregnancy outcomes and long-term metabolic health of mice progeny. *Chronobiology international*. 33(9):1171-1181.

- Vardhana PA, Illsley NP. 2002. Transepithelial glucose transport and metabolism in bewo choriocarcinoma cells. *Placenta*. 23(8-9):653-660.
- Vaughan OR, Fowden AL. 2016. Placental metabolism: Substrate requirements and the response to stress. *Reprod Domest Anim*. 51 Suppl 2:25-35.
- Velten M, Britt RD, Heyob KM, Welty SE, Eiberger B, Tipple TE, Rogers LK. 2012. Prenatal inflammation exacerbates hyperoxia-induced functional and structural changes in adult mice. *American Journal of Physiology - Regulatory, Integrative and Comparative Physiology*. 303(3):R279-R290.
- Ventura-Clapier R, Piquereau J, Veksler V, Garnier A. 2019. Estrogens, estrogen receptors effects on cardiac and skeletal muscle mitochondria. *Frontiers in Endocrinology*. 10(557).
- Veras MM, Damaceno-Rodrigues NR, Caldini EG, Maciel Ribeiro AA, Mayhew TM, Saldiva PH, Dolhnikoff M. 2008. Particulate urban air pollution affects the functional morphology of mouse placenta. *Biology of reproduction*. 79(3):578-584.
- Vidanapathirana AK, Thompson LC, Herco M, Odom J, Sumner SJ, Fennell TR, Brown JM, Wingard CJ. 2018. Acute intravenous exposure to silver nanoparticles during pregnancy induces particle size and vehicle dependent changes in vascular tissue contractility in sprague dawley rats. *Reproductive Toxicology*. 75:10-22.
- Vidanapathirana AK, Thompson LC, Mann EE, Odom JT, Holland NA, Sumner SJ, Han L, Lewin AH, Fennell TR, Brown JM et al. 2014a. Pvp formulated fullerene (c60) increases rho-kinase dependent vascular tissue contractility in pregnant sprague dawley rats. *Reproductive toxicology (Elmsford, NY)*. 49:86-100.
- Vidanapathirana AK, Thompson LC, Odom J, Holland NA, Sumner SJ, Fennell TR, Brown JM, Wingard CJ. 2014b. Vascular tissue contractility changes following late gestational exposure to multi-walled carbon nanotubes or their dispersing vehicle in sprague dawley rats. *J Nanomed Nanotechnol*. 5(3).
- Vlasova II, Kapralov AA, Michael ZP, Burkert SC, Shurin MR, Star A, Shvedova AA, Kagan VE. 2016. Enzymatic oxidative biodegradation of nanoparticles: Mechanisms, significance and applications. *Toxicology and applied pharmacology*. 299:58-69.
- Vogt Isaksen C. 2004. Maternal smoking, intrauterine growth restriction, and placental apoptosis. *Pediatr Dev Pathol*. 7(5):433-442.
- Vrijer Bd, Regnault TRH, Wilkening RB, Meschia G, Battaglia FC. 2004. Placental uptake and transport of acp, a neutral nonmetabolizable amino acid, in an ovine model of fetal growth restriction. *American Journal of Physiology-Endocrinology and Metabolism*. 287(6):E1114-E1124.
- Vykoukal D, Davies MG. 2011. Vascular biology of metabolic syndrome. *Journal of vascular surgery : official publication, the Society for Vascular Surgery [and] International Society for Cardiovascular Surgery, North American Chapter*. 54(3):819-831.
- Wai KM, Mar O, Kosaka S, Umemura M, Watanabe C. 2017. Prenatal heavy metal exposure and adverse birth outcomes in myanmar: A birth-cohort study. *International Journal of Environmental Research and Public Health*. 14(11):1339.
- Wainstock T, Shoham-Vardi I, Glasser S, Anteby E, Lerner-Geva L. 2015. Fetal sex modifies effects of prenatal stress exposure and adverse birth outcomes. *Stress (Amsterdam, Netherlands)*. 18(1):49-56.
- Walker N, Filis P, O'Shaughnessy PJ, Bellingham M, Fowler PA. 2019. Nutrient transporter expression in both the placenta and fetal liver are affected by maternal smoking. *Placenta*. 78:10-17.
- Wallace AE, Fraser R, Cartwright JE. 2012. Extravillous trophoblast and decidual natural killer cells: A remodelling partnership. *Human reproduction update*. 18(4):458-471.

- Wallis AB, Saftlas AF, Hsia J, Atrash HK. 2008. Secular trends in the rates of preeclampsia, eclampsia, and gestational hypertension, united states, 1987-2004. *Am J Hypertens*. 21(5):521-526.
- Wang H, Wu L, Sun X. 2020. Intratracheal delivery of nano- and microparticles and hyperpolarized gases: A promising strategy for the imaging and treatment of respiratory disease. *CHEST*. 157(6):1579-1590.
- Wang J, Chen C, Liu Y, Jiao F, Li W, Lao F, Li Y, Li B, Ge C, Zhou G et al. 2008a. Potential neurological lesion after nasal instillation of tio(2) nanoparticles in the anatase and rutile crystal phases. *Toxicol Lett*. 183(1-3):72-80.
- Wang J, Li Y, Li WEI, Chen C, Li BAI, Zhao Y. 2008b. Biological effect of intranasally instilled titanium dioxide nanoparticles on female mice. *Nano*. 03(04):279-285.
- Wang J, Liu Y, Jiao F, Lao F, Li W, Gu Y, Li Y, Ge C, Zhou G, Li B et al. 2008c. Time-dependent translocation and potential impairment on central nervous system by intranasally instilled tio(2) nanoparticles. *Toxicology*. 254(1-2):82-90.
- Wang J, Zhou G, Chen C, Yu H, Wang T, Ma Y, Jia G, Gao Y, Li B, Sun J et al. 2007a. Acute toxicity and biodistribution of different sized titanium dioxide particles in mice after oral administration. *Toxicology letters*. 168(2):176-185.
- Wang JX, Li YF, Zhou GQ, Li B, Jiao F, Chen CY, Gao YX, Zhao YL, Chai ZF. 2007b. [influence of intranasal instilled titanium dioxide nanoparticles on monoaminergic neurotransmitters of female mice at different exposure time]. *Zhonghua Yu Fang Yi Xue Za Zhi*. 41(2):91-95.
- Wang Y, S. Z. 2010. *Vascular biology of the placenta*. San Rafael CA: Morcan and Claypool Life Sciences.
- Wardoyo AYP, Juswono UP, Noor JAE. 2018. Varied dose exposures to ultrafine particles in the motorcycle smoke cause kidney cell damages in male mice. *Toxicol Rep*. 5:383-389.
- Weiler J, Tong S, Palmer KR. 2011. Is fetal growth restriction associated with a more severe maternal phenotype in the setting of early onset pre-eclampsia? A retrospective study. *PloS one*. 6(10):e26937-e26937.
- Weiner CP, Martinez E, Chestnut DH, Ghodsi A. 1989. Effect of pregnancy on uterine and carotid artery response to norepinephrine, epinephrine, and phenylephrine in vessels with documented functional endothelium. *American journal of obstetrics and gynecology*. 161(6 Pt 1):1605-1610.
- Weir A, Westerhoff P, Fabricius L, Hristovski K, von Goetz N. 2012. Titanium dioxide nanoparticles in food and personal care products. *Environmental Science & Technology*. 46(4):2242-2250.
- Weiss G, Sundl M, Glasner A, Huppertz B, Moser G. 2016. The trophoblast plug during early pregnancy: A deeper insight. *Histochemistry and cell biology*. 146(6):749-756.
- White V, Jawerbaum A, Mazzucco MB, Gauster M, Desoye G, Hiden U. 2018. Igf2 stimulates fetal growth in a sex- and organ-dependent manner. *Pediatric research*. 83(1):183-189.
- Wick P, Malek A, Manser P, Meili D, Maeder-Althaus X, Diener L, Diener PA, Zisch A, Krug HF, von Mandach U. 2010. Barrier capacity of human placenta for nanosized materials. *Environ Health Perspect*. 118(3):432-436.
- Wiebold JL, Becker WC. 1987. Inequality in function of the right and left ovaries and uterine horns of the mouse. *Journal of reproduction and fertility*. 79(1):125-134.
- Wilson R, Jenkins C, Miller H, McInnes IB, Moore J, McLean MA, Walker JJ. 2004. Abnormal cytokine levels in non-pregnant women with a history of recurrent miscarriage. *European Journal of Obstetrics & Gynecology and Reproductive Biology*. 115(1):51-54.

- Wojtyla C, Zielinska K, Wojtyla-Buciora P, Panek G. 2020. Prenatal fine particulate matter (pm(2.5)) exposure and pregnancy outcomes-analysis of term pregnancies in poland. *Int J Environ Res Public Health*. 17(16).
- Wollmann HA. 1998. Intrauterine growth restriction: Definition and etiology. *Hormone Research in Paediatrics*. 49(suppl 2)(Suppl. 2):1-6.
- Woods L, Perez-Garcia V, Hemberger M. 2018. Regulation of placental development and its impact on fetal growth-new insights from mouse models. *Front Endocrinol (Lausanne)*. 9:570-570.
- Wu F, Hicks AL. 2020. Estimating human exposure to titanium dioxide from personal care products through a social survey approach. *Integr Environ Assess Manag*. 16(1):10-16.
- Wu J, Sun J, Xue Y. 2010. Involvement of jnk and p53 activation in g2/m cell cycle arrest and apoptosis induced by titanium dioxide nanoparticles in neuron cells. *Toxicology letters*. 199(3):269-276.
- Xiao W, Wang R-S, Handy DE, Loscalzo J. 2018. Nad(h) and nadp(h) redox couples and cellular energy metabolism. *Antioxid Redox Signal*. 28(3):251-272.
- Xing AY, Challier JC, Lepercq J, Caüzac M, Charron MJ, Girard J, Hauguel-de Mouzon S. 1998. Unexpected expression of glucose transporter 4 in villous stromal cells of human placenta1. *The Journal of Clinical Endocrinology & Metabolism*. 83(11):4097-4101.
- Xu P, Wu Z, Xi Y, Wang L. 2016. Epigenetic regulation of placental glucose transporters mediates maternal cadmium-induced fetal growth restriction. *Toxicology*. 372:34-41.
- Xu X-F, Li Y-J, Sheng Y-J, Liu J-L, Tang L-F, Chen Z-M. 2014. Effect of low birth weight on childhood asthma: A meta-analysis. *BMC Pediatr*. 14:275-275.
- Xue C, Wu J, Lan F, Liu W, Yang X, Zeng F, Xu H. 2010. Nano titanium dioxide induces the generation of ros and potential damage in hacat cells under uva irradiation. *J Nanosci Nanotechnol*. 10(12):8500-8507.
- Xue Y, Wu J, Sun J. 2012. Four types of inorganic nanoparticles stimulate the inflammatory reaction in brain microglia and damage neurons in vitro. *Toxicology letters*. 214(2):91-98.
- Yamaguchi K, Mishina J, Mitsuishi C, Nakabayashi M, Nishida H. 1997. Neonatal hypoglycemia in infants with intrauterine growth retardation due to pregnancy-induced hypertension. *Acta Paediatr Jpn*. 39 Suppl 1:S48-50.
- Yamashita H, Shao J, Qiao L, Pagliassotti M, Friedman JE. 2003. Effect of spontaneous gestational diabetes on fetal and postnatal hepatic insulin resistance in lepr(db/+) mice. *Pediatric research*. 53(3):411-418.
- Yamashita K, Yoshioka Y, Higashisaka K, Mimura K, Morishita Y, Nozaki M, Yoshida T, Ogura T, Nabeshi H, Nagano K et al. 2011. Silica and titanium dioxide nanoparticles cause pregnancy complications in mice. *Nat Nanotechnol*. 6(5):321-328.
- Yamazaki F, Kuroiwa T, Takikawa O, Kido R. 1985. Human indolylamine 2,3-dioxygenase. Its tissue distribution, and characterization of the placental enzyme. *Biochem J*. 230(3):635-638.
- Yang H, Zhu S, Pan N. 2004. Studying the mechanisms of titanium dioxide as ultraviolet-blocking additive for films and fabrics by an improved scheme. *Journal of Applied Polymer Science*. 92:3201-3210.
- Yi J, Chen BT, Schwegler-Berry D, Frazer D, Castranova V, McBride C, Knuckles TL, Stapleton PA, Minarchick VC, Nurkiewicz TR. 2013. Whole-body nanoparticle aerosol inhalation exposures. *Journal of visualized experiments : JoVE*. (75):e50263-e50263.
- Yin J, Kang C, Li Y, Li Q, Zhang X, Li W. 2014. Aerosol inhalation exposure study of respiratory toxicity induced by 20 nm anatase titanium dioxide nanoparticles. *Toxicology Research*. 3(5):367-374.

- Yinon D, Lowenstein L, Suraya S, Beloosesky R, Zmora O, Malhotra A, Pillar G. 2006. Pre-eclampsia is associated with sleep-disordered breathing and endothelial dysfunction. *The European respiratory journal : official journal of the European Society for Clinical Respiratory Physiology*. 27(2):328-333.
- Yoshida S, Hiyoshi K, Oshio S, Takano H, Takeda K, Ichinose T. 2010. Effects of fetal exposure to carbon nanoparticles on reproductive function in male offspring. *Fertil Steril*. 93(5):1695-1699.
- Yu Q, Wang H, Peng Q, Li Y, Liu Z, Li M. 2017. Different toxicity of anatase and rutile tio<sub>2</sub> nanoparticles on macrophages: Involvement of difference in affinity to proteins and phospholipids. *Journal of Hazardous Materials*. 335:125-134.
- Yu Z-W, Burén J, Enerbäck S, Nilsson E, Samuelsson L, Eriksson JW. 2001. Insulin can enhance glut4 gene expression in 3t3-f442a cells and this effect is mimicked by vanadate but counteracted by camp and high glucose – potential implications for insulin resistance. *Biochimica et Biophysica Acta (BBA) - Molecular Basis of Disease*. 1535(2):174-185.
- Zamudio S, Baumann MU, Illsley NP. 2006. Effects of chronic hypoxia in vivo on the expression of human placental glucose transporters. *Placenta*. 27(1):49-55.
- Zamudio S, Torricos T, Fik E, Oyala M, Echalar L, Pullockaran J, Tutino E, Martin B, Belliappa S, Balanza E et al. 2010. Hypoglycemia and the origin of hypoxia-induced reduction in human fetal growth. *PLOS ONE*. 5(1):e8551.
- Zaretsky MV, Alexander JM, Byrd W, Bawdon RE. 2004. Transfer of inflammatory cytokines across the placenta. *Obstetrics and gynecology*. 103(3):546-550.
- Ze Y, Zheng L, Zhao X, Gui S, Sang X, Su J, Guan N, Zhu L, Sheng L, Hu R et al. 2013. Molecular mechanism of titanium dioxide nanoparticles-induced oxidative injury in the brain of mice. *Chemosphere*. 92(9):1183-1189.
- Zhang B, Tan L, Yu Y, Wang B, Chen Z, Han J, Li M, Chen J, Xiao T, Ambati BK et al. 2018a. Placenta-specific drug delivery by trophoblast-targeted nanoparticles in mice. *Theranostics*. 8(10):2765-2781.
- Zhang X, Fan C, Ren Z, Feng H, Zuo S, Hao J, Liao J, Zou Y, Ma L. 2020. Maternal pm<sub>2.5</sub> exposure triggers preterm birth: A cross-sectional study in wuhan, china. *Global Health Research and Policy*. 5(1):17.
- Zhang XF, Park JH, Choi YJ, Kang MH, Gurunathan S, Kim JH. 2015. Silver nanoparticles cause complications in pregnant mice. *Int J Nanomedicine*. 10:7057-7071.
- Zhang Y, Xu B, Yao M, Dong T, Mao Z, Hang B, Han X, Lin Z, Bian Q, Li M et al. 2018b. Titanium dioxide nanoparticles induce proteostasis disruption and autophagy in human trophoblast cells. *Chem Biol Interact*. 296:124-133.
- Zhao R, Xu L, Wu ML, Huang SH, Cao XJ. 2018. Maternal pre-pregnancy body mass index, gestational weight gain influence birth weight. *Women Birth*. 31(1):e20-e25.
- Zhao Y, Chen L, Li L-x, Xie C-m, Li D, Shi H-j, Zhang Y-h. 2014. Gender-specific relationship between prenatal exposure to phthalates and intrauterine growth restriction. *Pediatric research*. 76(4):401-408.
- Zheng T, Zhang J, Sommer K, Bassig BA, Zhang X, Braun J, Xu S, Boyle P, Zhang B, Shi K et al. 2016. Effects of environmental exposures on fetal and childhood growth trajectories. *Ann Glob Health*. 82(1):41-99.
- Zhong H, Geng Y, Chen J, Gao R, Yu C, Yang Z, Chen X, Mu X, Liu X, He J. 2020. Maternal exposure to ceo(2)nps during early pregnancy impairs pregnancy by inducing placental abnormalities. *J Hazard Mater*. 389:121830.
- Zhu N, Ji X, Geng X, Yue H, Li G, Sang N. 2021. Maternal pm<sub>2.5</sub> exposure and abnormal placental nutrient transport. *Ecotoxicology and Environmental Safety*. 207:111281.

- Zhu Y-C, Lin L, Li B-Y, Li X-T, Chen D-J, Zhao X-L, Cui S-H, Ding H-J, Ding G-F, Meng H-X et al. 2020. Incidence and clinical features of fetal growth restriction in 4 451 women with hypertensive disorders of pregnancy. *Maternal-Fetal Medicine*. 2(4).
- Zia S. 2013. Placental location and pregnancy outcome. *Journal of the Turkish German Gynecological Association*. 14(4):190-193.
- Zuo J, Tang J, Lu M, Zhou Z, Li Y, Tian H, Liu E, Gao B, Liu T, Shao P. 2021. Glycolysis rate-limiting enzymes: Novel potential regulators of rheumatoid arthritis pathogenesis. *Frontiers in Immunology*. 12.
- Zygula A, Kosinski P, Wroczynski P, Makarewicz-Wujec M, Pietrzak B, Wielgos M, Giebultowicz J. 2020. Oxidative stress markers differ in two placental dysfunction pathologies: Pregnancy-induced hypertension and intrauterine growth restriction. *Oxidative Medicine and Cellular Longevity*. 2020:1323891.